Micro and Macro-scale Characterisation of an Agarose-based Physical and Computational Model for the Testing and Development of Engineered Responsive Living Systems

Javier Rodriguez Corral

BSc Construction Engineering

MSc Civil Engineering

A thesis submitted for the degree of

Doctor of Philosophy

Abstract

The use of microbially-mediated processes to deal with geo-environmental problems has raised the interest of geotechnical engineers over the last decade. Of particular interest to this study is the use of bacteria cells to catalyse chemical reactions that can potentially improve the properties of the ground. These bio-mediated methods are based on naturally-occurring processes and provide effective, sustainable and economic engineering solutions. A frontier of this area of research is the development of the so-called *engineered responsive living systems*. These systems normally involve the use of bacteria cells that have been engineered to respond intelligently to inputs from their environment, and they provide benefits that conventional bio-mediated processes are not able to offer.

The work presented in this thesis contributes to the development of engineered responsive living systems for their use in geotechnical applications. One possible way of developing these responsive systems is to use *agarose gels* as a substitute for soils for the development of early stage physical and computational demonstrators. Agarose gels allow easier monitoring of the performance of the microbes, greater control of the chemical composition of the environment, a controlled simulation over the mechanical properties and a minimised risk of contamination, compared to soils. Thus, the ultimate aim of this research is to characterise at the micro and macro-scale an agarose-based system capable of testing engineered bacteria in a highly controllable environment and monitoring their response to external stimulus.

The first part of this thesis involves a full-scale characterisation of Agarose Low Melt gel through a series of geotechnical testing techniques, including SEM, triaxial and oedometer testing; the second part focuses on understanding the growth and distribution of bacteria colonies within a volume of agarose gel and exploring the factors that influence their behaviour; and the final part describes the development of a computational model that integrates geotechnical simulations with biological data and simulates the effect of a pressure-responsive gel-based biocementation system. The successful implementation of such gel-based model will help in the early development of a pressure-responsive bacteria-based system and will assist in the validation of the proof of concept.

Acknowledgements

Table of Contents

List of Figures

List of Tables

List of terms, abbreviations and symbols

MICP	Microbially-Induced Calcite Precipitation
SynBio	Synthetic Biology
DNA	Deoxyribonucleic acid
LM	Low Melting Point
EPS	Extracellular Polymeric Substances
OD	Optical Density
M	Molar concentration
GMO	Genetically-Modified Organism
GFP	Green Fluorescent Protein
M/kPa	Mega/kilopascal
σ_1	Major Principal Stress
σ_3	Minor Principal Stress/Cell Pressure
SEM	Scanning Electron Microscopy
UCS	Unconfined Compressive Strength
m/v	Mass per volume
M/kN	Mega/kiloNewton
u	Pore Water Pressure
a	Pore size
$C_{agarose}$	Agarose concentration
$\rho_{agarose}$	Agarose dry density
$\omega_{agarose}$	Mass fraction of agarose in a fibre
n	Porosity
Φ	Volume fraction of fibres
w	Moisture content
m_w	Mass of water
m_{dry}	Mass of dry solids
e	Void ratio
G_s	Agarose specific gravity (dry)
C_u	Undrained shear strength
q_u	Unconfined compression
C_v	Coefficient of consolidation
A	Area of sample

L	Length of Sample
M	Mass of Sample
B	Skempton B Value
D	Diameter of Sample
E	Young's Modulus
M_v	Coefficient of compressibility
k_v	Coefficient of vertical permeability
γ_w	Water specific weight (or unit weight)
LB	Lysogeny or Luria Broth
SSM	Spizizen Minimal
V_{medium}	Volume of medium
V_{flask}	Volume of flask
CFU	Colony Forming Unit
R^2	Coefficient of determination
S_e	Standard deviation of the residuals
PPE	Personal Protective Equipment
w.r.t.	With respect to
I	Influence
N_c	Skempton Factor
PWP	Pore water pressure
g	Gravitational acceleration
F	Force
δ	Vertical displacement
ε	Vertical strain
h	Original thickness of the sub-layer
H	Height of the layer
U	Urease activity
GUI	Graphic User Interface
XRD	X-Ray Diffraction
XRT/CT	X-Ray Computer Tomography
v	Poisson's Ratio

List of Publications

Rodriguez-Corral J, Mitrani H, Dade-Robertson M, Zhang M, Maiello P. Agarose Gel as a Soil Analogue for the Development of Advanced Bio-mediated Soil Improvement Methods. *PLOS ONE.* Under review.

Dade-Robertson M, Mitrani H, Rodriguez-Corral J, Zhang M, Hernan L, Guyet A, Wipat A. Design and modelling of an engineered bacteria-based, pressure-sensitive soil. *Bioinspiration & Biomimetics*, 2018, 13(4), 046004

Best paper award: Rodriguez-Corral J, Mitrani H, Dade-Robertson M, Zhang M. Agarose Gel as a Soil Analogue for Novel Ground Improvement Applications. *In: 3rd World Congress on Civil, Structural and Environmental Engineering (CSEE '18)*, 2018, Budapest, Hungary.

Dade-Robertson M, Rodriguez-Corral J, Guyet A, Mitrani H, Wipat A, Zhang M. Synthetic Biological Construction: Beyond 'bio-inspired' in the design and of new materials and fabrication systems. *In: 3rd International Conference Biodigital: Architecture & Genetics*, 2017, Barcelona.

Dade-Robertson M, Rodriguez-Corral J, Mitrani H, Zhang M, Wipat A, Ramirez-Figueroa C, Hernan L. Thinking Soils: A synthetic biology approach to material-based design computation. *In: ACADIA 2016 – Posthuman Frontiers: Data, Designers and Cognitive Machines*, 2016, Ann Arbor, Michigan: Association for Computer Aided Design in Architecture.

Chapter 1

Introduction

1.1. Background

Microorganisms and microbially-mediated processes are present in every environment on the Earth (Lopez-Garcia et al., 2005). Of particular interest to this thesis is the use of *living bacteria cells* to mediate geoenvironmental processes such as *soil biomineralization*. Mitchell and Santamarina (2005) reported that the most abundant microorganisms in soils are bacteria (between 10^1 and 10^9 cells per gram of soil) and they are able to survive in extreme conditions, e.g. low to high acidity environments, below freezing to above boiling temperatures or resist very high pressures (Madigan et al., 2008). Their growth and survivability depends on the environmental conditions they live in such as temperature, pH, oxygen concentration, soil suction, pore structure of the matrix or presence of toxic substances (Jiang G, Noonan MJ, 2006; Phadnis and Santamarina, 2011). According to (Gadd, 2007), many of the physical and chemical alterations occurring in geomaterials are generated by bio-mediated processes, including biomineralization, oxidation/reduction of chemical compounds and dissolution/degradation of minerals, amongst others.

Researchers have realised the potential of using bio-mediated processes for effective and sustainable ground improvement processes and extensive studies have been performed worldwide over the last decade (Umar et al., 2016). Following this growing interest, a new and promising area of investigation has emerged called *Construction Microbial Biotechnology* which includes *microbially-mediated construction processes* and *microbial production of construction materials* as the two main pillars (Stabnikov et al., 2015).

Focusing on the former, it has been shown that construction-related microbial biotechnologies offer many advantages over conventional construction processes,

including low cost and sustainability – both environmental and socio-economic (Chu et al., 2009; Ivanov and Chu, 2008; Stabnikov et al., 2015).

In particular, the use of *living bacterial cells* to mediate construction processes has raised great interest amongst researchers. Microbially-mediated or bio-mediated methods could be implemented in a wide range of geotechnical engineering applications, including soil erosion control, liquefaction mitigation or remediation of contaminated soil (DeJong et al., 2010; James K. Mitchell and Santamarina, 2005a). Bio-mediated processes have the potential for significant reduction in embodied energy and carbon emissions, relative to conventional practices which mainly rely on the use of Portland cement. Additionally, another advantage of bio-mediated methods is that they can cover large distances due to their low viscosity, and can be deployed beneath and around existing structures, generating a lower impact on the society (e.g. less noise or reduced disruption of congested sites).

The above-mentioned bio-mediated construction processes can be divided into three main categories:

1) *Soil biocementation.* A process in which bacteria acts as a catalyst for soil biomineralization through Microbially-Induced Calcite Precipitation (MICP), bonding the soil particles, reducing the hydraulic conductivity and strengthening the soil matrix (DeJong et al., 2010; Ivanov and Chu, 2008; Whiffin et al., 2007).

2) *Soil biodesaturation.* A process by which the saturation of soils is decreased due to the bio-mediated production of biogas in-situ, reducing the potential of liquefaction (Burbank et al., 2013; Jian Chu et al., 2009).

3) *Soil bioremediation.* A process by which microorganisms remove or immobilize soil pollutants and contaminants (Stabnikov et al., 2015).

Of particular interest to this project is the process of soil biocementation through MICP, which has been proved to be a more sustainable and cheaper alternative to mechanical or chemical ground improvement methods, as well as having a reduced impact on the geoenvironment (see 2.4.4. Biocementation through Microbially-Induced Calcite Precipitation

(MICP)). The precipitation of calcium carbonates by bacteria via urea hydrolysis is the most commonly exploited mechanism and, although the production of ammonium through this mechanism increases considerably the pH of the environment, it is believed to be a more eco-friendly solution than, for instance, cement-based practices.

Overall, microorganisms for ground improvement offer many potential advantages over traditional geotechnical engineering practices. However, significant multidisciplinary research is still required to optimise and develop these complex processes for industrial use. One of the reasons geotechnical engineers are reluctant to implement microbially-mediated practices in-situ is the poor control over the bio-mediated processes and the uncertainty of the final outcomes, which in turn has a strong dependency on the conditions of the environment.

1.2. Engineered responsive living systems

The microbially-mediated construction processes defined in the previous section rely on the potential of bacteria to change the composition of the ground at scales relevant to the built environment (Dade-Robertson, 2015). For instance, treating the soil with MICP processes involves the insertion of certain types of urease-producing bacteria into the ground in order to induce specific reactions that change the chemical composition of the soil matrix and ultimately precipitate calcium carbonate crystals, leading to soil cementation (see 2.4.4. Biocementation through Microbially-Induced Calcite Precipitation (MICP) for more details). This bio-mediated process depends on many parameters such as bacteria concentration, pH of the environment or calcium ions concentration and consequently, the magnitude and location of the cemented areas is often uncertain (DeJong et al., 2010; Ng et al., 2012; Whiffin et al., 2007). Additionally, the MICP process lacks real-time measurements and there is limited scope to control the performance of the microbes and their influence in changing the mechanical properties of the ground.

The process of bio-mediated soil cementation through MICP is in a certain way *responsive* to the conditions of the environment – e.g. crystal precipitation will only occur if a certain pH level is reached or if the amount of reagents exceeds a specific concentration. Another example of *responsive systems* using living organisms is the potential of bacteria cells to

seal cracks in concrete by responding to changes in the environment. This research demonstrates that bacteria spores introduced into the matrix of concrete materials can react to concrete cracking by germinating the spores into living cells and precipitating sealing materials – such as carbonates – that close partially or fully the cracks generated (Jonkers et al., 2010). In addition, another process in which a *responsive living system* is employed as an economical and sustainable solution is the process of soil bioremediation. This technique uses living bacteria cells to *detect* pollutants in the geoenvironment – such as heavy metals – and degrade them through processes of oxidation-reduction (Li et al., 2013; Megharaj et al., 2011; Tabak et al., 2005). To some extent, all these processes respond naturally to stimulus from the environment, however, having a tight control over the response and outcomes of these bio-mediated processes is often very complicated.

A new field of research is therefore arising which goes beyond the use of bio-mediated naturally-occurring processes and aims to *engineer* biological systems to detect stimulus that they would not instinctively detect or to behave in ways that they would not naturally do. Thus, by engineering these biological systems to react to specific instructions from their environment, a greater control and, therefore, a better optimised response over their behaviour can be achieved. For instance, the process of bio-cementation is not responsive to external inputs such as physical forces, it only occurs in areas where the bacterial solution and the reagents have been injected. However, if the behaviour of bacteria cells could be engineered to detect pressure changes from their environment and respond by synthesizing bio-cements, a responsive bio-cementation system could be developed.

In connection to this, it is known that some types of bacteria (e.g. barophilic) can only live under high-pressure conditions, meaning that some of their genes are capable of sensing the level of stress in their environment (Kato and Barlet, 1997). Therefore, by using the pressure-sensing capability of some genes, a bio-cementation system – based on genetically-modified bacteria cells – that responds to pressure changes in the environment could potentially be developed.

A system of this kind would go beyond the use of the natural behaviour of microorganisms to change the properties of the ground, and it would establish the fundaments of a new generation of *engineered responsive systems* that would couple the capability of living

bacteria to synthesize bio-cements with the ability to respond to meaningful inputs from the environment.

Therefore, a frontier of microbially-mediated construction processes is the development of these so-called *engineered responsive living systems* which would perform in ways they would not naturally do (Dade-Robertson et al., 2018; Nguyen et al., 2018).

Synthetic Biology (SynBio) has the potential to promote the development of such engineered systems, by genetically altering (programming) microorganisms to respond intelligently to inputs from the environment (Dade-Robertson, 2015). This discipline is defined as *"the design and construction of novel artificial biological pathways, organisms and devices as well as the redesign of existing natural biological systems"* (Voigt, 2012). In other words, Synthetic Biology, which is based on Genetic Engineering, offers the ability to modify the DNA of microorganisms and engineer them in such a way that their properties and functions are controllable (Endy, 2005). A section describing the principles of SynBio and the mechanism to engineer biological systems can be found in section 2.5.1. Definition of Synthetic Biology and Design Principles.

SynBio systems are traditionally used for biomedical applications and industrial biochemical synthesis of materials (König et al., 2013; Voigt, 2012). However, such systems offer an enormous range of possibilities in many other fields. An example of this is *Thinking Soils* (Dade-Robertson et al., 2016)*,* a research project at Newcastle University which aims to develop an *engineered responsive living system* through SynBio approaches for its use in geotechnical applications. The work described in this thesis contributed to this project and the preceding pilot project *Computational Colloids*, described in the following section.

1.2.1. Introduction to the Computational Colloids and Thinking Soils project

Thinking Soils (EP/R003629/1), and the preceding pilot project *Computational Colloids* (EP/N005791/1), are EPSRC (Engineering and Physical Sciences Research Council) funded projects which involve the collaboration between researchers from Newcastle University and Northumbria University. Both projects propose a system of *responsive bio-cementing*

in which engineered bacteria cells living within the soil matrix detect pressure changes in their environment upon loading and respond by synthesizing crystals that bind the soil particles together and increase the strength of the ground only where it is needed.

As described above, the proposed system goes beyond the use of biological systems to mediate natural processes. Instead, *Thinking Soils* is trying to develop an intelligent system, based on programmable bacteria cells, able to synthesize materials in response to physical changes in their environment. Developing such a system would not only have practical implications for geotechnical engineers by creating a responsive bio-mediated ground improvement method which would strengthen the soil itself when loaded, but also it would lead to the development of the first generation of a responsive and self-assembling bio-based material system. For a more comprehensive description of the *Thinking Soils* project, see 2.5.3. Computational Colloids and Thinking Soils Projects.

The Thinking Soils project is still in its early stages and the main priority is to find *gene promoters* sensitive to pressure changes of the same magnitude of those found in loaded soils. The next steps will involve the assembling and development of an engineered pressure-sensitive urease-producing strain of bacteria using SynBio methods and the *validation of the proof of concept.*

The validation of the proof of concept involves an *assessment of the feasibility* of this responsive self-assembling system for real-world applications. This process is part of a series of actions that assess the level of maturity of the proposed application. Thus, for an application to be proven successful for its use in an operational environment (i.e. real world), its development process must go through nine levels of technological maturity or *Technology Readiness Levels (TRL)* (Mankins, 1995). This procedure was originally conceived in the early 70s by NASA, who formally adopted the current nine level scale in 1990, and has since then gained acceptance worldwide both in industry and applied research (see Figure 1-1 for a brief description of each of the TRL).
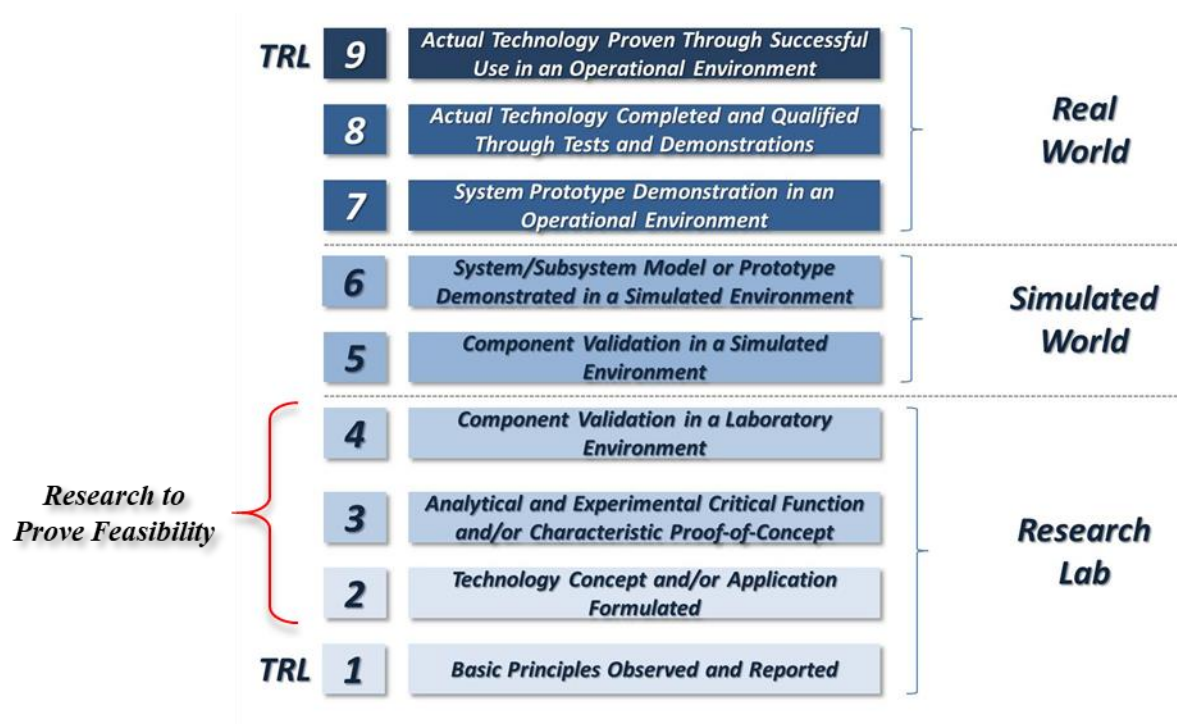
Figure 1-1. Technology Readiness Levels

(extracted from https://alopexoninnovation.com/2013/09/10/innovation-diffusion-from-university-rd/)

TRL 3 and TRL 4 include the validation of the proof of concept in a *research laboratory* environment and an assessment of the technical feasibility for *real world* applications, **which are the actions that this research project aims to resolve.**

In order to achieve the above-mentioned proof of concept validation, a scenario is proposed where the engineered bacteria cells are inoculated into a small volume of material, and a differential pressure is generated through the application of an external force onto the surface, to model the effect of a shallow foundation. Thus, as the force is applied, the engineered microbes will detect these pressure changes and will respond by producing more urease which will lead to increased calcium carbonate precipitation (through the process of MICP), leading to a differential soil bio-cementation. That way, the level of stress will dictate the amount of crystals precipitated (for more details on how stresses distribute through the soil underneath a foundation, see section 5.3.4. Mechanical behaviour).

In our case, an ideal scenario would involve laboratory trials in which the engineered bacteria are tested in a prototype soil-based demonstrator to evaluate their responsive behaviour to stress changes in a realistic environment and assess the feasibility as a responsive ground improvement method. However, the implementation of SynBio systems into a dynamic, complex and difficult to control environment such as soil presents several challenges, including risk of cross-contamination, poor control over the physical and chemical conditions and poor monitoring of the bacterial growth rates and cell distribution. Engineered biological systems are very complex and sensitive to their environment so, in early development processes such as a proof-of-concept physical demonstrator, a high degree of control over the testing conditions is required (Rodriguez-Corral et al., 2018).

1.3. Research rationale

One possible way of developing engineered biological systems is to use *agarose gels* as a substitute for soils for the development of early stage physical and computational demonstrators. Agarose gels are routinely used in microbiology for culturing and monitoring bacterial growth. They allow easier monitoring of the performance of the microbes, greater control of the chemical composition of the environment, a controlled simulation over the mechanical properties and a minimised risk of contamination, compared to soils. Additionally, these type of gels have a porous structure comparable to cohesive or organic soils and have similar relevant mechanical properties to soils, as described in *Chapter 3. Agarose gel as a Soil Analogue*. The reasoning behind the selection of this particular type of hydrogel is also described in Chapter 3. Use of this type of gel enables cultivation of the engineered bacteria homogeneously within the matrix of the gel and control of the forces exerted onto the gel volume, so that the response of the bacteria-based responsive system can be evaluated. Furthermore, the implementation of agarose gels allows studying the behaviour of bacteria in a three-dimensional volume in a detailed and rather simple way (on the contrary, obtaining an accurate representation of the behaviour of bacteria in a soil environment is a challenging process). Additionally, it allows equivalents to be drawn to the expected behaviour of the system in a soil-based

environment. Therefore, the implementation of agarose gels as a soil analogue for bacteria testing presents many advantages and will promote the development of engineered living systems for the geoenvironment.

This thesis presents the design of gel-based physical and computational models that can be used to study the behaviour and performance of *engineered bacteria cells*. In particular, the implementation of such model will help in the early development of a pressure-responsive bacteria-based system, as well as assist in the validation of the proof of concept and assess the feasibility of the system as a bio-mediated responsive ground improvement method for real-world applications. This gel-based model bridges the gap between nano-scale biological laboratory experiments and the macro-scale context in which the engineered organisms may be deployed.

Furthermore, the successful implementation of such gel-based model would establish the first steps towards the development of a new type of biotechnology that uses SynBio approaches to deal with geo-environmental problems.

1.4. Aim and objectives

The ultimate aim of this research is to develop physical and computational hydrogel-based models, in which genetically modified bacteria can be tested under specific conditions and the outcomes of the associated bio-mediated processes can be assessed. In order to achieve this aim, the following objectives will be considered:

1) To review the established understanding of ground improvement involving microorganisms and the associated bio-mediated processes as well as review the current literature on SynBio approaches and the possibilities to engineer bacteria in order to deal with geo-environmental problems.

2) To characterise the mechanical properties of agarose gels at a macro-scale relevant to geotechnical engineering.

3) To establish an experimental procedure for mixing bacteria cells uniformly with agarose gels and visualise their growth and activity in a volume of hydrogel.

4) To analyse the effect of agarose concentration on the microstructure of the gel and the interaction with bacteria cells

5) To develop a methodology to analyse cell distribution and patterning in order to study the formation of bacterial communities as colloids within the matrix of the gel.

6) To determine the effects different environmental conditions such as pH or temperature have on the growth behaviour of bacterial colonies both at the micro and macro scale.

7) To design and build a computational model that integrates all the experimentally-obtained data as well as hypothetical data of a pressure-sensitive crystal-producing strain of bacteria in order to develop a full nano-micro-macro characterisation of the so-called *responsive ground improvement method*.

8) To provide model simulations that display the outcomes/behaviour of such a system and allow comparison with a prospective gel-based physical demonstrator.

Figure 1-2 illustrates the three main components of the gel-based prototype model alongside some parameters investigated in this thesis. The figure clearly shows how the data obtained experimentally feeds the computational model, which in turn supports the development of a physical demonstrator. Furthermore, all these actions are part of a strategy to validate the Thinking Soils proof of concept.
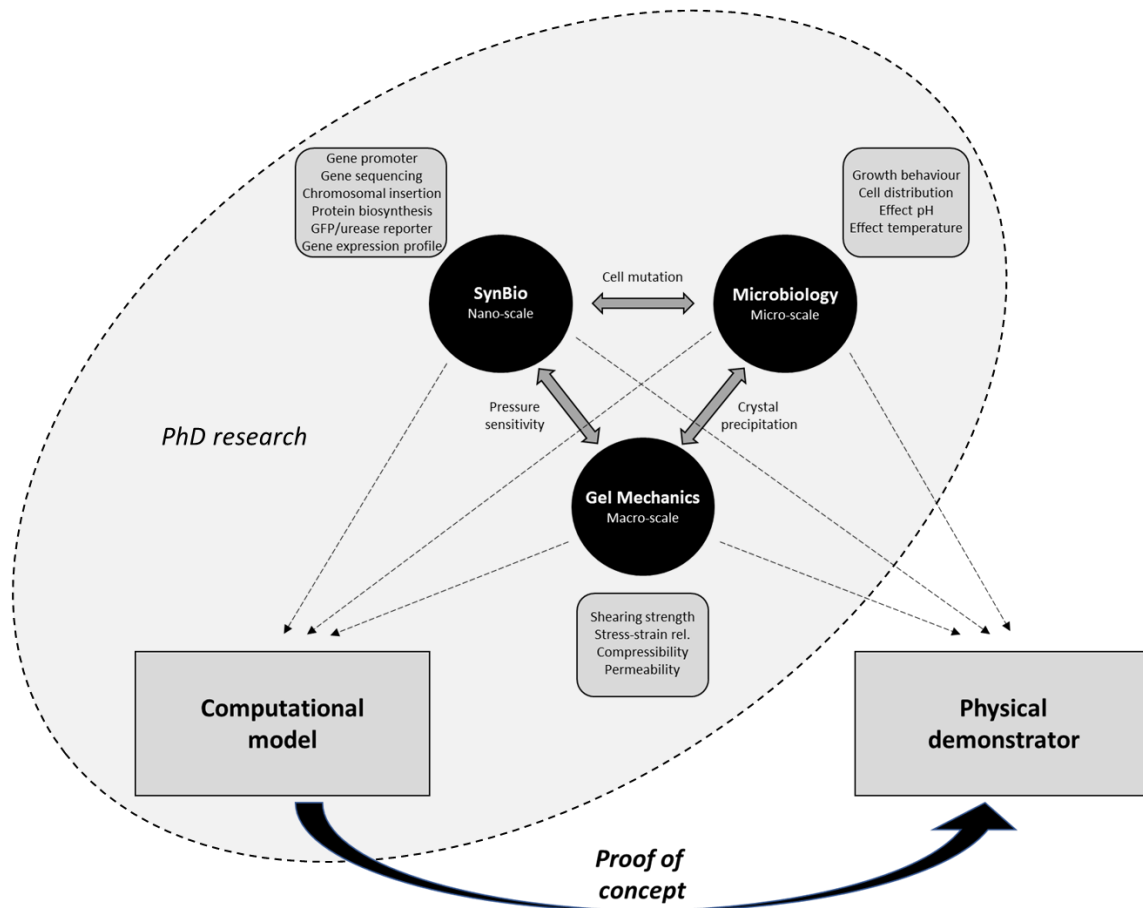
Figure 1-2. Thinking Soils proof of concept strategy

1.5. Thesis structure

Chapter 1 introduces this research as part of a bigger investigation related to the use of Synthetic Biology approaches to engineer microorganisms to detect inputs from their environment and respond in a useful (synthetic) way. The term *engineered responsive living systems* is introduced here alongside the relationship between this research and the EPSRC-funded *Thinking Soils* project.

Chapter 2 constitutes a comprehensive literature review on the use of microbial-mediated processes to deal with geoenvironmental problems, with an emphasis on the process of *bio-cementation through urea hydrolysis.* This chapter also presents a section describing the properties and parts of bacteria cells and their interaction with the geoenvironment. Additionally, this chapter introduces the field of Synthetic Biology and

discusses the current advances on the development of responsive bacteria-based living systems. This chapter addresses *objective 1.*

Chapter 3 describes a program of geotechnical testing to determine the mechanical properties of low melting point (LM) agarose gels. The microstructure of the gels is also analysed in this chapter alongside the effect agarose concentration has on the porous matrix. In addition, this chapter describes the similarities between agarose gels and some types of soils and assesses their suitability as a soil analogue for the development of a bio-mediated responsive gel-based prototype system. This chapter addresses *objective 2* and part of *objective 4*.

The methods to prepare and monitor the growth and distribution of bacteria-seeded agarose gels are presented in **Chapter 4**. This chapter analyses the growth of bacterial communities within the matrix of agarose gels as well as the effect of a range of environmental conditions on the growth behaviour. Chapter 4 addresses *objectives 3,4,5 and 6.*

Finally, **Chapter 5** integrates the data obtained experimentally and presented in chapters 3 and 4, by developing a computational model that simulates the behaviour of a pressure-sensitive and crystal-producing gel-based prototype system. The chapter defines the basis of this *bio-mechanical* coupled system that combines the nano-scale behaviour of pressure-sensitive cells with the macro-scale behaviour of loaded gels. The chapter also describes, step by step, the development of the software and the features included in the model. Simulations of the model representing the behaviour of this pressure-responsive system under different growing conditions and loading scenarios are also included in this chapter. Additionally, the limitations of the model and suggestions for further improvement are presented at the end of the chapter. This chapter addresses *objectives 7 and 8.*

Chapter 6 draws together the main conclusions of the research, highlighting the integration of the experimental work into the computational model. This is followed by recommendations for future work as the next phase of the project, and suggestions for the development of the proof-of-concept physical demonstrator.

Chapter 2

Literature Review

2.1. Introduction

The previous chapter set out the aim and objectives of this research project and introduced several key topics that give context to the overall research/thesis. The purpose of this chapter is to explore further on these topics, by reviewing the current understanding of the processes and methods relevant to this research. The chapter is divided into four sections. Section 2.2 describes the microbial mediated processes that naturally occur in soils. The impact these processes have on the behaviour of the geoenvironment is also discussed, highlighting the process of biomineralization. This section also introduces a new practice of research in which soils are not considered biologically inert, and where microorganisms are defined as the *fourth parameter* of the soil's matter.

Section 2.3 reviews the classification of unicellular organisms, providing with a comprehensive description of bacteria and their properties. The bacterial growth behaviour is also described in this section along with the parameters that play a role in the growth behaviour of bacteria. Additionally, the interaction between bacteria and soils is also discussed in this section.

Section 2.4 aims to review the current understanding on soil improvement practices and critically discusses the necessity for alternative and more sustainable techniques. The potential of using microbial-mediated processes as a soil reinforcement solution is examined, with an emphasis on the process of *Microbially-Induced Calcite Precipitation (MICP)*, including the latest research trends on the topic.

The last section, section 2.5 introduces the field of Synthetic Biology and its role in the design of engineered living systems. The design principles are briefly described in this section alongside a review on the most promising engineered living systems for the geoenvironment.

Finally, this section provides an in-depth description of the techniques and methods used for the development of the pressure-sensitive bacteria strain, reviews the results obtained experimentally and discusses the latest advancements and direction of work.

2.2. Microorganisms as the fourth parameter in soils

Traditionally, the study of soil behaviour has been focused on mechanical principles, geological processes, mineralogy and the chemistry of colloids within their structure (Mitchell & Santamarina 2005). Likewise, geotechnical engineering has concentrated on the mechanical and physical properties of geomaterials (i.e. materials of geological origin), without taking into consideration the effect biological activities may cause on them. For instance, Terzaghian soil mechanics ignores the influence of microbial activities on the matrix of geomaterials and the alteration they produce on the overall engineering behaviour.

In addition, according to conventional geotechnical engineering, geomaterials are considered to be biologically inert and the effect of microorganisms and plants on soil behaviour has been neglected (Shashank et al., 2016a).

However, it is known that microorganisms have lived in the geoenvironment for more than 3 billion years (Kennedy 1999) and have been 'active geotechnical engineers' for much longer than humans (Kohnhauser, 2007). Microorganisms are present in soils at notably high concentrations and great part of these microorganisms are bacteria and archaea (DeJong et al. 2013). According to some authors (Mitchell & Santamarina 2005; Fragaszy et al. 2011; Christensen et al. 1999; Sharma et al. 2014) more than 10^{12} bacteria cells are expected to be found in a kilogram of soil near the surface. Bacteria are also found at depths relevant to geotechnical engineering - i.e. 2 to 30m - although the population decreases to about 10^{11} to 10^{6} cells per kilogram of soil as the depth increases (Whitman et al., 1998).

It has been shown by many researchers that microorganisms play a crucial role in the formation of fine-grained soils and may modify the properties of coarse-grained soils, such as stiffness or permeability (Burbank et al., 2011; DeJong et al., 2010; Fukue et al., 2011; Whiffin et al., 2007), as well as stimulate some geochemical reactions which, in turn, accelerate the

weathering of rocks (Barkay and Schaefer, 2001; Gadd, 2010; Stocks-Fischer et al., 1999; Wierzchos and Ascaso, 1998).

Some bio-mediated processes such as bio-weathering and bio-mineralization also alter the initial composition of the soil matrix, consequently changing the mechanism of interaction between phases. These alterations further lead to changes in the pore structure, such as pore dimensions or porosity, which are critical parameters for the identification of the hydrological properties of the soil (Shashank et al., 2016a).

Furthermore, it is known that microorganisms secrete enzymes near nucleation sites (Wilson and Jones, 1993), consequently producing different fluids such as Extracellular Polymeric Substances(EPS), a principal component of biofilms (Decho, 2010; Edwards et al., 2005; Hazen et al., 2008) and altering the composition of the pore fluid. Thus, this phenomenon contradicts the traditional assumption of one single pore fluid within the pore space (Sharma et al. 2014).

Additionally, the presence of microorganisms within the saturated soil matrix leads to several processes of cellular metabolism (i.e. the chemical reactions occurring in living organisms in order to maintain life) which, in turn, contributes to the generation of gases (Dettling et al., 2007; Rebata-landa and Santamarina, 2012; Unger et al., 2009) and can result in an unsaturated soil.

Therefore, even though traditional soil mechanics ignores the influence of microorganisms on the mineralogical alteration of soil's matter, the impact of microbial activity on the mechanical behaviour of geomaterials is clearly demonstrated.

Due to this permanent biological presence in soils, there has been a lot of research in the last few decades in understanding the relationship between microorganisms and soils and their involvement in promoting most geochemical reactions (Mitchell & Santamarina 2005). From this a new geotechnical perspective has arisen in which soils are not treated as an inert construction material but a living ecosystem (DeJong et al. 2013).

Classical soil mechanics clearly defines three phases of matter – soil solids, water and air – and the interaction between them is well understood. However, if microorganisms are demonstrated to change soil behaviour and alter the interaction between the three phases of matter, traditional theory requires the introduction of *microbial organisms* as the fourth

parameter of matter (Sharma et al. 2014). Hence, some authors are beginning to consider living organisms as the *fourth parameter* of soil matter, in addition to the conventional three phase system (soil solids, water and air) (Shashank et al., 2016b).

2.2.1. Natural microbial mediated processes in soils and impact on the geoenvironment

This section explores the several processes caused by the effect of biological activities in soils and how they impact on the geoenvironment, from a geotechnical engineering point of view. Mitchell (1975) observed that the macro-scale behaviour in the geoenvironment strongly depends on the chemical reactions occurring at the micro-scale structure of soils. It is therefore essential to analyse all the processes happening at the micro-scale in order to understand the macro-scale changes taking place in soils and to be capable of *controlling* and *monitoring* them.

However, before further detailing the processes regulated by microorganisms and how they influence the behaviour of soils, it is important to understand that biological activity by itself does not affect directly the properties of the geomaterials. Instead, this change in the soil properties is governed by the geochemical reactions occurring at the micro-scale level and stimulated by the presence of microorganisms (Dejong et al. 2010; DeJong et al. 2013). Furthermore, it is known that geochemical processes also occur without the presence of microorganisms – but at a smaller rate. Hence, the role of microbes is to create particular conditions around cell populations in order to trigger the geochemical reactions. That way, microorganisms act as *biocatalyst* and can control where, when and the rate at which the geochemical process will occur (DeJong et al. 2013).

The main microbial mediated processes that have been identified in soils are listed as follows, alongside a list of references which describe their nature and how they impact the environment. However, only biomineralization is strictly relevant to this project/study and it is the only biogeochemical process that is further reviewed.

1) Oxidation/reduction of chemical compounds *(Chapelle, 2001; Dupraz et al., 2009; Ehrlich, 1998; Madigan et al., 2000; James K. Mitchell and Santamarina, 2005b; Nordstrom and Alpers, 1999)*

2) Dissolution/degradation of minerals *(Burns, 1982; Ehrlich, 1998; Mapelli et al., 2012; Rogers and Bennett, 2004; Xiao et al., 2012)*

3) EPS and biofilm formation *(Bhaskar and Bhosle, 2005; Flemming et al., 2000; Lear and Lewis, 2012; Staudt et al., 2004; Sutherland, 2001)*

4) Biomineralization

Biomineralization is a common phenomenon occurring in the geoenvironment which refers to the precipitation of minerals due to its chemical alteration caused by biological activity (Stocks-Fischer et al., 1999). According to Sarikaya (1999), biomineralization can lead to the formation of more than 60 different mineral species. A review of the different biomineralization processes and engineering applications is presented in (Phillips et al., 2013). As reported by several authors (Dupraz et al., 2009; Frankel and Bazylinski, 2003), there are three different mechanisms for the formation of such minerals:

- *Biologically induced mineralization,* a process whereby the microorganisms secrete metabolites (i.e. intermediate products of metabolic reactions) in the geoenvironment which consequently react with the present ions or organic compounds, and due to supersaturated conditions (i.e. concentration increment beyond the saturation point of a solution), mineral precipitation occurs (Stocks-Fischer et al., 1999). The formation of minerals through this mechanism does not involve any control from the microorganisms on the mineral morphology, structure or crystallinity (Gadd, 2010; Hamilton, 2003).

- *Biologically controlled mineralization,* in which the nucleation, location and growth of the precipitated mineral together with the structure and morphology are controlled by the microorganisms (Benzerara et al., 2011; Gadd, 2010; Phillips et al., 2013).

- *Biological influenced mineralization,* where the mineral is precipitated due to the effect of external geoenvironmental factors on microbial metabolites, independently of microbial activity. In this case, the structure, morphology and composition of the precipitated mineral is influenced by a *'passive formation of minerals by the organic matrix'* (Dupraz et al., 2009). This process is mainly caused by the presence of EPS substances and biofilms (Phillips et al., 2013).

Additionally, as reported by Dhami et al. (2013), the minerals precipitated by biomineralization can be either extracellular inorganic crystals (e.g. carbonate precipitation) or intracellular inorganic crystals (e.g. sulphates or phosphates).

Of special interest to this project is the process of *microbiological precipitation of CaCO₃*, which is thoroughly analysed in Stocks-Fischer et al., (1999).

In relation to the impact of biomineralization in the geoenvironment, it has been reported by some authors (e.g. Dejong et al. 2010) that the precipitation of minerals in the soil matrix due to the effect of microorganisms does affect the properties of the geomaterials such as permeability, compressibility or strength, amongst other factors. In particular, some bacteria species (e.g. *Bacillus* type) are known to crystallise calcium carbonates in calcium rich environments. This biomineralization process called *Microbially-Induced Calcite Precipitation* is of great interest for this study and it is therefore reviewed further in section 2.4.4. Biocementation through Microbially-Induced Calcite Precipitation (MICP), where its impact on the soil mechanical properties, the chemical reactions involved in the process and the potential applications of the process as a soil improvement technique are thoroughly analysed.

2.3. Bacteria and their properties

This section reviews the classification of unicellular microorganisms, with an emphasis on bacteria and their properties. The interaction between microorganisms and soils is also discussed as well as the bacterial growth behaviour and the different parameters that play a role in the growth rate of bacteria.

2.3.1. General classification microorganisms

Living organisms can be divided into two main categories – *prokaryotes* and *eukaryotes* – and although the former are only single-celled organisms and the latter can be either single or multi-celled organisms, the main difference lies in their structure. Figure 2-1, extracted from Mitchell and Santamarina (2005), presents an overview on the different types and properties of living organisms. Prokaryotes – which include bacteria and archaea – have a simple cell structure, without a nucleus within their cell wall. Eukaryotes – which include algae, fungi and protozoa – possess a nucleus within the cell structure. Moreover, while the genetic information in prokaryotic cells is not membrane-bound, the DNA of eukaryotic cells is contained within the nuclei (Prescott et al. 2002; Madigan et al. 2000).

Additionally, according to Madigan et al. (2000), some microorganisms (including bacteria) can live in harsh conditions such as extreme pH concentrations (ranging from 2 to 10) and

salinities greater than seawater. Also, according to Doran et al. (2003), bacteria can resist pressures of hundreds of atmospheres and extreme temperatures, both below freezing and above boiling. Therefore, due to this ability to withstand extreme conditions, some microorganisms such as bacteria can be expected to be omnipresent.

2.3.2. Bacteria cell structure

Bacteria are a type of prokaryotic microorganism which are present in almost every habitat on Earth, due to their ability to live in very harsh environments (Chapelle, 2001; Ehrlich, 1996; Madigan et al., 2000). Their entire organism consists of a single cell, without the nuclear membrane typical of an eukaryotic organism, in which the bacterial *chromosomal DNA* floats freely forming loops, which in turn generate a twisted thread mass called the nucleoid (Figure 2-2). The DNA is a single molecule which is found inside the cytoplasm (i.e. all the material within the cell). Additionally, bacterial cells contain a type of spherical units in which the proteins are assembled from individual amino acids. Furthermore, bacterial DNA can also be found in small pieces called plasmids, separated from the nucleoid, which can easily be transmitted from one cell to another. This ability to exchange genes makes bacteria a very adaptable microorganism and the favourite of genetic engineers, due to their ability to adopt new genes easily (Kohnhauser, 2007).
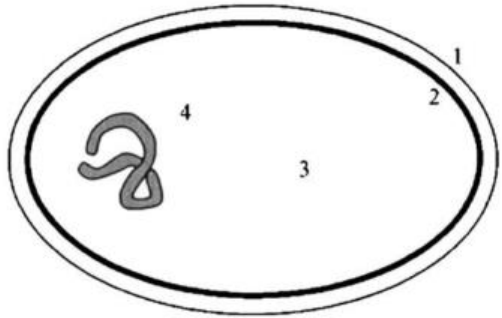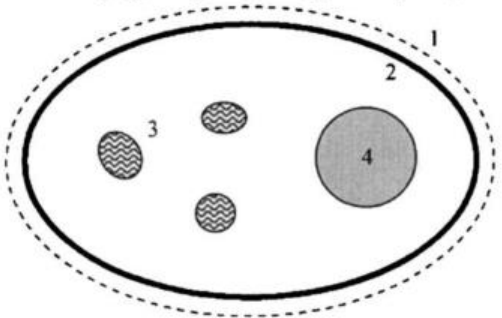
Bacteria	Archea	Eukarya
• Peptidoglycan in the cell wall is unique to bacteria (attacked by some antibiotics) • Some bacteria can survive harsh conditions by forming spores.	• Most cell walls contain significant amount of protein. • They are primarily present in anaerobic subsurface environments and around organic compounds.	• This domain includes: algae (photosynthetic eukarya - produce most of the oxygen in the world), fungi (gather energy by decomposing sources of organic carbon - includes tube-like filaments call mold), and protozoa (complex single cell decomposers).

Common Characteristics	Eukarya (continued)
• Bacteria and archea have different chemical composition but similar cellular structure: a strong cell wall in most cases (1), membrane (2), cytoplasm (3), folded chromosome (4). They have no membrane-enclosed nucleus. • The semi-permeable cell membrane controls the transport of chemicals and electrical charges in-and-out of the cell. In addition, the cell membrane conducts many functions including energy generation. • They are spherical, rod and curved shaped, and typically 0.5-to-3 µm long. Size reflects optimal conditions between volume-related internal functions and surface-related transport of input and waste. • There are cells that can live under extreme pH, temperature, and salt concentration. Therefore, they are present in most subsurface environments. • They reproduce by fission into two (reproduction time: from minutes to few days). Flagela may protrude from the surface to propel the cell, and pili to attach the cell to surfaces.	• They may not have a cell wall (1). Many cell functions are not implemented by the membrane (2), but by specialized membrane-enclosed organelles (3). They always have a membrane-enclosed nucleus (4). • Diatoms are eukarya with cell walls. Foraminiferan have internal shells. • Compartmentalization allows eukarya to be larger (diameter 2-100 µm) than bacteria and archea • Most eukarya are aquatic. The population size is expected to be small in pristine aquifer sediments, but it increases in sediments contaminated with organic compounds. • Most eukarya require oxygen. Therefore, they are less common microorganisms in the subsurface.. • There are multiple forms of reproduction and motion in the eukarya domain (e.g., flagela, cilia, pseudopods).

Figure 2-1. Properties unicellular microorganisms (after Mitchell and Santamarina, 2005)

The cytoplasm is comprised of a layered structure called the *cell envelope*, which serves to protect bacteria from hostilities in the environment. This cell envelope is composed of an inner cell membrane and an outer cell wall and can be divided into two categories: a *gram-positive* type and a *gram-negative* type (see following section for definition), which at the same time is used to classify bacteria (Goering et al., 2013; Kleanthous and Armitage, 2015) Additionally, according to Saunders (2013), the surfaces of a bacterial cell are often covered by *pilus*, which help the cell to attach to host surfaces, and some types of bacteria also present a *flagellum*, which facilitates mobility.
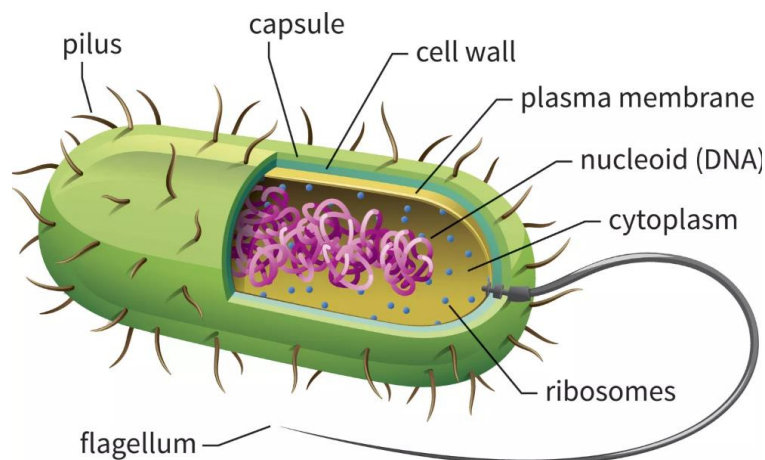
Figure 2-2. Different parts of a bacteria cell

(extracted from https://www.thoughtco.com/prokaryotes-meaning-373369)

In relation to their morphology, bacteria can have a number of different shapes, including spheres, rods or spirals.

2.3.3. Bacterial classification

Bacteria can be classified according to different classification systems, which include *Gram stain*, *Cell morphology* or *Growth requirements*, amongst others. The former was invented by H.C. Gram in 1884 (Gram, 1884) and it still remains as a very useful and quick technique to identify and classify bacteria. The method consists of dyeing bacteria cells using crystal violet (e.g. iodine). Gram-positive bacteria retain the purple colour when stained with iodine,

destained with alcohol and counter-stained again with safranin. Gram-negative bacteria lose their initial purple colour when the alcohol is added and stains pink as the counter-stain is used. This difference in staining behaviour is associated with the peptidoglycan layer present in the cell wall, which is much thinner in Gram-negative types and it dissolves after alcohol is added.

Another important classification system is to group bacteria according to their oxygen needs for growth (Slonczewski and Foster, 2013). For instance, strictly anaerobic bacteria only grow in environments where there is limited or no oxygen. On the contrary, aerobes only grow if significant amounts of oxygen are present in the environment. Additionally, facultatively anaerobic bacteria can grow under both oxygen-rich or oxygen-limited conditions, which makes them the most versatile type. Figure 2-3 represents the above-mentioned classification systems and provides examples of bacteria species for each category.
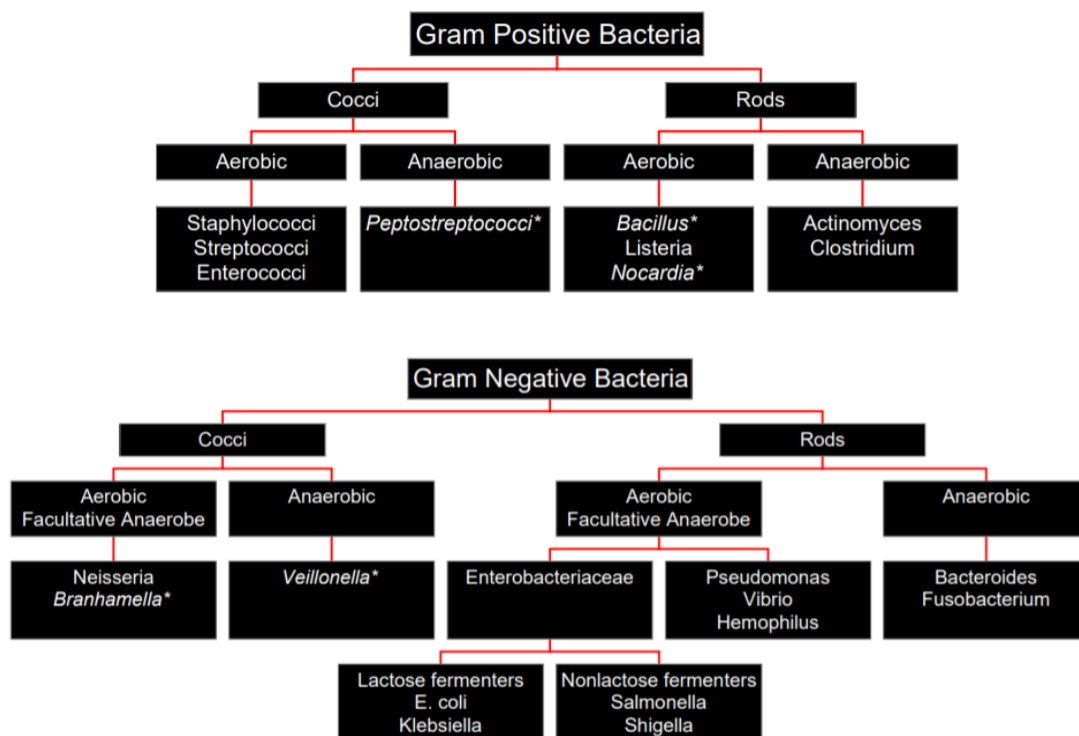
Figure 2-3. Bacterial classification system

(extracted from http://www.columbia.edu/itc/hs/medical/pathophys/id/2009/introNotes.pdf)

Additionally, bacteria can also be classified according to the environmental parameters that control their growth, such as temperature or pH (see section 2.3.5. Factors affecting bacteria growth for more details).

2.3.4. Bacterial growth

Bacterial growth refers to an increase in the number of cells and it occurs by a process called *binary fission*.

A bacteria cell, typically known as the *parent*, replicates the DNA within the cytoplasm and grows in size until the point where the cell splits into two genetically identical new cells, called *daughter cells*. Binary fission is a rather simple process and the rate at which it occurs is mainly dictated by the conditions of the environment. In rod-shaped cells – such as *Bacillus subtilis* or *Escherichia coli* – the division point usually lies at the midpoint of the rod, and it occurs perpendicular to the long axis of the cell (Harry et al., 2006). The cell division process by binary fission is illustrated in Figure 2-4.
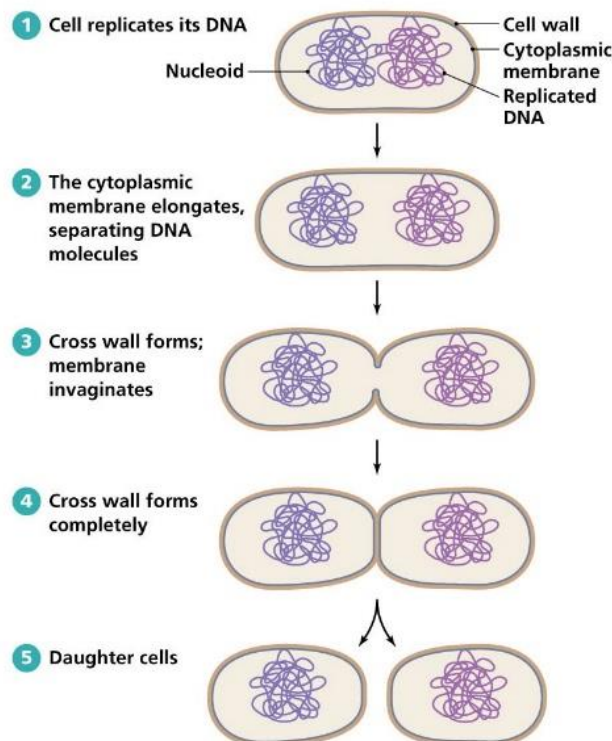
Figure 2-4. Representation of binary fission in bacteria

(extracted from http://biology-pictures.blogspot.com/2011/11/binary-fission-in-bacteria.html)

In a laboratory environment, bacteria are grown under high levels of nutrients in order to produce large amounts of cells in a cheap and relatively quickly manner. However, in a soil environment, the amount of nutrients is limited and bacteria do not reproduce indefinitely. Additionally, the physicochemical conditions in soils are often not ideal for optimum growth and the growth rates are considerably lower than the maximum experimental rates obtained in a laboratory environment (Konhauser, 2007).

All bacteria undergo the same growth cycle when entering a new environment. This cycle is composed of four phases, which can be distinguished in Figure 2-5, and it is commonly known as a *growth curve* or *growth profile*.
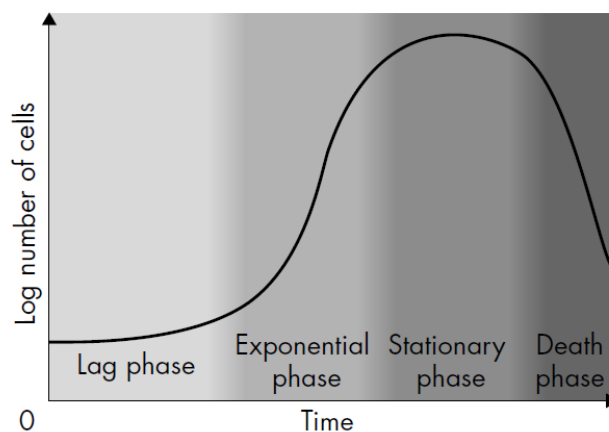
Figure 2-5. Typical growth curve of a bacterial culture. Time (0) represents inoculation (after (Konhauser, 2007))

The first phase is known as *lag phase* and it refers to the period of time when the cells are still adapting to the new surroundings and grow at a very low rate. Once the cells are acclimatized, a second phase called the *exponential* or *log phase* begins, in which cells reproduce very rapidly. As an example, *E. coli* cells tend to divide every 20-30 minutes under standard laboratory conditions (i.e. a liquid batch containing highly-rich nutrients) during the exponential phase. During this phase nutrients are metabolised very efficiently until the point where the cells begin to run out of required nutrients and the growth rate slows down. Additionally, towards the end of the exponential phase, the amount of waste accumulates and the new composition of the environment reaches toxic levels, impacting negatively the

microbial cells and limiting their growth. Is it at this point when the *stationary* phase begins. During this phase, some cells continue dividing and others begin to die, and it is considered that the cell population remains constant. This phase often last much longer than the other preceding phases together. The stationary phase is finally followed by the *death* phase, where the amount of cells dying exceeds the amount of new formed cells and the population begins to decrease in number (Konhauser, 2007; Slonczewski and Foster, 2013; Zwietering et al., 1990).

2.3.5. Factors affecting bacteria growth in soils

Microorganisms are found everywhere in soils, independently of the physical and chemical conditions of the system (DeJong et al. 2013). However, the microbial activity and the growth rate are dependent on two '*limiting parameters*': the availability of space for their growth or *geometric compatibility,* and the environmental conditions (DeJong et al., 2010; Shashank et al., 2016a). The former refers to the space that microorganisms need for their motility and reproduction, and is mainly restricted by the soil pore size. According to Mitchell and Santamarina (2005), "*the maximum bacteria count in soil pore fluid can be estimated as the ratio between the pore fluid volume and the volume of a bacterium".* Therefore, the *geometric compatibility* limits the maximum amount of cells that can be found within the pore space as well as restricting their motility. Figure 2-6 compares the size of microorganisms and soil particles (reproduced from Mitchell and Santamarina (2005)) and shows that bacteria are not likely to move through pore throats smaller than 0.4 μm.
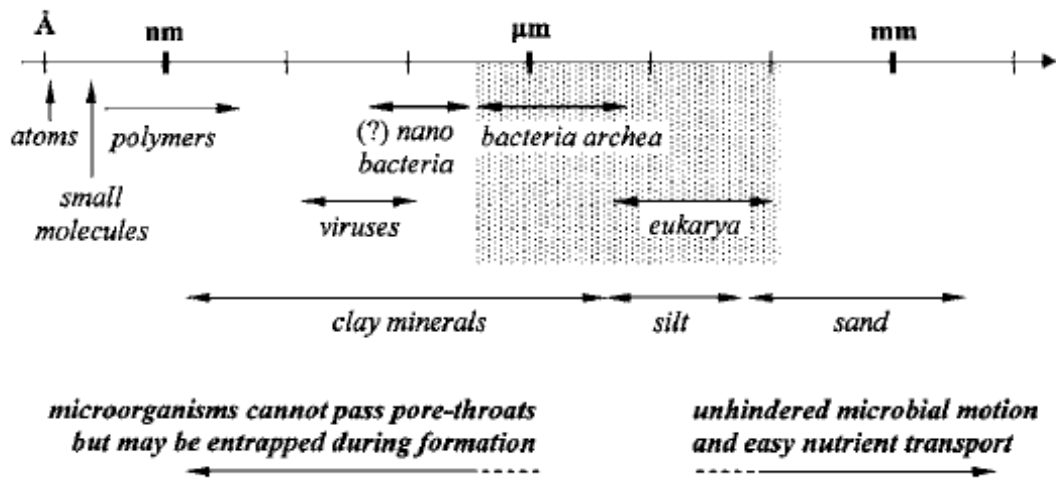
Figure 2-6. Comparative size of microorganisms and soil particles

(after Mitchell and Santamarina, 2005)

Although geometric compatibility is the most restrictive parameter, the environmental conditions also affect the survival and reproduction rate of microorganisms (Ehrlich, 1998). Each particular species is subject to different environmental conditions that affect their microbial activity and growth rate. These environmental conditions can be divided into three '*restrictive factors*': nutrient availability, water availability and other environmental factors (Mitchell & Santamarina 2005).

- **Nutrient availability.** Nutrients are essential for the growth and survival of microorganisms as they are used as both cellular material and as energy source (Shashank et al., 2016a). Additionally, according to Mitchell & Santamarina (2005), bacterial reproduction in many soil systems might be hindered due to the absence of organic constituents.

- **Water availability.** Water is fundamental for microorganisms since it constitutes a great part of their cellular material. It also plays an important role by stimulating nutrient transport, triggering many chemical reactions and controlling the pH of the system amongst many other functions (Hattori, 1973). It is therefore evident that systems with poor water availability will hinder microbial activity and reproduction. Nonetheless, when the system is close to a saturated state, the availability of oxygen is then limited due to the low diffusion rate of oxygen through water - leading to anaerobic conditions (Mitchell &

Santamarina 2005). According to Horn & Meike (1995) the optimum condition for aerobic microbial activity occurs when the degree of saturation in the soil is about 60% to 80%.

- **Other environmental factors.** The main factors affecting microbial activity and growth in soils are the following (Ehrlich, 1998; Paul and Clark, 1996; Slonczewski and Foster, 2013):

  - Temperature

  Microbial cells cannot control their own temperature and therefore changes in temperature affect every aspect of their physiology and consequently affect the rate at which they divide and grow. Each species has an optimum growth temperature as well as *limits of growth,* which are defined by the range of temperatures at which the cells grow. Microorganisms can be classified according to their limits of growth into: *psychrophiles*, *mesophiles*, *thermophiles* and *hyperthermophiles.* Figure 2-7 shows the relationship between growth rate and temperature for the different groups of microorganisms.
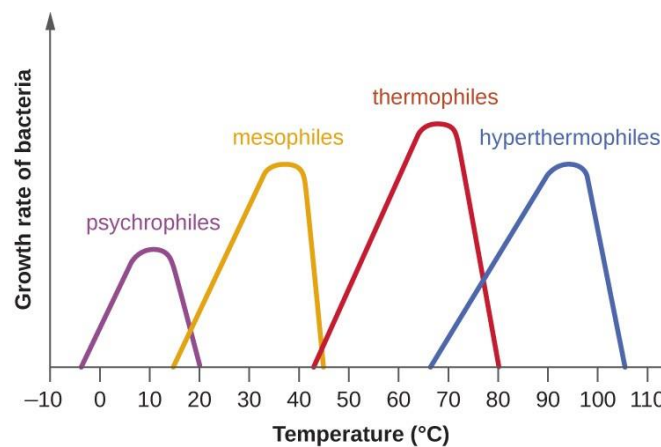
Figure 2-7. Optimum growth temperatures for different bacterial groups

(after Slonczewski and Foster (2013))

  - pH

  Similarly to temperature, each species of microorganisms has a range of pH (i.e. concentration of hydroxide ions) at which growth occurs. The hydrogen ion concentration has an effect on cell molecular structures and therefore an impact on

the growth rate. Bacteria can be classified according to their optimum growth pH into *acidophile*, *neutrophile* and *alkaliphile* (Figure 2-8).

However, while bacterial cells cannot regulate their internal temperature and it normally equals the external one, microbial cells have developed a mechanisms called *homeostasis* which maintains their internal pH within the 5-8 range in order to prevent destruction of its cytoplasmic macromolecules, independently of the pH of the environment.
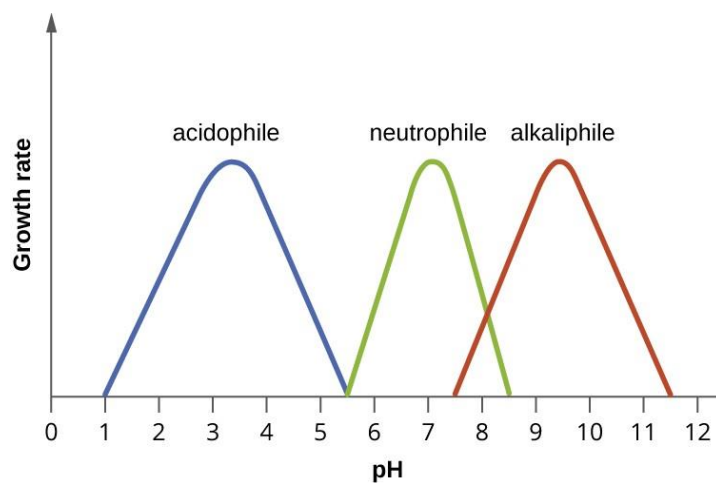
Figure 2-8. Optimum growth pH for different bacterial groups

(after Slonczewski and Foster (2013))

- *Oxygen*

As described in section 2.3.3. Bacterial classification*,* bacteria can be classified according to their oxygen needs for efficient growth into be strictly aerobic, strictly anaerobic or facultative aerobic. For instance, *E. coli* is a facultative aerobic microorganism since it can metabolise energy both aerobically and anaerobically. On the contrary, *B. subtilis* only grows under the presence of oxygen, being considered traditionally a strict aerobe. However, some evidence exists that *B. subtilis* can also grow under specific anaerobic conditions, making it a facultative anaerobe (Nakano and Zuber, 1998).

Additionally, other parameters such as osmotic pressure, redox potential, presence of growth inhibitors, soil suction or cation exchange capacity are also expected to influence microbial

activity in soils, but at a lesser extent (Ehrlich, 1998; Jiang et al., 2006; Paul and Clark, 1996; S et al., 2014).

2.4. Bacteria and ground improvement

This section outlines the importance of soil improvement to civil engineering practices, provides a classification of the most traditional ground improvement methods, discusses the necessity for alternative soil improvement techniques and reviews the potential of microbial mediated processes for soil reinforcement, highlighting one of the most promising processes: *bio-cementation through Microbially-Induced Calcite Precipitation.*

2.4.1. Ground improvement – a worldwide necessity

The current rapid growth of population and the consequent urbanisation and growth of cities requires the development of new infrastructure. However, this demand for infrastructure can sometimes be restricted by the existence of inadequate soil conditions (Shahin, 2016). In the past, engineers used to avoid construction on problematic soils, but today treatments are required to improve the quality of these unstable soils due to the limitation of land (Kumar et al., 2015). These problematic soils – being the majority collapsible and soft soils – raise some concerns for geotechnical engineers due to low bearing capacity and high compressibility (Shahin, 2016).

In order to allow the development of infrastructure in poor soil conditions, it is therefore necessary to employ techniques that improve the quality of the ground (Moseley and Kirsch, 2004).The purpose of soil improvement techniques is to transform a problematic and unstable soil into a good-quality, workable and reliable soil – i.e. soil with adequate strength, good settlement resistance, proper permeability and high durability (resistant to deterioration) (Purushothama, 2005). DeJong et al. (2010) reported that more than 40,000 soil improvement projects are executed worldwide annually.

2.4.2. Traditional methods of ground improvement

Soil improvement methods have been used extensively since ancient times – as an example, the soil underneath the Great Wall of China was reinforced using branches of trees acting as

tensile elements (Kumar et al., 2015). However, the concept of modern soil reinforcement was developed by Henry Vidal, a French engineer, in 1966, after patenting a soil reinforcement method called *'Reinforced earth'* (Vidal, 1969). Since then, ground improvement techniques have been employed widely in civil engineering applications (Kumar et al., 2015).

Many different techniques and processes have been developed throughout the years, from the inclusion of metal strips into the soil (Vidal, 1969) to the development of grouting techniques to inject additives into the ground in order to improve its properties. A universal classification of ground improvement methods has, however, not been established and the processes can be classified according to different parameters, i.e. physical, hydraulic, mechanical or chemical methods; grouting techniques or soil mixing; reinforcement, improvement or treatment techniques; ground improvement in cohesive soils v non-cohesive soils, ground improvement with or without admixtures, etc. One such classification of ground improvement methods is show in Figure 2-9, with examples for each category.
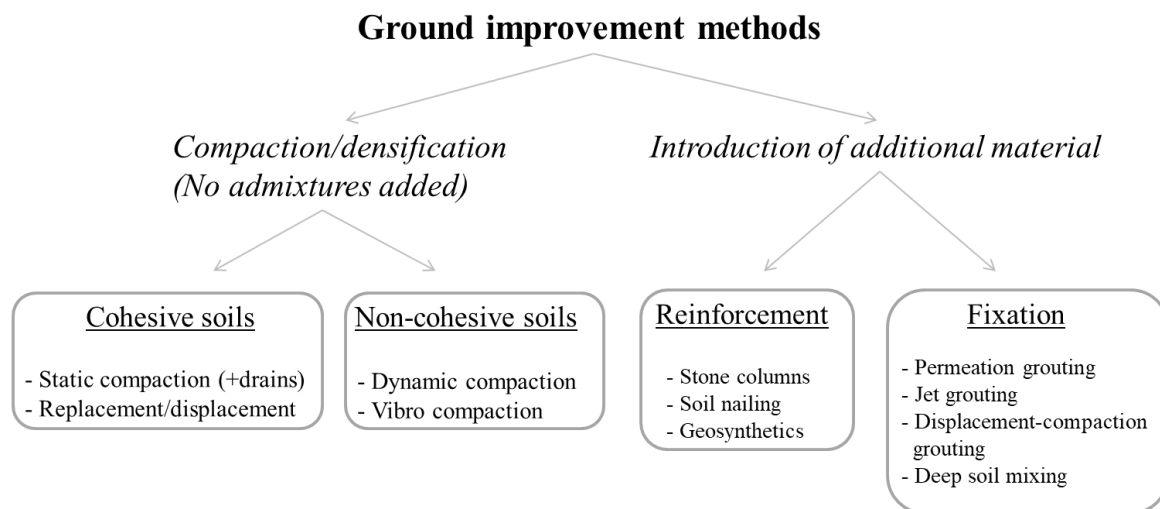
Figure 2-9. Classification ground improvement methods (based on Moseley & Kirsch 2004)

2.4.3. Need for alternative methods

All the processes included in Figure 2-9 have been proved to be successful in many applications throughout the years. However, the implementation of these methods often generates sustainability issues such as high energy demands and use of fossil fuels, the continuous modification and consequent degradation of natural ecosystems or the increasing use of

natural geo-resources which will limit future generations from using them (Fragaszy et al., 2011).

Amongst the most environmental unfriendly soil improving methods is the injection of chemical grouts. Increasing the pH of the groundwater to highly alkaline levels or contamination of the geoenvironment due to their toxicity are some consequences of the use of chemical grouts to improve soils (Karol, 2003; DeJong et al. 2006). Moreover, the use of chemical grouts is an expensive solution for soil improvement and also involves other problems such as non-uniform distribution along the soil mass and a relatively high uncertainty of execution (DeJong et al. 2009). Additionally, one of the most common materials used for grouting techniques is Portland cement, which according to Li et al. (2013) accounts for more than 7% of the global carbon dioxide emissions. Countries like USA have started to ban some chemical grouts due to their potential hazard for the geoenvironment and the need of reducing cement usage considering the associated environmental issues (DeJong et al., 2010).

On the other hand, methods involving compaction/densification of the ground might appear to be less hazardous for the environment, however, these methods have associated problems of noise and vibration, which can be an issue for existing buildings and congested sites. Therefore, considering the continuing demand for soil reinforcement projects, there is an extreme need for developing alternative, sustainable, harmless and cost-effective methods (DeJong et al. 2009; Shahin 2016).

One method that shows good potential to fulfil these requirements is the use of biological microorganisms, and in particular, the use of bacteria (Mitchell and Santamarina, 2005) to improve soil properties. Bio-mediated soil improvement is a relatively new method in which microorganisms are used to stimulate some chemical reactions within the soil matrix, and is currently being investigated by many researchers across the world as a potential soil improvement method (DeJong et al., 2010). The implementation of these so-called bio-mediated processes has the potential to modify many soil properties, including physical (density, saturation or porosity), conduction (hydraulic, thermal or electrical), mechanical (compressibility, stiffness, cohesion or friction angle) and chemical properties (reactivity or cation exchange capacity) (DeJong et al., 2010; Shahin, 2016; Whiffin et al., 2007). This can enhance bearing capacities, reducing liquefaction risk and controlling soil erosion, amongst

many other benefits (DeJong et al. 2010; Whiffin et al. 2007). Additionally, their further development would provide with the ability of dealing with some current geotechnical problems that traditional techniques are unable to solve or that involve an excessive cost, such as the creation of subsurface storage spaces, carbon dioxide sequestration at great depths, subsurface hydraulic flow control or stabilization of sink holes (DeJong et al. 2013).

The potential development of bio-mediated soil improvement methods could provide many advantages, including (DeJong et al. 2013):

- Low impact to the geoenvironment since they are based on natural processes.

- Reduced levels of energy required.

- Applicability to both new and existing structures (without disturbance to the existing ones).

- Ability to cover large areas due to their low viscosity and injection pressure.

In addition, the use of living organisms provides a higher degree of control over the response of the reinforcement system, and this response can be further enhanced by genetically modifying the DNA of the microbes (see section 2.5. The role of Synthetic Biology for further details).

Additionally, Ivanov and Chu (2008) performed an approximate analysis between the raw material cost for microbial grouting ($0.5-9 per cubic meter of soil) and chemical grouting ($2-72 per cubic meter of soil), being the bio-mediated solution considerably cheaper. Therefore, since the scale of geotechnical construction tends to be relatively large – e.g. land reclamation – microbial mediated treatments could provide with a cost effective solution in comparison to the expensive treatments involved in the use of traditional methods.

Many bio-mediated ground improvement processes have been investigated during the last two decades, although only one method has shown promising potential for industrial use. This method is called biocementation through Microbially-Induced Calcite Precipitation (MICP) and a lot of emphasis has been put in the development and upscaling from laboratory to field-scale applications (Ivanov & Chu 2008; DeJong et al. 2013). The next section describes the mechanisms involved in soil cementation through MICP and reviews the latest research on the topic.

2.4.4. Biocementation through Microbially-Induced Calcite Precipitation (MICP)

Microbial cementation or *biocementation* is a bio-mediated process by which the soil particles bind together due to the precipitation of inorganic materials – carbonates, silicates, phosphates, sulphides and hydroxides (Ivanov and Chu, 2008) – which leads to an increased soil strength and stiffness (DeJong et al., 2007).

MICP is a biological process that occurs naturally in geomaterials (e.g. digenesis from sand to sandstone) and researchers have attempted to imitate it in a laboratory under controlled conditions in order to use it as a ground improvement technique (Soon et al., 2013; Whiffin et al., 2007).

In MICP, a process of biomineralization (calcium carbonate or *calcite* precipitation) occurs as a consequence of metabolic microbial activity via several pathways, such as hydrolysis of urea (Ivanov and Chu, 2008, Burbank et al., 2011). Although other microbial processes have been proved to potentially lead to biocementation – i.e. denitrification (Montoya, 2012; van Paassen et al., 2010), sulphate or iron reduction (Boquet et al., 1973; Frankel and Bazylinski, 2003), etc. – enzymatic hydrolysis of urea is the most energy efficient process in terms of Gibbs Free energy (see DeJong et al., (2010) for more details on urea hydrolysis).

2.4.5. Mechanism for calcite precipitation

Urease positive bacteria are widespread in the environment and some particular strains – such as *Sporosarcina pasteurii* and *Bacillus megaterium* – produce relatively high levels of urease (Anbu et al., 2016; Bachmeier et al., 2002).

The idea of MICP is to use these urease-producing bacteria strains in order to hydrolyse urea (urease catalyses the hydrolysis of urea 1014 times faster than the normal urea hydrolysis (Mobley et al., 1995)) and produce carbonate ions in situ which then react with a calcium-rich solution and precipitate calcium carbonate (Cheng et al., 2013; De Jong et al., 2009; Hammes et al., 2003; Li et al., 2013; Ng et al., 2012; Stocks-Fischer et al., 1999). The process is described as follows:

1) The urease enzyme produced in situ by bacteria - which is a by-product of bacterial metabolic activity – decomposes urea injected within the soil matrix through a process called *hydrolysis of urea*. The resulting products of this reaction are ammonium and carbonate ions.

$$CO\,(NH_2)_2 + 2H_2O \rightarrow 2NH_4^+ + CO_3^{2-}$$
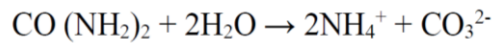
2) The generated carbonate ions react with calcium ions (the presence of a calcium source such as calcium chloride is needed) due to an increase in the local pH of the environment generated by the production of ammonia in the system. If there is a sufficient concentration of Ca^{2+} and CO_3^{2-} in the environment, calcium carbonate crystals begin to precipitate at the bacterial nucleation sites (Figure 2-10).

$$Ca^{2+} + CO_3^{2-} \rightarrow CaCO_3$$
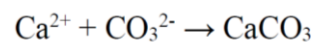
These crystals (commonly known as *calcite*) are then responsible for the soil particle binding and the consequent bio-cementation process (Ng et al., 2012).
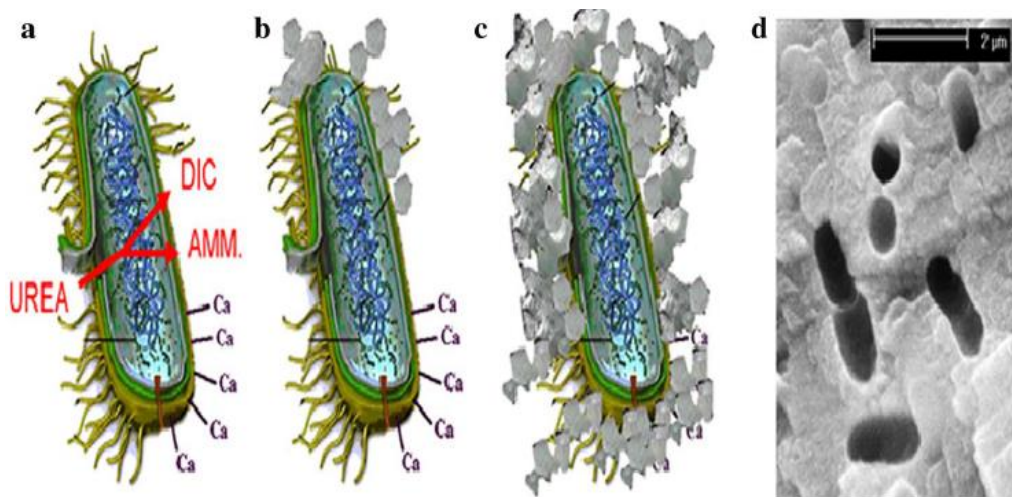
Figure 2-10. Ureolysis-driven calcite precipitation

(after De Muynck et al. 2010)

The urease enzyme generated by the microbial activity is therefore essential for calcite precipitation to take place (Bachmeier et al. 2002). Phang et al., (2018) performed an investigation to understand the relationship between cell concentration and urease activity

for different *Bacillus* species. The results (see Figure 2-11) demonstrated that the amount of urease released in the environmental is not proportional to the number of cells. This has clear implications for the biomineralization process since a larger number of cells does not necessarily lead to a higher degree of calcite precipitation. Therefore, understanding the optimum cell concentration that produces larger quantities of urease activity is an essential factor. Additionally, it was demonstrated by Singh et al., (2017) that the urease activity increases linearly from 20°C to 37°C, and decreases considerably after that point. Several authors (e.g. Stocks-Fischer et al. 1999; D. J. Evans et al. 1991; Arunachalam et al. 2010) have confirmed that urease activity reaches its peak at pH 8 and gradually decreases with a further increase in pH.
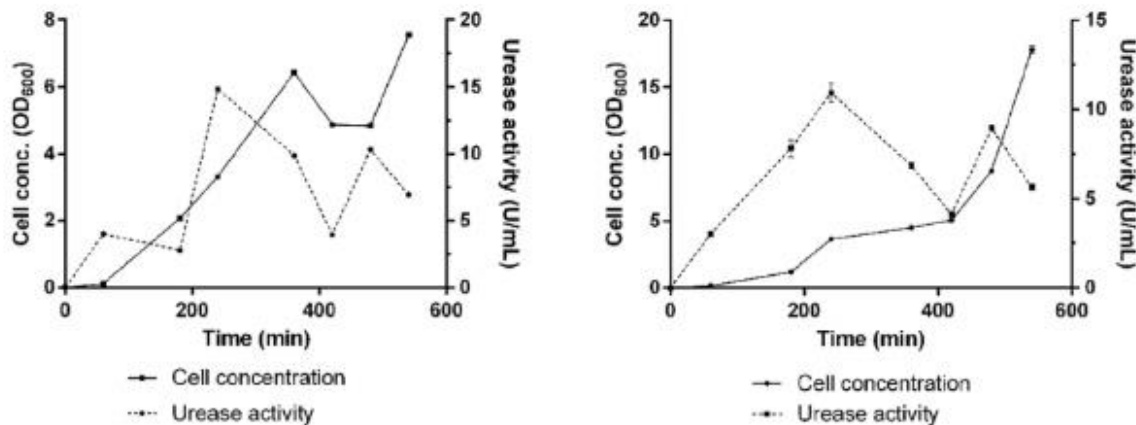
Figure 2-11. Correlation between urease activity and cell concentration for two different species

(after Phang et al., (2018))

Additionally, Achal & Pan (2014) stated that, although many calcium sources can be used to induce calcite precipitation, calcium chloride provides with the best results.

According to several authors, the rate at which calcite precipitates is mainly governed by four parameters – the calcium ion concentration, the dissolved inorganic carbon concentration, the pH of the environment and the availability of nucleation sites within the soil matrix (Castanier et al., 1999; Kile et al., 2000; Ng et al., 2012).

In addition, Phillips et al. (2013) stated that in order to have stable and continuous $CaCO_2$ formation, the availability of nucleation sites is essential. In the biomineralization process, bacteria are used as nucleation sites due to their negatively charged cell surfaces, attracting divalent cations – such as Ca^{2+} – and attaching them onto their surface at neutral pH, providing ideal conditions for calcite precipitation (Ferris et al., 2004; Li et al., 2013; Lian et al., 2006; Stocks-Fischer et al., 1999).

2.4.6. Macromechanics of bio-cemented soils

In bio-cemented soils, the $CaCO_3$ precipitated through MICP bridges between adjacent soil grains at the particle-particle contact (Figure 2-12), forming a cemented soil structure similar to that of calcareous rocks (DeJong, Jason T., Michael B. Fritzges, 2006).
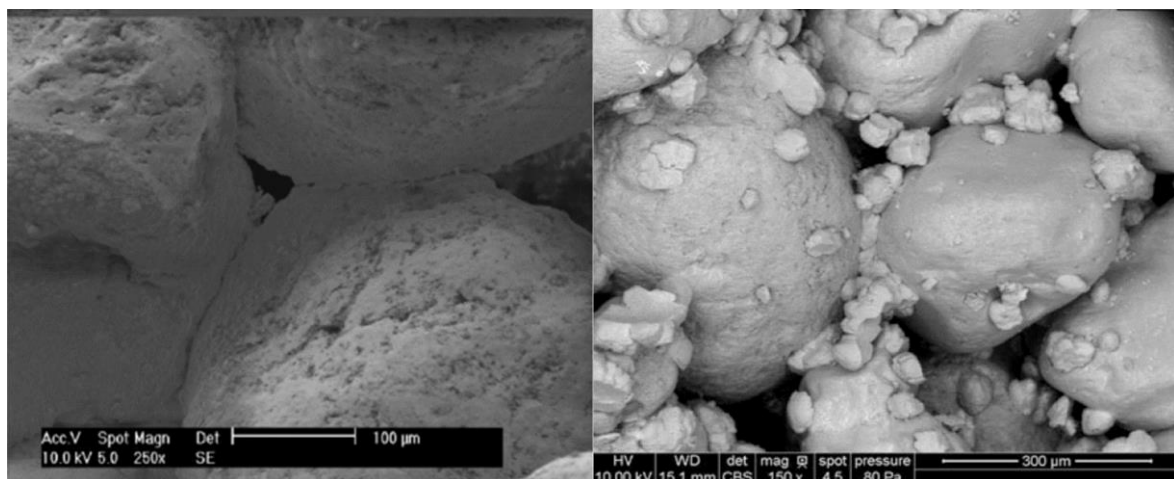
Figure 2-12. Examples of calcite precipitated between soil particles

(after Cheng et al. 2013 (left) and Ivanov et al., (2015) (right)).

Thus, this new bio-cemented soil structure has enhanced mechanical properties, some of which are summarised as follows:

- Substantial increases in shear strength has been demonstrated by many researchers (Chu et al., 2012; DeJong, Jason T., Michael B. Fritzges, 2006; Whiffin et al., 2007), as well as increases in small-strain stiffness by three orders of magnitude (DeJong, Jason T., Michael B. Fritzges, 2006; van Paassen, 2011).

- Decreased compressibility of the soil has also been demonstrated by many researchers, e.g. DeJong et al. (2010), where a ten-fold change was obtained.

- Permeability can be also reduced due to the precipitation of calcite in the pore space and the partial plugging of the soil that reduced water flow through the pore throat (Anbu et al., 2016; Chu et al., 2012; DeJong, Jason T., Michael B. Fritzges, 2006; Whiffin et al., 2007). Martinez et al. (2013) showed hydraulic conductivity decreased by greater than two orders of magnitude. However, one of the key properties of MICP treated soils is the capacity to retain sufficient permeability, providing enough drainage and dissipation of the excess pore water pressure upon loading (Cheng et al., 2014; Shahin, 2016).

2.4.7. Factors/parameters affecting MICP performance

The performance of MICP treated soils depends on several physical and environmental parameters which have been comprehensively analysed by many authors. This section outlines the main factors analysed in the literature and proposes the best conditions for optimum MICP soil treatment. Additionally, section 2.4.8. Applicability, limitations and upscaling principles discusses some other factors that might also impact the effectiveness of MICP for field-scale projects – such as the geometric compatibility of bacteria, the fixation and distribution of bacteria in soil and the injection method.

- Type of bacteria

The preferred organisms for MICP are facultative anaerobic bacteria due to their ability to respond under both aerobic and anaerobic conditions (Ivanov and Chu, 2008). Additionally, bacteria used in MICP applications must be able to catalyse the hydrolysis of urea. Hence, most of the species commonly used are urea positive bacteria such as the Bacillus group (Hammes et al., 2003; Kucharski et al., 2008).

- Bacteria cell concentration

The importance of bacteria cells in providing nucleation sites for calcite precipitation was discussed in previous sections. It was confirmed by Okwadha and Li (2010) and (Stocks-Fischer et al., 1999) that higher bacterial cell concentration leads to an increased amount of calcite precipitation (from to 10^6 to 10^8 cells). Hence, if enough cementation reagents are provided

to the system, the rate of urea hydrolysis is directly proportional to the bacterial cell concentration (Ng et al., 2012).

- *pH*

The urease enzyme is essential in the process of decomposing urea and triggering calcite precipitation. As described above, urease activity is highly dependent on the pH of the environment and, therefore, the amount of calcite precipitated is also influenced by the pH.

Therefore, it must be taken into consideration that the production of ammonia will increase the pH of the system, consequently reducing urease activity. Additionally, Lowenthal and Marais (1976) stated that if low pH levels are present in the environment, calcium carbonate crystal will dissolve, rather than precipitate.

Ferris et al. (2004) and Dupraz et al. (2009) demonstrated that most calcium carbonate precipitation takes place under alkaline conditions from pH 8.7 to pH 9.5, and Cheng et al. (2014) performed an analysis which shows the effect of acidity and alkalinity on the strength of MICP treated soil samples (Figure 2-13). The figure also shows that, although the amount of $CaCO_3$ precipitated was higher, the unconfined strength of the soil samples might be lower. This phenomenon might be associated to the morphology and attachment of the crystals to the soil grains. In addition, Harkes et al. (2010) stated that the pH of the system also alters the transport and adhesion of bacteria, leading to non-homogenous distribution problems.
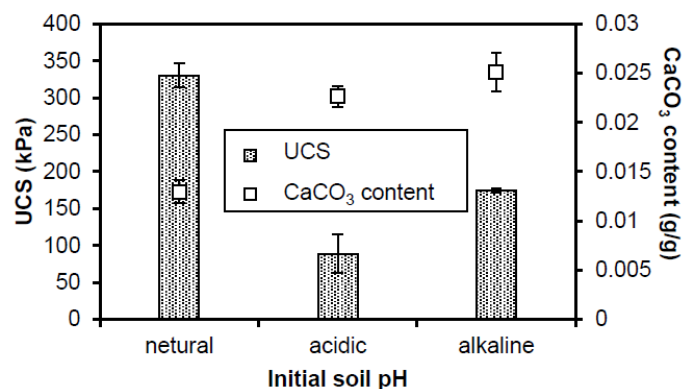
Figure 2-13. Unconfined compressive strength and $CaCO_3$ content of MICP treated soil samples at different pH

(after Cheng et al. 2014)

- *Temperature*

According to Mitchell & Ferris (2005) and Okwadha & Li (2010), the rate of hydrolysis is temperature dependent, with optimum values reached between 20 and 37°C for most urease-producing bacterial species. Nemati et al. (2005) stated that hydrolysis rate is higher at 30°C than 20°C and an increase of further temperature does not lead to an accelerated urea decomposition rate.

In addition, Cheng et al. (2014) demonstrated that MICP samples treated at 25°C are stronger than the same samples treated at 50°C, the latter ones showing 60% less strength. It can be seen from Figure 2-14 that, although the amount of $CaCO_3$ increases, the shear strength of the samples decreases. According to the author, this behaviour occurs due to the fact that the crystals formed at 50ºC are considerably smaller (2-5 μm diameter) than those formed at 25°C (15 – 20 μm). Hence, the formation of bigger crystals contributes to strength development due to the gap filling effect between soil grains. It is therefore concluded that the strength improvement is not governed by the amount of $CaCO_3$ crystals, but the size of them (Cheng et al., 2014).
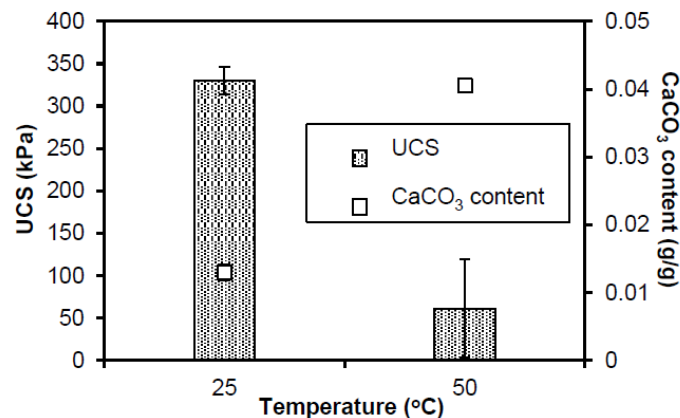
Figure 2-14. Unconfined compressive strength and CaCO₃ content of MICP treated soil samples at different temperatures

(after Cheng et al. 2014)

- *Reactant (Urea and Ca+) concentration*

The introduction of urea and calcium chloride (or other calcium source) into the soil is essential to precipitate calcium carbonate. Achal & Pan (2014) analysed the calcite precipitated through MICP using different calcium sources and concluded that calcium

chloride is the most efficient one. Rivadeneyra et al. (2004) stated that the concentration of the reagents influences the rate at which calcite precipitates. Nemati et al. (2005) and De Muynck et al. (2010) demonstrated that increasing the urea and calcium chloride concentrations results in larger amounts of calcite precipitation. Moreover, De Muynck et al. (2010) reported that 0.5M and 0.25M concentrations of urea and CaCl2 respectively are the optimal ones for efficient calcite precipitation. In addition, Okwadha & Li (2010) reported that higher reactant concentrations than 0.5M decrease the efficiency of calcium carbonate precipitation.

On the other hand, the negative effect of high salinity solutions was analysed by Rivadeneyra et al. (2000) and it was stated that large amounts of calcium would inhibit microbial activity and further calcite precipitation due to the high salinity. Additionally, Okwadha & Li (2010) demonstrated that Ca^{2+} concentration has a bigger influence than urea concentration on the process of $CaCO_3$ precipitation.

- *Nutrient availability*

It is well-known that nutrients are the source of energy for bacteria and are essential for their survivability and growth (Ng et al., 2012). Mitchell and Santamarina (2005) provided a list of the most common nutrients, including CO_2, N, K, Mg, Fe, P, Ca, etc. Hence, it is crucial to supply the ground with these nutrients during the treatment process since geological systems often lack them or they are not present in sufficiently large amounts (DeJong et al., 2007). DeJong et al. (2006) and Qabany et al. (2011) introduced 3g per litre of nutrient broth into the treatment solution in order to maintain a desired growth rate of urease positive bacteria long enough for the biocementation process to be effective.

2.4.8. Applicability, limitations and upscaling principles

Bio-cementation through MICP stands as a promising environmentally-friendly and cost-effective soil reinforcement method; however, in order to establish this technique for industrial applications, a few considerations must be taken into account and a few limitations must be overcome.

Bio-mediated processes have a considerably lower impact on the geoenvironment than chemical grouting techniques. Nevertheless, the by-products generated from the urea hydrolysis process such as ammonium and nitrate are toxic and hazardous to humans and microorganisms if present at high concentrations, which makes MICP not completely environmental friendly (van Paassen et al., 2010). In addition, microbial processes are more complex than chemical processes since they depend on many environmental factors such as pH, temperature, concentration of nutrients and concentrations of donors and acceptors of electrons (Ivanov and Chu, 2008). Thus, the design of bio-mediated applications must consider many other aspects apart from soil conditions and grouting solutions – e.g. microbiological aspects (growth, biosynthesis, enzymatic activity, etc.), ecological aspects, physico-chemical processes (precipitation, formation insoluble compounds, etc.) – which makes their applicability much more complex than conventional grouting techniques (Ivanov and Chu, 2008).

The nutrients used to grow bacteria cultures in the laboratory are relatively cheap. However, for field applications, where large amounts of nutrients are needed, the use of laboratory grade nutrient sources may become an economic limitation (Anbu et al., 2016). Therefore, alternative economical nutrient sources need to be investigated in order to successfully upscale MICP projects from laboratory to field-scale applications. According to Mitchell et al. (2010) and Phillips et al. (2013), other nutrient sources such as *corn steep liquor* or *lactose mother liquor* could provide an inexpensive solution to address this problem.

Similarly, the production of large volumes of reactants (e.g. calcium chloride) may be seen as an economic disadvantage in comparison to traditional grouting and, therefore, prevent the progress of bio-cementation into a commercial scale. The use of alternative calcium sources has been investigated by Cheng et al. (2014). The author proposed the use of seawater as a substitute to conventional bio-cementation reagents in order to reduce the cost of MICP-based projects and position this soil improvement technique one step closer to its commercialisation. Figure 2-15 shows the results of using seawater as a chemical reagent compared to a *cementation solution* (i.e. calcium chloride). It can be seen that, as reported previously, the strength increases exponentially by increasing the amount of calcite precipitated. However, samples treated with seawater clearly show an increased strength compared to samples treated with a cementation solution, for the same amount of carbonate

precipitation. As commented in previous sections, this phenomenon may occur due to the fact that, although higher concentrations of urea and calcium chloride produce a relatively large amount of calcite, the efficiency of the crystals formed is lower than those crystals formed at reduced concentrations of calcium – i.e. using seawater. However, in order to achieve these results, the amount of seawater flushed through the specimens is much larger than the amount needed using conventional calcium chloride. Hence, this result shows the potential of using seawater as a cementation reagent and could position bio-cementation as the preferred ground improvement method for marine environments.
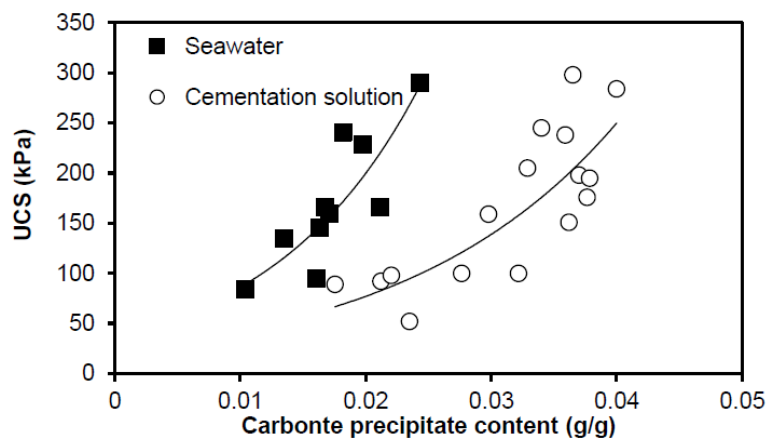
Figure 2-15. Unconfined compressive strength and CaCO$_3$ content of MICP treated soil samples with seawater as a calcium source

(after (Cheng et al., 2014)

Another study where an alternative calcium source is used for bio-cementation of sand is the one presented by Choi et al., (2016). The authors investigated the effect of using eggshell as the calcium source to induce calcium carbonate precipitation via MICP. The study demonstrated that samples treated using calcium from eggshell generate the same strength and permeability values than samples treated with calcium chloride, indicating that the use of calcium from eggshell for soil improvement is a feasible option.

On the other hand, the geometric compatibility between bacteria and soil is essential for successful implementation of a bio-cementation project. According to (De Jong et al., 2009), sufficiently large pore throats are necessary in order to allow microbial mobility through the soil structure. Small soil pore throats restrict the transport of bacterial cells leading to non-uniformity problems. Maier et al. (2009) stated that bacteria cells with diameter between 0.3

to 2 μm can move freely through the pore structure of sandy soils with size particles between 0.05 and 2 μm. However, the presence of fine particles would have a negative effect on the distribution of bacteria cells due to an obstruction of some pore throats (Ng et al., 2012). Cheng and Shahin (2015) analysed the effect of clay particles on MICP treated sand samples and concluded that bio-cementation treatment using conventional injection methods may not be suitable for sandy soils containing a clay content higher than 5% due to filter effect and further accumulation of cells at the injection end and the consequent bio-clogging, impeding a uniform distribution of cementation.

Another important consideration that needs to be further analysed is how to achieve a uniform distribution of the bio-cementation reagents and the bacteria-medium solution. A uniform cementation distribution is essential for ground improvement field applications. However, achieving uniform distribution through the soil matrix is not a straight-forward process since filtration of bacteria cells through the porous structure results in a logarithmic reduction of cell concentration (Ginn et al., 2002). Hence, since lower concentration leads to reduced cementation, injection methods need to be improved in order to achieve an even distribution of microbes and reactant concentrations across the injection path (De Jong et al., 2009). Martinez et al. (2011) demonstrated that the stopped-flow injection (intermittent injections, opposite to continuous injection) of cementation fluids provides a more uniform distribution than continuous injection methods due to the accumulation of precipitated calcite next to the injection port by the latter method and a decreased concentration as distance from injection increases. Therefore, stopped-flow injection is capable of distributing evenly all the fluids before calcite begins to precipitate. Alternatively, Boving et al. (2008) have developed a method called push-pull injection through which uniform cementation can be achieved. The idea of this method is to inject microbes at an artificial hydraulic gradient and nutrients at a reversed hydraulic gradient. In this way, areas with lower concentration of microbes are supplied with more nutrients than areas with higher concentration (i.e. near the injection point) and uniform distribution of the treatment is accomplished throughout the treated area.

In addition, another aspect that must be taken into consideration is the original composition of the pore fluid. According to Lebron and Suarez (1996), the chemical composition of the pore fluid can influence the reactions taking place and may benefit or inhibit the production

of carbonates. These authors stated that while high calcium concentration groundwater assists in the production of calcite, groundwater with high organic content may hinder its precipitation. Therefore, analysing the groundwater chemistry is essential prior to treatment application.

Lastly, the permanence of MICP treated soils is crucial for successful field implementation, although fewer investigations have been performed on this aspect to date. The design life of MICP bio-cementation projects must equal that of the associated civil infrastructure. Therefore, for areas where calcite stability is not completely assured, it is extremely important to monitor the state of the treated soil throughout its service life (De Jong et al., 2009).

All these limitations are currently hindering the commercialisation of MICP as a ground improvement method, mainly due to the poor control and uncertainty of the outcome. However, there have been a few field-scale projects worldwide in which bio-mediated processes, including MICP, have been performed. The contractor *Visser and Smit Hanab* applied a MICP treatment in the Netherlands in 2010 using bio-augmentation (injection urea-positive microbes into the ground) of bacteria with urea and calcium chloride as cementation reagents in order to induce calcite precipitation and stabilise a gravel soil before horizontal drilling. The successful treatment allowed the drilling for gas pipelines without failure of the loose gravel ground (van Paassen, 2011). Another field trial was performed in the United States using bio-stimulation (stimulation of native urea-positive bacteria) of the indigenous species. The aim of this project was to analyse the performance of calcium carbonate precipitation as a heavy metals immobilisation method. The trial took place in the US Department of Energy site in Rifle, Colorado (Fujita et al., 2010). Additionally, according van Meurs et al. (2006) and Blauw et al. (2009), a few field trials have been performed in the Netherlands and Austria using bio-clogging to reduce the leakage through water retaining structures.

2.4.9. Potential applications

The main objective of bio-cementation through MICP is to provide a cost-effective and eco-friendly soil reinforcing technique in order to increase the strength and reduce compressibility of weak soils (De Muynck et al., 2010; Ng et al., 2012). However, there are specific areas in

which MICP has been recognised as a particularly promising substitute for conventional ground improvement techniques, which are listed as follows:

- Creating impermeable barriers for catchment facilities (Chu et al., 2012).

- Piping prevention for dams and levees (DeJong et al., 2007).

- Reducing dust levels (Kucharski et al., 2008).

- Treating waste (J. Chu et al., 2009).

- Improving resistance to liquefaction (Montoya et al., 2013).

- Increasing resistance to petroleum borehole degradation (Kucharski et al., 2008).

- Remediation of heavy metals (Li et al., 2013).

- Soil stabilisation prior to tunnelling or underground construction (DeJong et al., 2007).

- CO_2 sequestration (Manning, 2008).

- Reducing erosion induced by wind and water (Bang et al., 2011).

- Coastline erosion prevention (using seawater as a chemical reagent) (Shahin, 2016).

2.5. The role of Synthetic Biology

This section presents the new field of Synthetic Biology (SynBio) describing its design principles and the methods used to engineer microorganisms, and provides a review of the most promising engineered living systems and their applications for the geoenvironment.

2.5.1. Definition of Synthetic Biology and Design Principles

SynBio is a relatively new field of research based on the molecular level manipulation of microorganisms through genetic modification. Although the term Synthetic Biology has been around for more than 100 years, it was at the beginning of this century when SynBio considerably took off as a field of research, due to the publication of several articles discussing the creation of synthetic biological circuits and the combination of genes within *E. coli* cells (Elowitz and Leibler, 2000; Gardner et al., 2000). SynBio is often associated with Genetic

Engineering, although clear differences exist between the two fields. While Genetic Engineering essentially enhances existing biological functions or transfers them between organisms, SynBio focuses on the combination of multiple genes in order to construct new biological pathways and functions that are not present in nature and redesign existing biological systems to perform new functions (Endy, 2005). In other words, the aim of SynBio is to create new biological systems that can be programmed by changing and reassembling biological components or "parts" so that they perform beneficial functions (Silver et al., 2014).

SynBio follows an engineering approach, where these interchangeable *biological parts*, which are genes that encode a specific function, are treated as components to create a synthetic genetic circuit, or *device* (Voigt, 2006). These circuits can be assembled to form complex systems that are capable of responding to a range of physical and chemical inputs (Khalil and Collins, 2010). The response to these inputs is normally in the form of protein synthesis or other molecules, which ultimately have useful applications (see section 2.5.2. Engineered living systems for the geoenvironment for some examples). Furthermore, the rational design and customisation of these genetic parts into devices is normally guided by computer modelling (König et al., 2013). In this way, SynBio creates libraries containing well-defined parts so that they can be combined in cells in order to generate predictable outcomes (Silver et al., 2014). Thus, the aim of SynBio is to program cells by introducing new genes to their DNA with specific instructions so that the cell performs a specific function.

Genetic engineering practices are frequently used in laboratory environments and many applications exist where Genetically Modified Organisms (GMOs) are used. Living organisms contain long chains of deoxyribonucleic acid (DNA), called chromosomes, which contain all the genetic information needed for growth, functionality and reproduction. Using recombinant DNA techniques, sequences of DNA from one organism, the donor, can be extracted and attached onto the genome of another organism, the host, so that the new organism presents some features of the donor. A common practice in a microbiology environment is to introduce a fluorescence protein obtained from a type of jellyfish in the genome of another organism in order to report its expression under specific light conditions. This protein is called Green Fluorescence Protein (GFP).

The above-mentioned genetic *parts* can be assembled into *devices* which can be represented by symbols comparable to those of electrical circuits (Endy, 2005; Khalil and Collins, 2010).

These symbols belong to a basic language called *Synthetic Biology Modelling Language* which is used to genetically program bacteria. An example of these genetic circuits is represented in Figure 2-16.
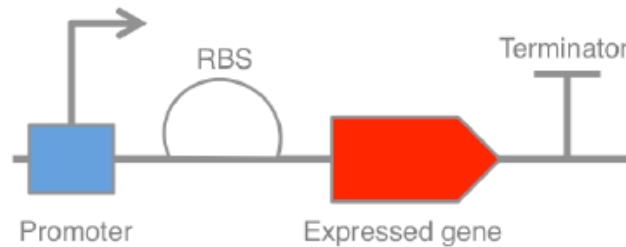
Figure 2-16. Diagram of a genetic 'device'

(after Dade-Robertson et al., (2016))

For a more in depth description of all the components present in genetic *devices*, see Endy (2005).

2.5.2. Engineered living systems for the geoenvironment

The rise of SynBio provides the capacity to design living organisms to respond to environmental conditions or external stimulus, opening up a wider range of bio-mediated ground improvement possibilities. As described in the previous section, SynBio gives the possibility to engineer organisms to detect specific environmental conditions and act in a desired way. Thus, SynBio brings a new dimension to the field of *microbially-mediated construction processes* since microorganisms are not only used as a catalyst of natural processes but they can potentially be engineered to induce particular reactions under specific conditions that will ultimately produce a desired function.

Some examples of *Engineered Living Systems* that are currently being investigated for use in the geoenvironment are described as follows:

- *Environmental biosensors.* Bacteria are engineered by attaching to their DNA circuits a gene responsive to pollutants in the geoenvironment and a reporter gene (such as Green Fluorescent Protein). The idea is to detect and monitor the amount of contaminants present in soils such as heavy metals or pesticides. This method would

allow large scale monitoring of contaminated areas in an efficient way (Loren L. Looger, Mary A. Dwyer and Department, 2003; Prindle et al., 2012; Ripp et al., 2000; Trang et al., 2005).

- *Bioremediation by Genetically Modified Organisms.* Although removal of pollutants from the environment can occur with non-engineered microorganisms, SynBio would enhance the clean-up performance of bacteria by implementing novel and complex metabolic pathways for biodegradation which would make the technique more attractive to industrial organizations (Haro and De Lorenzo, 2001; Megharaj et al., 2011; Sinha et al., 2010).

- *Pressure-sensing bacteria.* (Dade-Robertson et al., 2018) propose a system in which bacteria cells are engineered to respond to pressure changes in the geoenvironment and synthesize bio-cement through Microbially-Induced Calcite Precipitation where the higher pressures are located. The development of this idea would change the way geotechnical infrastructure is designed and would open a broad range of design possibilities (see section 2.5.3. Computational Colloids and Thinking Soils Projects for a more detailed description of the methods and techniques used by the *Thinking Soils* researchers).

The implementation of these engineered living systems would allow for cheaper and more efficient geotechnical and geoenvironmental strategies (Singh et al., 2011; Urgun-demirtas et al., 2017). However, the application of these techniques to geological systems would come with associated risks and challenges. For instance, the release of engineered organisms may have a negative impact to the indigenous organisms already living in that environment (Urgun-demirtas et al., 2017), and these environmental concerns lead to constraints of the commercialization of Genetically Modified Organisms (GMOs) for in-situ applications (Megharaj et al., 2011). Therefore, new approaches need to be taken in order to make the use of GMOs a more appealing solution for applications outside a controlled laboratory environment (Ramos et al., 2011).

2.5.3. Computational Colloids and Thinking Soils Projects

Thinking Soils is an ongoing project, which followed on from the pilot project *Computational Colloids*. This project aimed to develop a new type of system based on engineered responsive bio-materials which would react to inputs from the environment and act in a desired way. Section 1.3. Research rationale describes how the work performed in this thesis relates to the Thinking Soils and Computational Colloids projects.

As described briefly in Chapter 1, Computational Colloids and Thinking Soils introduce the concept of a pressure-responsive system based on engineered bacteria cells inoculated into the ground that would sense increases in local pressure upon loading and would respond by synthesizing materials that would cement the soil matrix, consequently increasing the strength and stiffness. The first steps towards the implementation of such system required identifying pressure-sensitive gene promoters which show an increase in expression when they are subjected to certain levels of stress. Some preliminary work carried out in the Computational Colloids project involved the use of a technique called RNA-seq. in order to characterise the response of the whole genome to pressure changes and target potential pressure-sensitive gene candidates. Out of all the genes analysed, 75 were found to be responsive to a pressure increase of 1 MPa, and in particular one gene (*AzuC*) showed a considerable increase in expression (Guyet et al., 2018).

The next step was to build a genetic circuit, using several molecular biology techniques, in which the *AzuC* gene was used as an input or *sensor* from the pressure of the environment and would transmit this information into the cell's DNA. Additionally, in order to characterise the sensitivity of the genetic response to pressure changes, GFP was selected as the reporter protein, and a strain of *E. coli* was created (P_{azuC} *azuC-gfp*) which emitted fluorescence as changes in pressure were sensed.

The fluorescence signal was monitored for different pressure values ranging between 0 and 1 MPa and it was confirmed that an increase in genetic activity occurred in response to a pressure increase. However, the engineered cells only exhibited relatively small *expression* changes in respond to elevated pressures of up to 1 MPa, with less than a 2-fold increase in expression. Pressures of such magnitude are not likely to be found is shallow soil systems and, therefore, more work needs to be done to refine and enhance the response of the bacteria strain to a suitable range of pressures (Guyet et al., 2018).

Although the complexity of the project was associated to the genetic manipulation of bacteria at the nano-scale level, the novelty of the system was demonstrated through the development of a computational model that combines this work performed at the nano and micro-scale with real geotechnical scenarios. By using this model, it is possible to predict the macro-scale biocementation behaviour of soils by modifying the gene profile of the bacterial cells at the nano-scale level. For a more detailed description of the micro and molecular biology methods and protocols, see Guyet et al., (2018), and for a comprehensive description of the rationale behind the design of the computational model, see Dade-Robertson et al., (2018).

All the limitations aside, this preliminary work demonstrated the ability to engineer bacteria to sense pressure changes from the environment and, ultimately, a more complex strain will be designed to respond to changes in stress by synthesizing crystals through a process of biomineralization. This pressure-sensitive crystal-producing system will potentially involve the precipitation of calcium carbonates crystals through the hydrolysis of urea (see section 2.4.5. Mechanism for calcite precipitation), where the urease expression will be dictated according to the level of pressure exerted on the cell.

Beyond the potential engineering applications of the system, which include for example the development of self-assembling foundations, self-strengthening of collapsible soils or self-construction of subsurface structures upon loading, the aim of the project is to develop a new class of biotechnology where sensing and response are performed in-situ by engineered living organisms (Dade-Robertson et al., 2017).

Chapter 3

Agarose Gel as a Soil Analogue

3.1. Introduction

The implementation of agarose gels as a soil analogue for the testing and monitoring of bacteria-based engineered living systems presents many advantages, as described in section 1.3. Research rationale, which are summarised as follows:

- Routinely used in microbiology to culture and grow bacterial colonies
- Easier monitoring of the performance of the microbes
- Greater control of the chemical composition of the environment
- Controlled simulation over the mechanical properties
- Minimised risk of contamination

Hence, understanding the mechanical properties relevant for the development of a physical and computational prototype testing model is a crucial aspect of this study. This chapter describes an experimental program performed on agarose gel to determine some of these relevant physical and mechanical properties as well as assess its suitability as a soil analogue. Agarose gels have been extensively studied for biomedical applications and they are commonly used as the medium for electrophoretic separation of proteins and DNA fragments (Jeppsson et al., 1979). The vast majority of literature on the mechanical properties of agarose focuses on analysing the stiffness and permeability of the gel for different concentrations and thermal conditions. Some examples of stiffness calculations are presented by Normand et al. (2000), Oflaz and Baran (2014) and Aymard et al. (2001), where small-scale cylinders of agarose (<10mm diameter) were tested under compression and tension and the stress-strain relationship was evaluated. Examples on permeability calculations can be found in Johnson and Deen (1996), Gu et al. (2003) and Liu et al. (2011), in which the authors flowed water through thin membranes of agarose gel under a pressure gradient in order to obtain the

hydraulic conductivity. However, little information exists about the behaviour and properties of agarose hydrogels at the macro-scale relevant to geotechnical engineering (for example, shear strength or consolidation). Therefore, their mechanical properties need to be well understood in order to successfully implement agarose as the testing medium for engineered bacteria and the development of physical and computational demonstration models.

Agarose gels present a porous structure comparable to soils and they provide ideal conditions for growing and monitoring bacteria. They are very easy to produce and their low degree of chemical complexity makes them less likely to influence the behaviour of engineered bacteria cells and allow controlled simulation of a variety of chemical, physical and mechanical properties. For these reasons, they stand as the most suitable material to be used for an early stage physical demonstrator.

The chapter is divided in three main sections: *Materials and methods*, where the composition of agarose, the method to produce agarose gels and the different tests performed are described; *Results and analysis*, where the physical and mechanical properties of the gel obtained from the experimental program are evaluated; and *Discussion*, where the gel properties are compared with some types of soils and their suitability as a soil analogue is critically discussed.

Additionally,

Table 3-1 presents an overview of the experiments described throughout the chapter.

Experiment	Specification	Location
Effect agarose concentration on pore size (SEM)	*Agarose concentration: 2%, 4% and 6% m/v*	Figure 3-3 and Figure 3-4
Unconfined Compression	*Preliminary test and effect agarose concentration (2%, 3%, 4%, 5% and 6% m/v) on shear strength*	Figure 3-6
Unconsolidated Undrained Triaxial	*Stress-strain relationship at different confining pressures (100kPa, 200kPa, 300kPa, 400kPa and 500 kPa)*	Figure 3-8 and Appendix A
	Plastic behaviour at different strain levels (2%, 4%, 6%, 8% and 10%)	Figure 3-9
	Stress-strain relationship kaolinite clay sample – comparison with 6% m/v gel	Figure 3-17
Isotropic consolidation (triaxial)	*Samples consolidated isotropically at different effective stresses*	Figure 3-11
Anisotropic consolidation (oedometer)	*Samples consolidated anisotropically at different stress levels*	Figure 3-12 and Appendix B
Effect consolidation on microstructure (SEM)	*Raw 6% m/v agarose sample v sample consolidated isotropically at 100kPa for 21 days*	Figure 3-14

Table 3-1. List of experiments Chapter 3

3.2. Materials

3.2.1. Agarose composition and formation

Agarose is a linear polysaccharide material extracted from marine red algae and it is one of the main components of agar. Agarose gels are formed by a reversible, physical association of polysaccharide chains, consisting of large fibre bundles held together by non-covalent hydrogen bonds and microvoids holding water (Johnson and Deen, 1996; Stellwagen and Stellwagen, 1995). Different models of gel formation have been identified, depending on the way the polymer chains are associated to form the bonds between the junction zones of the gel-forming elements (Morris, 1986). These models are presented in Figure 3-1A.
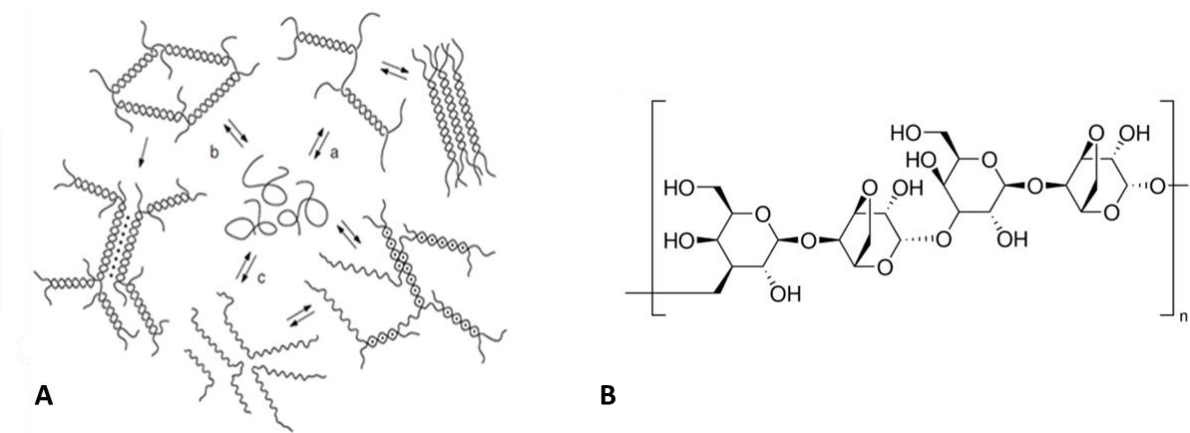
Figure 3-1. (A) different models of gel formation and (B) Fundamental unit of agarose low melt

(after (Normand et al., 2000; Tuvikene et al., 2008) and https://www.gbiosciences.com/Buffers-Reagents-Chemicals/Agarose-Electrophoresis-Running-Buffers-Chemicals/Agarose-II-Low-Melting*)*

Agarose gels are formed when a homogeneous solution (agarose chains are soluble in water at temperatures above 80°C, depending on agarose type) is cooled down to temperatures between 35-40°C, developing an infinite three-dimensional network of agarose fibres, formed by the above-mentioned helices distribution. Furthermore, the melting of agarose occurs at temperatures above 80°C (Johnson and Deen, 1996; Normand et al., 2000). Thus, the mechanical properties of the gels are mainly dictated by the fibre-pore structure which in turn depends mainly on agarose type, concentration and setting temperature (Narayanan et al., 2006). Agarose Low Melt (or 2-Hydroxyethyl Agarose) supplied by Melford Laboratories was the type of agarose selected for the experimental program (see Figure 3-1B for the chemical structure).

3.2.2. Kaolinite clay

Kaolinite clay was used to prepare clay samples so that a comparison regarding the stress-strain behaviour upon loading can be done. The kaolinite used was *Kaolin* provided by IMERYS Ceramics.

3.3. Experimental program

A range of experimental tests was performed to determine the physical and mechanical properties of Low Melt agarose gel and assess its suitability as a soil analogue. The porous microstructure of the gel was visualised at different concentrations before and after loading using Scanning Electron Microscopy (SEM), which allowed the measurement of the pore size and porosity of the gel. Unconfined Compression tests were performed to agarose gel samples in order to obtain an initial insight of the strength and deformation behaviour of the samples for different concentrations. The undrained shear strength (c_u) and the stress-strain relationship of the gels were determined using Unconsolidated Undrained triaxial tests, where the samples were subjected to a confining pressure or radial stress, σ_3 and to an axial stress, σ_1 applied vertically. This type of test does not involve pore pressure or volume change measurements and only provides information in terms of total stress. The isotropic consolidation behaviour and permeability of the gels were also investigated by performing Isotropic Consolidation triaxial tests, where drainage of the pore water at different consolidation pressures was allowed. Finally, the one-dimensional consolidation of the gels was investigated using an oedometer cell, where samples were constrained laterally and a load was applied in the vertical direction.

3.3.1. Agarose gel preparation and specimen moulding

The agarose gel was formed by dissolving agarose powder in distilled water or LB media. Agarose powder has low solubility in these solvents at room temperature, therefore the heterogeneous mixture was heated to above 100°C in order to achieve a homogeneous solution. The solution was then immediately poured into aluminium moulds for geotechnical testing or 25mm Petri dishes for SEM. Agarose gels present a fully saturated matrix, assuming all the bubbles generated in the liquid solution migrate to the surface and eventually disappear. For the triaxial tests, 38mm diameter cylindrical moulds filled with gel to approximately a height-to-diameter ratio of 2 were used. The cylinders were immediately covered with tape in order to avoid evaporation and were then stored in the fridge at 4°C for approximately 15 minutes until gelation. For the oedometer tests, samples were prepared in the same way, although the moulds used in this case were 50mm in diameter and 20mm in

height. Samples with different mass concentrations, ranging from 0.5% to 10% m/v (mass/volume), can be prepared depending on the amount of agarose powder dissolved in the solution. For all the mechanical tests, a concentration of 6% m/v was used. This was chosen after initial investigation determined that this was the highest concentration possible that allowed homogeneous growth of bacteria (see section 4.4.3. Effect of agarose concentration and reasoning behind choosing 6% m/v for more details).

3.3.2. Kaolinite sample preparation

Kaolin powder was thoroughly mixed with water until a homogeneous mixture was achieved. The mixture was then consolidated at 100kPa for a week in a consolidometer. Cylindrical samples of clay were obtained by introducing hollow cylinders (38mm diameter) into the consolidometer acting as a mould for the clay samples. The top and bottom of the cylinders were then covered with wax in order to avoid changes in the water content and stored in a cool environment until testing.

3.3.3. Scanning Electron Microscope (SEM) imaging

The scanning electron microscope used was a field emission TESCAN MIRA 3. Agarose gel was prepared as described in Section 3.3.1. Agarose gel preparation and specimen moulding. Upon gelation, 5mm cubes of gel were cut and placed inside 10mL beakers. Liquid nitrogen was then poured into the beakers to guarantee rapid freezing of the samples and avoid structural deformations during the freeze-drying process. The use of ultrafast freezing techniques avoids distortions and deformations of the specimens' structure to as little as the nanometre scale (Robards, 1991). The beakers were then placed into a vacuum cell and were freeze-dried under vacuum at -80°C for 24h. Finally, before SEM inspection, the samples were sputter-coated with a layer of platinum approximately 3-4nm thick using a High Resolution Sputter Coater. The samples were visualised at a very low voltage (1.5-2 kV) in order to avoid any damage to the structure.

3.3.4. Unconfined Compression tests

Unconfined compression tests were performed to agarose samples using an *Instron 5585H* load frame. in order to analyse the shear strength and deformation occurring upon loading. This type of test measures the shear strength of cylindrical specimens as well as providing an insight into the deformation behaviour.

The cylinders were demoulded, prepared and tested in accordance to (British Standard 1377, 1990a) and the loading rate applied was 1mm/min.

3.3.5. Triaxial tests

Triaxial tests are one of the most widely used methods to test the shear strength of soil samples as well as analyse the stress-strain relationship and isotropic consolidation behaviour. Two different series of triaxial tests were performed using a GDS 50kN digital load frame: Unconsolidated Undrained tests and Isotropic Consolidation tests.

Details of the triaxial testing setup can be found in Figure 3-2.

Calibration of the system was performed before the testing program and every three months thereafter to ensure accuracy and reliability of the results. The process involved calibration of the pressures measured by the GDS software against a standard reference value measured by conventional pressure gauges.
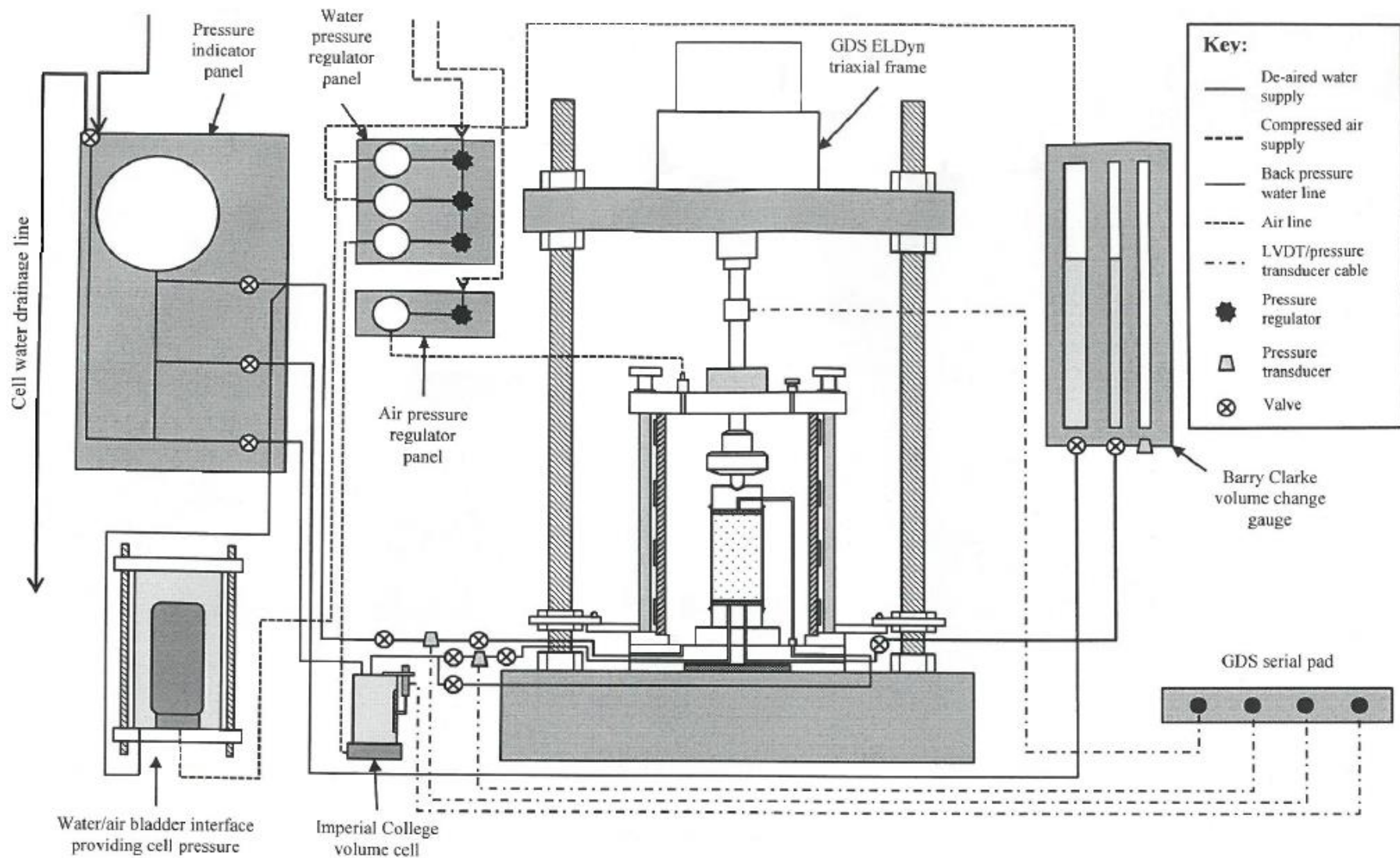
Figure 3-2. Representation triaxial apparatus including pressure and volume regulators/indicators

58

Additionally, the saturated state of the samples was confirmed for each specimen by performing a B-test prior to triaxial compression or consolidation. The B-test aims to establish the relationship between an increase in radial pressure in an undrained manner and the consequent increase in pore pressure by measuring the pore pressure coefficient, B, or Skempton's B-value (Skempton, 1954). This values can be obtained using the following equation:

$$B = \frac{\Delta u}{\Delta \sigma_3}$$

(Equation 3-1)

where Δu refers to the increase in pore pressure due to an increase in radial stress, $\Delta \sigma_3$. If a B-value of 0.95 or greater is achieved, saturation of the sample is confirmed, and the sample is ready for testing.

- *Unconsolidated Undrained triaxial tests*

Agarose cylinders were produced as described in section 3.3.1. Agarose gel preparation and specimen moulding, and then demoulded, prepared and tested according to (British Standard 1377, 1990a). For these tests the samples were wrapped in an impervious membrane and confined between impervious end caps before being introduced into the triaxial cell and pressurized with water. This allows maintenance of the same moisture content before and after the test. The kaolinite clay samples were also demoulded and tested to failure following the same procedure.

- *Isotropic Consolidation triaxial tests*

In order to measure and control pore pressures and volumes drained from the sample, pressure-volume controllers were attached to the triaxial cell and connected to the top and bottom of the sample. The tests were performed according to (British Standard 1377, 1990b) and the isotropic consolidation behaviour was obtained for samples consolidated at different effective stresses (25kPa, 50kPa, 100kPa, 150kPa and 200 kPa). The back pressure was set to 300 kPa for all the test.

Note that for this test, special caps including porous stones were placed either side of the sample which allowed drainage and consequent consolidation.

3.3.6. Oedometer tests

An oedometer test is a type of test used to study the anisotropic – i.e. one-dimensional – consolidation behaviour of saturated specimens.

50mm diameter disks were prepared as described in section 3.3.1. Agarose gel preparation and specimen moulding*,* and tested in accordance to (British Standard 1377, 1990c). Drainage was allowed from both top and bottom of the sample and filter paper was added between the sample and the porous stone to ensure that no gel entered the pores of the stone during the consolidation stage.

Agarose gel samples were consolidated anisotropically at different consolidation pressures (3kPa, 6kPa, 12kPa, 25kPa and 50kPa) by applying increments of axial stress. At the end of the consolidation test, the samples were unloaded following the same increments as during loading.

3.4. Results and analysis

3.4.1. Effect concentration on gel microstructure

Increasing gel concentration leads to the fibres becoming more densely packed and consequently the pore size being reduced (Stellwagen and Stellwagen, 1995). Depending on the agarose type and the setting temperature, the honeycomb microstructure presents different patterns – especially at lower concentrations – leading to different pore sizes (Narayanan et al., 2006; Tuvikene et al., 2008). In addition, since agarose gels are formed by physical linkages among multiple chains, a distribution of fibre radius also develops, ranging from 1 to 20nm, also affecting the strength of the gels (Johnson and Deen, 1996; Spencer, 1982).

Figure 3-3 shows SEM images of agarose LM gel samples at different concentrations (2%, 4% and 6% m/v), at the same scale. It is clear qualitatively from this figure that increasing gel concentration results in more densely packed fibres and reduced pore size.
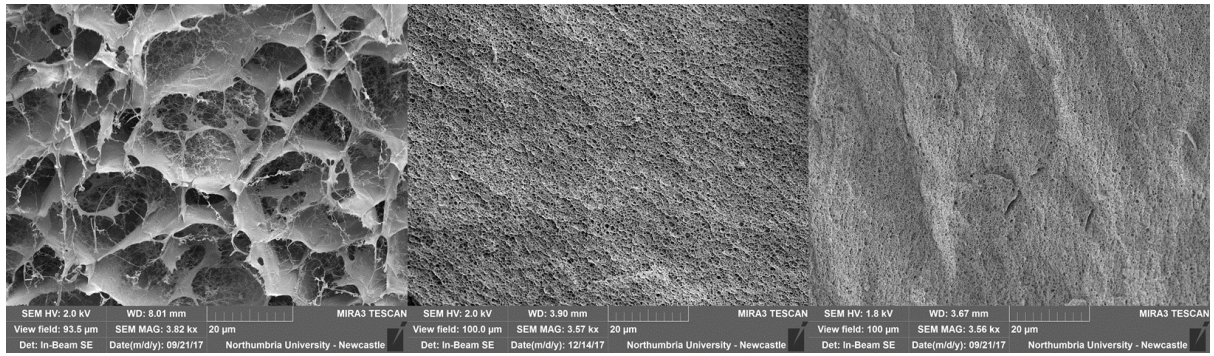
Figure 3-3. SEM images of agarose gel microstructure at 2% m/v (left), 4% m/v (middle) and 6% m/v (right)

The pore diameters shown in each images were measured using ImageJ (an open-source image processing software) and the results are represented in Figure 3-4.

$$y = 148x^{-3.6}$$
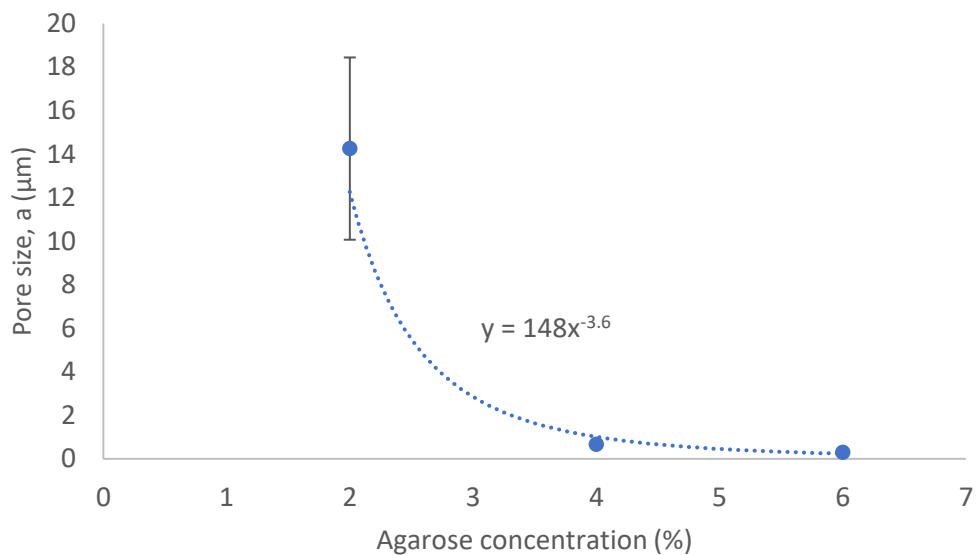
Figure 3-4. Pore size, a, as a function of agarose concentration

The error bars in Figure 3-4 show the variation of pore size that exists at lower concentrations (2% m/v), where pores of sizes ranging 10-20 μm could be measured. However, for higher concentrations of agarose, variations in pore size were very small and the standard deviation of the pore size values measured was very low (and therefore the error bars are almost negligible). Considering the implications for our work, this small variation in pore size will ensure homogeneous distribution and transport/diffusion of nutrients throughout the matrix of the gel.

61

The results from the graph indicate a relationship between the concentration of agarose *C* and the pore size, *a*, of the form:

$$a \sim C^{-\gamma}$$

where *γ* is a constant that depends on the agarose type and the setting temperature(Narayanan et al., 2006) and is found to be 3.6 in this case. This result differs from those found by previous researchers, for example, (De Gennes, 1979; Ogston, 1958) who give values of *γ* between 0.5 and 0.75. This difference may be related to the use of LM agarose over standard agarose.

3.4.2. Porosity and void ratio

(Ogston et al., 1973) developed a method to determine the volume fraction of fibres *φ*, which can be calculated as:

$$\Phi = \frac{C_{agarose}}{(\rho_{agarose} * \omega_{agarose})}$$

(Equation 3-2)

where $C_{agarose}$, $\rho_{agarose}$ and $\omega_{agarose}$ are concentration of agarose in the gel (m/v), dry agarose density and mass fraction of agarose in a fibre, respectively. The last two values can be estimated as 1.64 g/mL (Laurent, 1967) and 0.625 (Johnson et al., 1995). From the volume fraction of fibres, *φ* , the porosity *n* and the void ratio *e* can be obtained with the following expressions (Pluen et al., 1999):

$$n = 1 - \phi$$

(Equation 3-3)

$$e = \frac{n}{1 - n}$$

(Equation 3-4)

The moisture content – i.e. the relationship between the amount of water and the amount of dry solids of a sample – can be also be calculated according to the following expression:

$$w = \frac{m_w}{m_{dry}}$$

(Equation 3-5)

where m_w and m_{dry} are the mass of water and mass of dry solids, respectively.

However, in reality the moisture content might slightly vary due to possible water evaporation during sample preparation. Hence, the moisture content was also obtained experimentally for cylinders (50mm in diameter and 20mm in height) of agarose gel, according to (British Standard 1377, 1990d).

Additionally, an experimental void ratio can also be obtained with the relationship between void ratio, moisture content and specific gravity (G_s) for a saturated soil (Smith, 2014):

$$e = w * G_s$$

(Equation 3-6)

where w is the water content and G_s is the specific gravity of dry agarose (1.64). Table 3-2 represents the theoretical and the experimental values obtained for the porosity, void ratio and moisture content of 6% m/v agarose LM gel.

	Porosity, *n*	Void ratio, *e*	Moisture Content, *w*
Theoretical	0.94	16.1	16.7
Average Experimental	0.96	26.0	15.8

Table 3-2. Theoretical and experimental values of porosity, void ratio and moisture content of 6% concentration agarose LM gel

3.4.3. Strain-stress relationship

The shear strength of 6% m/v agarose samples was initially determined by performing Unconfined Compression tests. The undrained shear strength, or C_u , was obtained by dividing the value of the Unconfined Compression, or q_u, by 2, as described in (British Standard 1377, 1990a). The results obtained are presented in Table 3-3.

Sample	Undrained Shear strength, c_u (kPa)	Maximum strain (%)
1	25.0	22
2	21.5	22
3	24.1	24

Table 3-3. Undrained shear strength and maximum axial strain obtained from the Unconfined Compression tests

The average undrained shear strength obtained from the Unconfined Compression tests was **23.5 kPa** and the average maximum vertical strain was **22.7%**. Figure 3-5 shows one of the agarose samples while being tested. As it can be appreciated, the vertical strains developed are considerably large, leading to an increased cross-sectional area. Furthermore, water drainage can also be observed due to the increase in water pressure generated within the sample.
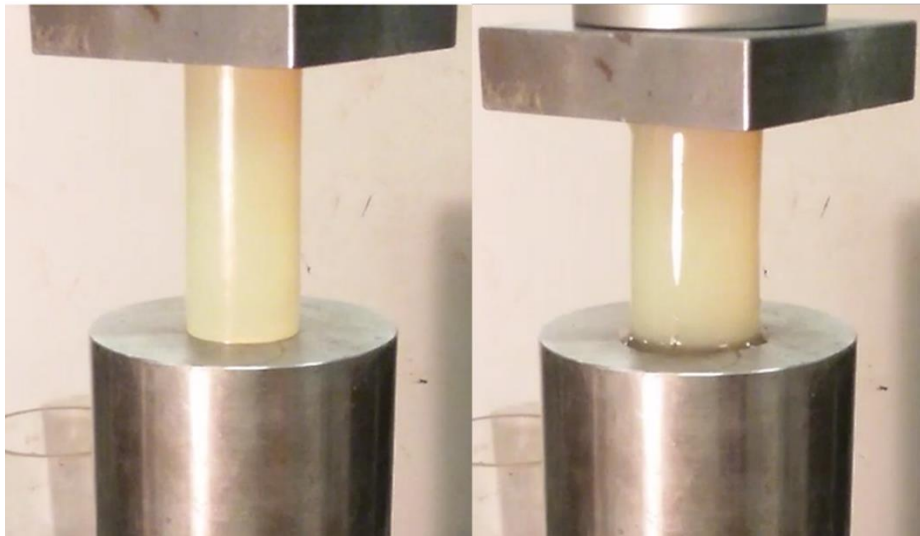
Figure 3-5. Agarose gel sample being tested

Additionally, Unconfined Compression tests were also performed on a range of samples produced with several agarose concentrations, and it was confirmed that increasing the concentration of agarose leads to stronger gel samples (see Figure 3-6). Note that no replicates were taken for this experiment (except for the 6% concentration samples,

where three replicates were tested) and, therefore, the results only provide an estimation of agarose strength at different concentrations.
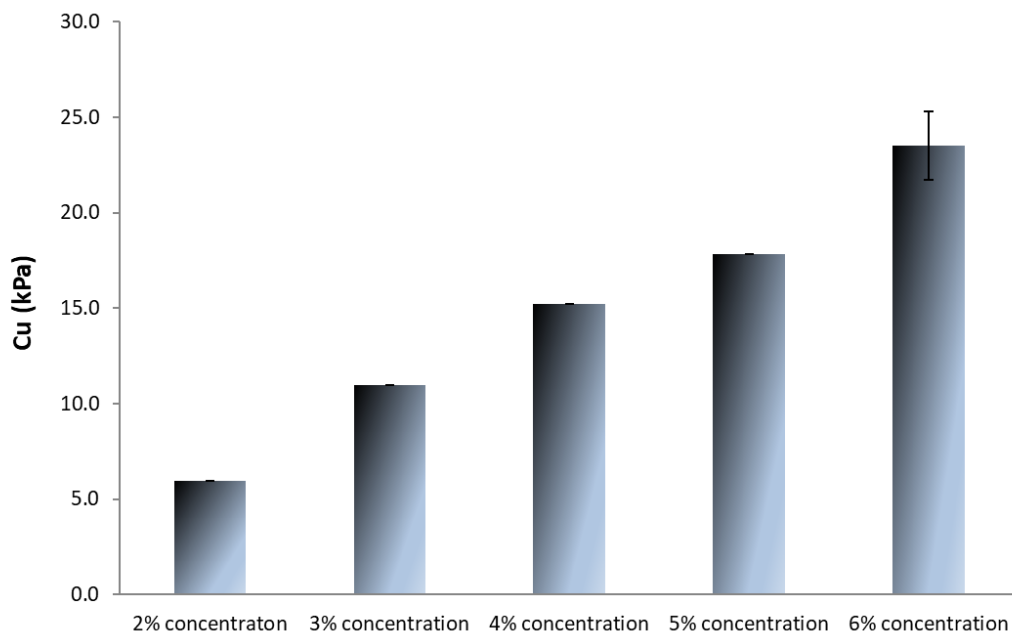
Figure 3-6. Increase in Undrained shear strength by increasing agarose concentration (results obtained from the Unconfined Compression tests)

Unconfined Compression tests provided an estimation of the strength of 6% m/v agarose samples as well as an indication of the deformation behaviour upon loading. However, this type of test was not appropriate to obtain an accurate representation of the stress-strain relationship of the gel due to the lack of confinement – causing the specimens to slide out of the load ring before reaching shear failure. Therefore, these results, and the ones presented in Table 3-3, were only preliminary and were not considered further in the characterisation of the gel.

Unconsolidated Undrained Triaxial (UUT) tests were then performed to agarose gel samples in order to analyse their stress-strain relationship upon loading. This type of test applies a radial stress to the specimens, thus preventing any horizontal movement of the gel cylinders throughout the duration of the test. Saturation of the samples was confirmed before beginning the shearing stage by measuring the increase of pore pressure under undrained conditions and ensuring the Skempton's B-value was higher than 0.95, as

described in section 3.3.5. Triaxial tests. Figure 3-7 shows how the B-value increases over time for a sample confined at 200 kPa.
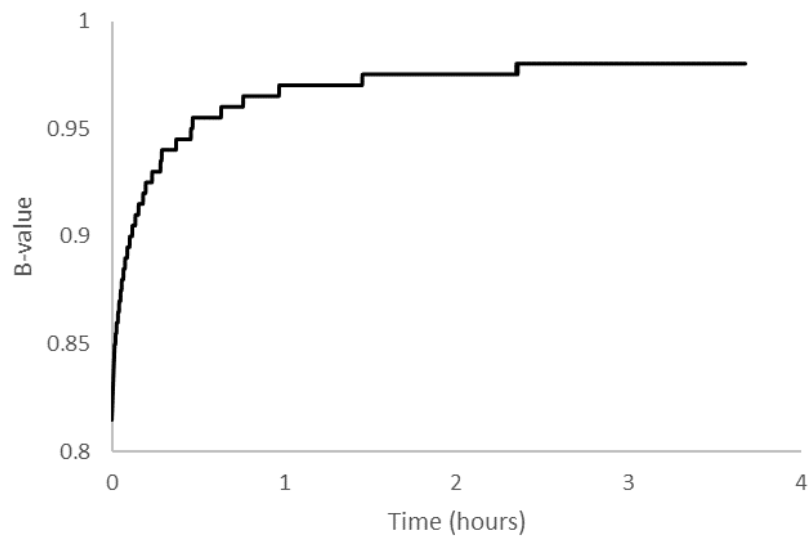
Figure 3-7. Evolution of the Skempton's B-value over time

The stress-strain relationship for samples at different confining pressures is presented in Figure 3-8, along with an inset photo showing the failure plane of two agarose LM samples. As it can be seen from Figure 3-8, the maximum deviator stress (σ_1 - σ_3) increases with confining pressure (35.5% between the samples tested at 100kPa and 500kPa). In addition, the elastic modulus also increases with confining pressure (31.7% higher for the sample tested at 500kPa in comparison to the sample tested at 100kPa).

Considering Mohr's circle theory in soils, an increase in confining pressure should not affect the undrained shear strength value C_u of the material. However, the results from the UUT tests performed on agarose gel show a different behaviour, where a significant increase in undrained shear strength occurs as the confining pressure is increased. The reasons for this abnormal behaviour are currently unknown and further analysis will have to be performed in the future to explore this behaviour. However, it is believed that the formation of leaks due to the high confining pressures and the consequent consolidation of the samples might be associated to this phenomenon.

The results for undrained shear strength, maximum strain and elastic modulus for each of the specimens were obtained as explained in (British Standard 1377, 1990a) and are summarised in Table 3-4. In the absence of further understanding of the gel's elastic behaviour upon loading, the average values were considered for further analysis. These average values are **27 kPa** for undrained shear strength, **18%** for maximum strain and **309 kPa** for the modulus of elasticity.
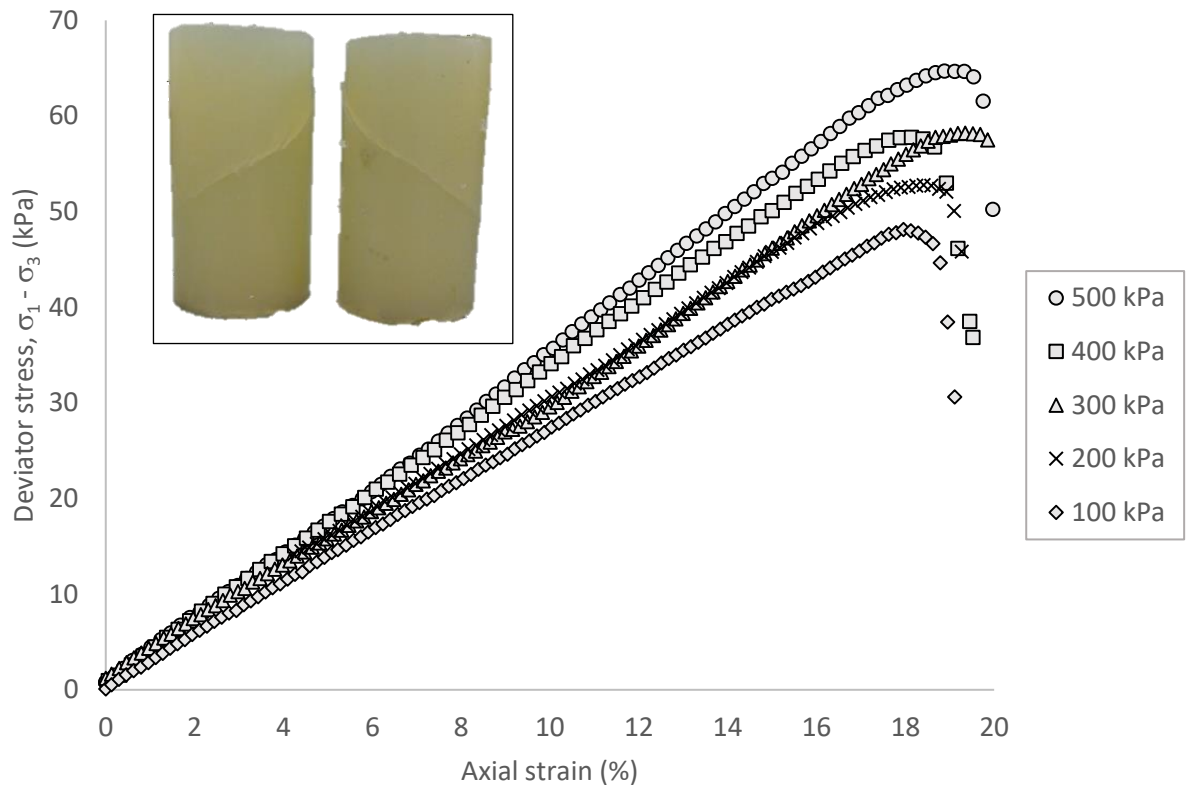
Figure 3-8. Stress-strain relationship of agarose LM gel at different confining pressures, with samples showing failure surface inset

Confining pressure (kPa)	Undrained Shear strength, c_u (kPa)	Maximum strain (%)	Elastic modulus (kPa)
100	23	18	268
200	25	18	297
300	28	19	299
400	28	18	328
500	31	19	353

Table 3-4. Shear strength, maximum axial strain and elastic modulus of 6% m/v agarose gels

Agarose LM gel samples were also loaded to different levels of axial strain (2,4,6,8 and 10%) under a confining pressure of 500kPa, and immediately unloaded, as it can be seen from Figure 3-9. The residual/plastic axial strains developed after unloading are also summarised in Figure 3-9.

Sample loaded to	Plastic strain developed
2% strain	0.18%
4% strain	0.4%
6% strain	0.74%
8% strain	1.07%
10% strain	1.29%
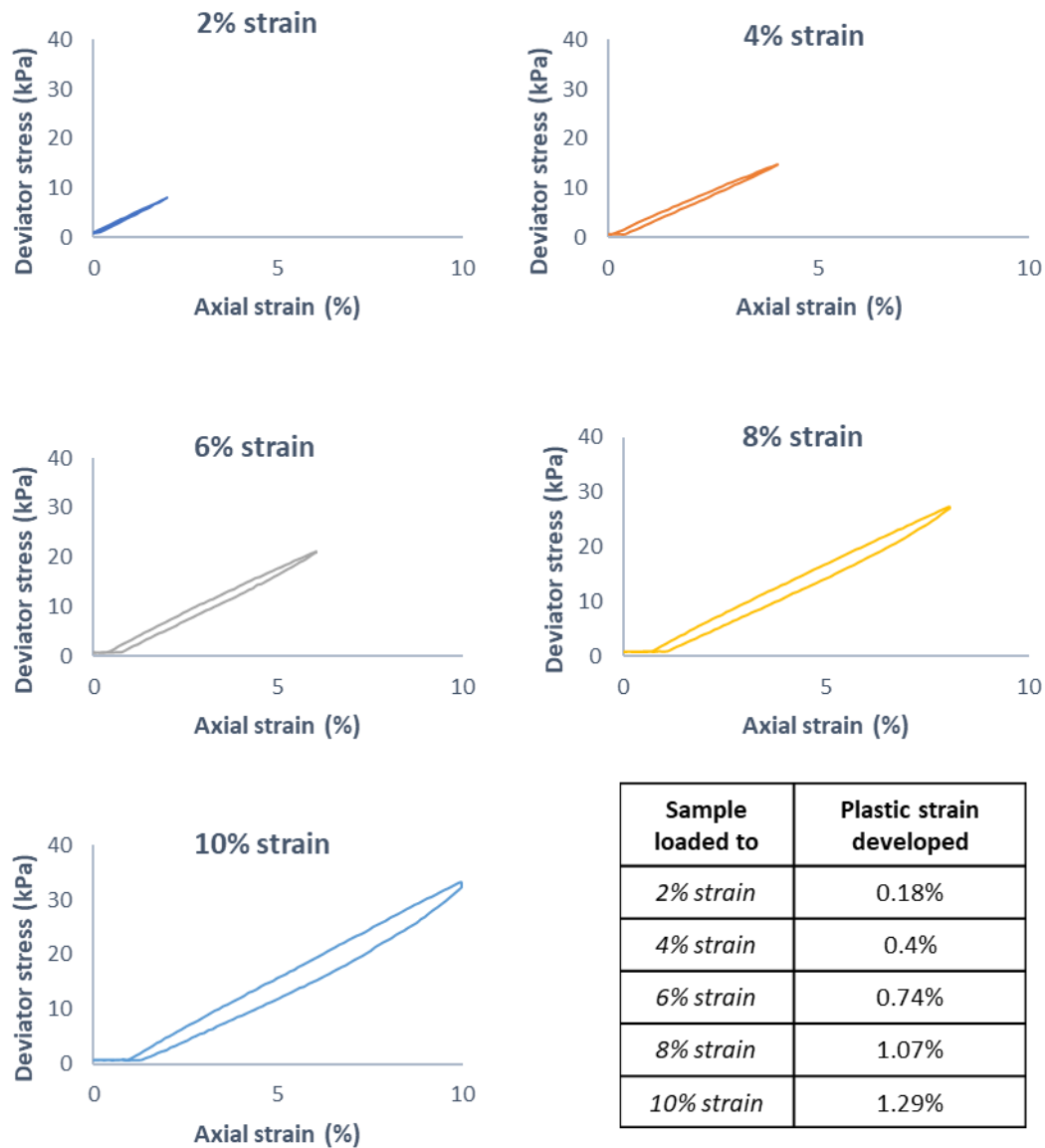
Figure 3-9. Loading and unloading behaviour at different strain levels

These results show that agarose LM gel presents short term elasto-plastic behaviour and permanent strains develop. Greater residual strains also develop at higher strain levels. However, these values were obtained with an immediate unloading of the specimens and,

therefore, the plastic strains generated might potentially increase if the load is applied for longer periods of time.

3.4.5. Consolidation

Terzaghi (1943) defined consolidation as *"every process involving a decrease of the water content of a saturated soil without replacement of the water by air"*. This decrease in water content occurs due to a change in the volume of voids when applying an effective stress to a compressible soil. Due to the fully saturated nature of agarose gels, consolidation is expected to occur when an effective stress is applied, leading to drainage of water through their porous structure. On one hand, the *isotropic consolidation* behaviour of the gels was analysed by performing consolidation tests on a triaxial cell. On the other hand, the *anisotropic consolidation* behaviour was analysed using an oedometer cell.

- Isotropic consolidation

Determining the isotropic consolidation behaviour of agarose LM gel was found to be problematic as the volume change did not occur isotropically – the cross-sectional area near the drainage ends decreased considerably in comparison to the average cross-sectional area (Figure 3-10). This phenomenon is presumably related to an elevated effective stress generated near the drainage end and the consequent large volumetric strains occurring in the agarose gel upon consolidation. Several samples were consolidated under different effective stresses over a 21 day period and all of them showed the same behaviour, as shown in Figure 3-11. A very high magnitude of volume change was measured and all tests had to be stopped manually before reaching a final degree of consolidation. There was an initial non-linear rate of volume change, possibly due to the reduced cross-sectional area and this became linear after a few days.

Figure 3-10. Deformation agarose sample during isotropic consolidation
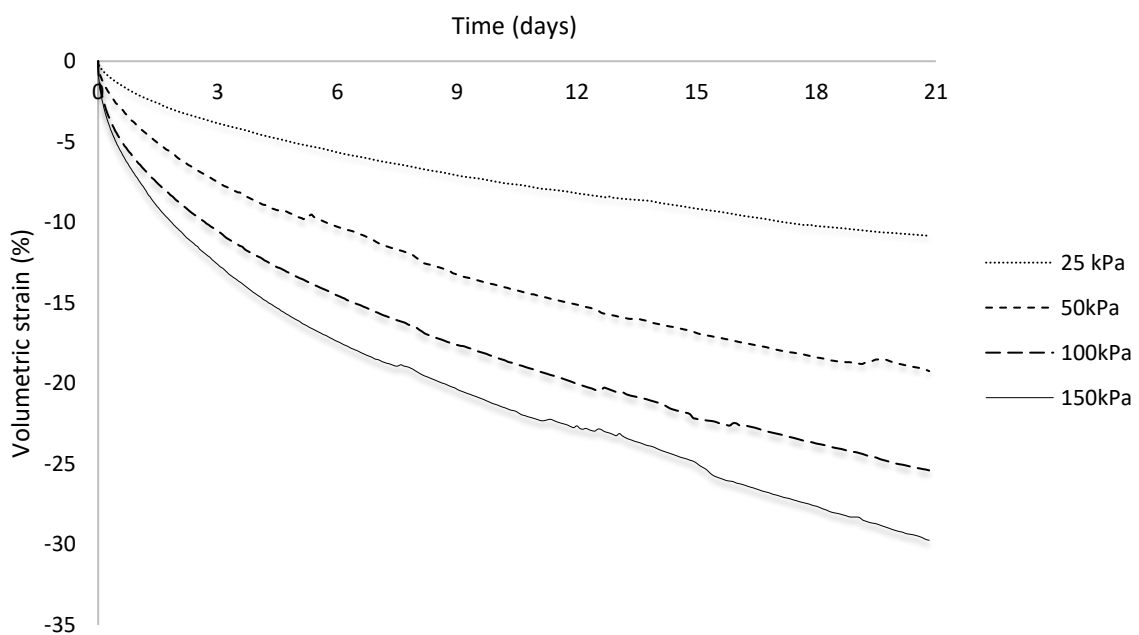
Figure 3-11. Samples isotropically consolidated at different effective stresses

Therefore, it is suggested that this method of consolidation analysis is not appropriate due to the large deformations occurring near the drainage end, causing the sample to generate a non-constant cross-sectional area, as well as not being time-efficient due to the long consolidation process.

- *Anisotropic consolidation*

The samples tested in the oedometer cell (one-dimensional consolidation) showed a different behaviour than those tested isotropically. The rate of axial strain change in the

70

samples decreased for every stage as consolidation occurred, allowing calculation of the coefficient of consolidation. Figure 3-12 shows all the stages of an agarose gel sample consolidated anisotropically at 3, 6, 12, 25 and 50 kPa, including both the loading and unloading stages.

Taylor's method (Taylor, 1948) for one-dimensional consolidation was used to calculate the coefficient of consolidation, c_v for each loading stage. This method is based on the approximation that the relationship between axial displacement and time is parabolic for degree of consolidation < 60%, therefore the relationship between the axial displacement and the square root of time is linear. Secondary consolidation is also assumed to be negligible for a degree of consolidation > 90%.
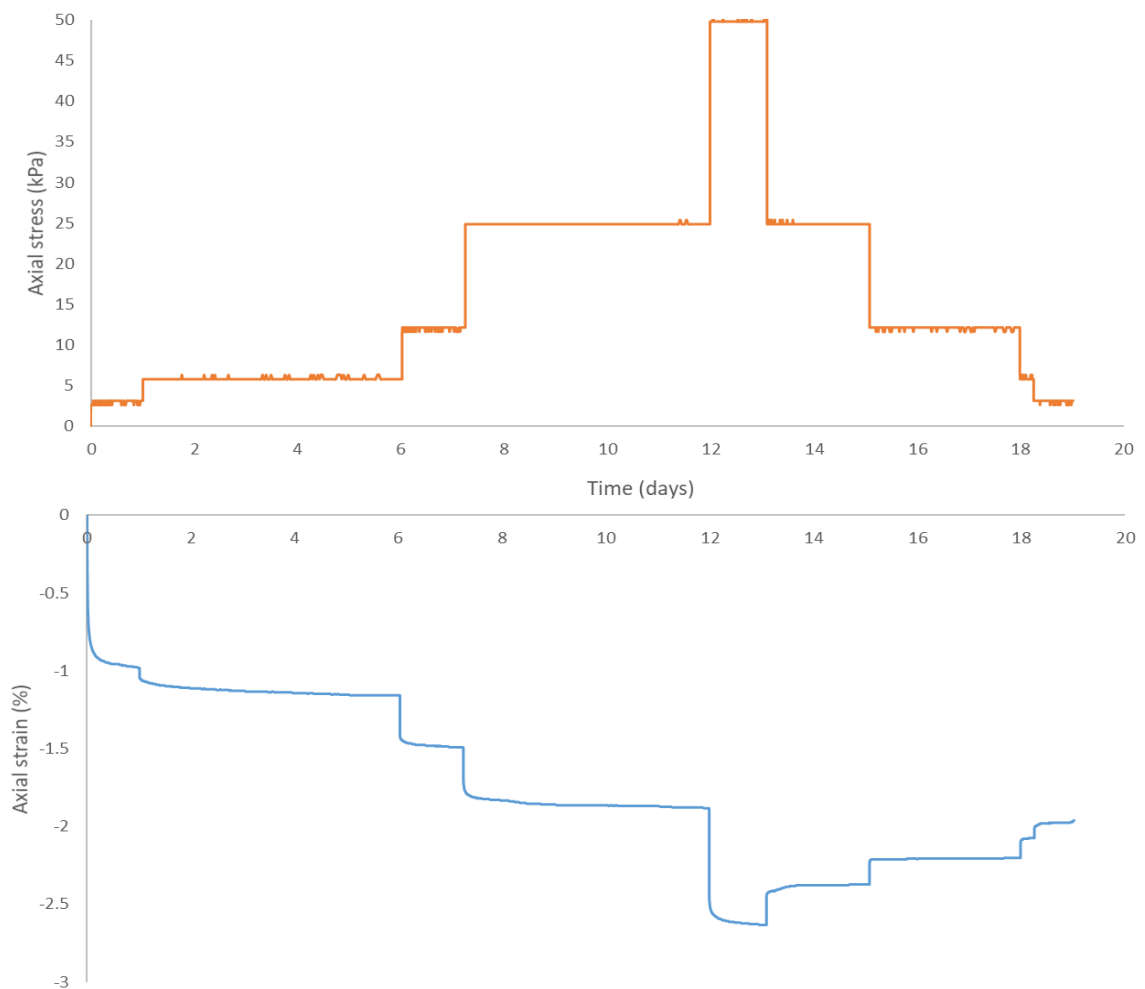
Figure 3-12. Sample consolidated at different stress levels. Top: stress v time. Bottom: axial strain v time

Thus, c_v was calculated using t_{90}, according to the following expression (British Standard 1377, 1990b):

$$C_v = \frac{0.446 * \overline{H}^2}{t_{90}}$$

(Equation 3-7)

where $\overline{H}$ is the average height of the specimen between the start and the end of the consolidation stage and t_{90} is the time for 90% of consolidation. Figure 3-13 shows the steps used to derive the value of t_{90} for one of the consolidation stages. Several tests were performed to 6% m/v agarose the samples, and the coefficient of consolidation was found to range between 0.1-1.36 m^2/year.
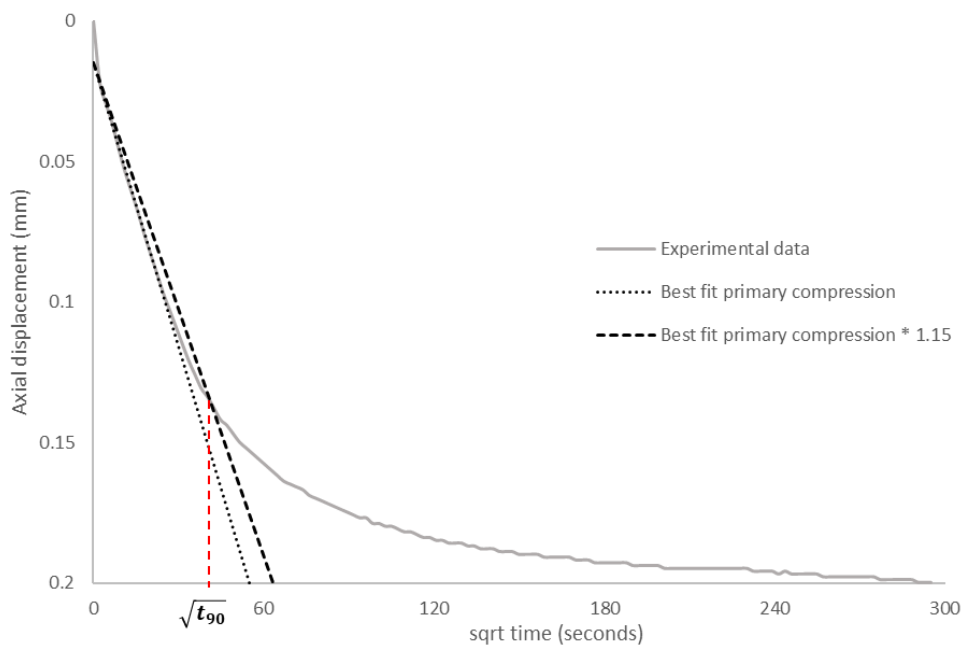
Figure 3-13. Derivation of t_{90}

Additionally, the coefficient of volume compressibility was calculated according to (Equation 3-8) (British Standard 1377, 1990b):

72

$$m_v = \left(\frac{H_2 - H_1}{H_1}\right)\left(\frac{1000}{P_2 - P_1}\right)$$

(Equation 3-8)

where H_2 and H_1 are the height of the specimen at the end and start of the load increment, and P_2 and P_1 are the pressures applied to the specimen for the previous and the considered loading stage, respectively. The results obtained were found to range between 1.82 and 4.78 m²/MN.

3.4.6. Effect of consolidation on microstructure

5 mm per side cubes were extracted from one of the samples isotropically consolidated for 21 days at 100kPa and were prepared for SEM inspection as described in section 3.3.3. Scanning Electron Microscope (SEM) imaging. Figure 3-14 shows the microstructure of an unconsolidated sample and a sample consolidated for 21 days. It can be clearly seen how the structure is denser and the sizes of the pores are smaller for the consolidated sample than the unconsolidated sample, due to the drainage of water during consolidation. This reduction in pore size is expected to result in a consequent decrease in permeability.
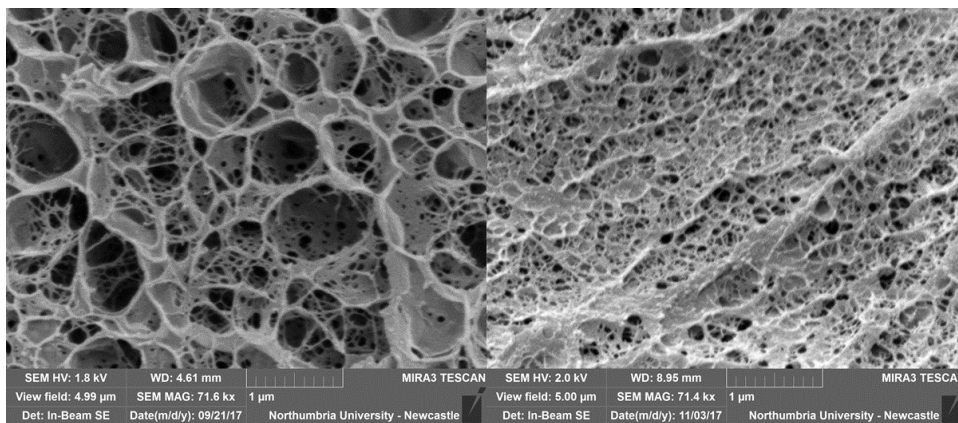
Figure 3-14. Microstructure of consolidated (right) and unconsolidated (left) agarose LM gel

The average pore size for the samples consolidated isotropically at 100kPa for 21 days was measured using the ImageJ software and it was found to be 0.07 μm, 76.7% lower than the non-consolidated samples (approximately 0.3 μm). The difference in pore size upon

consolidation is considerably large after 21 days, and it is therefore expected to be greater if full consolidation was achieved.

3.4.7. Permeability

Permeability is particularly important as it determines the transport and distribution of nutrients and microbes through the porous structure. In order to estimate the vertical permeability, k_v, of 6% m/v agarose gels the following expression derived from Darcy's law was used:

$$k_v = \frac{1.63 * q * L * 10^{-4}}{A * (p_1 - p_2)}$$

(Equation 3-9)

where q is the mean rate of flow through the bottom of the specimen, L is the length of the specimen prior to testing, A is the area of the specimen prior to testing and $p_1 - p_2$ is the pressure difference, or consolidation pressure in this case. Thus, the vertical permeability k_v for 6% m/v agarose LM gel was found to range between $4.1 \ x \ 10^{-11}$ and $8.8 \ x \ 10^{-11}$ m/s depending on the effective stress applied, as it can be seen from Table 3-5.

Pressure gradient (kPa)	Flow rate (mL/min)	Specimen length (mm)	Area (mm^2)	k_v (m/s)
25	0.000088	74.35	1046.35	4.1x10^{-11}
50	0.00038	75.40	1046.35	8.8x10^{-11}
100	0.00041	74.96	1081.03	4.6x10^{-11}
150	0.00045	75.60	1086.86	3.4x10^{-11}

Table 3-5. Values used to calculate the vertical permeability

It should be noted that these results do not express measured values of the vertical permeability, but an estimation made from the amount of fluid drained from the samples. However, they provide a good indication of the permeability and allow a comparison with soils.

Additionally, according to Terzaghi's consolidation theory (Terzaghi, 1943), the total amount of water drained from the soil depends on the final amount of settlement, which in turn depends on the compressibility of the soil:

$$C_v = \frac{k_v}{(m_v * \gamma_w)}$$

(Equation 3-10)

where γ_w is the specific weight (or unit weight) of the pore fluid which in the case of our samples is distilled water and its value is approximated to 9.807 kN/m^3. Using this relationship and taking both the lower and upper limit values for C_v and m_v calculated in the previous section, the vertical permeability of 6% m/v agarose gels was found to range between **8.29E-11** and **3.93E-9 m/s**, values reasonably similar to those found using Darcy's equation.

3.5. Discussion: comparison to saturated cohesive soils

An experimental investigation was performed in order to analyse the mechanical and physical properties of 6% m/v agarose LM gel and Table 3-6 summarises the results and provides a comparison to saturated cohesive soils for each of the properties.

Properties	Values	Comparable to
Water content (%)	1583%	-
Porosity	0.96	-
Void ratio	26.0	-
Pore size (µm)	0.21 – 0.39	Homogeneous clay soils
Shear strength (kPa)	27	Medium-firm saturated cohesive soils
Maximum axial strain (%)	18	Medium-firm saturated cohesive soils
Elastic modulus (kPa)	309	-
Coefficient of consolidation ($m^2/year$)	0.10-1.36	Organic silts (1.8 $m^2/year$), glacial clays (2.35 $m^2/year$) and Chicago silty clays (2.7 $m^2/year$) [61]
Coefficient of volume compressibility (m^2/MN)	1.82-4.78	Sensitive clays (0.9 m^2/MN) and highly organic soils (1.5 m^2/MN) [61]
Vertical permeability (m/s)	4.1– 8.8x 10^{-11}	Homogeneous clay soils

Table 3-6. Physical and mechanical properties 6% m/v agarose gels and comparison to soils

It can be seen from Table 3-6 that there are a number of similarities between agarose LM gel and clays, silts and peats, particularly the pore size, shear strength and coefficient of consolidation. The permeability values obtained from the tests on agarose LM gel are also comparable to clays, as shown more clearly in Figure 3-15. The permeability of agarose LM is also expected to be higher in specimens produced with lower concentrations of agarose (Narayanan et al., 2006; Pernodet et al., 1997).
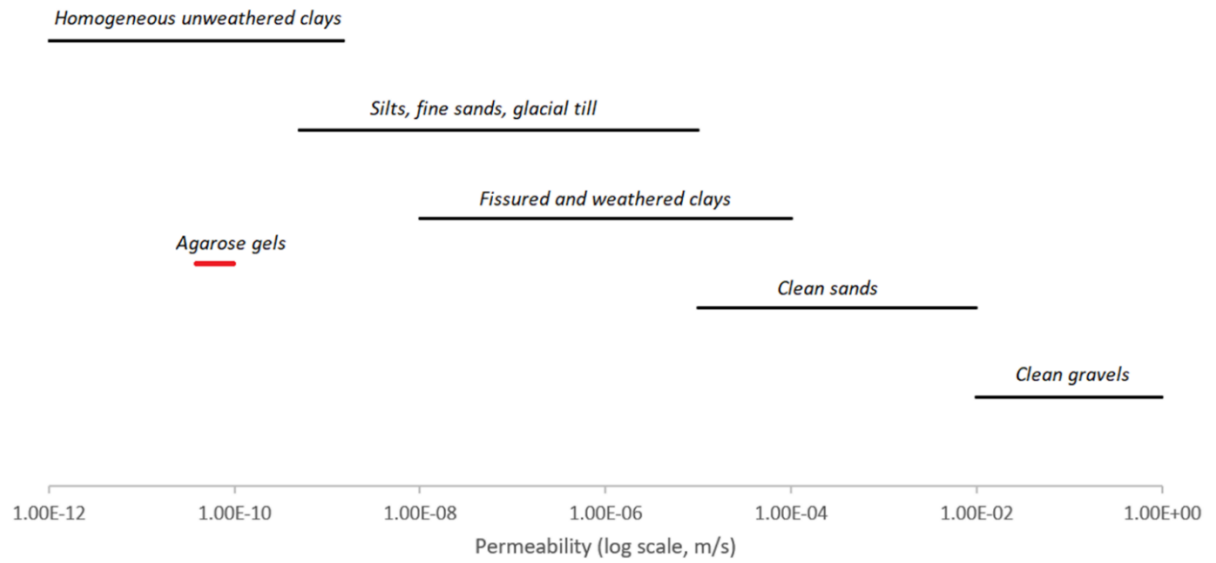
Figure 3-15. Permeability chart for soils and 6% m/v agarose gel

(adapted from Carter and Bentley, (1991))

Agarose LM gel has a three-dimensional fibrous microstructure that, although it is not granular, has a porous structure similar to soils, especially organic soils such as peats. Figure 3-16 shows an SEM image extracted from Rezanezhad et al. (2016) which confirms the similarities between agarose gels and peat soils in relation to the porous structure. The size of the pore in peat soils is of the same magnitude as the pores present in 2% m/v agarose gels (see Figure 3-3 for a comparison).
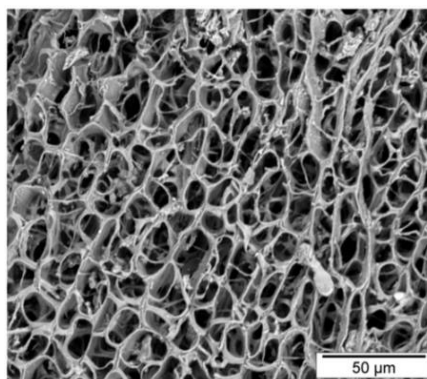
Figure 3-16. SEM image showing the porous microstructure of peat soils

(after Rezanezhad et al. (2016))

However, there are also significant differences between the properties of agarose LM gel and soils. Agarose LM gel has a significantly higher water content than any soil and consequently a much larger coefficient of volume compressibility than most soils. Only sensitive clays and highly organic clays and peats present similar values (Carter and Bentley, 1991). This is also demonstrated by the isotropic consolidation behaviour of agarose.

The stress-strain relationship of one of the kaolinite clay samples was analysed and compared to the behaviour of 6% m/v agarose gels. This comparison is represented in Figure 3-17.
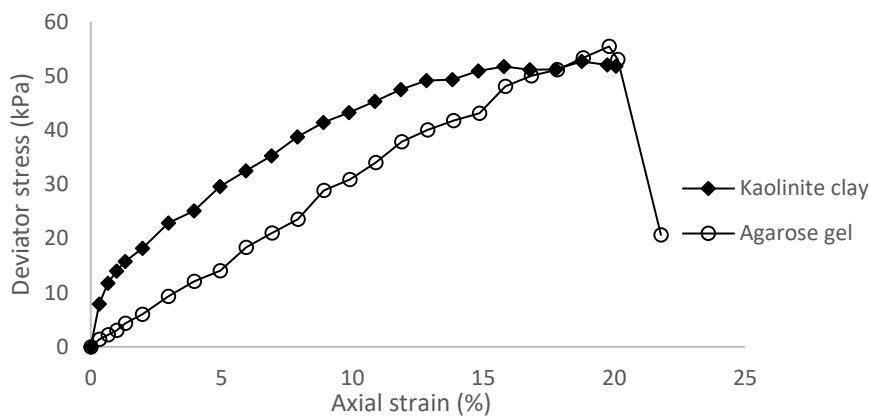
Figure 3-17. Comparison stress-strain relationship agarose gel v kaolinite clay

Note that the density of this particular clay sample was 1.78 Mg/m^3 and the moisture content was 0.44 (or 44%). The shear strength, C_u, of the clay sample was found to be approximately 25-26 kPa and the maximum strain was found to be 20%. Both values are similar to that present in agarose gels. Additionally, the relationship is linear until failure (about 18-19% axial strain) for agarose gels and non-linear for the kaolinite clay samples, where yield point was reached at 12-14% deformation and failure at 20%, as established by (British Standard 1377, 1990a). In addition, according to (Bowles, 1996), the Young or elastic modulus of very soft clays ranges between 2 and 15 MPa, as it can be seen from the slope of the graph at small strains (<1%). Thus, it can be confirmed that the elastic modulus (i.e. stiffness at the elastic region) is significantly higher than agarose gels (0.3

MPa), however, as plastic strains develop in the clay sample, the stiffness seems to be similar to that of agarose gels.

However, the above-stated similarities between clay and agarose gel have to be treated very carefully since the two materials are only comparable for certain conditions. For instance, if properties of the tested clay samples such as density or water content were different, the samples would have exhibited a completely different testing behaviour and therefore different stress-strain relationship.

Regarding plasticity of the gels, it is clear from Figure 3-9 than gels experience both elastic and plastic deformations. For instance, the sample loaded at 10% strain showed a 8.71% elastic recovery upon unloading in comparison to the 1.29% plastic strain developed. This behaviour confirms that the elastic range in agarose gels is considerably higher than in soils, where the elastic behaviour only occurs at very small axial strains (<1%).

Additionally, SEM analysis (see Figure 3-14) showed that a more densely packed structure is formed during consolidation, suggesting that shear strength and stiffness of agarose gels will increase as water is drained upon loading, which is similar to the behaviour of most soils.

3.6. Concluding remarks

The development of bacteria-based engineered responsive systems often requires laborious testing procedures and monitoring of the performance of the microbes in a contamination-free environment. This thesis proposes a gel-based prototype system where the testing conditions can be controlled with accuracy and the response of the system to external stimulus can be easily monitored. Agarose gel is believed to be the ideal medium for such prototype testing system due to its ability to provide great control of the chemical composition of the environment alongside a controlled simulation over the mechanical behaviour. Thus, an experimental investigation was performed to agarose LM gels in order to obtain a thorough understanding of their physical and mechanical properties relevant for the development of such prototype system.

The testing programme confirmed that this type of gel has similar properties to some saturated cohesive soils such as soft clays or peats. It has also been found that the permeability and consolidation behaviour of agarose LM gel is very similar to that occurring in soft saturated soils. It can therefore be confirmed that agarose gels are suitable to model the geotechnical behaviour of saturated cohesive soils for our particular application, and it is expected that an agarose-based physical demonstrator will mimic some of these soils properties such as stress distribution, pore pressure dissipation or deformation upon loading.

As a conclusion, this chapter has successfully performed an investigation on the physical and mechanical properties of agarose gels needed for the development of the computational model and future implementation of the system in a gel-based physical demonstrator.

Next chapter will focus on understanding the growth and distribution of bacteria colonies within the matrix of agarose gels.

Chapter 4

Bacteria Growth in Agarose Hydrogel

4.1. Introduction

As described in Chapter 3, agarose gels are a purified version of agar gels and do not carry any biological information – they do not interfere in the behaviour of microorganisms grown within their matrix. Additionally, their lower gelling temperature prevents causing thermal shock to microorganisms suspended in the liquid hydrogel. The porous structure of agarose gels allows bacteria motility and seeded cells are expected to slowly migrate through the pore throats and form networks of colonies. The microbial growth rate of bacteria colonies in the three-dimensional matrix of agarose hydrogels, however, is believed to differ from the growth in standard liquid cultures, mainly due to the restrictions of space and oxygen availability. Hence, if agarose gels are going to be implemented as the growth medium to develop and demonstrate engineered responsive bio-systems, a good understanding of the growth behaviour and motility of bacteria colonies within their matrix is essential.

Little previous research exists on the growth behaviour of different types of bacteria in 3D hydrogels. One such study used agar as the growth medium and monitored the growth of colonies in 24-well plates using absorbance measurements (Tuson et al., 2012). This method, however, does not monitor the growth rate of individual colonies seeded within the gel, but rather provides an estimation of the turbidity of the sample, through optical density (OD) measurements. These turbidity measurements can then be associated to cell density; however, the inconvenience of this method is that not only living cells contribute to increase the OD of the samples but also dead cells and metabolic waste.

Our gel-based system is expected to simulate with accuracy the concentration of cells throughout a volume of gel. Therefore, a different growth monitoring method must be employed.

This chapter describes the development of a new method to prepare 3D homogeneously seeded agarose gels and monitor their growth using the fluorescence behaviour of certain engineered strains. This method allows measurements of the fluorescence of individual colonies, which can then be associated to cell concentration values. Additionally, the effect of external stimulus on the cell behaviour can also be monitored using fluorescence measurements.

The differences between *B. subtilis* and *E.coli* in relation to their growth and distribution in hydrogels are also discussed in this chapter. The chapter also describes the effects of different environmental conditions on the growth behaviour, cell distribution and colony formation throughout a gel volume. The growth behaviour of the selected bacteria strains in liquid media (rich and minimal) is also assessed, since liquid cultures are used to grow bacteria previous to inoculation into the 3D hydrogels. In this way, the amount of cells seeded within a volume of gel can be estimated with a relatively high degree of accuracy.

The effect different environmental conditions have on the growth rate was first analysed in small hydrogel samples (30mm Petridishes). The reasoning for that was to assess whether the method to grow bacteria in the hydrogels and the techniques utilized to monitor the growth rate were adequate for the analysis. Once it was confirmed that our method could assess the impact of different conditions on the growth behaviour, an experimental programme was performed where the growth in large hydrogel samples (100mm height cylinders) was monitored. Finally, the different growth profiles obtained from the experiments in cylindrical samples were converted into numerical equations using non-linear regression, where mathematical expressions were generated from series of data points. These expressions will ultimately be integrated in the computational model in order to represent and predict the distribution and formation of bacterial colonies over time in 3D agarose gels (*see Chapter 5 for more details*).

The chapter is divided into four sections: *Materials,* where the bacteria strains and the other components used in the experimental program are described, *Methods,* which describes the techniques and methodology employed to grow and monitor liquid and gel cultures; *Results and Discussion*, where the main results obtained are analysed and discussed; and *Conclusions*, where the outcomes of the investigation and their relationship with the overall research are discussed.

Additionally, Table 4-1 presents an overview of the experiments described throughout the chapter.

Experiment	Specification	Location
Effect of agarose concentration		Figure 4-12
Initial concentration of cells (serial dilution)		Figure 4-11
B. subtilis growth in liquid media	*Comparison of minimum media v rich media*	Figure 4-9
	Minimum media	Figure 4-10
Comparison colony formation of *B. subtilis* v *E. coli*		Figure 4-8
B. subtilis growth in agarose hydrogel (small samples)	*Effect of initial concentration of cells*	Figure 4-14 and Figure 4-15
	Effect of incubation temperature	Figure 4-16
	Effect of pH	Figure 4-17
B. subtilis growth in agarose hydrogel (large cylindrical samples)	*Differential growth rate with depth*	Figure 4-20
	Effect of initial concentration of cells	Figure 4-21, Figure 4-22 and Figure 4-23
	Effect of incubation temperature	

Table 4-1. List of experiments Chapter 4

4.2. Materials

4.2.1. Agarose LM

The type of agarose used for the experimental program is agarose LM (Low Melting Point). For more information about this type of agarose and its properties see section 3.2.1. Agarose composition and formation*.*

4.2.2. Bacteria strains

Escherichia coli (E. coli)

The gram-negative bacterium *E. coli* was chosen to study microbial growth in agarose gel. *E. coli* is a facultative aerobic, rod-shaped prokaryotic organism. Cells are typically approximately 0.25-1.0 μm width and 2 μm length. The strain HS524 was selected for this

study. This strain contains the protein GFP (Green Fluorescent Protein) attached to a plasmid, allowing visualisation of the cells under a fluorescent microscope (Ouzounov et al., 2016).

Bacillus subtilis (B. subtilis)

The gram-positive bacterium *B. subtilis* was also used in this study. LH158 was the strain selected which also expresses constitutively fluorescence due to the protein GFP attached on the chromosome. Similar to *E. coli*, this strain of bacteria is rod-shaped and the dimensions of the cells are 0.8-0.9 µm width and 3.8-4 µm length.

4.2.3. Growth media

Rich media

Lysogeny Broth or *Luria Broth* (Miller, Sigma Aldrich, UK) – traditionally named LB –, containing 10g/L Tryptone, 10g/L NaCl and 5g/L Yeast Extract, was used as the highly nutritive growth medium.

Minimal media

Two different media were used to grow cultures under minimal-nutrient conditions. This type of media provides with the minimum set of nutrients needed for bacterial growth, i.e. carbon and inorganic salts. M9 medium was required to grow cultures with *E. coli*, whereas SMM (Spizizen Minimal) medium was used when working with *B. subtilis*. Both media were made up of two different components, the *base* medium (Table 4-2), in which different chemicals were dissolved in distilled water and autoclaved with a sensitive cycle (115°C), and the *complementary salts*, which were prepared by dissolving them in distilled water until the solution was homogeneous and were then filter-sterilised. The complementary salts were stored in a fridge at 4°C. It must be noted that the addition of phosphates to the minimal media will have implications for the biomineralization process due to the precipitation of apatite when mixed with calcium ions. However, for the purpose of this work, the addition of phosphate salts is considered to be acceptable.

Additionally, in order to hinder the formation of spores during the experiments performed at high temperatures (in particular for the *B. subtilis* experiments), glucose was added to the mixture since it is believed that its addition slows down sporulation due to catabolite repression (Schaeffer et al., 1965; Takahashi and MacKenzie, 1981). The recipes to prepare the two minimal media can be seen in Table 4-3.

M9 base	SMM base
- 1 L distilled H_2O	- 2g $(NH_4)_2SO_4$ (*Ammonium sulphate*)
- 30g Na_2HPO_4 (*Sodium phosphate dibasic*)	- 14g K_2HPO_4 (*DiPotassium hydrogen phosphate*)
- 15g KH_2PO_4 (*potassium phosphate monobasic*)	- 6g KH_2PO_4 (*Potassium dihydrogen phosphate*)
- 2.5g NaCl (*sodium chloride*)	- 1g $C_6H_5Na_3O_7.2H_2O$ (*Trisodium citrate dihydrate*)
- 5g NH_4Cl (*ammonium chloride*)	- 0.2g $MgSO4·7H2O$ (*Magnesium sulphate heptahydrate*)

Table 4-2. M9 and SSM base medium composition

M9 minimal medium	SMM minimal medium
- 10mL M9 base	- 10 mL SMM base
- 500 µl 40% *Glucose*	- 125 µl 40% *Glucose*
- 100 µl 1M $MgSO_4$ (*Magnesium sulphate*)	- 100 µl 2mg/mL *Tryptophan*
- 250 µl 20% CAA (*Casamino acids*)	- 60 µl 1M $MgSO4·7H2O$ (*Magnesium sulphate*)
- 50 µl 0.1M $CaCl_2$ (*Calcium chloride*)	- 10 µl 20% CAA (*Casamino acids*)
- 39.1 mL H_2O	- 5 µl 0.22% $(NH_4)_5[Fe(C_6H_4O_7)_2].2H_2O$ / $C_6H_8FeNO_7$ (*Ammonium ferric citrate / ferric ammonium citrate*)

Table 4-3. M9 and SMM media recipes

4.3. Methods

4.3.1. Liquid culture preparation

Prior to any experiment, bacteria liquid cultures were prepared with the required strain of bacteria so that a source of living cells was available. This liquid culture was then used to inoculate living cells into fresh liquid medium or a hydrogel solution to evaluate the growth behaviour. The protocol followed to prepare liquid cultures of bacteria is

explained as follows. On day 1, the surface of a glycerol stock (solution containing living bacteria cells stored at -80°C which is used to store bacterial cultures for a long time) was scratched with a sterile loop and streaked onto the surface of an LB agar plate. The plate was then stored in a static incubator at 37°C (*E.coli*) or 30°C (*B. subtilis*) overnight to promote bacteria growth. On day 2, individual bacteria colonies of similar size should be visible on top of the plate, as illustrated in Figure 4-1.

Figure 4-1. Agar plate containing isolated bacteria colonies

The medium solutions were prepared – as described in section 4.2.3. Growth media – in a 50 mL plastic tube. The $V_{medium}:V_{flask}$ ratio used was 1:5 (i.e. the volume of media did not occupy more than 20% of the flask volume). A single colony was then transferred from the plate into the medium solution using a sterile loop and the plastic tube was then stored overnight in a rotating incubator at 37°C (*E.coli*) or 30°C (*B. subtilis*) and 150 rpm.

B. subtilis cells tend to sporulate (create endospores) if the culture is incubated at 37°C over long periods time. Endospores or *spores* are a dormant form that some types of bacteria adopt when subjected to unfavourable conditions. Therefore, considering the aim of the experiments is to inoculate living cells, all the *B.* subtilis liquid batches were incubated at 30°C in order to minimise endospore formation.

4.3.2. Growth monitoring of a liquid culture

Growth of bacterial cultures refers to an increase in the number of cells in a population and it occurs due to the division of a bacterium into two genetically identical new cells by a process called *binary fission*. The rate at which bacteria grows depends on many parameters including oxygen level, pH, availability of space, amount of nutrients or temperature, amongst others. If nutrients are provided to the growth medium and the right temperature is selected, bacteria cells are expected to divide and grow in number (more details about bacterial growth can be found in *Chapter 2. Literature review*).

Several methods exist for microbial cell growth monitoring in a liquid culture. The methods adopted in our experimental program are *cell count by serial dilution* and *growth monitoring by absorbance*. The former was used to count the total amount of cells present in a liquid culture at a certain time, whereas the latter was used to monitor the growth over a period of time.

- *Cell count by serial dilution*

A serial dilution experiment was performed to count the number of cells present in a liquid culture at a specific time point. The biggest advantage of this method of cell counting is that it only counts viable (i.e. living) cells. This method consists of performing a series of 10-fold dilutions to the original culture by inoculating 1mL of each solution onto 9 mL of cell-free medium. The first step is to transfer 1mL of the overnight culture onto 9mL of medium (Note: autoclaved distilled water can also be used instead). Once the new 10mL solution has been thoroughly mixed, 1mL is taken and transferred into 9mL of medium. This procedure was performed several times, resulting in different solutions with 10-fold change in cell numbers. 100 μL of each solution is then transferred onto the surface of LB agar plates and the inoculum is spread homogeneously across the plate using a sterile glass spreader. The samples are then incubated for 24 hours at 37°C (*E.coli*) or 30°C (*B. subtilis*) inside a static incubator in order to promote bacteria growth.

This method assumes that each colony originates from a single bacterial cell and that the original inoculum (i.e. the overnight culture) is homogeneous. After the 24-hour

incubation period, individual cells will appear on the surface of the plate, allowing cell counting. For the method to be accurate, only counts between 25 and 250 CFU (Colony Forming Unit) are pertinent.

Once the number of CFU has been counted, the expressions to determine the final dilution and the cell concentration (CFU/mL) of a liquid culture at a specific time point are the following:

$$\text{Final dilution} = \frac{\text{Amount inoculum (mL)}}{\text{Final volume (mL)}}$$

(Equation 4-1)

$$\text{Cell concentration} \left(\frac{\text{CFU}}{\text{mL}}\right) = \frac{\text{number colonies on plate}}{\text{amount plated}} * (-\text{Final dilution})$$

(Equation 4-2)

- *Absorbance*

As described in *Chapter 2*, the rate at which bacteria grows over time is not always the same. Hence, a method is needed to measure the number of cells in a liquid culture over a period of time. Bacteria cells absorb and scatter light and, as they grow, the medium becomes turbid and allows the measurement of the absorbance, which is the ability of a substance to absorb light. A spectrometer is a piece of equipment that measures the amount of light that goes through a liquid culture of bacteria (Figure 4-2).

Figure 4-2. Spectrometer used to measure the absorbance of the bacterial culture

Samples were taken from the liquid culture at specific time points and the absorbance was measured. Organic material has high optical density at light with wavelengths of 600 nanometres. The optical density of a sample at 600 nanometres is referred to OD_{600}. The measured OD_{600} of the bacterial culture relative to the OD_{600} of a plain reference sample is the final value adopted for the analysis. The different OD_{600} values obtained for every time point are then mapped onto a graph that represents cell concentration over time and allows estimation of the different growth phases of the bacterial population.

4.3.3. Bacteria-seeded agarose gel preparation

Due to the high water content, agarose gels provide an ideal matrix for cell growth (Johnson and Deen, 1996). A method was developed to create 3D agarose gels homogeneously seeded with bacteria cells, which is similar to that used by Xu et al. (2011).

LM (Low melting and gelling temperature) agarose was used to avoid heat shock of the bacteria cells when inoculated into the liquid gel. The method consisted of preparing a solution of growth medium and agarose at the desired concentration then autoclaving it to dissolve the agarose and ensure homogeneous mixing as well as to sterilise the flask.

The solution was then stored inside a water bath at 40-45°C (just above the gelling temperature) and once it cooled down, the bacteria culture was inoculated into the flask at the desired ratio. The solution was then thoroughly mixed using a mechanical stirrer to ensure homogeneous distribution of the cells and was immediately poured onto 30mm diameter and 10mm height Petri dishes. Due to the viscosity of the gel at high concentrations, the bubbles generated did not migrate instantly to the surface of the solution, and it was decided to wait a few seconds before pouring the solution onto the plates so that the majority of these bubbles disappeared.

The dishes were then stored in a fridge at 4°C for 10 minutes to allow gel formation before they were transferred to an incubator where bacteria growth was promoted at the desired temperature.

4.3.4. Growth monitoring in bacteria-seeded hydrogels

Bacteria cells are expected to divide and grow in number within the matrix of the gel. However, due to the lack of motility and oxygen, the growth rate will differ from that in liquid medium. Agarose gels present a porous microstructure, as explained in chapter 3, however, the size of the pores are not big enough for bacteria cells to swim through. According to Mitchell and Santamarina (2005), the minimum diameter of the pore throat that allows cell motility is 0.4 µm. It can be confirmed from chapter 3 that the pore size of 6% agarose gels varies between 0.21 µm and 0.39 µm. Hence, it is assumed that cell motility is non-existent and that the seeded cells are embedded within the matrix of the gel and bacterial colonies grow in size by breaking the fibres of the gel and expanding.

Additionally, if movement of the cells is hindered, a differential consumption of the nutrients in the gel might develop, i.e. areas where the original cells are seeded might rapidly consume all the nutrients of its surroundings, potentially resulting in starvation and further death. Although diffusion of nutrients through the porous structure will occur, the consumption of nutrients by the microbes might occur at a higher rate, potentially leading to the above-mentioned starvation, and possibly modifying the growth behaviour. However, this behaviour is out of the scope of this thesis and therefore no evidence has been found.

A method was designed to assess the growth behaviour of bacteria cells in agarose gels by using *E. coli* HS524 and *B. subtilis* LH158 (strains containing GFP). This method consists of analysing the amount of fluorescence present in a slice of agarose gel to quantify the cell density over time, and to do that, a laser scanning microscope (e.g. CONFOCAL microscope) is needed.

A CONFOCAL microscope is a type of microscope that uses a technique called *confocal microscopy.* This technique enables the visualisation of 3D stacks due to the action of a pinhole that allows penetration of the light from the laser into the specimen. Thus, a series of two-dimensional images can be captured over the desired depth of the specimen and the reconstruction of this images enables the creation of a three-dimensional structure. The CONFOCAL microscope used was a Leica TCS SPE (Figure 4-3).

Figure 4-3. Leica TCS SPE microscope

A series of images were taken at different depths within the gel to provide a 3D representation of the bacterial distribution across the sample. Figure 4-4 shows a screenshot of the software used to obtain and process the visualisations (LAS X) alongside all the parameters used to generate 3D stack.
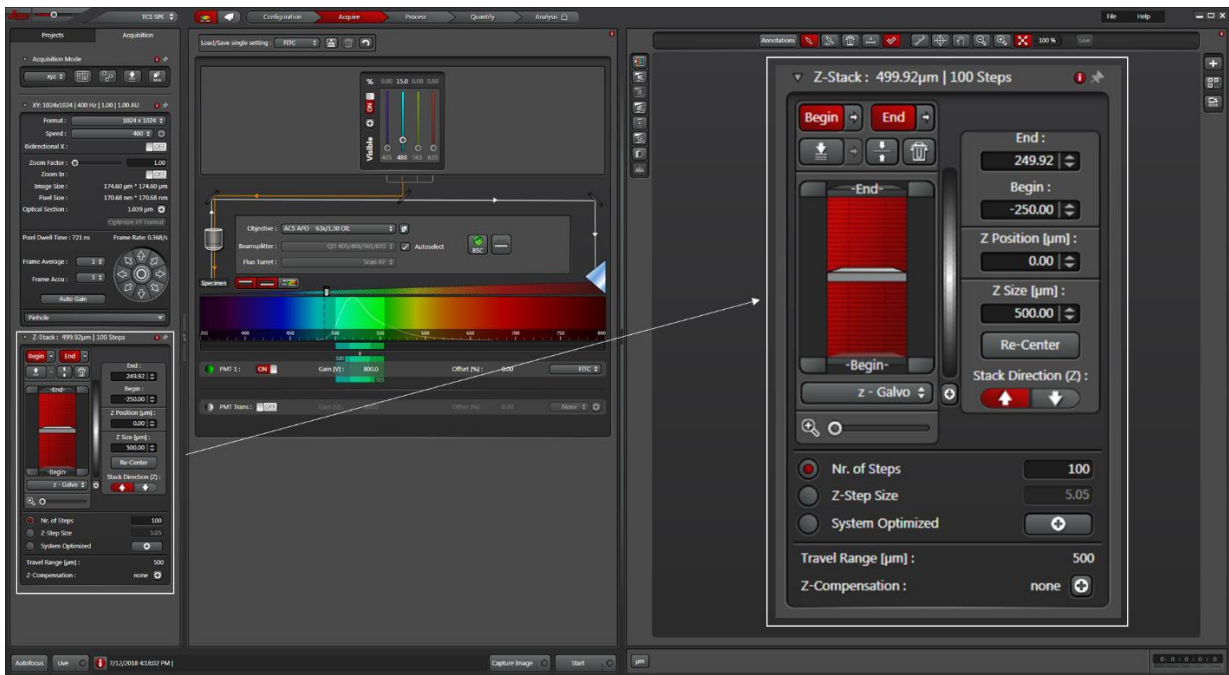
Figure 4-4. Screenshot taken from the LAS X software showing the parameters used for the analysis

As it can be seen, the depth of the z-stack was set to 500 µm, the maximum possible thickness. It provides a good estimation of the cell concentration within the sample, considering homogeneous CFU distribution. In addition, three different slices from different locations within the sample were analysed in order to increase the accuracy of the results.

- *Image post-processing and cell quantification*

Two-dimensional (2D) and three-dimensional (3D) images were captured to aid analysis. Figure 4-5 shows a representation of the bacteria-seeded 3D volume of gel. On the other hand, Figure 4-6 shows an image perpendicular to each of the three two-dimensional planes of the gel volume with their corresponding dimensions. The image selected for cell quantification is the image perpendicular to the x-y axis (i.e. Figure 4-6-A).
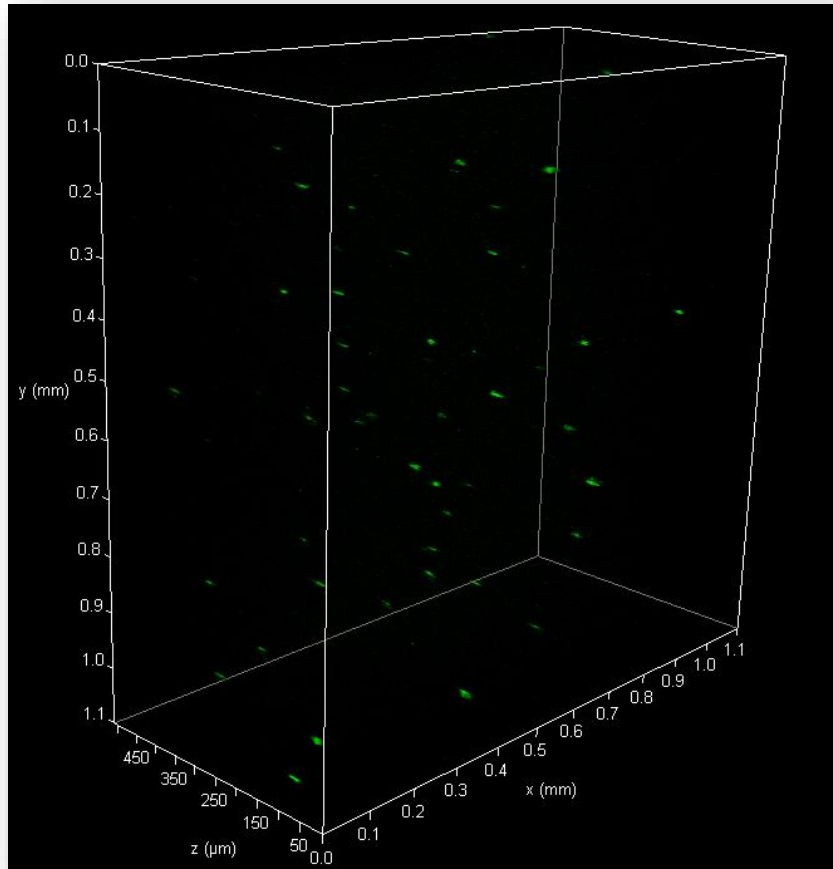
Figure 4-5. Colony distribution within the 3D volume of gel analysed

The green spots represent the bacteria colonies composed of hundreds of cells that developed after a single cell was seeded in the gel.

Although cell superposition occurs due to only analysing the 3D volume using a 2D plane, it is assumed that the x-z plane provides the most accurate representation of the amount and distribution of colonies within the gel.
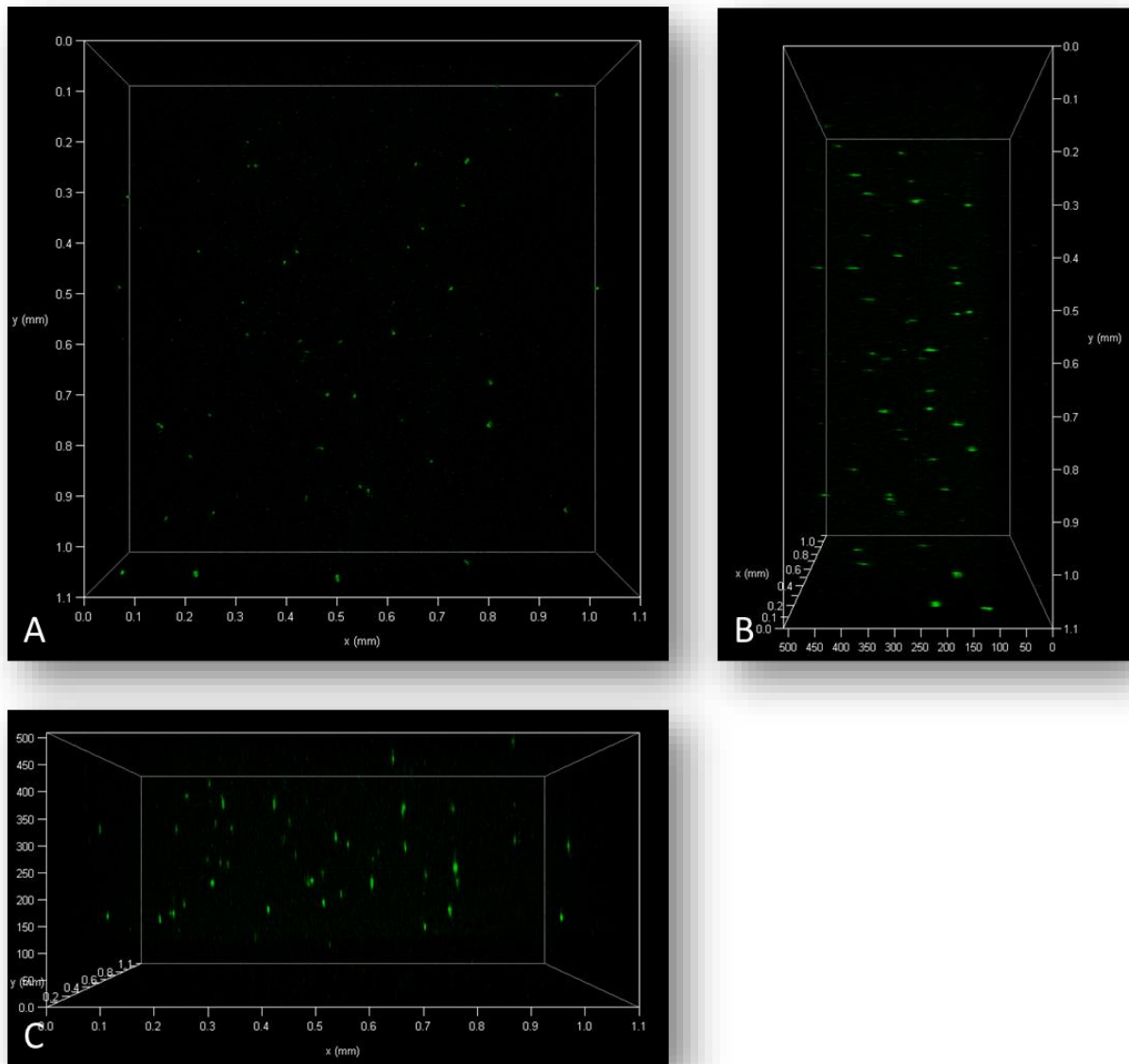
Figure 4-6. (A) x-y plane, (B) z-y plane and (C) x-z plane

The images were obtained using the LAS X software and the cell concentration was measured using an application called ImageJ. This application is a Java-based image processing program that allows the installation of Plugins into their built-in editor. A 3D Object Counter plugin was installed and used to analyse the amount of fluorescence on the slices. This plugin analyses every single pixel of the images and detects whether there is fluorescence or not. From a 800x800 pixels image, the 640,000 pixels are analysed and the plugin calculates the total amount of pixels that emit fluorescence. Figure 4-7 shows the process utilized to measure the amount of fluorescence (i.e. concentration of bacteria cells) using the 3D Object Counter plugin.
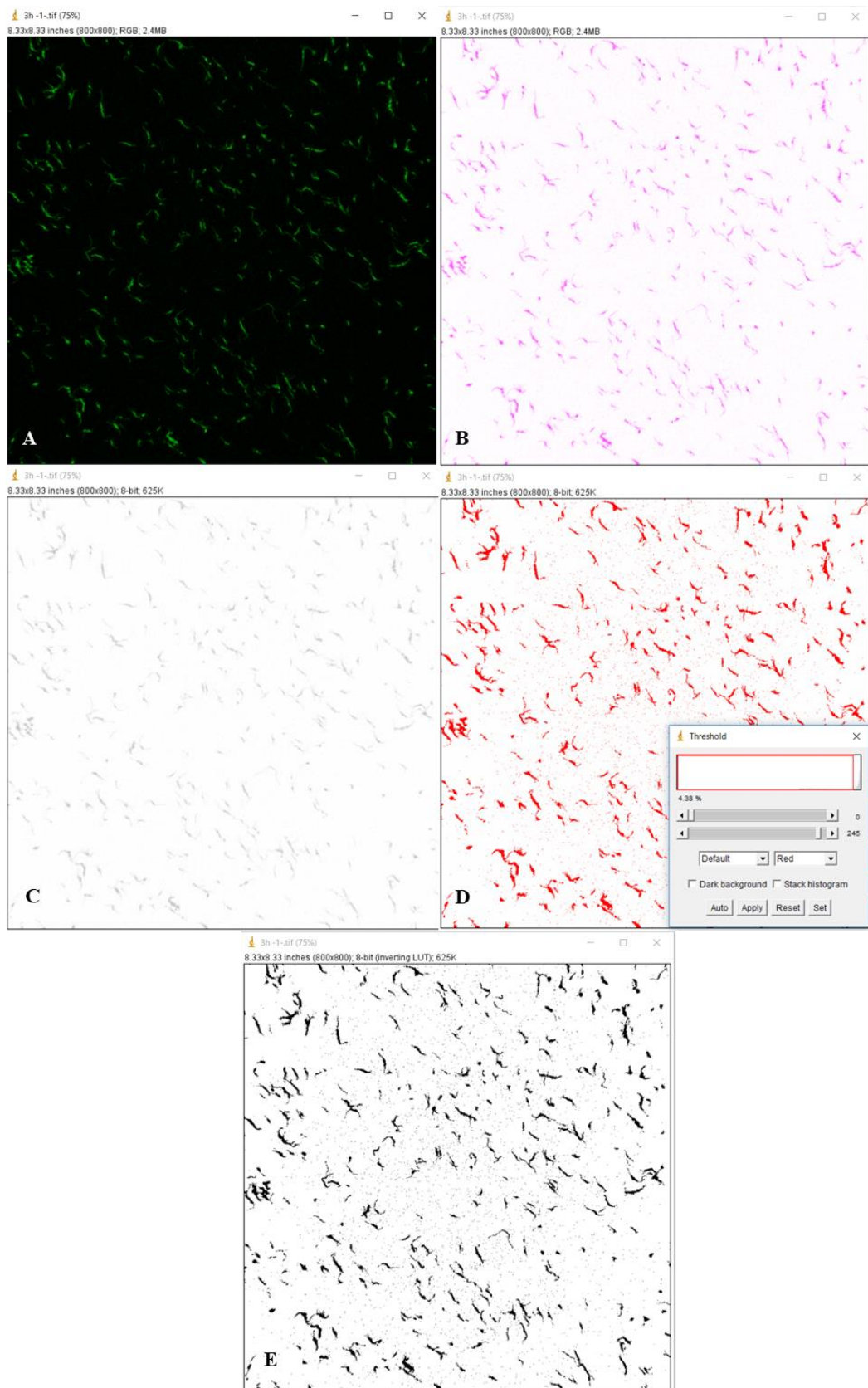
Figure 4-7. Process for cell quantification using ImageJ - (A) original image, (B) invert tool applied, (C) greyscale applied, (D) threshold applied, (E) image ready for quantification

Figure 4-7-A shows the raw image before post-processing. The first step is to invert the colours in order to change the background from black to white (Figure 4-7-B). The second step is to change the colour of the slice to a greyscale (Figure 4-7-C) before a threshold is applied (Figure 4-7-D). The role of this threshold is to assign a value of 255 – i.e. white – to pixels without fluorescence (image background) and 0 – i.e. black – to pixels with fluorescence (i.e. bacteria cells). Once the threshold is applied, the image is ready for analysis (Figure 4-7-E) by applying the 3D Object Counter function. The equation used to obtain the total amount of fluorescence within the agarose slice is expressed as follows:

$$\text{Amount fluorescence (\%)} = \frac{\text{Amount pixels with fluorescence (GFP)}}{\text{Total amount of pixels}} * 100$$

(Equation 4-3)

This method does not provide the total number of cells within the volume of gel, however it does provide a relatively accurate representation of the total amount and distribution of fluorescence within the sample, which can then be related to cell concentration. Greenhalgh et al., (2017) confirmed that there is a strong correlation between fluorescence and cell number. However, the study was performed on *E. coli* cells and, therefore, it cannot be confirmed that the same theory applies for *B. subtilis* cells, although it is quite likely that the same correlation will occur.

GFP is commonly used to evaluate cell viability. However, (Ann-Muriel et al., 2001; Fortin et al., 2005; Greenhalgh et al., 2017) confirmed that GFP fluorescence can also be used to assess cell death, by evaluating the loss of fluorescence after the induction of cell death. Ann-Muriel Steff et al., (2001) suggested that the fluorescence level of death cells decreased due to cell shrinkage until the point where the cells where indistinguishable from the background. Nevertheless, this study was not performed on *B. subtilis* cells so the correlation between fluorescence loss and cell death cannot be confirmed for our type of bacteria.

These limitations aside, it was assumed for our study that analysing the GFP fluorescence of bacteria-seeded agarose gels provides a good representation of the growth-decay behaviour of *B. subtilis* cells.

- From growth points to growth profiles: curve fitting

Analysing the growth behaviour of bacteria cells is a long and laborious process which requires the evaluation of multiple time points in order to obtain an accurate profile. For our experimental program, it was assumed that measuring the growth of bacteria-seeded gels over time with intervals of one hour would be accurate enough to obtain a solid representation of the growth behaviour. However, due to the large amount of growth experiments performed, some growth profiles were obtained with intervals of two hours, especially those with a very slow growth rate – e.g. incubation at low temperature. Additionally, the growth/decay rate of bacteria between the 12h and the 24h time point might be inaccurate since no readings were obtained.

The cell concentration values obtained for the different time points analysed were plotted onto a scatter graph in order to display the growth profile for each of the tested conditions. A process called *Curve fitting* was used to obtain the mathematical equation that best fits the series of data points (Brandreth, 1968; Hauser, 2009). The aim of using a *curve fitting* method is to generate a smooth curve that goes near the data points in order to interpolate unknown values (Motulsky and Christopoulos, 2003).

Due to the complexity of the bacterial growth profiles, a professional curve fitting software called *FindGraph (UNIPHIZ Lab Software)* was used. This software performs a regression analysis in order to find the best fit equation for a series of data points. Non-linear regression provides with more flexibility in fitting curves due to the wider range of non-linear functions to choose from, in comparison to linear regression (Hauser, 2009). From all the catalogue of non-linear functions that *FindGraph* offers, *rational equations* provided the most accurate fit. These type of non-linear functions are the quotient of two polynomic functions *P(x)* and *Q(x)*, taking the following form:

$$f(x) = \frac{P(x)}{Q(x)}$$

(Equation 4-4)

97

Rational functions can adopt an extremely wide range of shapes and they are relatively easy to handle computationally. However, rational functions did not provide a good fit for some of the cases, and a non-linear function called *Rodbard* was used instead. This function is represented as follows:

$$f(x) = d + \frac{(a - d)}{\left(1 + \left(\frac{x}{c}\right)^b\right)}$$

(Equation 4-5)

where *a, b, c* and *d* are the parameters of the equation and depend on the shape of the curve.

A statistical regression analysis was performed in order to assess how well the function fits the observed data. Two parameters were calculated in order to quantify the accuracy of the fitted curve: the *coefficient of determination R^2* and the *standard deviation of the residuals S_e*. The former is a fraction between 0 and 1, where higher values indicate that the observed data points are closer to the fitted equation. The latter represents the average distance between the observed data points and the regression line, in the units of the dependent variable (*amount fluorescence* or *cell concentration* in our case), and smaller values indicate that the observations are closer to the fitted equation.

According to (Hauser, 2009), 95% of the experimentally obtained data points should fall within $\pm 2 * S_e$ from the fitted curve. Therefore, for all the lines of best fit obtained from non-linear regression, these parameters were calculated, evaluated accordingly, and it was confirmed that this condition was satisfied.

4.4. Results and discussion

4.4.1. Escherichia coli v Bacillus subtilis

An initial investigation was performed in order to visualise the growth patterns of *E.coli* and *B. subtilis* cells in agarose gels. The strains HS524 and LH158 were the ones selected

for the experiment due to the constitutively-expressed GFP which would allow visualisation of the bacterial colonies.

Bacteria-seeded agarose gels were prepared with both strains and visualised on the CONFOCAL microscope after 5 hours of incubation at 37°C and 30°C, respectively (Figure 4-8).
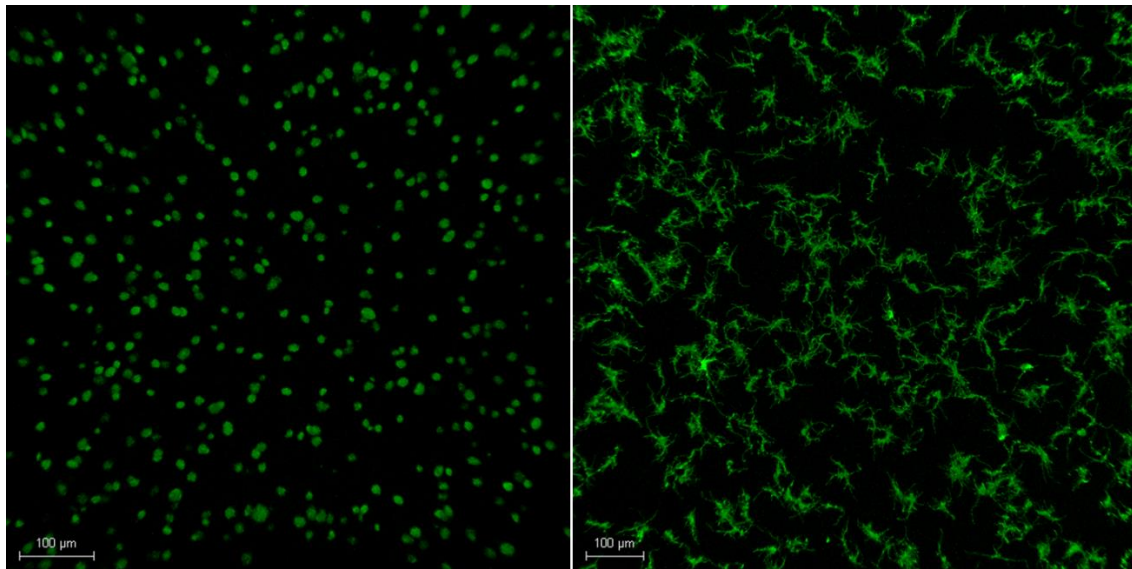
Figure 4-8. Colony formation and patterning for E. coli HS524 (left) and B. subtilis LH158 (right)

As can be seen from the images, both strains show different distribution patterns. While *E. coli* cells tend to form disk-like colonies, *B. subtilis* cells tend to form *branches* through the matrix of the gel as the colonies grow.

One of the main benefits of using agarose gels is the homogeneous distribution of cells that is generated within their structure. Both bacteria strains can grow colonies uniformly distributed within the gel, however, *B. subtilis* seem to be more appropriate due to the formation of long chains of cells that might potentially cover a bigger volume upon growth.

B. subtilis was the strain selected for our experimental program for several reasons. Firstly, the use of *B. subtilis* will lead to a larger spread of cells due to this peculiar *branching* behaviour, which will ultimately contribute to widespread biomineralization along the 3D space. Furthermore, *E. coli* is a urease-negative bacterium, whereas most *B.*

subtilis strains release urease naturally, which will presumably facilitate the cloning of the engineered responsive strain. In addition, the ultimate aim of the Thinking Soils project is to inject the engineered strain of bacteria into the ground, and it is more likely that the strain used will be *B. subtilis*, since this type of bacteria is commonly found in soils and the cells would easily integrate with the geo-environment.

4.4.2. Bacillus subtilis growth in liquid media

As described in the introduction, the growth of *B. subtilis* in liquid media was initially studied in order to count the number of cells present in a culture at a certain time before introducing the inoculum into the agarose solution.

The strain LH158 was inoculated into six cylindrical bottles, three with rich media (LB) and three with minimal media (SMM) and incubated at 30°C and 150rpm. The absorbance (OD_{600}) was then measured with a spectrometer at different time points (number of technical replicates, n = 3) and the results are represented in Figure 4-9. Note that the error bars displayed in red represent the standard deviation of the three technical replicates.
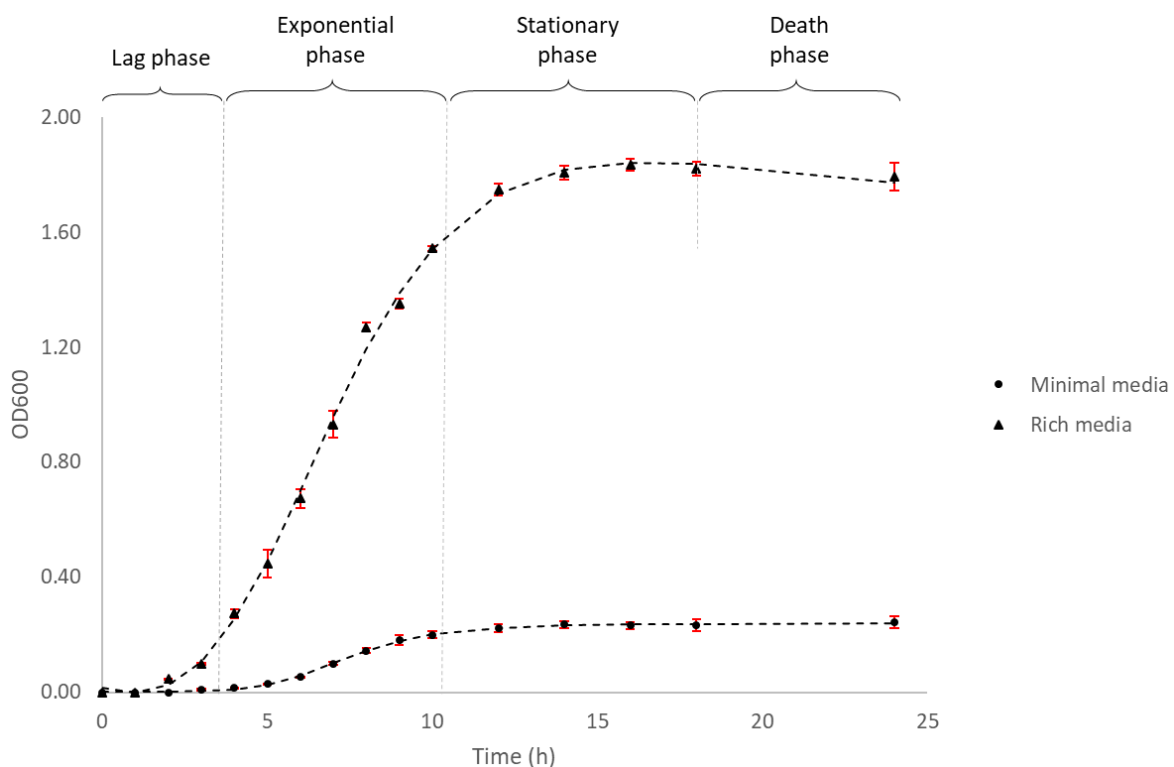
Figure 4-9. Comparison LH158 growth in rich and minimal media

The graph shows the four different phases of microbial growth for the samples grown with rich media, however, the fourth phase (death phase) is not present in the samples grown with minimal media, and it is expected to start after periods longer than 24h. As expected, the cell concentration is much higher for the samples grown with rich media, where OD_{600} values close to 1.9 are obtained, in comparison to the much lower values obtained with minimal media (max. $OD_{600} \sim 0.25$).

However, the amount of nutrients present in most type of soils are very limited, and the growth of microorganisms is more similar to that occurring under minimal medium conditions. Additionally, the use of minimal medium facilitates microbial visualisation under the microscope, generating clearer and sharper images due to a much-reduced background (or *noise)*. This is very important since our method to monitor growth rates relies on CONFOCAL microscopy. SMM was therefore selected as the medium for LH158 and all the microbiology experiments (unless otherwise stated) were performed using the same medium. Figure 4-10 shows the growth curve of LH158 in minimal media.
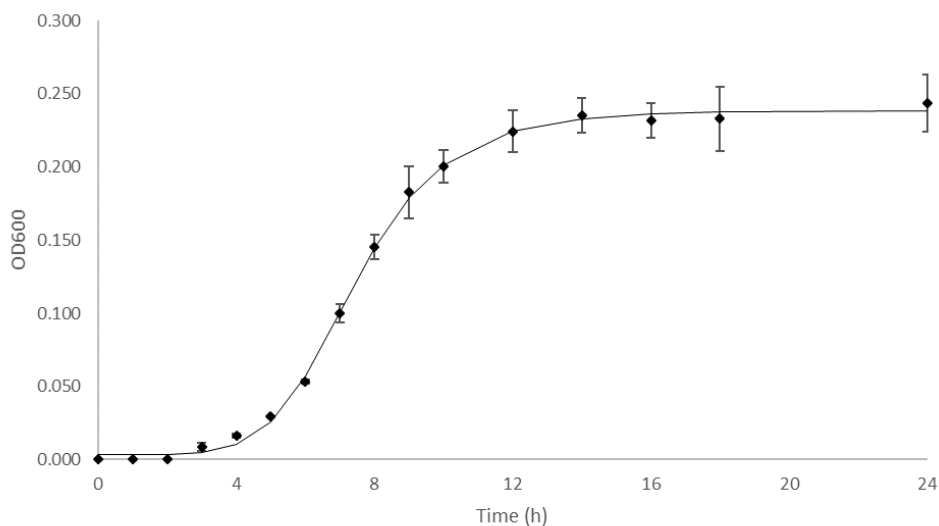
Figure 4-10. Growth behaviour of LH158 in liquid minimal media

As it can be appreciated from the graph, the exponential phase begins at approximately 4 hours and ends after 12 hours.

- Initial cell concentration

As mentioned in earlier sections, the first step to analyse the bacterial growth behaviour is to prepare an overnight liquid culture saturated with bacteria cells that will be used as the inoculum for the growth experiments. For every new set of experiments, an overnight culture of LH158 was grown on minimal media for 12 hours before inoculation. The OD_{600} of the culture was measured at the 12-hour time point every time a new culture was set up in order to make sure the microbial growth was consistent, and that no contamination was present in solution. Following this procedure, it was guaranteed that approximately the same number of bacteria cells are inoculated into the fresh medium or agarose solution.

However, the OD_{600} measured does not give us an indication of the total number of cells present in the overnight solution. Therefore, a serial dilution experiment was performed to determine the cell concentration of the overnight culture after 12 hours of incubation.

Figure 4-11 shows the total amount of CFU present on two plates after a 10^{-5} (left) and a 10^{-6} dilution (right). The images were taken with a standard phone camera. The plates have 199 and 19 CFU, respectively. Note that the colonies were highlighted with blue marker at the bottom of the plate in order to facilitate counting.
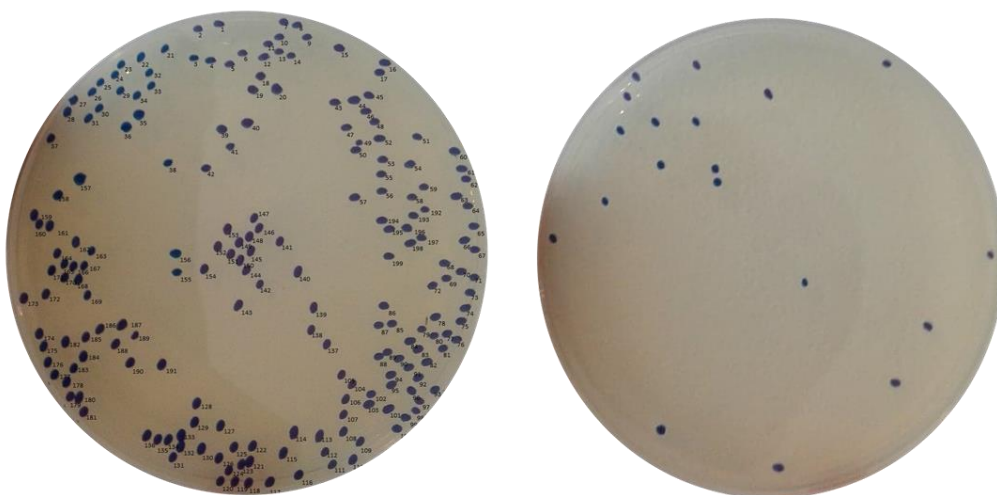
Figure 4-11. CFU grown on the top of agar plates after a serial dilution experiment

The cell concentration after 12h of growth at 30°C and 150rpm can be calculated according to (Equation 4-2):

$$Cell\ concentration\left(\frac{CFU}{mL}\right) = \frac{number\ colonies}{amount\ plated\ (mL)} * (-Final\ dilution)$$

$$= \frac{199}{0.1} * (-10^{-5}) = \mathbf{1.99\ x\ 10^8\ CFU/mL}$$

$$Cell\ concentration\left(\frac{CFU}{mL}\right) = \frac{number\ colonies}{amount\ plated\ (mL)} * (-Final\ dilution)$$

$$= \frac{19}{0.1} * (-10^{-6}) = \mathbf{1.9\ x\ 10^8\ CFU/mL}$$

Hence, there are approximately $2x10^8$ cells in 1mL of inoculum.

4.4.3. Effect of agarose concentration and reasoning behind choosing 6% m/v

The mechanical properties of 6% w/v agarose gels were thoroughly analysed in Chapter 3. This section therefore aims to provide justification for the selection of 6% concentration for the experimental program.

As described in Chapter 3, increasing the concentration of agarose powder leads to two aspects critical to this project: an increase in gel strength and a decrease in pore size. Generally, soils are stronger than agarose gels, and therefore increasing the strength of the gel is clearly one of the objectives of the project – to prove their suitability as a soil analogue. However, increasing gel strength leads to a reduction of the pore throat within the gels and the fibres becoming stronger, which ultimately affects the growth and distribution of bacteria cells. It was confirmed experimentally (*see section* 3.4.1. Effect concentration on gel microstructure) that the size of the pores at low concentrations – i.e. < 2% – are large enough for bacteria cells to swim through and move across the matrix of the gel. However, as more agarose is added to the matrix (>4%), the pores decrease in size considerably and become smaller than the actual cells, potentially hindering their movement through the matrix of the gel. Furthermore, at high concentration gels (>6%), the fibres become so dense that microbial growth might also be affected.

A study presented by Yañez et al., (2010) investigated on the pore size threshold for bacteria penetration into hydrogels. The study analysed the success rate of bacteria penetration at different pore sizes and it was found that between 1μm and 10μm the relationship adopts the shape of a cumulative distribution function, i.e. 0% cell penetration through pores smaller than 1μm and 100% cell penetration through pores larger than 10μm. However, this relationship cannot be implemented for our study since the type of hydrogel and bacteria strain are different. Therefore, an investigation was performed to find the most suitable concentration of agarose for our experimental program.

As it was confirmed in Chapter 3, increasing agarose concentration leads to stronger samples, therefore, the concentration selected must be the highest one possible that allows homogeneous bacterial growth across the gel sample. Bacteria-seeded agarose samples were then prepared as explained in section 4.3.3. Bacteria-seeded agarose gel preparation for concentrations ranging from 1% to 10%. As expected, increasing the concentration of agarose led to more viscous solutions, causing mixing problems when bacteria were inoculated. The plates were then incubated at 30°C for 24h in order to promote bacteria growth. Additionally, samples without added bacteria were also prepared in order to act as a control. After the incubation process, the plates were visually analysed and the results showed that bacteria growth was homogeneous throughout the plate for concentrations ranging 1-6%. However, for concentrations higher than 6%, bacteria-seeded samples showed a non-uniform growth. Figure 4-12 shows a capture of the two plates with bacteria-seeded agarose gels at 6% and 7% concentration respectively. The one on the left (6%) shows homogeneous growth across all the plate. However, the plate on the right (7%) shows a non-uniform behaviour – with the light-coloured areas showing the gel containing bacteria and the darker areas showing the parts of the plate where bacterial growth did not occur.

A) 6%   **B) 7%**
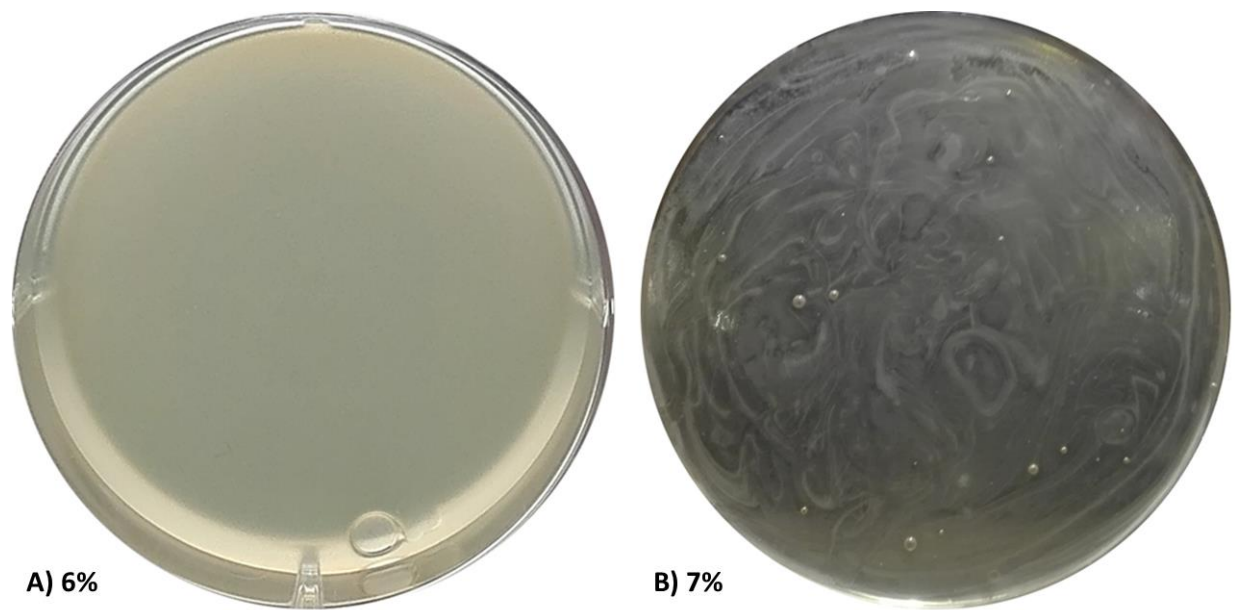
Figure 4-12. Homogeneous (A) versus non-homogeneous (B) bacterial growth

Considering both bacterial growth and strength-stiffness of the gel, the optimum concentration for the mechanical experiments is 6% w/v since it provides with relatively strong gel samples and allows homogeneous bacterial growth across its matrix.

4.4.4. Bacteria growth in agarose hydrogels

As stated previously, the aim of this chapter is to understand the growth behaviour and distribution of bacteria colonies in 3D agarose gels under different conditions. Considering that the amount of nutrients available is the factor that affects the most microbial growth and the growth medium has already been established (SMM), the other remaining factors that are to be analysed are temperature, pH and initial cell concentration (or initial dilution). Hence, this section aims to analyse the effect of each of these parameters on the growth behaviour of *B. subtilis* in agarose gels. Furthermore, another aim of this section is to demonstrate that agarose gels can be used to study the effect different environmental conditions have on the growth rate of bacteria.

The samples were prepared as described in section 4.3.3. Bacteria-seeded agarose gel preparation and following the visualisation and post-processing techniques described in section 4.3.4. Growth monitoring in bacteria-seeded hydrogels.

The growth points measured for each of the conditions were obtained by analysing three technical replicates ($n = 3$) – i.e. three images were taken from three different areas of the plate for each time point –but only one biological replicate – i.e. the experiment was only performed once. Additionally, as explained in previous sections, the final representation of each growth profile was generated using non-linear regression and finding the best-fit curve.

- *Effect of initial cell concentration*

The initial number of cells inoculated into the gel is a crucial parameter. The total amount of Colony Forming Units (CFU) present in each of the agarose slices analysed can easily be estimated. It was calculated in section 4.4.2. Bacillus subtilis growth in liquid media that the amount of CFU in 1mL of inoculum after 12h of incubation at 30°C and 150rpm is approximately $2x10^8$ CFU/mL. Therefore, if 1mL of this LIQUID inoculum is introduced into 100mL of an agarose-medium solution – i.e. a 1/100 dilution – the resultant concentration of cells within the gel is $2x10^6$ CFU/mL. Furthermore, considering the dimensions of a CONFOCAL slice are approximately 1mm x 1mm x 0.5 mm (=0.5mm^3 or 0.0005mL), it can be estimated that every slice analysed will have approximately **1,000 CFU** embedded into its matrix. Additionally, some of the growth experiments were performed using a 1/1000 dilution, which will lead to a reduced number of CFU in each slice analysed (approx. **100 CFU**). Figure 4-13 shows a comparison of two CONFOCAL images (slices) with different initial dilutions in which the difference in cell concentration can clearly be appreciated.
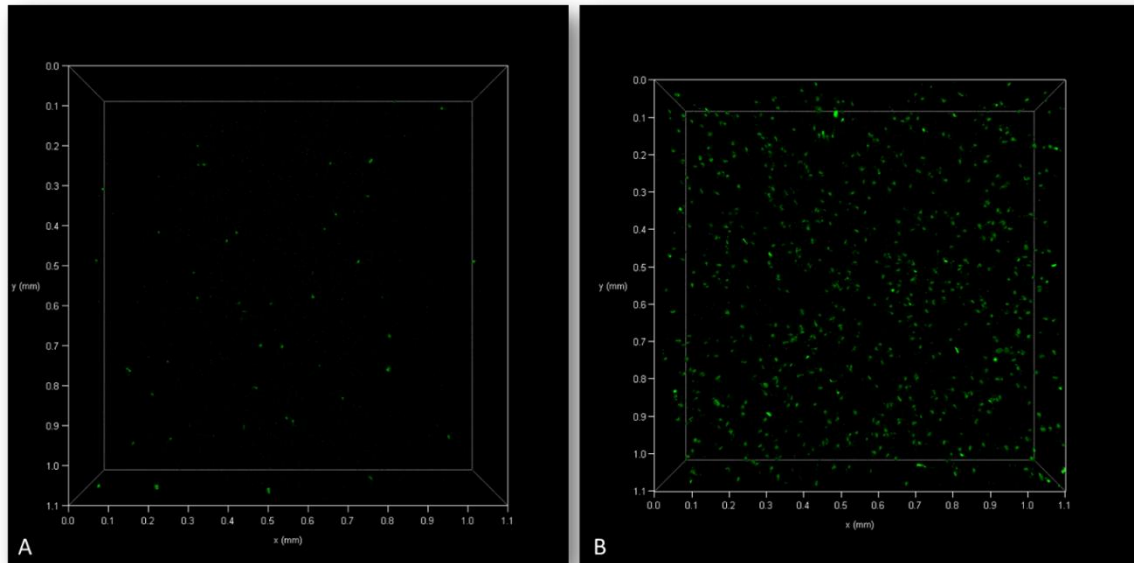
Figure 4-13. Comparison B. subtilis LH158 growth at 1/1000 dilution (A) and 1/100 dilution (B) after 9h of incubation at 25°C

An ImageJ plugin called *ITCN* was used to count the number of colonies present in every slice. This plugin was originally designed to count cells, however, due to the low magnification used to obtain our images, the plugin can be used to count colony formations instead. *ITCN* detected **93 CFU** for the case of the gel produced with a 1/1000 dilution (left) and **923 CFU** in the gel slice generated with a 1/100 dilution (right). Hence, comparing these values to the results estimated above, it can be confirmed that most of the *B. subtilis* cells inoculated into the agarose solution do form colonies.

Three series of experiments were prepared in which the overnight culture was inoculated at different dilutions ($^1/_{100}$, $^1/_{300}$ and $^1/_{500}$). Figure 4-14 shows the effect the initial dilution has on the growth profile in hydrogel samples incubated at 30°C. The y axis represents the amount of fluorescence in a CONFOCAL slice or *cell concentration*, as described in section 4.3.4. Growth monitoring in bacteria-seeded hydrogels, and calculated in accordance to (Equation 4-3) (% refers to the percentage of bacteria present in the slice of gel analysed).
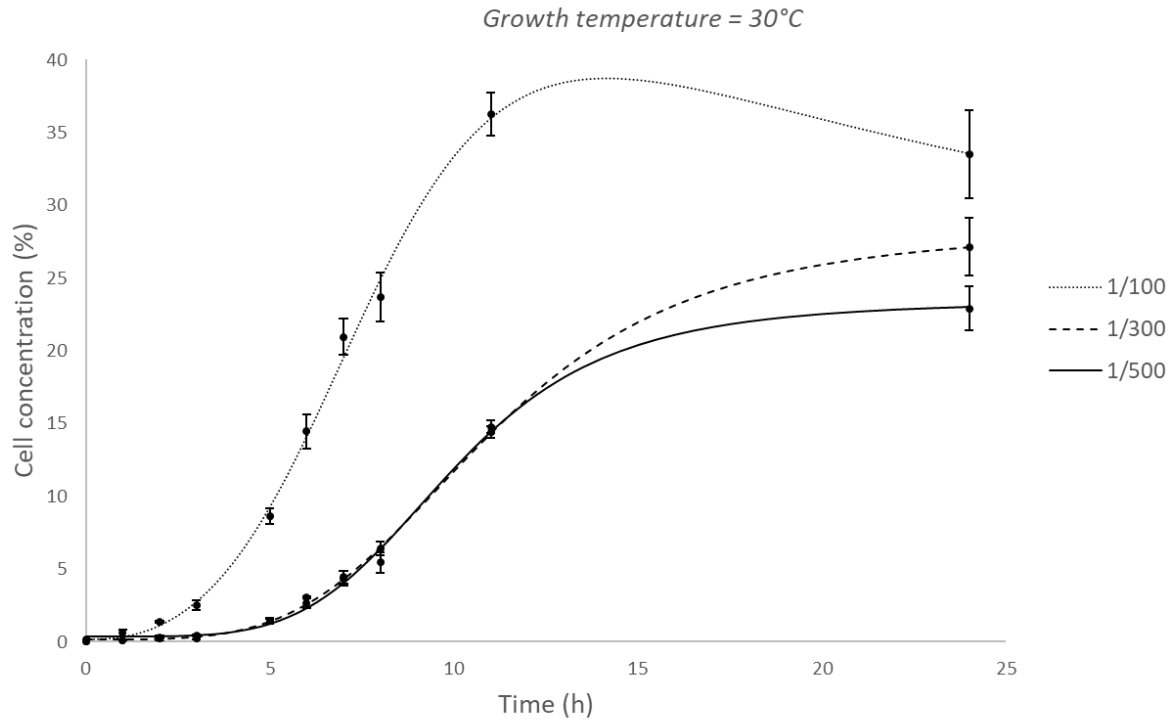
Figure 4-14. Effect initial dilution on bacterial growth profile

As expected, the lower the dilution – i.e. higher initial concentration of cells –, the higher the total amount of cells generated during the 24-hour period. Furthermore, it can clearly be seen that there is a different behaviour between the gel samples inoculated at 1/100 dilution and those inoculated at 1/500. However, for the case of the samples inoculated at 1/300 dilution, although the total amount of cells after 24 hours is larger than those inoculated at 1/500, the behaviour is very similar, starting exponential phase after 6 hours and stationary phase after approximately 16 hours. Therefore, in order to reduce the number of conditions analysed, it was decided that only two different dilutions (1/100 and 1/500) would be analysed in future experiments.

The effect of initial dilution was also analysed for temperatures of 25°C and 35°C and the results are represented in Figure 4-15.
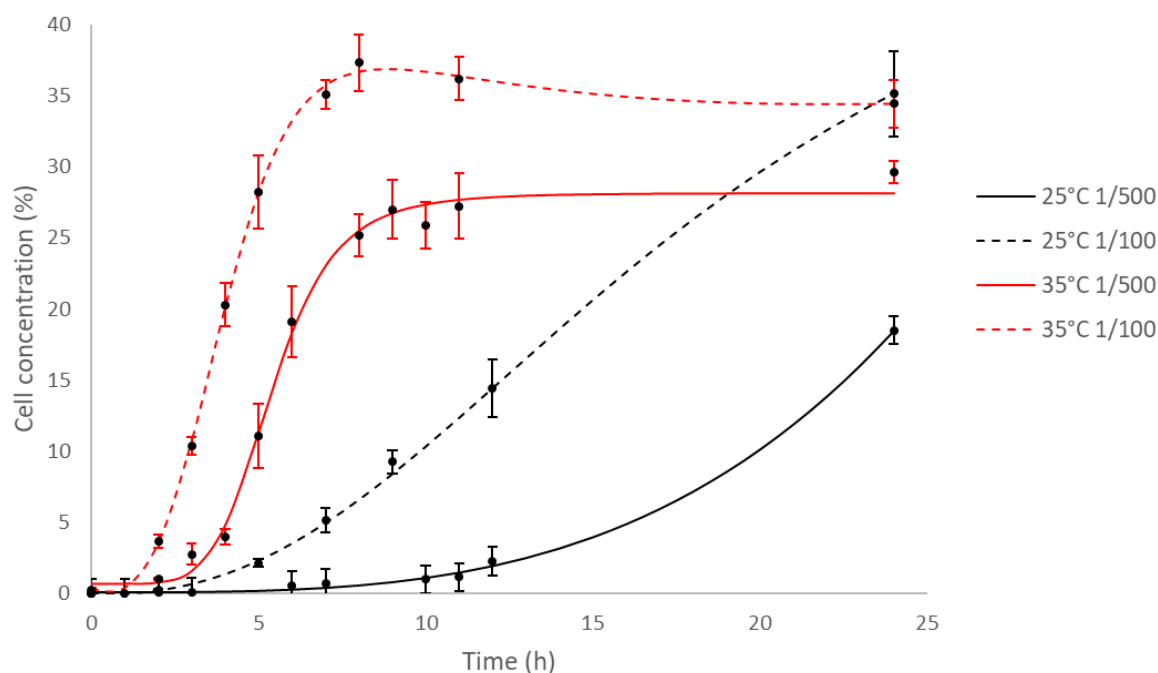
Figure 4-15. Effect initial dilution w.r.t. incubation temperature

Again, as expected, the samples inoculated with a lower initial dilution generate a higher concentration of cells throughout the 24 hour period (excluding the first 2-3 hours, in which the difference cannot be appreciated). In addition, it can be seen how the temperature has a major effect on the growth behaviour, which will be thoroughly analysed in the next section.

It can then be concluded that increasing the initial concentration of cells inoculated into the matrix of the gel – or decreasing initial dilution – leads to an increased cell concentration during the 24 hour period.

- Effect of temperature on growth rate

Temperature is another parameter that plays an important role on the growth behaviour of bacteria. *B. subtilis* is considered to be a mesophilic microorganism – i.e. it grows best at moderate temperatures, typically between 20°C and 45°C. However, if incubation temperatures higher than 37°C are used, it is quite likely that the cells will sporulate -i.e. hibernate. As described in section 4.2.3. Growth media, glucose was added to the growth media in order to hinder the possible formation of spores at 35°C.

It was reported by Singh et al., (2017) that the production of the urease enzyme is optimised between 25-35°C. Hence, the temperatures selected for the experimental program were 25°C, 30°C and 35°C.

Figure 4-16 shows the significant effect temperature has on the growth behaviour of *B. subtilis*.
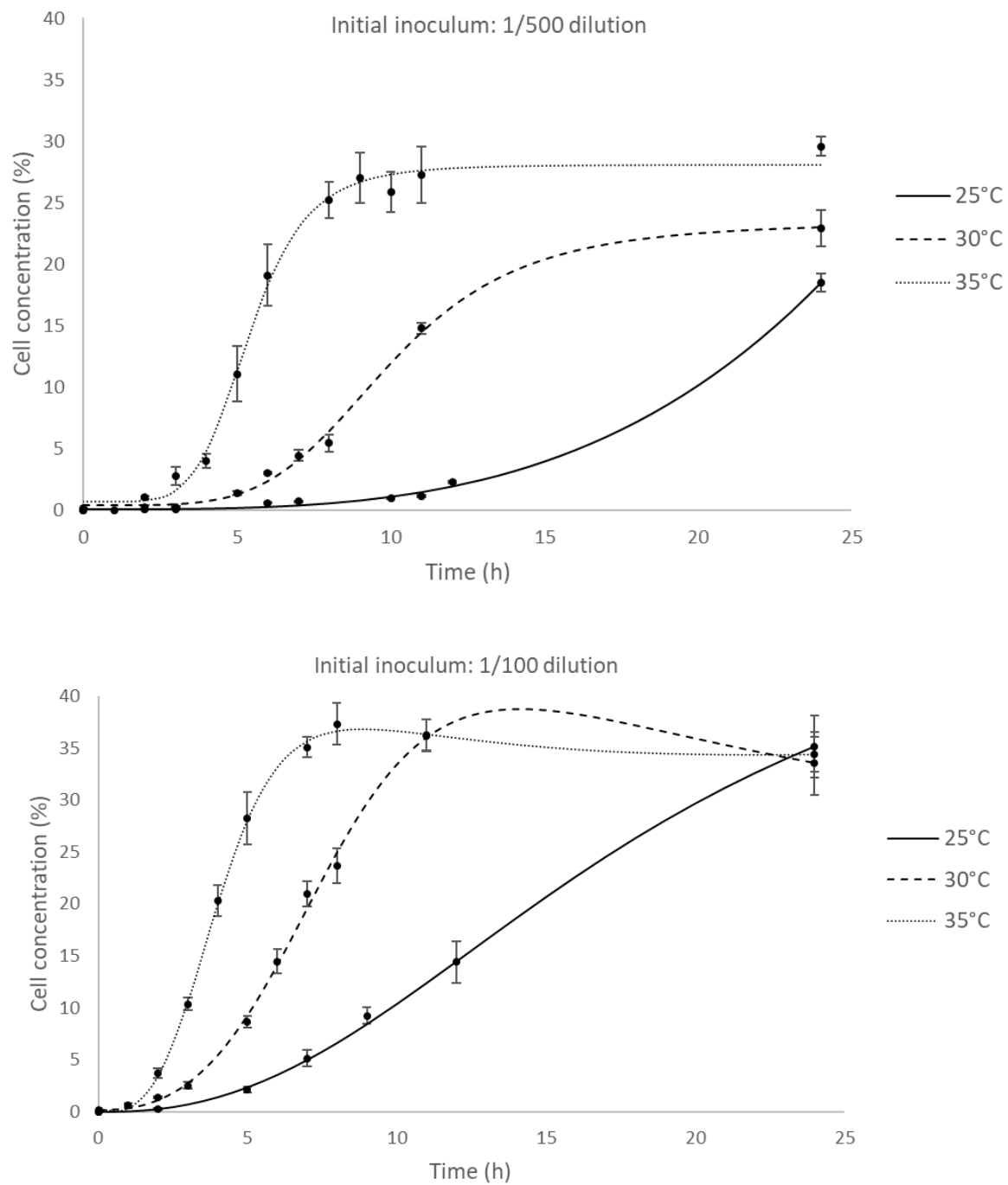
Figure 4-16. Effect temperature on microbial growth. Low initial concentration (top) and high initial concentration (bottom)

It can be seen how both exponential and stationary phases occur earlier as the temperature increases. In addition, the steepness of the growth expression during exponential phase is also higher as the temperature increases, suggesting cells divide more quickly at higher temperatures.

However, whilst the total amount of cells after 24 hours increases as the temperature increases for the case of the samples inoculated at 1/500 dilution, a different behaviour is observed in the samples inoculated at 1/100 dilution: the total amount of cells after 24 hours growth is approximately the same, independently of the incubation temperature. This phenomenon occurs due to bacterial decay – i.e. bacterial death – happening in the samples incubated at 30°C and 35°C after exponential phase ends. Furthermore, the relatively high temperatures alongside the increasing lack of nutrients might promote the formation of spores - since growth conditions are not favourable – ultimately affecting the growth behaviour.

Contrarily, the samples incubated at 25°C do not show any signs of decay over the 24-hour period, suggesting most of the cells are still alive and dividing.

Therefore, these results suggest that temperature has a major effect on the growth behaviour of *B. subtilis* in agarose gels and also show that there is a saturation point at approximately 35% cell concentration for the samples with high initial concentration of cells which is not exceeded. This saturation point occurs at approximately 30% cell concentration for the samples with lower initial concentration.

- Effect of pH on growth rate

The effect of the incubation temperature and the initial dilution was analysed, and it was confirmed that both parameters play a crucial role in the growth behaviour of *B. subtilis* in agarose gels. This section investigates the influence that the pH of the gel has on the growth rate.

The pH measures the acidity or basicity of an aqueous solution and it is expressed as a logarithmic scale that ranges 0-14. The pH of pure water is 7 and solutions with a pH lower or higher than 7 are acidic and basic, respectively. Since the pH can only be quantified in

liquid solutions, the pH of the medium prior to mixing with the agarose powder was measured. It was then assumed that adding agarose (pH neutral) to the growth medium has a negligible effect on the pH of the gel. Note that the pH of the liquid agarose could not be measured due to the high viscosity of the solution.

The pH of SMM medium was first measured and was found to range between 7.12 and 7.15, similar to that of pure water. In order to evaluate the effect pH has on the growth behaviour of *B. subtilis* in the hydrogel, series of samples with pH=6 and pH=8 were prepared. 3M HCl and 3M KOH were the solutions used to reduce and increase the pH of the media respectively. Note that the mixing was performed inside a fume cupboard in order to limit exposure to the fumes generated whilst wearing the appropriate PPE since HCl and KOH solutions are highly corrosive.

Figure 4-17 shows the effect pH has on the growth behaviour of B. subtilis for incubation temperatures of 25°C and 30°C, and 1/500 initial dilution (i.e. lower initial concentration of cells).
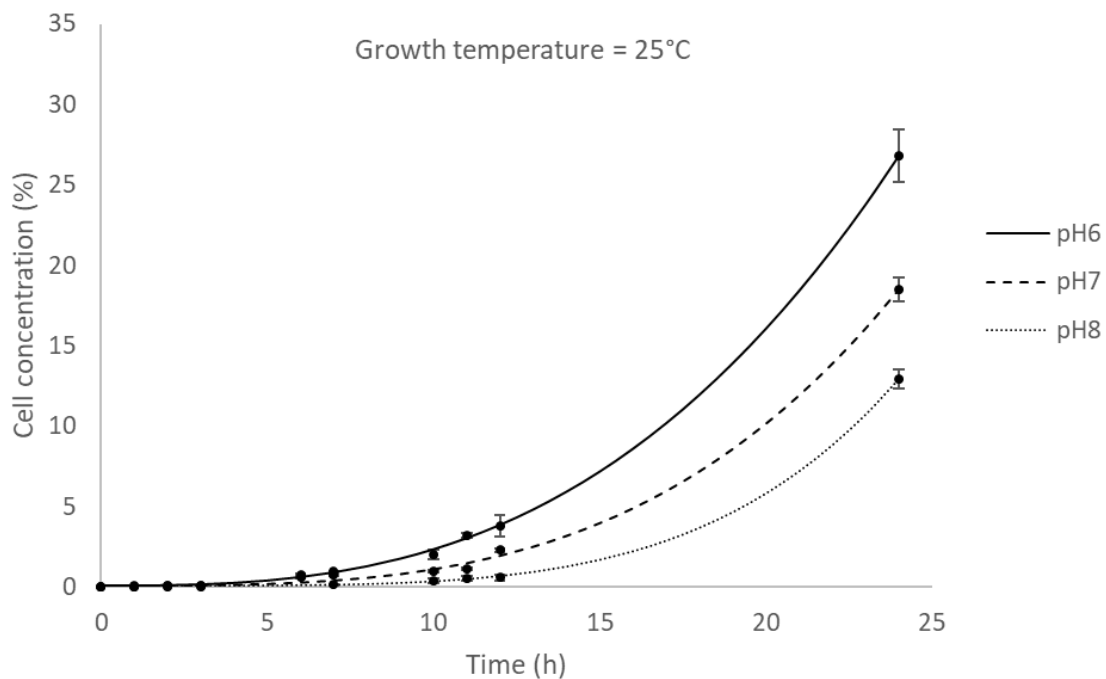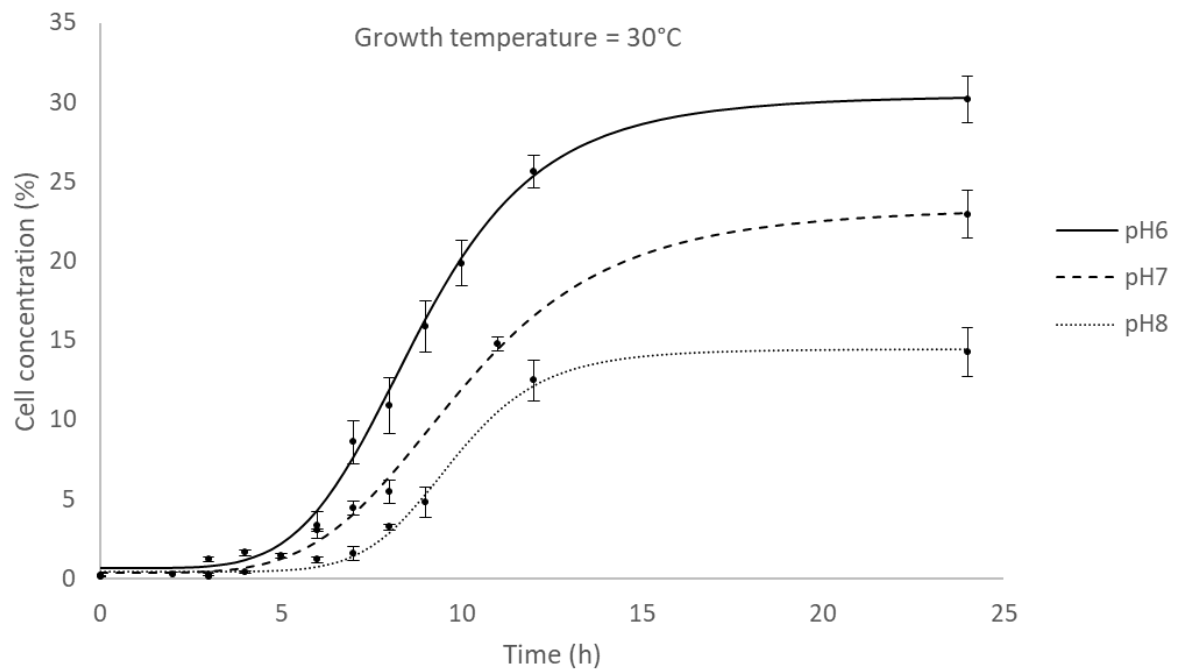
Figure 4-17. Effect pH on the microbial growth rate. Growth at 25°C (top) and 30°C (bottom), and initial dilution = 1/500

These results suggest that the pH of the medium also has an impact on the growth rate of bacteria in the hydrogel. For simplicity, the samples grown with standard SMM medium were considered to have a pH=7. As it can be seen from the graphs, an increased pH – i.e. a basic solution – leads to a reduced concentration of cells during the 24h analysed. On the contrary, the results suggest that reducing the pH of the medium to 6 contributes positively to the growth rate of bacteria. Thus, an increase of approximately 7% and 8% in the total concentration of cells after 24h can be obtained by decreasing the pH to 6, for samples incubated at 25°C and 30°C, respectively.

However, these results are not as straightforward as they seem. Although it can clearly be seen that the samples grown with the acidic medium exhibit a boosted growth rate when compared to samples grown with basic growth media, it cannot be confirmed that this behaviour only occurs due to the increase in pH, since the added components – i.e. KOH and HCl – might also slightly alter the growth rate of the microorganisms. In addition, Smith et al. (2002) evaluated the influence of different pH conditions on the GFP fluorescence of a *B. subtilis* strain in liquid media and confirmed that different pHs lead to

113

different levels of fluorescence, with pHs above and below 7 decreasing the fluorescence intensity of GFP.

It was therefore decided not to include pH as one of the parameters to be analysed in forthcoming experiments, due to the ambiguity of the results.

4.4.5. Growth characterisation in cylinders

In the previous sections, the effect of different temperatures and initial concentration of cells (or initial dilution) on the growth behaviour of *B. subtilis* in hydrogels was analysed and it was confirmed that both parameters have a major effect on the bacterial growth profile.

All the previous tests were performed in 35mm diameter Petri dishes (the thickness of the gel samples was approximately 5mm) which, amongst other factors, provided the samples with unlimited oxygen, due to the reduced dimensions of the gel sample. Additionally, the growth rate on the top layer of the samples was expected to be higher due to the free movement of the cells – in comparison to those cells trying to divide and grow within the micropores of the gel. Therefore, if the thicker gel samples are analysed, the microbial growth is expected to vary significantly with depth. In other words, analysing the bacterial growth in 30mm diameter and 10mm height Petri dishes does not provide an accurate representation of the growth behaviour in 3D hydrogels. Hence, an investigation was performed in order to analyse the 3D growth behaviour in larger samples of hydrogel, where slices from sections at a variety of depths were taken, and the growth within the matrix of the gel was examined.

The lack of oxygen is expected to have a major influence on the microbial growth, potentially leading to an accelerated decay rate. *B. subtilis* was believed to be a strict aerobe – i.e. they require oxygen to grow –, however, some studies have contradicted that theory and they can grow under anaerobic conditions too, becoming then *facultative aerobes* (Nakano and Zuber, 1998). The growth mechanisms are then the use of nitrates/nitrites as a terminal electron acceptor, or by fermentation.

The differential consumption of nutrients might also play an important role in the growth/decay rate since cells might quickly starve due to the unavailability of nutrients in their surroundings. In addition, these adverse conditions might lead to the formation of spores (as mentioned in previous sections), which might also lead to an alteration of the growth behaviour.

Regarding the dimensions of the new gel samples, it was believed that growing the microbes in cylindrical samples would allow inspection of the growth rate across the different layers within the gel, behaviour that could not be investigated using standard Petri dishes. Therefore, it was believed that, considering the overall objectives of the project (*see section* 1.4. Aim and objectives), investigating the growth on cylindrical samples would provide results comparable to the microbial growth behaviour occurring in a large volume of agarose gel.

- Design and 3D printing of the cylinders

The diameter of the new specimens had to be the same as the 35mm diameter Petri dishes in order to allow visualisation of the bacteria-seeded hydrogel on the CONFOCAL microscope. A cylindrical mould was designed using SketchUp (*see* Figure 4-18*)* with the appropriate dimensions: 35mm diameter and 100mm in height. The sketch was then sent to a FormLabs printer which 3D-printed the cylinders using transparent resin. A platform was also 3D-printed to support the gel slices on the CONFOCAL microscope. This platform was also designed and 3D-printed using the same procedure (Figure 4-18). Additionally, both the cylinder and platform were placed on a water and ethanol bath (equal parts) in order to eliminate impurities and cured under UV light in order to increase the stiffness of the resin.
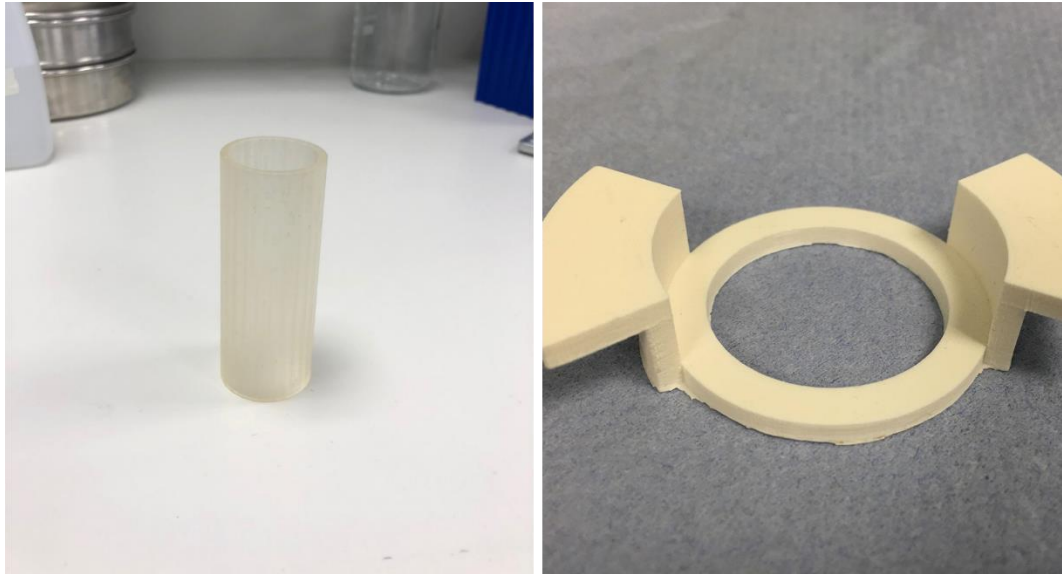
Figure 4-18. Final prototype of the 3D printed resin moulds and platform

- *Preparation of the slices*

The preparation of the gel samples is identical to the procedure used in section 4.3.3. Bacteria-seeded agarose gel preparation, with the only difference being the moulds used. The bacteria-inoculated gel was poured onto the cylinders, covered with tape in order to avoid contamination and placed in the fridge at 4°C for 10 minutes until the gel solidified. The cylindrical samples were then placed inside the incubator at the corresponding temperature to promote bacteria growth. For every selected time point, the cylinders were removed from the incubator and the gel samples were slid out of the mould. The 100mm long gel cylinders were then cut into approximately 5mm thick slices, generating 20 slices – which correspond to the 20 different layers within the gel that are to be analysed (Figure 4-19). The slices were then placed on the 3D-printed platform and analysed using the CONFOCAL microscope by following the procedure described in section 4.3.4. Growth monitoring in bacteria-seeded hydrogels.
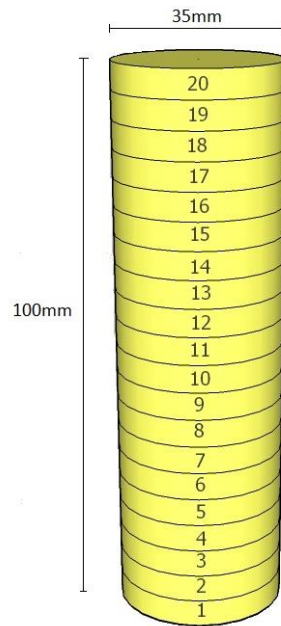
Figure 4-19. Representation of the cylindrical volume of hydrogel with its corresponding dimensions and number of layers

- *Data acquisition*

For each of the conditions evaluated, five cylinders were prepared, which correspond to the 3, 6, 9, 12 and 24-hour time points. Since 20 slices – i.e. layers of the cylinder – were to be analysed and three technical replicates were to be taken from each of the slices, the time needed for the analysis was too long to use more frequent time points. Hence, it was assumed that analysing the growth every 3 hours would give a relatively accurate representation of the growth behaviour of bacteria at each layer within the gel. Note that although it is not strictly true, it was assumed that no further bacteria growth occurred while the samples were being analysed on the microscope. Additionally, for each of the conditions evaluated, two biological replicates were analysed – i.e. the same test was performed from a different start culture under the same conditions – and the average of these two replicates was the value taken for further analysis. The reason for performing biological replicates is to increase the accuracy of the results since the data obtained from these tests will be used as an input for the computational model (see *chapter 5*).

Regarding the different growth conditions analysed, the effect of three different temperatures (25°C, 30°C and 35°C) was evaluated along with the effect of two different

initial dilutions (1/1000 and 1/100). The reason for using a 1/1000 dilution instead of 1/500 is to increase the difference between a high and a low initial concentration of cells and evaluate the impact on the growth behaviour. The two selected initial dilutions generated a 10-fold difference regarding the initial number of bacteria cells inoculated into the matrix of the gel and, therefore, a big variation is expected. Additionally, for simplicity purposes, the samples inoculated with an initial dilution of 1/1000 were referred as *low initial cell concentration* samples and those inoculated at 1/100 dilution were referred as *high initial cell concentration*.

After analysing the first cylinder, it was discovered that measuring the cell concentration for all the layers within the gel (including three replicates) was too demanding and the analysis time exceeded 3 hours, overlapping with the next time point. Therefore, it was decided to only analyse the odd layers within the gel, with the exception of the three top and bottom layers, where large variations regarding cell concentration are expected. Additionally, the results represented for the even layers (not obtained experimentally) are the average between the two confining layers, i.e. the cell concentration for layer 14 is the average between layer 13 and 15.

Appendix C shows the series of data points obtained from the experimental program for each of the layers and conditions analysed. Note that every single value represents the cell concentration (%) at each time point for each of the 20 layers within the gel. These results were calculated as the average of six values (two biological replicates and three technical replicates).

These series of data points obtained experimentally were represented in the form of scatter graphs for each of the conditions and layers of the gel to evaluate their growth behaviour and allow comparison between conditions (Figure 4-22).

- Differential growth rate between layers

As mentioned in previous sections, the growth rate of bacteria along the layers of the gel was expected to be variable. In order to analyse this behaviour, the cell concentration (%) after 12 hours of growth at two different initial dilutions and temperatures was

represented for each of the 20 layers of the gel, 20 being the top layer of the cylinder and 1 being the bottom (Figure 4-20).

Cell concentration (%) after 12h incubation at 35°C
Initial dilution = 1/1000

Cell concentration (%) after 12h incubation at 25°C
Initial dilution = 1/100
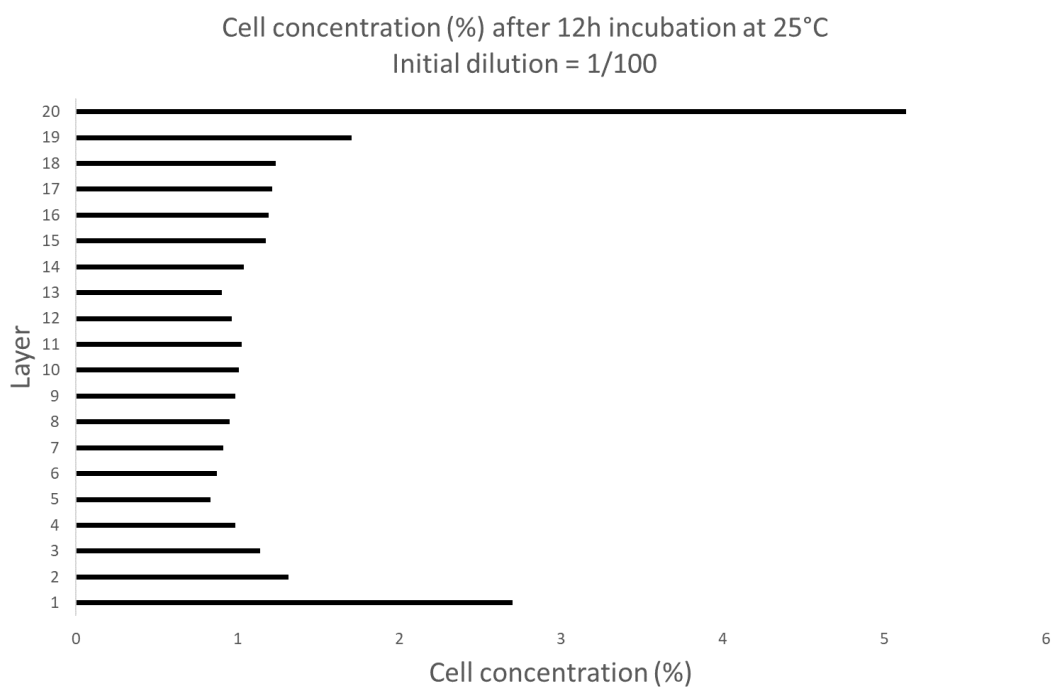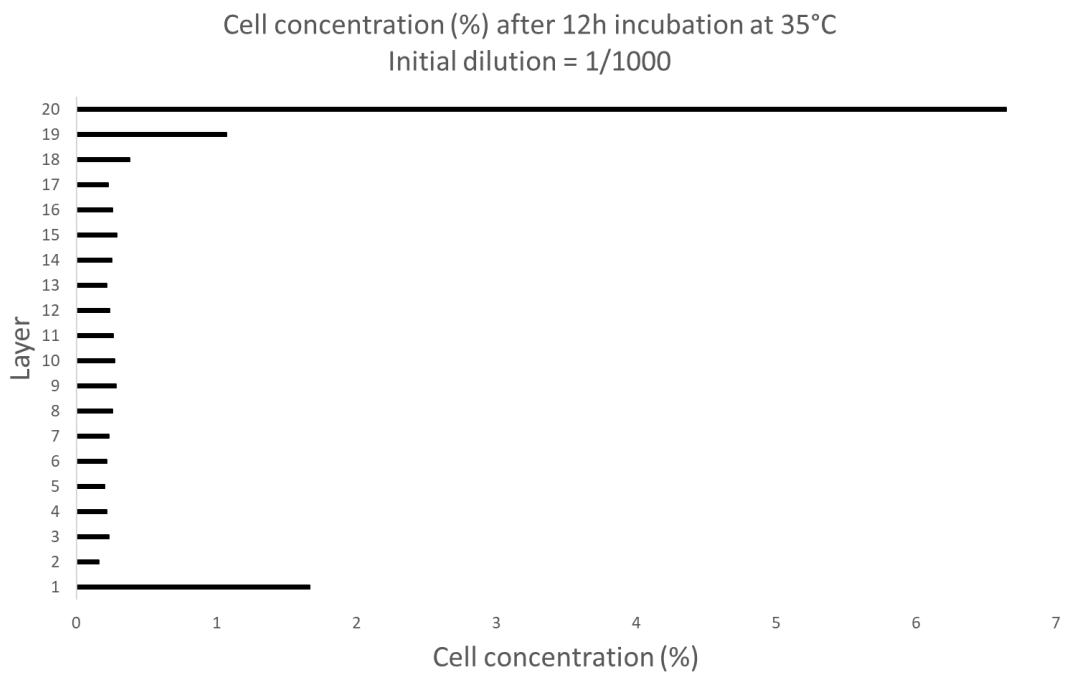
Figure 4-20. Differential cell concentration after 12h w.r.t. layer within the gel

The graph shows how the concentration of cells varies depending on the location within the gel, with the top and bottom layers exhibiting a higher concentration of cells than the middle layers. Figure 4-20 displays this behaviour for two different conditions: low initial concentration of cells and incubation at 35°C; and high initial concentration of cells and incubation at 25°C. However, the rest of the conditions analysed showed the same trend.

This differential growth rate between layers might be possibly related to the lack of oxygen in the middle layers of the gel which might ultimately lead to sporulation of the cells or a reduced growth rate. Although it was confirmed by Nakano and Zuber, (1998) that *B. subtilis* cells can grow under both aerobic and anaerobic conditions, the growth rate – and consequently the growth profile – is expected to be different. The behaviour observed after analysing the gel cylinders further strengthens this theory. Additionally, accumulation of metabolic waste within the pores of the gel might also be another factor which affects bacterial growth. Another possible cause of this differential growth behaviour might be the precipitation and accumulation of nutrients at the bottom layers of the samples, before the gel is formed. However, understanding the factors that generate the observed differential growth rate is beyond the scope of this study.

- *Effect of temperature and initial cell concentration on growth rate*

Preliminary inspection of the results suggested that the growth rate in the layers 20, 19 and 1 of the gel clearly showed a distinctive behaviour, while the microbial growth rate in the middle layers (2 to 18) tend to follow the same pattern, as it can be seen in Figure 4-21.
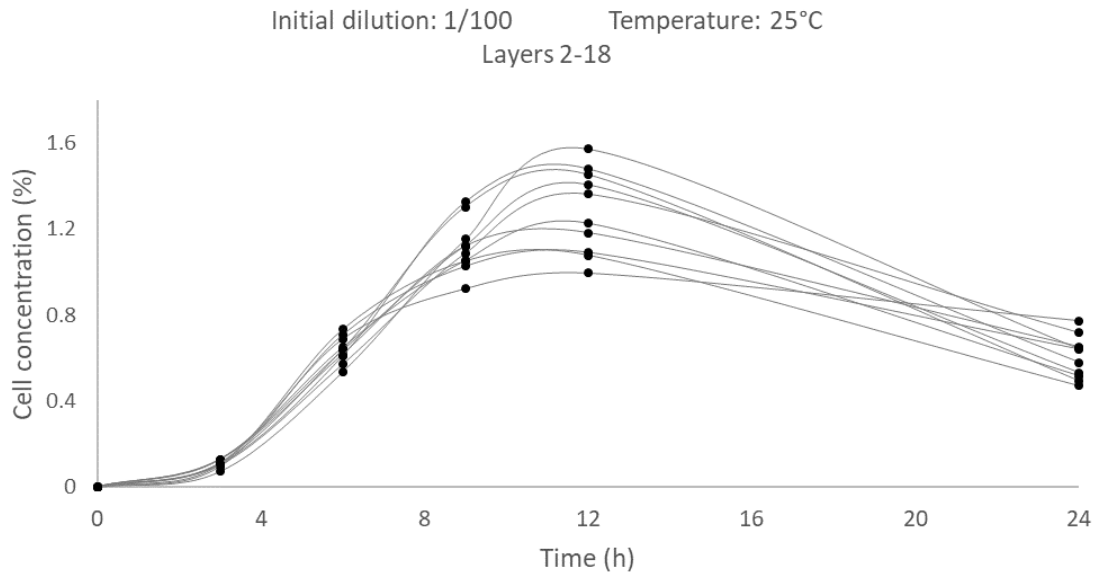
Figure 4-21. Growth curves obtained for layers 2-18

A layer from the middle of the cylinder was selected randomly (11) alongside layer 1, 19 and 20 and were the ones used to analyse the growth behaviour and make a comparison between the different conditions. Figure 4-22 shows the different growth profiles obtained from the experimental program corresponding to the different growth conditions analysed.

The effect of the initial concentration of cells on the growth profile is substantial, as it can be seen comparing the graphs on the left side of Figure 4-22 (1/1000 dilution) with those on the right side (1/100 dilution). However, the difference in cell concentration (%) throughout the 24-hour period is smaller than a 10-fold, suggesting that even though the initial amount of CFU is 10 times lower for the samples inoculated at 1/1000 dilution, the actual bacterial yield is higher in the samples with low initial cell concentration. This phenomenon might possibly be associated to a higher amount of nutrients available for each cell in the *low concentration* samples, promoting an accelerated microbial growth rate. Note that, similarly to the tests performed in Petri dishes (section 4.4.4. Bacteria growth in agarose hydrogels), sporulation of the cells might also occur within the cylinders due to adverse growing conditions, potentially having a significant effect on the growth-decay behaviour.

Figure 4-23 displays the growth profiles of the 4 layers selected and compares them to the growth profile obtained from the analysis in small samples (Petridishes) from section 4.4.4. Bacteria growth in agarose hydrogels. The shape of the growth profile in small agarose samples (red line) is somewhat similar to the growth profile at the top of the cylinders (layer 20), as expected. However, the growth rate and cell concentration values are much reduced in the cylinders, despite having the same initial concentration of cells and being incubated at the same temperature. This phenomenon is presumably associated to a lower concentration of cells due to reduced oxygen conditions; however, this might also be related to issues with the CONFOCAL microscope and the method used to obtain visualisations of the bacterial colonies at different depths within the gel. Either way, a more thorough analysis is recommended in order to get a more robust understanding.

In addition, the effect temperature and initial dilution have on the growth behaviour is similar for both small and large (cylindrical) samples. Incubating the cylinders at higher temperatures, leads to an increased growth rate and an early start of the exponential phase. Similarly, the stationary phase is reached earlier for samples incubated at higher temperatures and it is followed by a rapid decay – or death – phase. This behaviour is also observed in Tuson et al., (2012), where the growth of different bacteria strains was monitored in 24-well plates containing bacteria-seeded polyacrylamide (PA) hydrogels using absorption spectroscopy measurements (wavelength λ=595nm). Amongst all the strains grown at 37°C, *B. subtilis* was the only one that decayed very rapidly after reaching the peak concentration, similar to the profiles displayed in Figure 4-22 for samples incubated at 35°C.
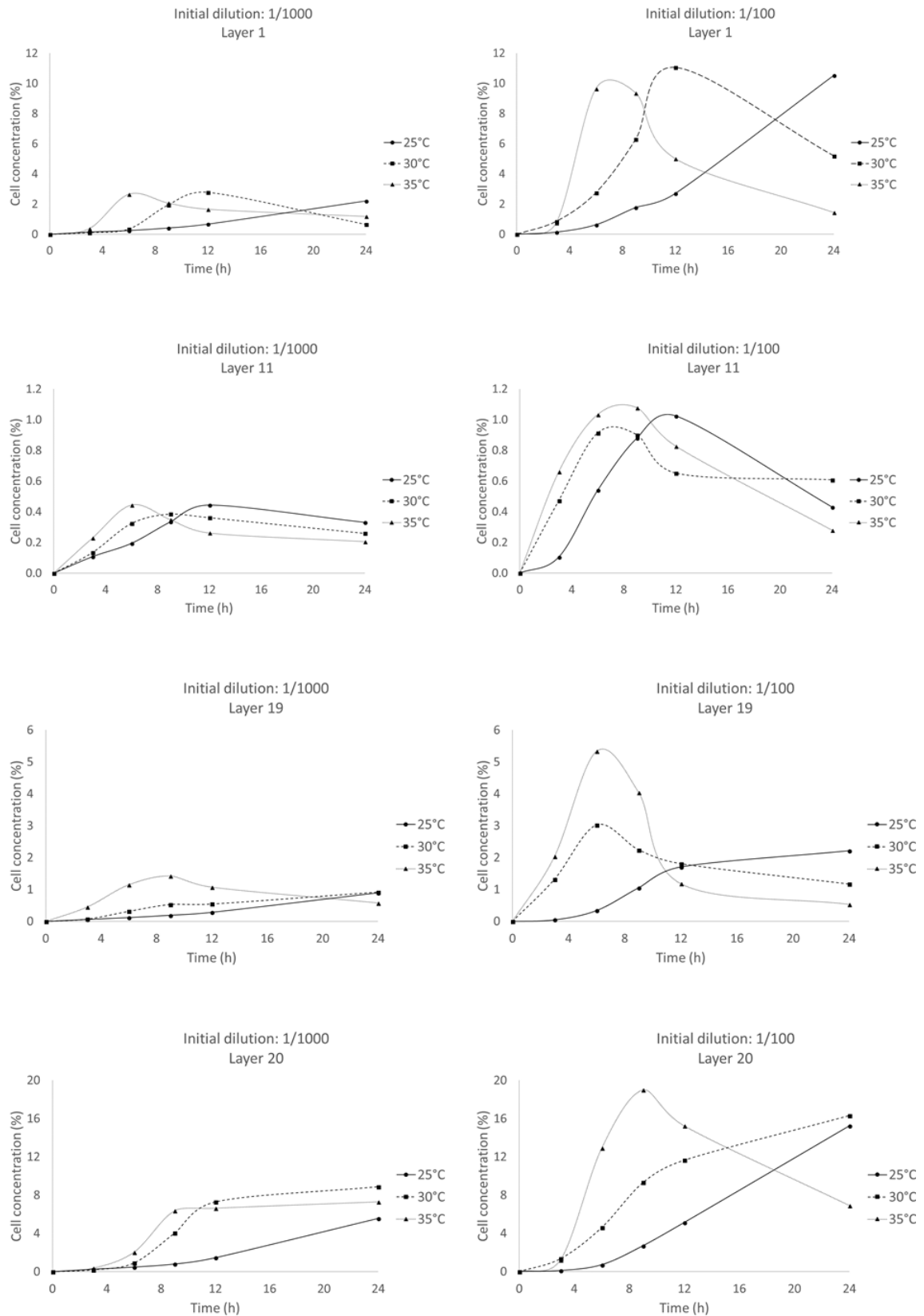
Figure 4-22. Effect initial cell concentration and temperature on growth profile for different layers

Initial dilution: 1/100

Initial dilution: 1/100

124
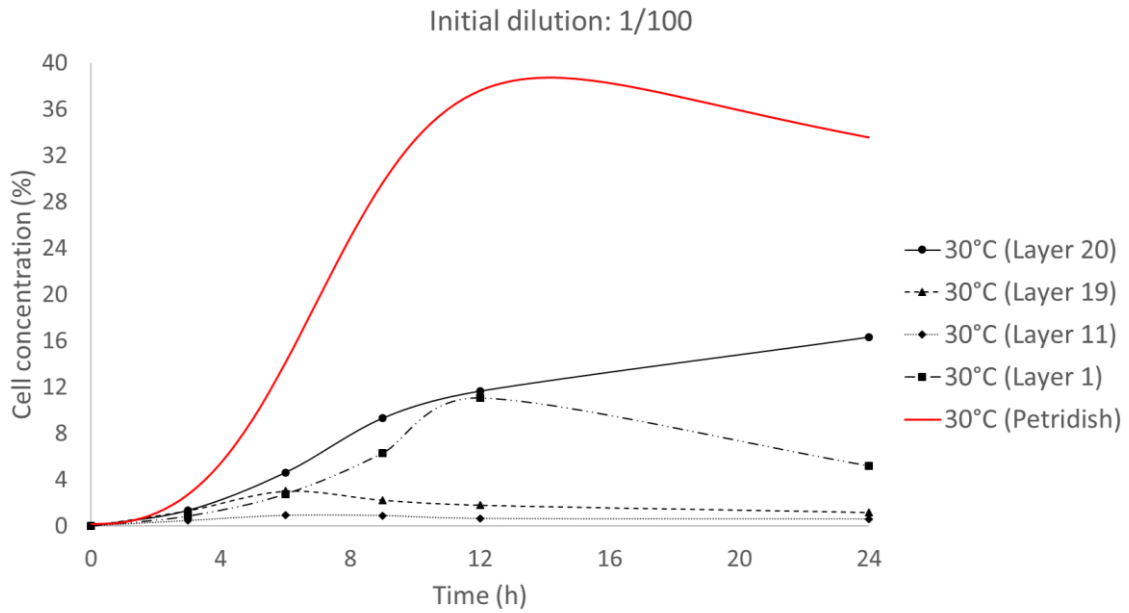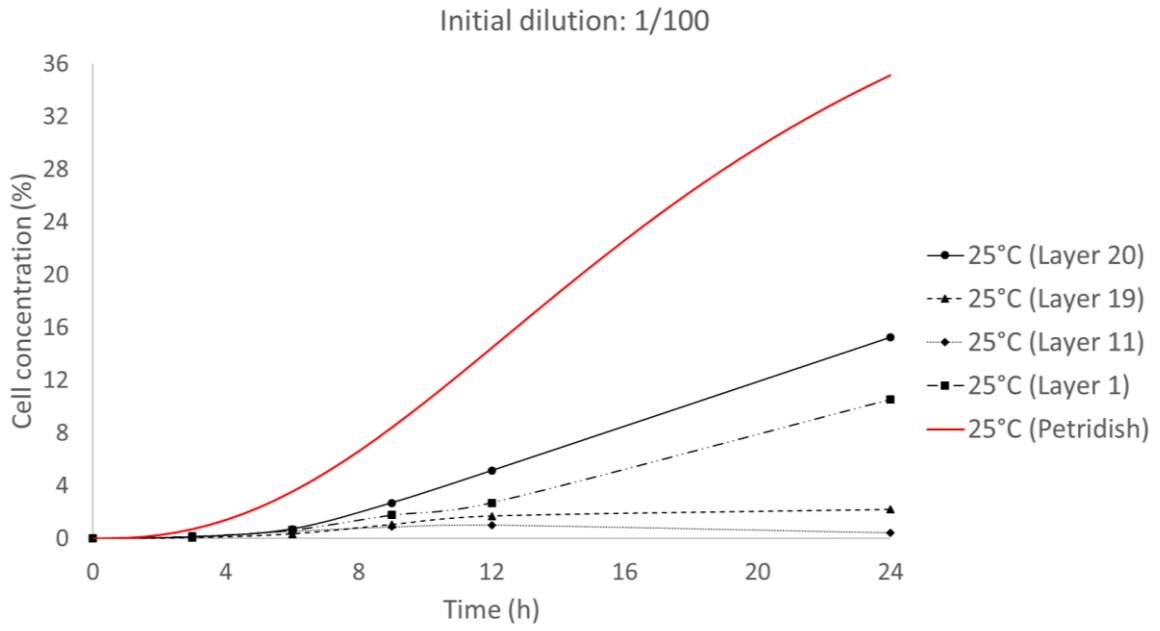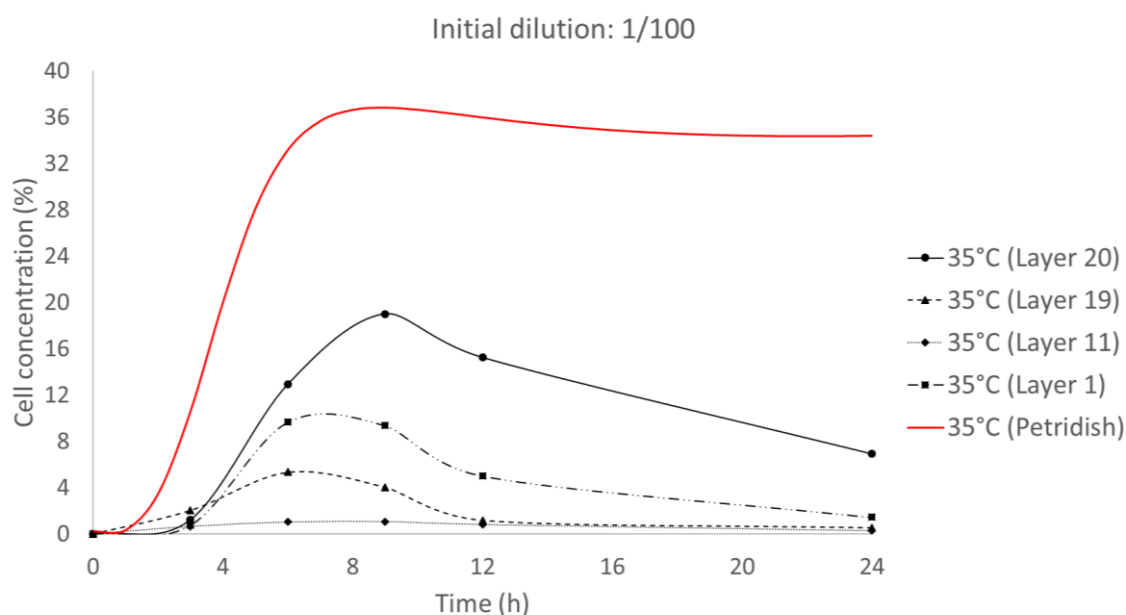
Figure 4-23. Growth profile for different layers at 1/100 dilution and 25°C (top), 30°C (middle) and 35°C (bottom). Red line represents the growth profile of B. subtilis in Petridishes for the same conditions, obtained from Figure 4-16

Finally, the data points obtained experimentally were used to generate the growth profile for each of the conditions and layers, by following the procedure described in section 4.3.4. Growth monitoring in bacteria-seeded hydrogels. Appendix D summarises the equations that best represent the growth behaviour for each of the conditions and layers within the gel. These profiles were then used as an input for the computational model so that the cell concentration over time under specific growth conditions can be easily simulated (*see Chapter 5*).

4.5. Concluding remarks

The above described experimental program investigates the growth and distribution behaviour of bacteria cells – and in particular *B. subtilis* cells – in 3D-seeded agarose gels. A method was developed to produce gels homogeneously seeded with bacteria cells, which also allowed visualisation of the 3D colonies within the porous structure. Additionally, the growth profiles of *B. subtilis* in cylinders of agarose gel were analysed

under different growing conditions. The following conclusions were summarised in accordance to the results obtained from the experimental program:

- A new method was successfully developed to produce 3D-seeded agarose gels with uniformly distributed bacteria cells throughout the volume of gel.

- CONFOCAL microscopy allowed exploration of the colony formation and distribution behaviour of bacteria cells as well as real-time monitoring of the growth rate and the relationship between bacteria cells and their environment

- For the growing conditions tested, 6% is the highest concentration of LM agarose that allows homogeneous cell growth and distribution. Samples prepared with higher concentrations of agarose show a non-uniform distribution.

- The colony formation patterns differ significantly depending on the bacterial strain. While *E. coli* colonies tend to form cluster-like colonies, *B. subtilis* colonies tend to form branches through the matrix of the gel as they grow.

- The growth rate of bacteria colonies in liquid media or in Petri dishes differs significantly to that occurring within the matrix of cylinders of agarose gel. The growth rate in 3D hydrogels is much reduced due to the limitation of space for the cells to grow and move as well as a reduced oxygen availability.

- Different growth rates appear at different depths within a cylinder of hydrogel. Layers in the middle of the cylinder show a much reduced growth rate in comparison to top or bottom layers. It is presumed that this behaviour occurs due to the different levels of dissolved oxygen available throughout the gel sample. Other factors such as differential nutrient consumption or sporulation might also have an effect on the growth behaviour, but understanding their impact is out of the scope of this thesis.

- The number of cells inoculated into the gel also have a considerable effect on the growth profile. However, the relationship between the amount of CFU inoculated and the cell concentration over time is not proportional.

- Temperature has a major effect on microbial growth behaviour. Similarly to the growth behaviour on liquid media, increasing the growing temperature leads to an accelerated growth rate over the first hours. However, increasing temperature also leads to an accelerated decay rate after the peak concentration is reached. It

is presumed that this phenomenon might be associated to the generation of spores at high temperatures.

- The bacterial growth profiles were numerically obtained using non-linear regression and are presented in Appendix D. These expressions are introduced into the computational model in order to simulate the distribution and concentration of *B. subtilis* cells over time throughout a volume of agarose hydrogel (see *Chapter 5* for more details).

The development of this novel method to prepare 3D bacteria cultures in hydrogels has implications for *Thinking Soils* since it allows real-time monitoring of the cell behaviour and the response to specific stimulus – such as pressure. However, the author believes this method might also be useful to the wider community of researchers, especially for research projects involving the use of engineered organisms, and the interaction between engineered cells and specific environments. A discussion about the possibilities of using this method for other applications is provided in *Chapter 6. Conclusions*.

The following chapter details the design of the computational model and provides with series of simulations describing the behaviour of a pressure-sensitive gel-based system under different environmental conditions and loading scenarios.

Chapter 5

Modelling of a Gel-based Pressure-responsive System

5.1. Introduction

This chapter aims to describe the development of a computational model that integrates geotechnical simulations with biological data and predicts the behaviour of a bacteria-based pressure-responsive system. The model reproduces the behaviour of agarose gels under loading by incorporating the *macro-scale* level data obtained in Chapter 3 (i.e. mechanical properties of the agarose hydrogel and behaviour under loading). The model also incorporates the *micro-scale* level data obtained in Chapter 4 relative to the growth and distribution behaviour of bacteria colonies homogeneously seeded within the 3D structure of agarose gels. Finally, the model integrates these mechanical and biological simulations with hypothetical data of the *nano-scale* behaviour of pressure-sensitive bacteria cells and their enzymatic activity in response to such stimulus.

The development of the model is described step by step in this chapter, alongside the governing equations that dictate the behaviour of the bacteria-seeded hydrogel under loading. The model is based on the computational work presented by Dade-Robertson (2015) and Dade-Robertson et al. (2016) where the behaviour of the ground underneath a raft foundation was represented for different loading scenarios – with the main difference being that the current model is specifically tailored for agarose hydrogels and their behaviour under loading, and real data about the growth behaviour of bacteria in 3D hydrogels and their distribution and colony formation throughout the volume is considered. Therefore, it is important to mention that the validity of the results obtained from Chapter 3 and 4 are recognised to be vital for the development of the computational model and the successful implementation of the gel-based physical demonstrator.

The *Design rationale* section describes the reasoning behind the selection of the parameters used for the development of the model. The section *Model development* describes the steps

taken to generate the model alongside the mathematical expressions used to represent and predict the behaviour of the hydrogel under different loading conditions. Furthermore, the different parameters and boundary conditions used for the development of the model are also described in this section as well as the assumptions adopted.

The *Model simulations* section provides with simulations taken from the 3D model that represent the behaviour of the system under different conditions and loading scenarios.

Finally, the *Model limitations* section critically discusses the limitations of the current model.

5.2. Design rationale and conceptual model

As described in Chapter 1, *Thinking Soils* aims to design a material that remodels itself in response to the forces from the environment. The framework used to develop this kind of responsive system is based on how the stresses distribute through the ground upon application of a load on top of a shallow foundation (see Dade-Robertson (2015)). The proposed model aims to use the same design framework and simulate how the pressure-sensing system responds to such stress distribution in a gel-based prototype demonstrator, which can be easily operated in a controlled laboratory environment and used to validate the proof of concept of such responsive system.

Therefore, the model aims to represent the behaviour of a small-scale gel-based soil-foundation system that integrates data from the nano to the macro scale and predicts the behaviour of the pressure-sensitive crystal-producing cells in a 3D gel-type structure, analogous to certain types of soils. Additionally, the model will allow for simulation of different loading scenarios and the consequent response of the system to such stimulus. As described in Chapter 2, the idea behind this pressure-sensing system is to generate localised changes in stress upon loading, which will be perceived by the cells living in the gel and will, ultimately, respond by inducing specific conditions in their microenvironment that will promote crystal precipitation.

The model represents three types of behaviour: the *mechanical* aspects, where the stresses upon loading, pore pressure generated, consolidation effects and settlements are analysed; the *biological* aspects, which contains the data obtained experimentally from Chapter 4

regarding microbial growth and cell distribution; and the *integrated system* that couples both the mechanical and biological aspects with hypothetical data on the nano-scale behaviour of a pressure-sensitive strain of bacteria and its response in terms of enzymatic activity. Such an integrated system allows for representation of different environmental conditions and simulates how the system will respond.

5.3. Model development

The model proposes a scenario in which a 100x100x100 mm volume of hydrogel is homogeneously seeded with bacteria cells and is subjected to different growing and loading conditions, depending on its boundary conditions. For this case, the model is based on a loading system similar to the one found in an oedometer setup (see section 3.3.6. Oedometer tests). Thus, the design of the future physical demonstrator is expected to involve the use of a oedometer cell modified in such a way that it can accommodate a mould containing the 1000 cm^3 volume of gel and to which a desired load can be applied on top of the gel, simulating the effect of a rectangular foundation. With such a setup, the oedometer apparatus would control the magnitude of the loads applied onto the simulated foundation or *loading platform* as well as the deformations occurring to the gel volume. In addition, the model not only provides graphical and numerical simulations of the system for future comparison but also informs the design of the physical demonstrator.

5.3.1. Software

The software used to develop the model was Processing (v3.3.6), an open-source, object-oriented programming language based on Java. This software was selected due to the many built-in features and the user-friendly coding environment, which allow a non-expert user to create relatively complex graphical applications in a simple way.

Appendix E contains the raw code used to develop the application, along with comments describing each line of code. Like most object-oriented coding environments based on *Java*, *Processing* follows a very simple syntax which starts by the definition of *objects* (e.g. variables

and classes) followed by the definition of *methods* (e.g. statements, functions, etc) that dictate the behaviour of such objects.

5.3.2. Mesh generation and Finite Element computation

Similarly to the earlier soil-based version of the model presented in Dade-Robertson (2015), the code implements a type of finite element analysis in which the analysed volume is divided into smaller parts, by generating a 3D mesh of cubic elements or *voxels*, allowing the evaluation of the behaviour at individual points within the 3D volume of gel. The volume of gel is divided into 40 voxels in each direction, leading to the formation of 64,000 voxels (see Figure 5-1). The simplicity of the mesh and the cubic shape of the voxels facilitates computation of the set of equations integrated in the model.
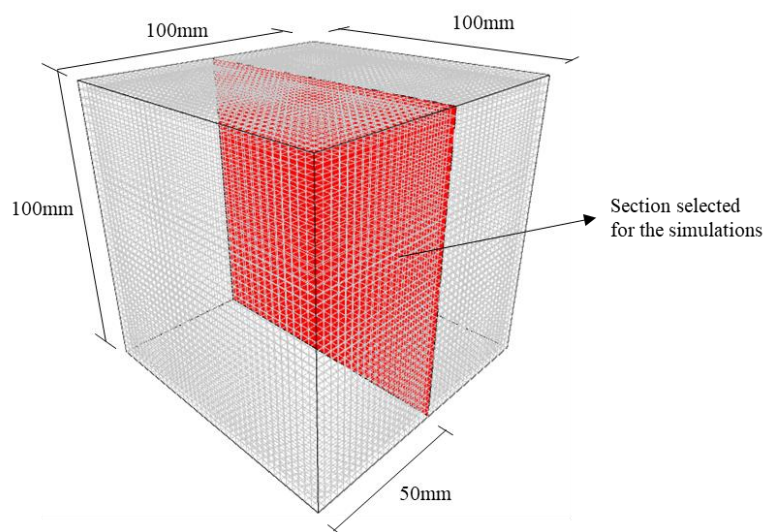
Figure 5-1. Diagram to illustrate the dimensions of the gel volume and the section through the centre used to produce the 2D simulations

In this way, every individual voxel within the gel volume shows a response to the different mechanical and biological parameters analysed, and the coupling of all the voxels together leads to the generation of the 3D simulations. Figure 5-1 shows the section selected to analyse the behaviour of the simulations.

5.3.3. Boundary conditions

The model proposes a system in which the 3D volume of gel is contained within a 100x100x100 mm solid mould, as described above. The boundary conditions play a major role in defining the behaviour of the gel volume upon loading. Three potential scenarios are studied, which are described as follows:

a) Fully constrained volume of gel under undrained conditions

This scenario considers the volume of gel to be *fully constrained* in all directions (does not allow deformation), as it is represented in Figure 5-2. Both the lateral walls and the base of the mould are impermeable and do not allow any movement – they simply limit the volume of gel. Additionally, no drainage of the pore water occurs through the impervious stone and, hence, consolidation does not take place – i.e. volume of the gel does not change. The load applied on top of the impervious surface generates a distribution of total stress (pore water pressure) equal in all parts of the volume and does not dissipate – i.e. the stress at a point located in the middle of the gel volume is equal to the stress at a point located next to the mould wall.
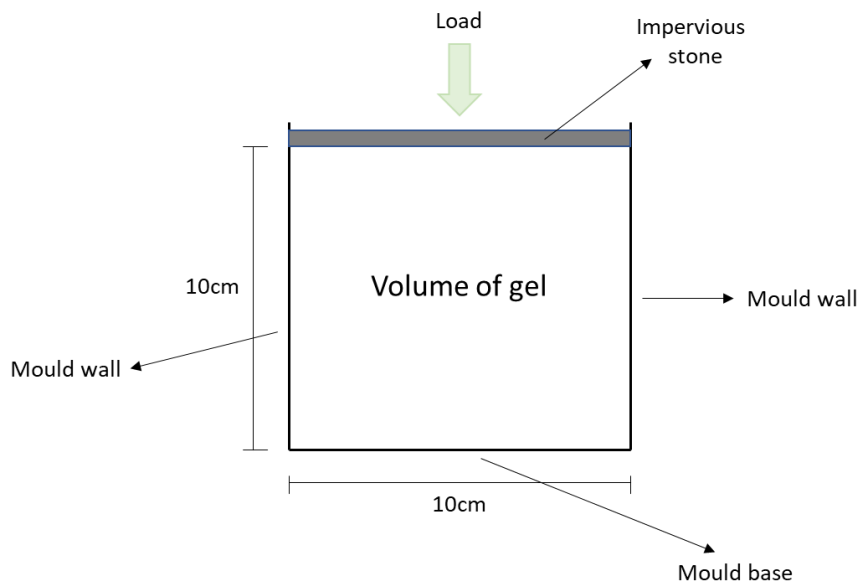
Figure 5-2. Representation of a fully constrained scenario under undrained conditions

b) Laterally constrained volume of gel under drained conditions

This scenario considers the volume of gel to be *constrained laterally* (no deformation allowed laterally) but allowing drainage of the pore water in the vertical direction, and consequent vertical deformation. The mould walls are impervious and do not allow any movement, but the porous surfaces at the top and bottom of the mould allow vertical drainage of water upon loading, as represented in Figure 5-3, leading to consolidation, volume reduction and pore pressure dissipation. Additionally, this setup allows the user to select between one-way and two-way drainage. The load applied on top of the porous surface generates a distribution of total stress (initially carried by the pore water) equal in all dimensions, which is gradually transferred to the gel skeleton as consolidation occurs (see section 5.3.4. Mechanical behaviour for more details). Also, note that this scenario is identical to that in an oedometer cell.
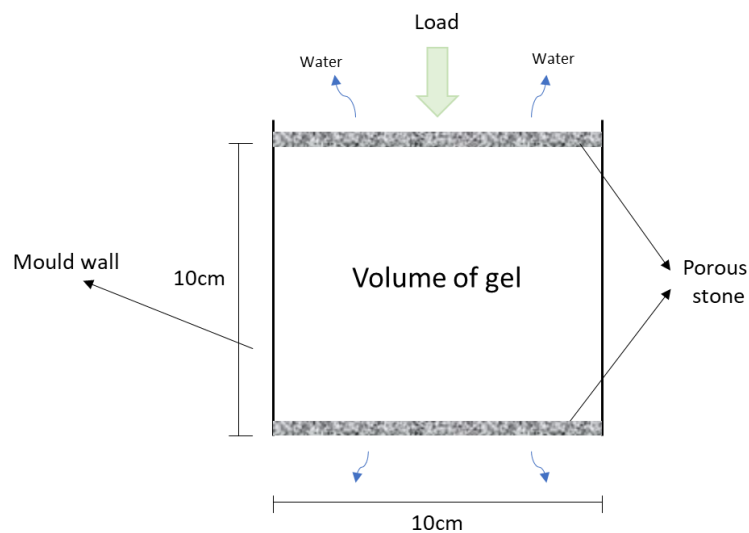
Figure 5-3. Representation of a fully constrained scenario under drained conditions

c) Semi-infinite volume of gel

This scenario aims to represent the behaviour occurring in a semi-infinite volume of gel – i.e. volume limited in one direction (vertical) and infinite in the other (horizontal). In order to achieve this behaviour, the volume of gel is constrained laterally (drainage and deformations are not allowed), similarly to case a) and b), however, in this case the dimensions of the *loading platform* are considerably smaller than the gel surface, as illustrated in Figure 5-4, developing a radial distribution of stresses (see section 5.3.4. Mechanical behaviour for more details on how stresses distribute upon loading). The dimensions of the loading surface must

134

be small enough so that the stresses developed at the lateral boundary upon loading are negligible. This way, the effect of the lateral confinement can be neglected and the stress distribution is not affected by the boundaries. In addition, this scenario also allows the user to choose between one-way or two-way drainage.
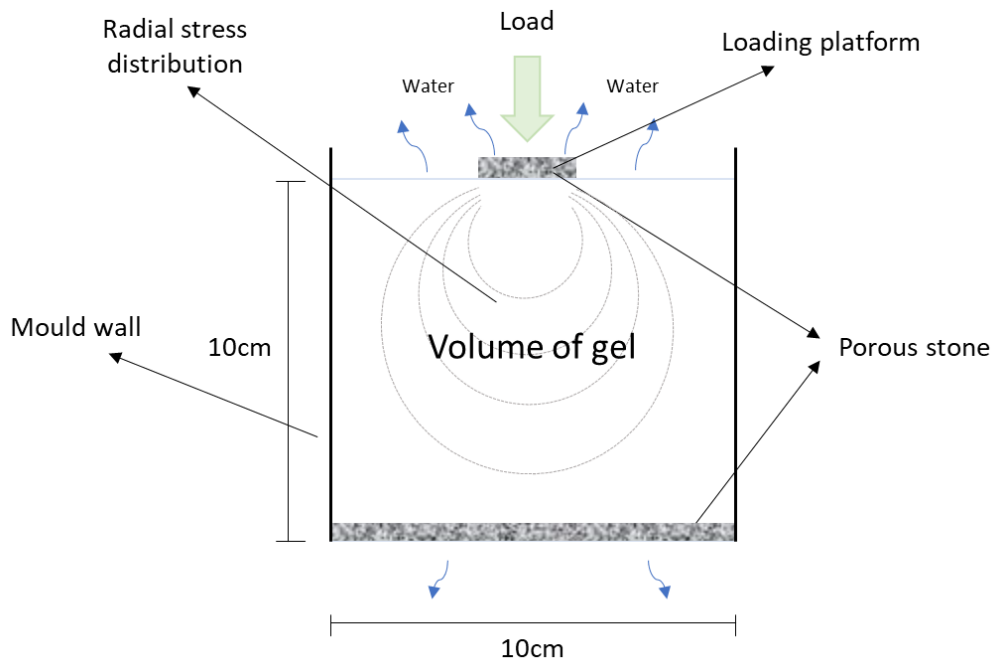
Figure 5-4. Representation of a scenario simulating the effect of semi-infinite volume of gel

5.3.4. Mechanical behaviour

This section describes the mechanical aspects taken into consideration in the design of the computational model in order to examine the mechanical behaviour of the hydrogel upon loading. The model aims to represent the stress distribution under different loading conditions as well as the generation and dissipation of pore pressures and the settlements occurring due to consolidation. Each of the following sections includes the mathematical expressions adopted to represent the relevant behaviour.

- Stress distribution upon loading

As load is applied onto the surface of the gel, a differential total stress distribution is generated, with greater values directly underneath the load area, and reduced levels of stress as depth increases. Boussinesq (Boussinesq, 1871) developed the mathematical relationships

for determining the normal and shear stresses at any point within a *homogeneous*, *elastic* and *isotropic* medium due to a concentrated load applied on the surface of it. For a soil scenario, it is assumed that the soil mass is isotropic, homogeneous and fully elastic and that the semi-infinite space is free of initial stress and deformation. In the case of hydrogels, due to the homogenous matrix structure, the material is expected to be isotropic and, additionally, hydrogels have an elasto-plastic behaviour upon loading, but the elastic region is greater than in soils. Hence, adopting Boussinesq's stress distribution in hydrogels is appropriate.

According to Boussinesq's solutions, the distribution of vertical total stresses upon loading is radially symmetrical and decreases with the square of the depth beneath the application point. Hence, the value of the total stress within a volume of soil directly depends on the value of the applied load as well as the location of the point considered.

Since the model aims to represent the stress distribution generated underneath a rectangular loading platform (simulating the effect of a loaded building foundation), an integration of the Boussinesq solution has to be adopted. Fadum (1948) developed a method to obtain the vertical stress value at the corner of a rectangle on which a pressure is applied uniformly and in the normal direction. In order to obtain the value of the vertical stress at any point within the gel, the analysed area needs to be divided into four rectangles, as illustrated in Figure 5-5, where P is the point of interest. The principle of superposition is applied so that the stress at any point of the 3D volume of gel can be calculated. As it can be seen from the illustration, the contribution of each rectangle is provided by the *Influence* value, *I*. This value can be calculated by using the following expressions (Fadum, 1948; Poulos and Davis, 1974).

$$I = \frac{1}{2\pi}\left[\arctan\left(\frac{m*n}{\sqrt{m^2 + n^2 + 1}}\right) + \left(\frac{m*n}{\sqrt{m^2 + n^2 + 1}}\right)\left(\frac{1}{1 + m^2} + \frac{1}{1 + n^2}\right)\right]$$

$$m = \frac{b}{z} \qquad n = \frac{l}{z}$$

(Equation 5-1)

136

where b and l are the breath and length of each of the resulting rectangles and z is the depth of the point of interest, as shown in Figure 5-5. The final vertical stress due to a rectangular loading at any point within the 3D volume of gel can be obtained by using the following expression:

$$\sigma_z = q * (I_1 + I_2 + I_3 + I_4)$$

(Equation 5-2)

where q is the pressure applied on the rectangular surface due to a constant load and $I_{1,2,3,4}$ is the influence value given by each of the rectangles.
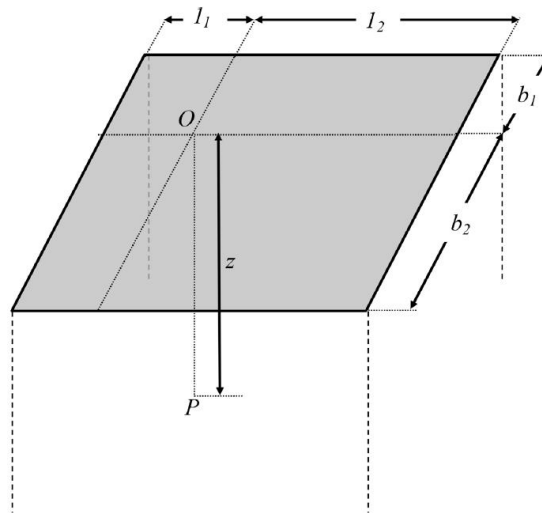
Figure 5-5. Diagram to illustrate the method adopted to calculate the stresses generated underneath a rectangular foundation

(after Dade-Robertson et al. (2018)).

Once the value of the vertical stress has been calculated for each of the *voxels* within the 3D volume of gel, the simulations are displayed by assigning a colour to each voxel, which depends on the stress level.

- _Bearing capacity of the gel system_

The scenario presented in Figure 5-4 relies on the gel being strong enough to withstand the pressures applied by the external load. If the stresses generated are greater than the _bearing capacity_ of the gel, the interface between the loading platform and the gel will collapse. Terzaghi (1943) investigated shearing failures occurring due to excessive load in areas underneath a shallow building foundation. Figure 5-6 represents the three possible sliding surfaces or _modes of failure_ that might occur after an excessive load is applied, which depend on the type of the soil. For the case of soft cohesive soils, failure is expected to occur by _punching shear_. Therefore, due to the similarities between the agarose gel and this type of soils, it is assumed that if the load applied exceeds the bearing capacity of the gel, the loading platform will collapse by p_unching shear_ failure.
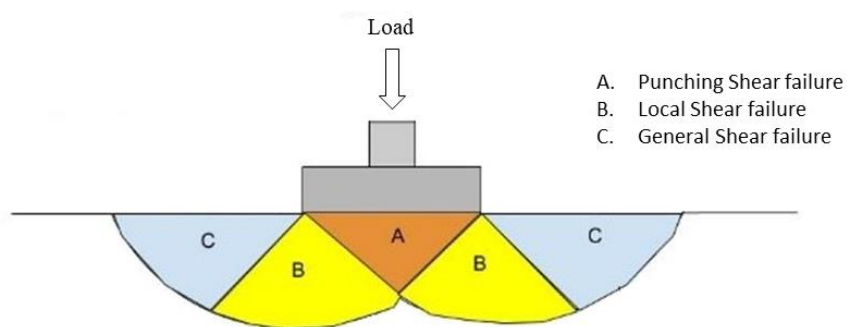
Figure 5-6. Different modes of failure upon excessive loading (representation of Terzagui's failure zones underneath a shallow foundation)

Independently of the different shearing failure modes, the system will not collapse if appropriate loads and dimensions of the loading platform are selected. Considering hydrogels are fully saturated, the most critical point is immediately after the load has been applied. Thus, undrained conditions must be adopted to calculate the maximum bearing capacity of the gel. Skempton (Skempton, 1951) developed a simplified version of Terzaghi's bearing capacity equation (Equation 5-3) for the case of saturated cohesive soils – i.e. loading in undrained conditions. Since the angle of internal friction is equal to 0, the expression only depends on the undrained shear strength C_u and the Skempton factor N_c :

$$q_f = C_u * N_c$$

(Equation 5-3)

where q_f is the ultimate bearing capacity of the system. If the foundation is square and located at the surface (i.e. z=0), the Skempton factor *Nc* is equal to **6.2**, as it can be seen from Figure 5-7.
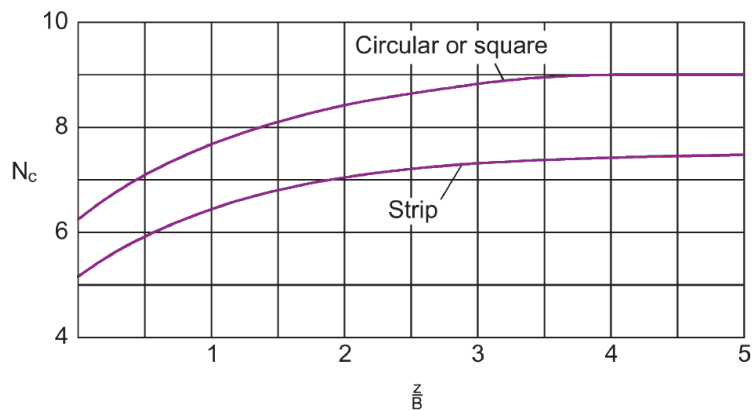
Figure 5-7. Diagram representing the variation of the Nc coefficient with depth

(reproduced after Skempton (1951))

As demonstrated in Chapter 3, the undrained shear strength of our hydrogel ranges between 23 and 31 kPa, depending on the value of the confining stress or σ_3. Without a better understanding of this behaviour, the average undrained shear strength value was adopted. This equals to approximately 27 kPa, and using Skempton's expression, the ultimate bearing capacity of the gel can be calculated, as approximately **167 kPa**.

The ultimate bearing capacity of the gel was integrated in the model in such a way that if the combination of load and loading platform dimensions selected does generate stresses greater than the ultimate bearing capacity, the model does not proceed and displays the text *"Bearing capacity exceeded"*.

Note that adopting an average C_u value is considered acceptable due to the preliminary nature of the model. However, the selection of the undrained strength value will have implications for the model, in particular the maximum load that can be applied and the associated bearing capacity of the gel. Therefore, it is recommended that, once this variation

on C_u is better understood, the computational model should be updated to reflect these changes.

- *Consolidation behaviour*

Similarly to saturated cohesive soils, the micropores of the gel are filled with water, and as a load is applied on to the surface of the gel, an excess pore pressure develops of the same magnitude. This behaviour occurs due to the incompressibility of water compared with that of the gel (fibre) microstructure. These excess pores pressures generated are only able to dissipate if drainage of water occurs, leading to *consolidation* of the sample (Terzaghi, 1943). As consolidation occurs, the load is gradually carried by the gel skeleton. When these excess pressures have dissipated entirely, the system has finished primary consolidation at that level of stress, and the pressures are equalised throughout the system. The excess pore pressure generated within the system upon loading depends on several parameters (Powrie, 2014):

- The magnitude of the applied vertical stress

- The permeability of the system

- The length of the drainage path

The consolidation effect upon drainage is accompanied by the restructuring and compression of the system (in this case the gel matrix). At the moment all the excess pore pressures have dissipated, the loading stress generated by the force applied onto the loading surface is only supported by the fibrous microstructure of the gel. The rate at which consolidation occurs is dictated by the coefficient of consolidation, c_v (calculated in Chapter 3).

The computational model is able to represent the dissipation behaviour of the pore pressures generated within the gel upon loading. In addition, the restructuration of the gel matrix upon consolidation leads to a reduction of the gel volume and consequent settlement – i.e. vertical displacement of the loading platform due to drainage.

Both the pwp (pore water pressure) dissipation effect as well as the settlement occurring to the loading platform are described in the following sections.

Excess pore pressure refers to the water pressures developed within the pores upon loading. As mentioned above, if the pores of the gel are fully saturated, the value of the stress applied due to loading is carried completely by the water within the pores, and it is gradually transferred to the fibrous microstructure as consolidation occurs.

Terzaghi's one-dimensional consolidation equation (Terzaghi, 1943, 1925) can be used to calculate excess pwp over time in the vertical direction. This is given as follows:

$$\frac{\partial^2 u}{\partial z^2} c_v = \frac{\partial u}{\partial t}$$

(Equation 5-4)

where *u* refers to the excess pwp at the time *t* and depth *z*, and c_v is the coefficient of consolidation, which, as defined above, determines the rate at which consolidation of the system occurs. The coefficient of consolidation can be calculated as follows:

$$c_v = \frac{k}{\rho_w * g * m_v}$$

(Equation 5-5)

where *k* is the permeability of the system, ρ_w is the water density, *g* is the gravitational acceleration and m_v is the coefficient of compressibility.

The solution to Terzaghi's one-dimensional consolidation can be solved mathematically by using Fourier series (Taylor, 1948). Abid and Pyrah (1988) developed a simplified version of the differential equation so that it can be easily implemented in a coding environment:

$$u_{z,t+\Delta t} = u_{z,t} + \beta * \left[u_{z-1,t} + u_{z+1,t} - 2 * u_{z,t} \right]$$

(Equation 5-6)

where β is a coefficient that directly depends on the coefficient of consolidation c_v and it can be calculated as follows:

$$\beta = \frac{c_v * \Delta t}{\Delta z^2}$$

(Equation 5-7)

This method of analysing the one-dimensional consolidation and excess pore water pressure dissipation relies on several assumptions:

- The voids within the system must be completely filled with water.
- Water and soil grains are considered perfectly incompressible.
- The coefficient of permeability is considered constant throughout the system.
- The excess pore water pressures at the drainage ends is considered to be 0, immediately after the load is applied.
- The system is assumed to only drain in the vertical direction
- The flow of water draining out of the system depends on the its permeability and the hydraulic gradient generated in the direction of the flow, i.e. Darcy's law applies (Darcy, 1856).

These assumptions are originally for granular materials, however, as explained above, due to the composition and structure of the gels (fibrous matrix containing micropores saturated with water), it is assumed that the same assumptions apply and that consolidation occurs in a similar way than in soils.

- Settlement

As described in previous sections, settlement refers to the compression of a soil layer due to the stress generated by loading the surface. This concept is originally used for granular materials and a soil-structure environment, however, it is assumed that the same theory applies for our hydrogel system. Modelling with accuracy the amount of settlement occurring in a gel volume upon loading is very important since its value strongly depends on the stiffness of the gel. By measuring the amount of settlement generated after the load is applied, an estimate of the stiffness of the sample as well as comparison between samples can be made. For instance, gel samples with a larger concentration of crystals precipitated will most likely be stiffer, and the settlement occurring upon loading will be reduced in comparison to more

compressible samples. More details on this are provided in *Chapter 6. Conclusions and Recommendations for Future Work*.

This study has focused on modelling the settlement behaviour in agarose gels so that the deformations occurring to the future physical demonstrator upon loading can be compared to the values obtained from the computational model, and the accuracy of the model in representing this behaviour can be assessed. The model evaluates two types of settlement: immediate settlement or *elastic deformation* and consolidation settlement.

1) *Elastic deformation*.

Immediately after the load is applied, elastic deformations occurs at the surface of the gel, as represented in Figure 5-8.
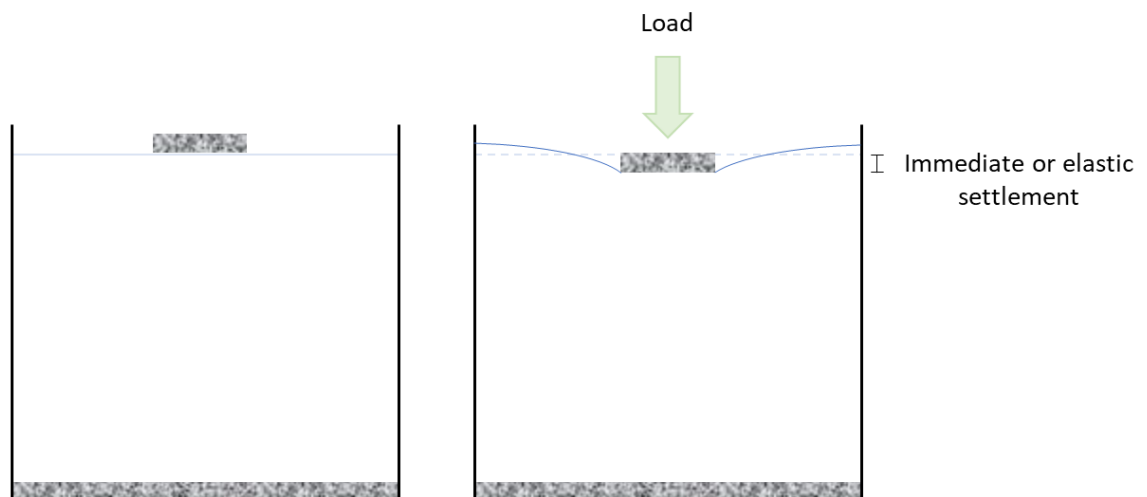
Figure 5-8. Representation of elastic settlement occurring upon loading

This elastic or *immediate settlement* purely occurs due to the elastic properties of the material. Therefore, it is assumed that it occurs under linear elastic conditions and the elastic or Young's modulus E is used for its calculation, amongst other parameters. The expression that calculates the total amount of immediate settlement (S_I) occurring in a homogeneous layer of gel due to uniform loading is represented as follows:

$$S_I = \left(\frac{1-v^2}{E}\right) * q * B * I_\rho$$

(Equation 5-8)

143

where v is the Poisson's ratio of the gel, E is the Young's modulus of the gel, q the contact pressure at the base of the loading surface, B the width of the loading surface and I_ρ the influence factor, which depends on the shape and rigidity of the loading surface. If a rectangular rigid loading surface is considered, the I_ρ is equal to 0.9 (Smith, 2014)

However, a different method was used for the computation of the immediate settlement. Rocscience Inc., (2007) developed a software (*Settle3D*) that, amongst other features, computes the value of the immediate settlement at each point within a volume of soil. The method relies on (Equation 5-10) – which is based on the principle of elasticity and the relationship between the total stress, strain and Young's modulus. For this method to be accurate, the longitudinal or *constrained* Young's modulus (E_s) must be used instead. This modulus is defined as the ratio of axial stress to axial strain in an uniaxial strain state – which are the conditions present in our setup. The expression to calculate E_s from the value of the Young's modulus is as follows:

$$E_s = \frac{E}{\left(\dfrac{(1+v)(1-2v)}{1-v}\right)}$$

(Equation 5-9)

where v is the Poisson's ratio of the material. Since the value of the Poisson's ratio has not been obtained for the agarose gel, a slider was added into the Graphic User Interface (see section 5.3.7. Graphic user interface) so that the user can select a value out of a range provided. It is expected that, in future experiments, more mechanical tests will be performed in order to provide an insight into some of the remaining unexplored properties of the gel, including the Poisson's ratio. Normand et al. (2000) estimated the Poisson's ratio to be equal to 0.5, for large deformations. Furthermore, Takigawa et al. (1996) discovered that the Poisson's ratio of Polyacrylamide gels – which have similar properties to agarose gels and are also used in molecular biology – is equal to 0.457.

The vertical strain at each of the layers of hydrogel can then be calculated with the elasticity relationship:

$$\varepsilon = \frac{\Delta\sigma}{E_s}$$

(Equation 5-10)

where $\Delta\sigma$ is the increase in vertical stress at every point. The vertical displacement δ at each of the layers can then be calculated using the strain values obtained:

$$\delta = \Delta z = \varepsilon * h$$

(Equation 5-11)

h being the original thickness of the sublayer. The immediate settlement is finally computed by using the following expression:

$$\delta_i = \delta_{i+1} + \varepsilon_i h_i$$

(Equation 5-12)

Figure 5-9 illustrates the way in which the computation of the immediate settlement is performed.
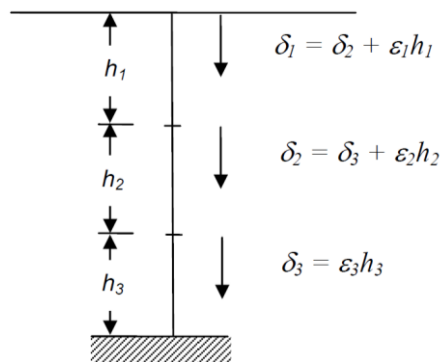
Figure 5-9. Diagram to illustrate the method used to compute the settlement

2) Consolidation settlement

The immediate settlement described above occurs immediately after the load is applied and does not involve any change in volume. However, after the initial load has been applied and the gel deforms elastically, a change in volume gradually occurs due to the process of consolidation, and vertical deformations (due to the *consolidation settlement*) are generated over time.

Vertical stresses transmitted from the surface load are initially carried by the water within the pores, since water is considered incompressible in comparison to the fibrous microstructure of the gel, as mentioned above. Therefore, immediately after the load is applied, primary consolidation begins. This process involves drainage of water from the pores. As mentioned earlier, as consolidation occurs, the load is transferred gradually from the pore water to the skeleton of the system. This load transfer is accompanied by a decrease in the gel volume which is equal to the volume of water drained from the gel. Primary consolidation finishes when all the excess pore water pressures have dissipated. The one-dimensional consolidation behaviour of the gels was analysed in Chapter 3, and the two important parameters that influence consolidation – i.e. the coefficient of compressibility m_v and coefficient of consolidation c_v – were obtained from the experimental program. Terzaghi's consolidation theory can be used to predict the rate and magnitude of the settlement occurring due consolidation.

There are several methods to calculate consolidation settlement, which depend on the parameters that are required for the calculation. The method that was selected relies on the compressibility values obtained in Chapter 3. The model calculates the amount of settlement occurring at each of the 40 horizontal layers of hydrogel, according to the following expression:

$$S_c = \Delta\sigma' * m_v * H$$

(Equation 5-13)

where S_c is the settlement due to consolidation, $\Delta\sigma'$ the increment in effective stress due to the external load, m_v the coefficient of compressibility and H the height of the layer.

The coefficient of compressibility in agarose gels was analysed in Chapter 3 and it was confirmed that its value depends on the stress level. However, for the computation of the settlement, the same value is used for all the layers within the gel and, considering the height of the layers is constant (i.e. 2.5mm), the value of the consolidation settlement only depends on the value of the stress applied at each point within the gel. In addition, the stresses used for the computation are *effective* stresses – i.e. vertical stress minus pore pressure – and, therefore, the pore pressure values were also used in the computation of the settlement, providing a time-dependant solution.

The computation of the total consolidation settlement was then performed by following the same procedure that was used for the computation of the total immediate settlement (Figure 5-9).

5.3.5 Biological aspects

As described in Chapter 2, urease is an enzyme produced by some microorganisms that catalyses the hydrolysis of urea into carbon dioxide and ammonia and under the right conditions, it leads to crystal precipitation. Our system assumes that the three-dimensional distribution of urease within the system directly depends on the location of the cells within the 3D matrix of the gel. However, the amount of urease or *urease activity* in the environment is not necessarily proportional to the cell concentration (see *Chapter 2. Literature review*). The computational model proposes a system where the experimental data from the bacterial growth experiments (Chapter 4) can be associated to hypothetical levels of urease expression. The relationship between cell concentration [%] and urease activity [U/mL] was implemented in the model in such a way that different profiles can be selected and their effect can be visualised.

It is also worth mentioning that some researchers within the *Thinking Soils* group are investigating how urease expression is activated and regulated in *B. subtilis*. Thus, once experimental data relating cell concentration and urease activity is available, the different profiles obtained can be easily introduced in the computational model. That way, the model will be able to generate different urease expression patterns across the gel depending on the growth conditions (see section 5.4. Model simulations).

- Bacterial growth data (cell concentration)

The microbial growth expressions obtained in Chapter 4, which are displayed in Appendix D, were introduced in the main code of the model. A slider was added in the Graphic User Interface to select the growth temperature (*25°C, 30°C or 35°C*) and two toggles were created to select the initial concentration of cells (*low or high*).

Additionally, the microbial growth data is displayed next to the volume of gel in the form of a horizontal bar graph, where the cell concentration [%] is represented for every vertical layer within the gel. Figure 5-10 shows how the cell concentration is represented in the model for one of the growth conditions after 3h of incubation.
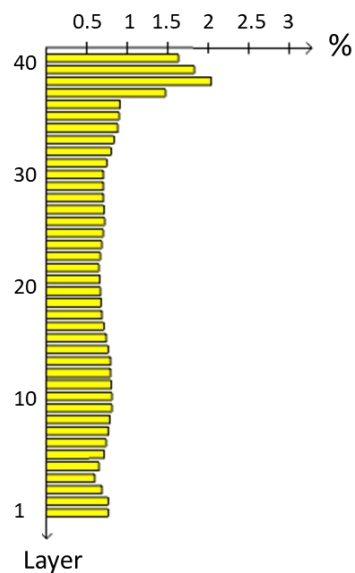
Figure 5-10. Cell concentration after 3h of growth at 35°C (high initial concentration of cells)

- Urease activity relative to cell concentration

The microbial growth data implemented in the code was associated to values representing urease activity, as mentioned above. Due to the lack of experimental data regarding urease activity, the range of values used to describe the behaviour of the urease enzyme were selected to range between 0 and 25 [U/mL] (urease activity units). These values were obtained from the work presented by Phang et al., (2018) where the urease activity is

measured in relation to the cell concentration for several *B. subtilis* species. Thus, the urease expression values produced by a wild-type (i.e. non-engineered) Bacillus strain are expected to be in that range. Furthermore, Omoregie et al., (2017) and Singh et al., (2017) also investigated on the urease activity of *B. subtilis* under different pH solutions, and the higher values obtained were approximately 30 [U/mL] for pH=7.

The model is able to calculate values of cell concentration over time for the required growth conditions, as described in the previous section, and associate these values to hypothetical values of urease expression (Figure 5-11). The results are then represented in the same way as the stresses or the settlements – i.e. assigning a colour to each of the voxels which depend on the urease level values. Hence, by changing the relationship between the urease expression values [U/mL] and the cell concentration [%], different patterns of urease levels within the gel volume are obtained (see section 5.4. Model simulations).

The release of the urease enzyme into the environment produced by some strains of bacteria is the parameter that controls the formation of crystals, as mentioned above. So, these levels of urease can then be associated to crystal formation. In this way, depending on the [%] – [U/mL] profile selected, different patterns of crystals precipitation are expected to be formed within the gel volume. Section 6.5. Recommendations for future work discusses in more detail the feasibility of the model for different situations, including how to monitor crystal formation in hydrogels.

Figure 5-11 shows three graphs displaying different [U]-[%] relationships, where the horizontal and vertical axis are cell concentration [%] and urease activity [U/mL], respectively.
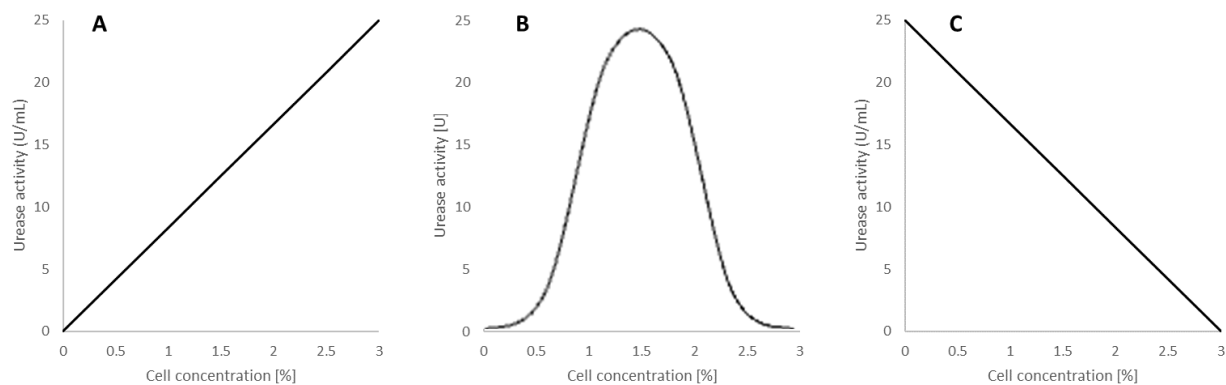
Figure 5-11. Different Urease Activity – Cell Concentration relationship: A) Linear increase, B) Peak, C) Linear decrease

Figure 5-11 (A) represents a scenario where the urease expression increases linearly as the cells grow within the system. Figure 5-11 (B) describes a scenario where a *peak* of enzyme activity is reached for a specific concentration of cells but the expression decreases as more bacteria cells grow within the gel. Finally, Figure 5-11 (C) represents a less likely scenario where the system generates high levels of urease that linearly decrease as the microbes grow within the gel. The relationship displayed in Figure 5-11 (A) is the one selected for the model simulations (see section 5.4. Model simulations). However, as it was described in Chapter 2, this relationship is not likely to be linear, since urease activity not only depends on the number of cells present in the system, but also on many other parameters. Therefore, a sensitivity study is recommended for the next phase of the project where the impact different urease activity – cell concentration functions have on the behaviour of the system is assessed.

5.3.6. Integrated system

This section aims to describe the methods adopted to integrate the biological data regarding cell concentration and urease activity values with the mechanical behaviour of the gel under different loading scenarios. The section is divided in two parts:

- Part one describing the development of a process that integrates hypothetical urease activity levels of a pressure-sensitive Bacillus strain relative to the stresses applied to the gel.
- Part two describing how the model couples the experimental microbial growth data of *B. subtilis* with associated levels of urease alongside the amplifying effect on urease expression due to the pressure-sensitivity. This integration leads to the development of a *bio-mechanical coupled system*.

- Urease activity relative to level of stress

The models of total stress and pore pressure dissipation described in previous sections were associated to urease activity values. Let's imagine a single engineered bacteria cell that constitutively expresses a certain amount of urease under no-pressure conditions. This level

of urease produced can be referred as the *baseline* level, which will increase or decrease depending on the urease activity profile. This variation in urease activity can be expressed as a percentage or, in our case, as an *expression ratio*. For instance, if the amount of urease expressed (i.e. urease activity) doubles as a certain pressure is applied, then the ratio between the urease activity under pressure and the *baseline* urease activity (under no-pressure conditions) equals 2.

If we propose a scenario where the *urease expression ratio* increases linearly with the level of stress (i.e. *pore water pressure*), as represented in Figure 5-12, high levels of urease are expected in the areas just underneath the loading surface, where higher pressures develop. The urease activity would then gradually decrease as distance from the loading surface increases (see section 5.4. Model simulations). The way the model integrates the pore pressure data with the *expression ratio* values is as following:

- The model calculates the levels of stress present across the gel due to a specific loading condition. These stresses are initially carried by the pore water, generating pore water pressures of the same initial value than the stresses due to loading.

- A value is assigned to the coefficient of consolidation so that consolidation takes place over time. Pore pressures dissipate at a rate which is proportional to the coefficient of consolidation. Section 5.5. Model limitations provides a critical discussion on why pore pressures are being modelled, instead of total stresses.

- The stress values (pore pressures) generated across the 3D volume of gel are then associated to urease expression ratio values, in accordance to Figure 5-12.

- Finally, the resulting *expression ratio* values are mapped to the 3D volume of gel, by displaying each voxel in a range of colours, depending on the *expression ratio* value.

Note that for the case of a linear relationship as the one displayed in Figure 5-12, the urease expression pattern is identical to the pore pressure patterns.

Researchers in the *Thinking Soils* project are currently working on developing a strain of bacteria significantly sensitive to pressure, and some preliminary results are presented in (Guyet et al., 2018). However, a comprehensive characterisation of the strain's pressure-sensitivity has not been obtained yet, and therefore estimated values for the *ratio* have been

selected. Thus, for Figure 5-12, the maximum *Expression ratio* value selected is equal to 5, which ultimately leads to a 5-fold increase in urease activity at the selected level of stress (in this case 175 kPa).
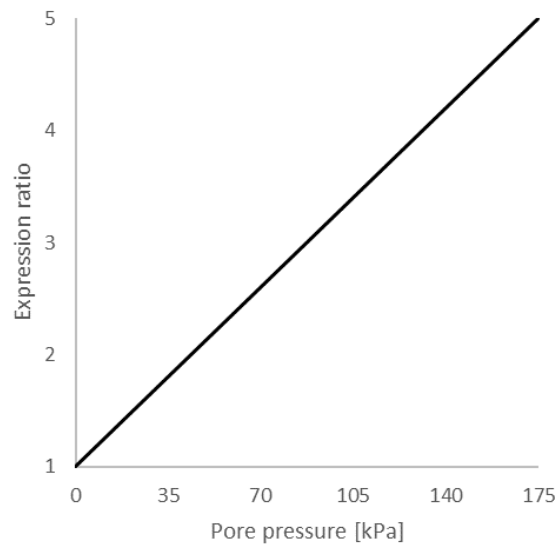
Figure 5-12. Diagram to illustrate the increase in urease activity (Expression Ratio) depending on the level of stress

- Bio-mechanical coupled model

The computational model is also able to incorporate the urease activity data corresponding to the cell concentration with the above-mentioned urease expression ratio relative to the level of stress within the system.

The way the model computes the resulting urease level (U/mL) at each point within the gel is by multiplying the baseline urease activity values associated to the amount of cells (non-pressurised urease expression, in U/mL) with the value of the *expression ratio* relative to the level of stress present at each point, i.e.

Pressurised urease expression (U/mL) = baseline urease expression (U/mL) ∗ expression ratio

(Equation 5-14)

Figure 5-13 describes the method to compute the resulting amount of urease expressed in a point located in the middle of the gel volume (i.e. x=20mm, y=20mm and z=20mm) under the following growth and loading conditions:

Load	150N
Loading base/platform	30mm
Initial dilution	High
Growth temperature	35°C
Time	3h

Table 5-1. Example of growing and loading conditions

The cell concentration at the required point after 3h of incubation under the specified growing conditions in Table 5-1 is equal to 0.66%, which according to Figure 5-13 (A), produces **5.5 U/mL**. This value refers to the urease level being expressed by the bacteria cells at that time and location within the gel under no-pressure conditions, i.e. *the baseline urease expression*. Additionally, the pore pressure due to the specified loading conditions at the required point is equal to 25.9 kPa. Thus, if the urease expression profile of the pressure-sensitive engineered strain is represented as displayed in Figure 5-13 (B), the *expression ratio* at 25.9 kPa is equal to **1.6**, which corresponds to a 1.6-fold or 60% increment in urease expression. This value can then be multiplied to the *baseline* urease level obtained from Figure 5-13 (A), and the resulting amount of urease expressed at the required point due to the effect of the local pressure is equal to **8.7 U/mL**.
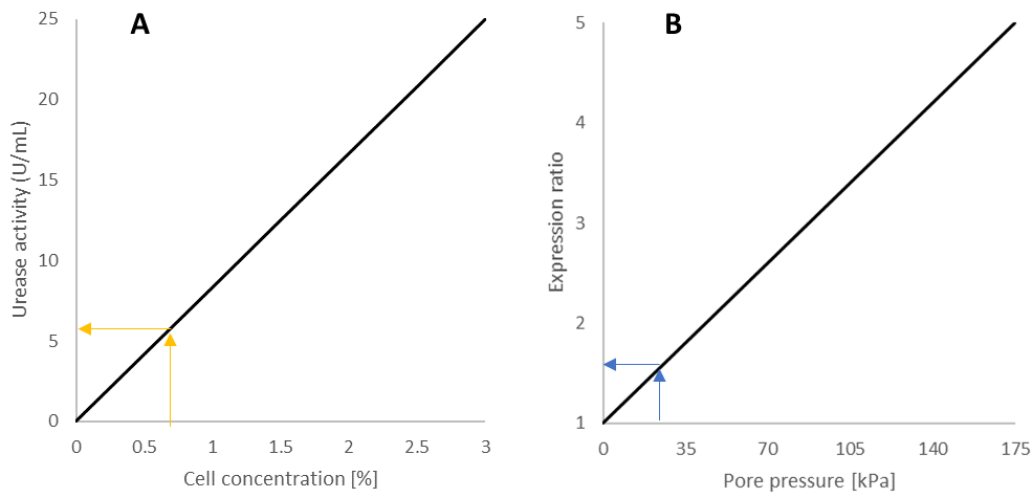
Figure 5-13. Diagram to illustrate the method used to calculate the resulting urease activity relative to cell concentration and stress level

The model performs the same procedure to all the points (voxels) within the gel and the results are displayed by assigning a range of colours to each of the voxels, which depend on the urease value expressed at each location. Additionally, the model is time-dependent due to the pore pressure dissipation effect upon consolidation.

5.3.7. Graphic user interface

A library called ControlP5 was introduced in the Processing directory to allow the creation of a Graphic User Interface (GUI). This GUI allows interactive exploration of the different parameters used for the analysis so that the resulting simulations can be visualised dynamically, without the necessity of having to access the main code. The GUI mainly uses Sliders to select the required values for each parameter. However, where a true/false response is needed (e.g. activate/deactivate one-way drainage), a parameter called Toggle is used. In addition, the GUI also allows for the different simulations to be exported as 2D models so that the effect of the different parameters and conditions can be compared. Figure 5-14 shows a screenshot of the model's Graphic User Interface.

Table 5-2 describes all the features and parameters included in the Graphic User Interface, with their respective description and range of values.

Parameter	Type	Description	Value range
Simulation Mode	Slider	Selects the analysis mode	1 - 8
Load	Slider	Selects the value of the load applied	0 - 1000 [N]
Loading platform dimensions	Slider	Selects the length of the square loading surface	10 - 100 [mm]
Time threshold	Slider	Stops the simulation when the value is reached	0 - 10 [h]
Temperature	Slider	Selects the required growth temperature	25 - 35 [°C]
Slice	Slider	Selects the required 2D section for analysis	1 - 20
Coefficient of consolidation	Slider	Selects the value of the coefficient of consolidation	0 - 3 [m^2/year]
Coefficient of compressibility	Slider	Selects the value of the coefficient of compressibility	0 - 1 [m^2/MN]
Poisson's ratio	Slider	Selects the value of the Poisson's ratio	0.4 - 0.49
High	Toggle	Selects a high initial cell concentration	-
Low	Toggle	Selects a low initial cell concentration	-
Drainage	Toggle	Allows/prevents water drainage	-
One-way	Toggle	Prevents the gel from drain through the bottom end	-
Local stress	Toggle	Allows the calculation of local stresses (only when length loading surface <= 50mm)	-
Lock	Toggle	Prevents rotation of the analysis volume	-
Isobars	Toggle	Displays the results as isobar zones/areas	-
Export_2D	Toggle	Exports a screenshot of the simulation	-
Run	Toggle	Runs the simulation	-
Graph 1	Graph	Relationship between cell concentration (%) and urease activity (U/mL)	-
Graph 2	Graph	Relationship between pore water pressure (kPa) and expression ratio	-

Table 5-2. Parameters included in the Graphic User Interface
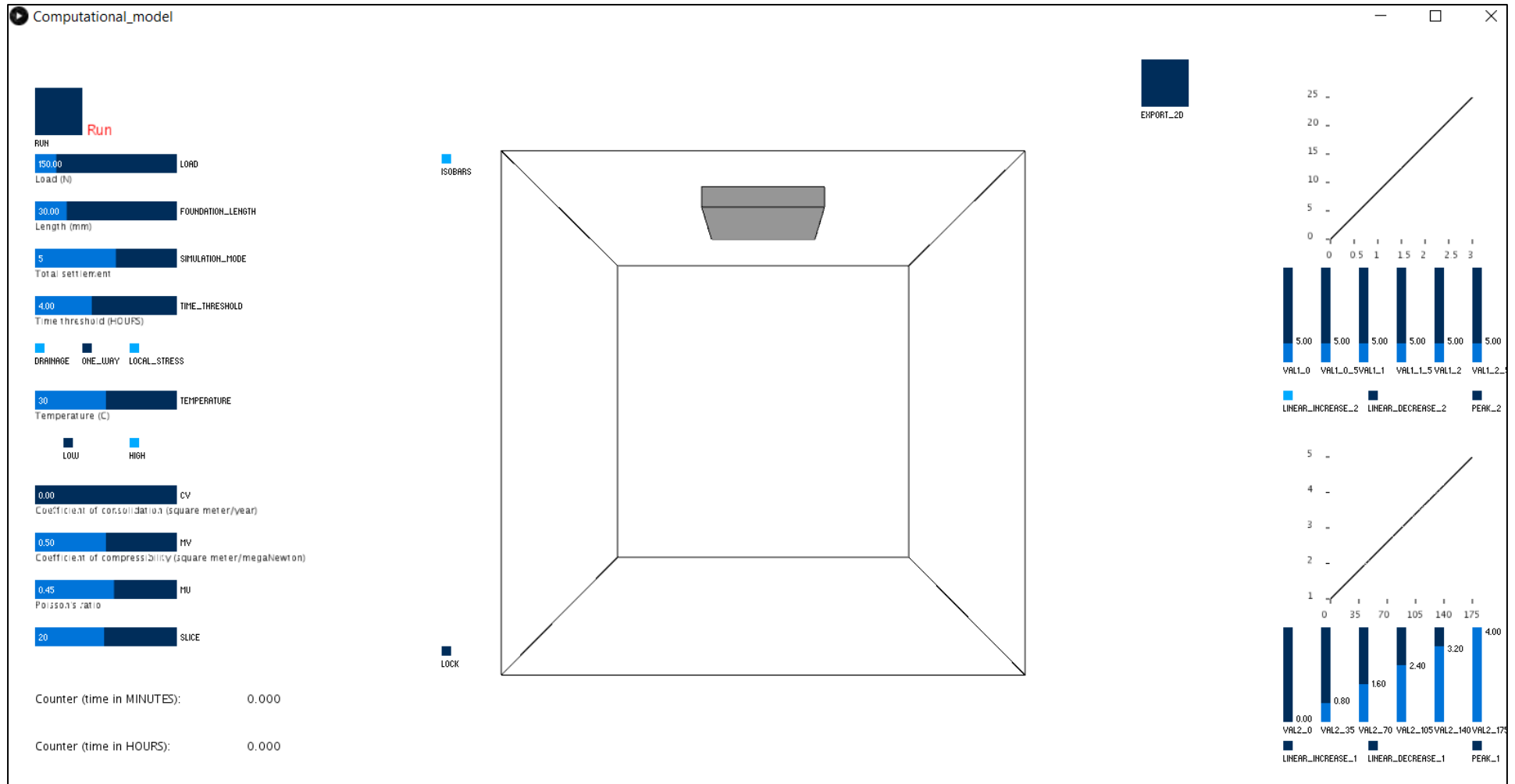
Figure 5-14. Screenshot taken from the software showing the gel volume and all the parameters described in Table 5-2

156

5.4. Model simulations

This section provides with series of 2D slices of simulations exported from the 3D model that describe the behaviour of the 100x100x100mm volume of gel homogeneously seeded with pressure-sensitive urease-producing engineered bacteria cells. As described in the previous section, the model is capable of displaying the performance of the system under different mechanical and biological conditions, and is ultimately able to integrate both aspects into a bio-mechanical coupled model. Eight different *Modes* were implemented in the code, each one of them aiming to represent a specific mechanical and/or biological aspect of the system. **Mode 1** represents the total stress distribution behaviour upon loading. **Mode 2** describes the pore pressure dissipation behaviour in agarose hydrogels. **Modes 3**, **4** and **5** illustrate the immediate, consolidation and total settlement upon loading, respectively. **Mode 6** models the levels of urease activity in relation to the concentration of bacteria cells. **Mode 7** displays the levels of urease activity in relation to the stresses generated in the system. **Mode 8** describes the behaviour of the so-called bio-mechanical integrated system.

5.4.1. Mode 1 – Total stress distribution due to loading

The stresses generated within the gel are a function of the load applied. If the loading surface equals the dimensions of the confinement – i.e. 100x100mm loading platform – the stresses developed throughout the gel volume correspond to the load applied divided by the loading surface, and all the points within the 3D structure are subjected to the same stress value. A *local stress* distribution only develops in the case of a semi-infinite volume of gel. As discussed in earlier sections, the stresses at the boundary must be negligible so that it can be assumed that the stresses distribute as they would in a semi-infinite volume. Therefore, considering that the maximum stresses generated underneath the loading platform are designed to be slightly smaller than the bearing capacity of the gel (~170 kPa), the maximum platform dimensions that generate negligible stresses on the gel boundaries is a 30mmx30mm square platform (the vertical stresses at the gel boundaries range between 0.2 and 2.8 kPa, which are assumed to be small enough so that they do not affect the stress distribution behaviour).

Figure 5-15 shows a series of simulations where total loads of 50N, 100N and 150N are applied onto the 30mm square loading platform at the surface of the gel. These 2D simulations correspond to the middle section within the gel volume, as described in Figure 5-1. As it can be appreciated from these stress distribution simulations, the load applied directly affects the level of stress generated within the system, as expected. Additionally, as described above, the maximum load that can be applied to the platform before the bearing capacity is exceeded is approximately 150N, which generates maximum stresses of approximately 167 kPa for the areas directly beneath the platform, as it can be seen from Figure 5-15. With this load-platform combination, the stresses generated along the vertical gel-confinement interface are considered negligible and it is therefore assumed that the system acts as a semi-infinite volume of gel.

These results show the behaviour expected in a gel volume when a rectangular surface load is applied. The simulations are generated from the computation of mathematical expressions that describe this behaviour in a soil environment, however, considering the limitations mentioned in earlier sections, it is assumed that the same distributions of stress occurs in the agarose hydrogel. Additionally, the simulations generated with our model were compared to simulations obtained with a licensed geotechnical analysis software (Settle3D) and it was confirmed that the results were identical.
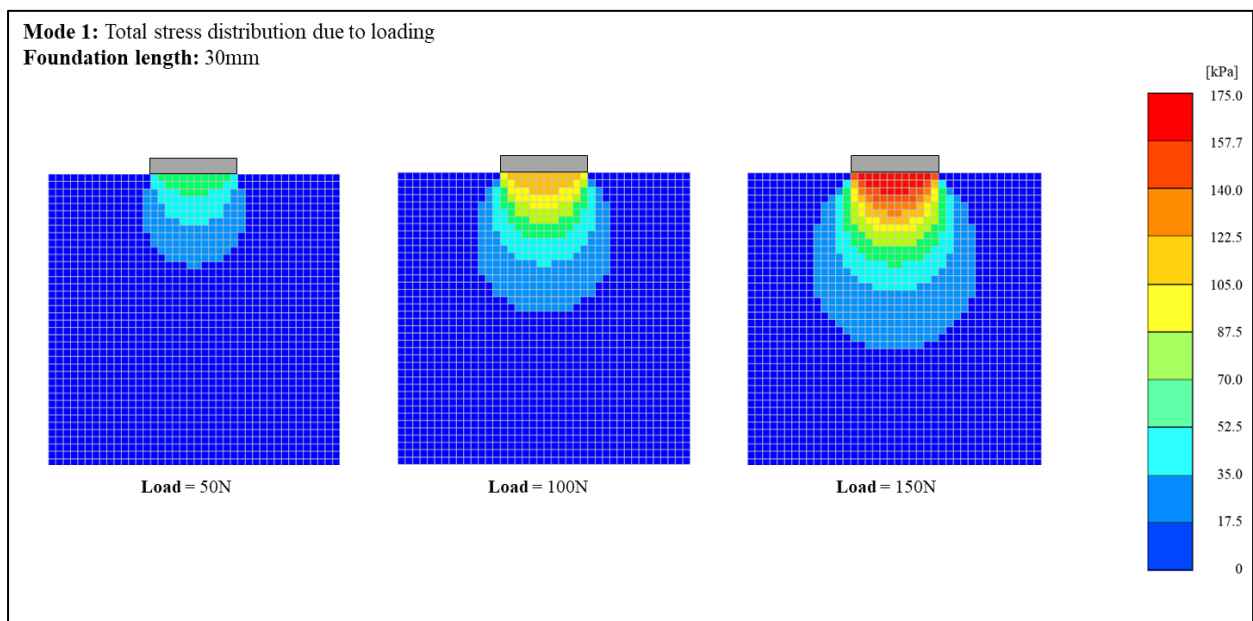
Figure 5-15. Simulations showing the stress distribution behaviour upon loading

5.4.2. Mode 2 – Pore water pressure dissipation over time

Similarly to *Mode 1*, if the dimensions of the loading platform are equal to the gel surface, the total stresses generated are the same throughout the gel volume. Hence, if drainage of the pore water is not allowed, the pore pressures generated equal the amount of the total stress produced due to loading. However, if drainage of the sample is allowed – e.g. by using porous surfaces at the top and bottom ends (see scenario 2 from section 5.3.3. Boundary conditions) – consolidation will occur, and the sample will decrease in volume. Since the sample is confined laterally – i.e. movement in the lateral direction is restricted due to the mould walls –, this volume reduction is directly proportional to the vertical displacement occurring to the loading surface.

For the case of a *semi-infinite volume* of gel (i.e. considering a 30mm square platform), a local stress distribution develops upon loading. As explained in section 5.3.4. Mechanical behaviour, the water within the pores will initially carry the stresses developed, and as consolidation occurs, these pore pressures generated will dissipate and the load will gradually be taken by the gel skeleton. Figure 5-16 shows a series of simulations taken at different time points where the gel system was uniformly loaded with 150N and the pore pressure dissipation effect can be seen, for two different c_v values. These simulations show how the value of the coefficient of consolidation directly affects the rate at which pore pressures dissipate, by accelerating the process as its value increases. Figure 5-17 shows a series of graphs that demonstrate the rate at which pore pressures dissipate, for different depths along the vertical line beneath the centre of the loading platform (i.e. x=50mm, y=50mm). As it can be seen from the graphs, points located near the top and bottom ends – e.g. z=5mm and z=97.5mm – show a very rapid pore pressure dissipation, due to the short distance from the drainage end. However, for points located in the middle of the gel volume, pore pressure dissipation tends to be slower due to an increased length of the drainage path. In addition, the model shows a temporary increase in pore pressure at some depths, before the dissipation effect begins. For some of the points analysed (e.g. Z=62.5mm), the pore pressure rises up to 40% of the original stress value without the application of any additional loads, and it can take up to seven hours to drop to the initial pressure value. This behaviour was also seen in a preliminary analysis performed on Settle3D, where a similar soil scenario was modelled and a temporary increase in excess pore pressure developed at certain regions.

Understanding the factors that generate this local increase in pore pressure is beyond the scope of this thesis, however, this behaviour is believed to be associated to the way the model computes the pressure dissipation effect. It is therefore recommended to explore this effect further in the future in order to understand the extent to which pore pressures might increase, and the consequences that this might have on our system – since it might lead to higher urease activity areas in particular regions of the gel volume.
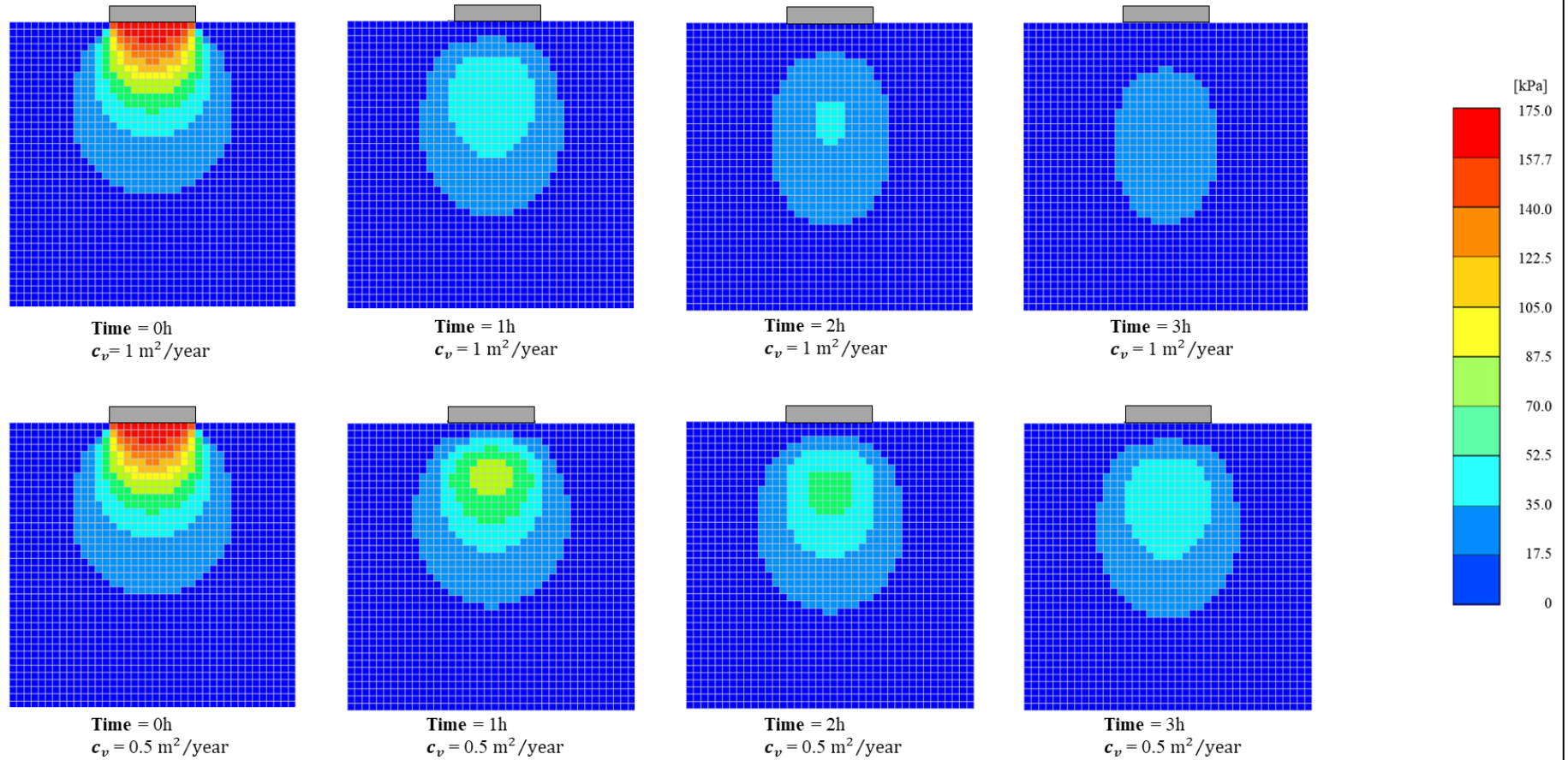
Figure 5-16. Simulations showing the pore pressure dissipation behaviour upon consolidation
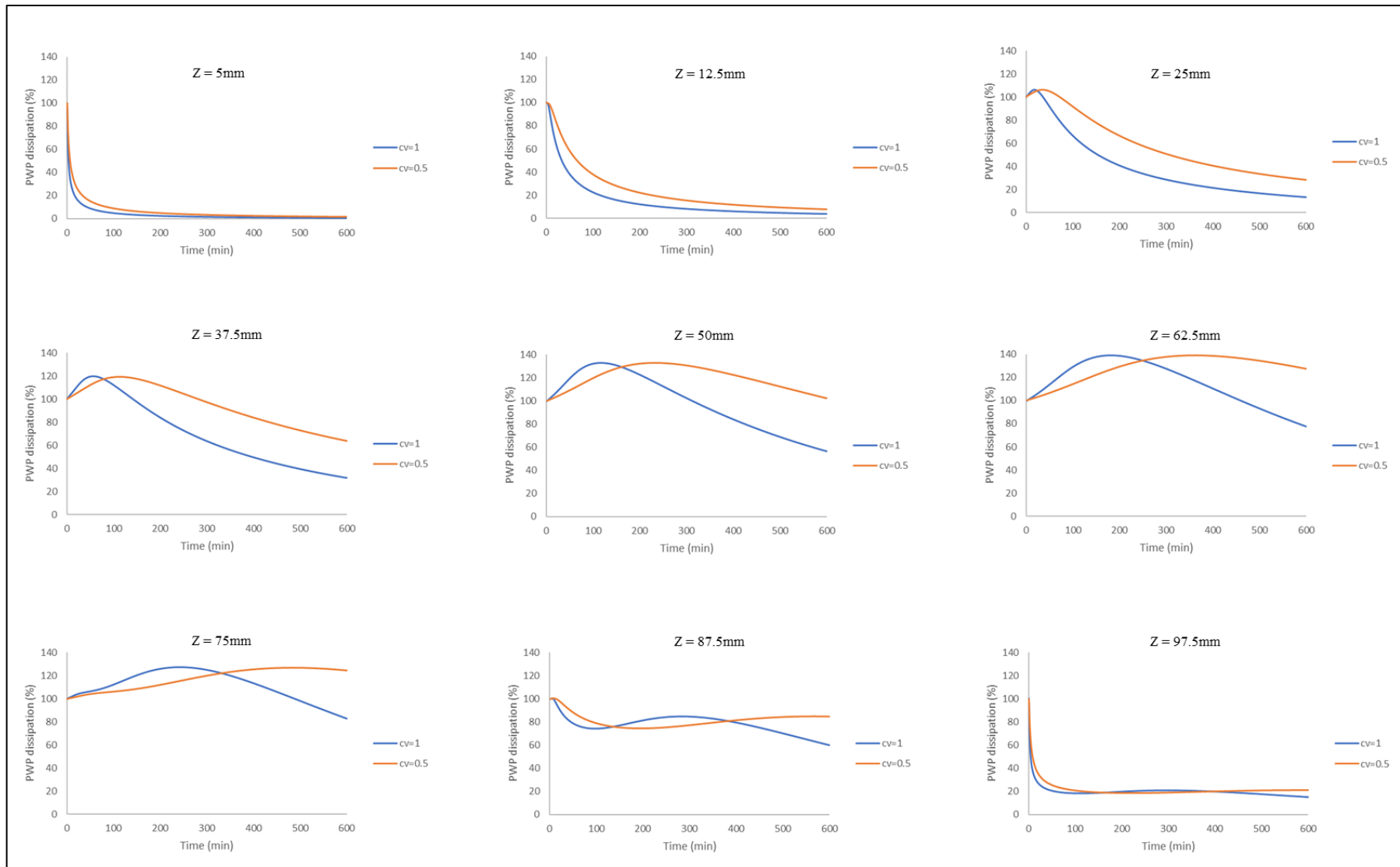
Figure 5-17. Pore pressure dissipation over time for different depths within the gel

162

5.4.3. Mode 3 – Immediate settlement

Mode 3 explores the elastic settlement occurring to the loading platform immediately after the load is applied, without considering any change in volume due to consolidation.

As described in previous sections, the immediate or elastic settlement directly depends on the load applied, the Young's or elastic modulus (E) of the gel and the Poisson's ratio (v). Considering the value of E was calculated in Chapter 3 and is equal to approximately 300 kPa, several simulations were run with different loading pressures (Figure 5-18). The Poisson's ratio selected for these simulations was 0.45 (obtained from Takigawa et al. (1996), for a similar type of gel. These series of simulations clearly show how the immediate settlement increases with an increase in the load applied. This behaviour is expected since the higher the load applied, the higher the stresses generated within the gel, which ultimately leads to larger elastic deformations (according to the Young's modulus and the principle of elasticity described in Chapter 3). Additionally, Figure 5-18 also shows a series of simulations where the immediate settlement is displayed for different Poisson's ratio, ranging between 0.45 and 0.49, and a constant load of 150N. For this case, it can clearly be appreciated how the value of the settlement decreases as the Poisson's ratio of the material increases. The Poisson's ratio measures the facility of a material to expand in the direction perpendicular to the direction of compression. Therefore, the results seem to be reasonable since gels with higher Poisson's ratio will prevent longitudinal deformations upon vertical loading, which can be associated to a higher gel stiffness, and consequent reduced settlement.

In addition, similarly to the previous modes, the simulations obtained from the computational model matched the results obtained from Settle3D, confirming the computation of the immediate settlement is accurate.
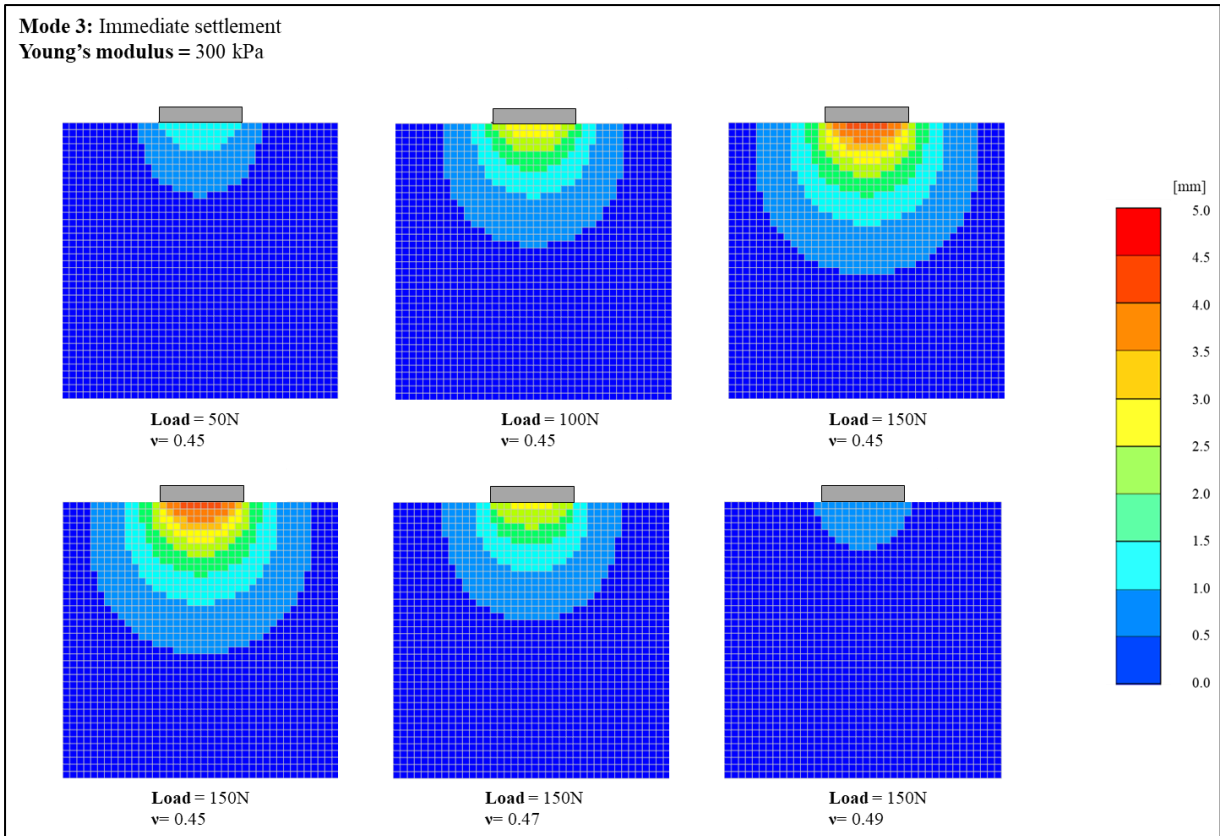
Figure 5-18. Simulations showing the immediate settlement behaviour upon loading

5.4.4. Mode 4 – Consolidation settlement

Mode 4 focuses on the consolidation settlement behaviour. As described in previous sections, this is a time-dependent phenomenon, which depends on the load applied as well as the coefficient of consolidation and the coefficient of volume compressibility. Both coefficients were experimentally calculated in Chapter 3 and, although the coefficient of consolidation was found to be approximately equal to 1 m^2/year, the coefficient of compressibility varied depending upon the stress level applied. Terzaghi's consolidation equation was used to compute the rate and magnitude of settlement upon consolidation, and a series of simulations are displayed in Figure 5-19. These simulations show how the consolidation settlement increases over time, as expected. The results seem reasonable since the longer the load is applied, the more pore water is drained out of the gel, which contributes to a reduction in gel volume and consequent settlement of the loading platform. As described in earlier sections, this time-dependency is associated to an increase in effective stress, as pore pressures dissipate.

164

Furthermore, the effect of the coefficient of compressibility can also be appreciated in Figure 5-19, where simulations with two different m_v values are compared. The coefficient of volume compressibility is a property of the material and measures the magnitude of volumetric deformations in relation to pressure changes. Therefore, as expected, simulations performed with higher m_v values will lead to larger volumetric deformations, and consequently larger settlement values.
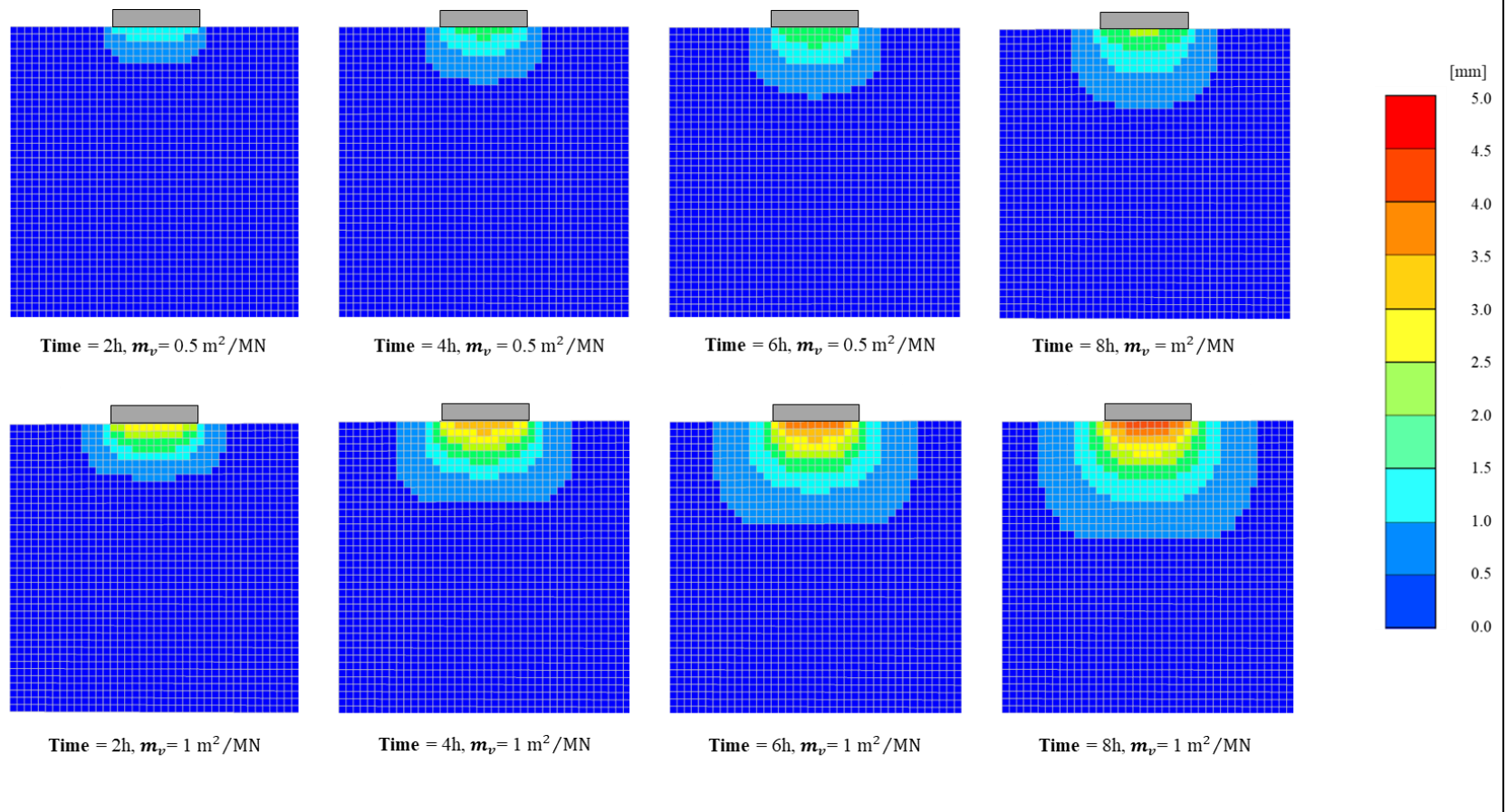
Figure 5-19. Simulations showing the consolidation settlement behaviour upon loading

5.4.5. Mode 5 – Total settlement

Model 5 couples both the immediate and the consolidation settlement together. The total settlement is a time-dependent phenomenon which depends both on elasticity and consolidation. Figure 5-20 shows the relationship between total settlement and time for different $c_v - m_v$ combinations, and two different Poisson's ratios: 0.45 and 0.49.
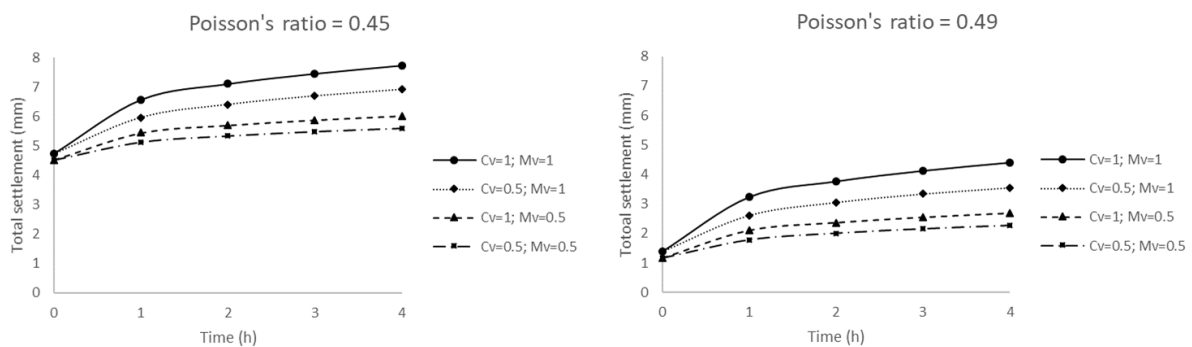
Figure 5-20. Relationship between total settlement with respect to different c_v, m_v and Poisson's ratio values over time

As expected, the total settlements values are reduced as the Poisson's ratio of the material increases, as described in Mode 3. Furthermore, the results also show how larger coefficients of consolidation and compressibility lead to larger total settlements over time. This behaviour seems reasonable since both c_v and m_v dictate the rate and magnitude of consolidation settlement, as described in Mode 4.

If a Poisson's ratio value of 0.45 is assumed (most cautious scenario), the maximum total settlement that would occur to a point at the surface of the gel after 4h of loading ranges between 5.6mm and 7.7mm, depending on the $c_v - m_v$ combination.

Also, note that for all the simulations, the load applied is 150N, which is load that generates the maximum allowable stress before the loading platform fails/collapses.

However, the actual total settlement values are relatively unimportant for our study. As mentioned in earlier sections, the point of modelling settlements with accuracy is being able

to compare the stiffness of samples with different compositions in a simple way. More details on that are discussed in Chapter 6 (Recommendations for future work).

5.4.6. Mode 6 – Urease Activity relative to Cell Concentration

The modes described in the previous section simply model the behaviour of the gel when it is subjected to a vertical uniaxial load. The computational model uses governing equations to represent the properties described and it is supported by the data obtained experimentally.

The modes described in the following sections, however, go one step further by integrating the biological aspect into the system and describing the behaviour of a bacteria-based pressure-sensitive hydrogel.

Simulation mode 6 integrates the data obtained from the Bacillus growth experiments with hypothetic values of urease expression – or *urease activity*. Bacteria-seeded hydrogels can be seeded homogeneously by following the procedure described in 4.3.3. Bacteria-seeded agarose gel preparation, however, the growth rate throughout a volume of gel is not uniform, as demonstrated in Chapter 4. Therefore, this mode represents the concentration of cells in a gel volume under different growing conditions and the associated *urease activity*.

Figure 5-21 displays the urease activity levels along all the layers within the gel after 3h of incubation and compares the effect of three different incubation temperatures: 25°C, 30°C and 35°C (left to right). The cell concentration (%) is also displayed to the right of every simulation for all of the 40 horizontal layers of the gel. Additionally, two different *cell concentration [%] – urease activity [U/mL]* profiles are compared: a *linear* relationship (see Figure 5-11 (A)) for the top simulations, and a *peak* relationship (see Figure 5-11 (B)) for the bottom simulations. For clarification purposes, a *linear* relationship means that the urease activity increases proportionally with cell concentration (most likely scenario); and a *peak* relationship displays high levels of urease activity for a specific cell concentration, and reduced levels for the rest (less likely scenario).

For the case of a linear relationship, the layers of the gel with higher concentration of cells lead to a higher urease activity, as it can be seen from Figure 5-21. However, the simulations generated with a *peak* relationship show a different behaviour. As mentioned above, this

peak profile simulates a less likely scenario where the urease activity increases exponentially until a certain cell concentration is reached and, beyond this point, the level of urease within the system starts to decay. Therefore, the urease distribution patterns that develop using this *peak* profile differ significantly from the simulations generated with a *linear* relationship. Figure 5-21 also shows how temperature plays an important role in the distribution of urease. The simulations run with higher temperatures lead to higher urease activity levels, since temperature is one of the major parameters that determine the growth rate of bacteria cells in hydrogels, as described in Chapter 4.

By interpreting the results obtained from the model, and assuming that high levels or urease activity lead to more crystal precipitation, it is suggested that more crystals would precipitate towards the top end of the gel volume (layers displayed in orange-red colours), independently of the loading conditions. Furthermore, the results also suggest that an increase in temperature from 25°C to 35°C leads to significant changes in the amount and distribution of urease activity within the gel.

As mentioned in earlier sections, these urease activity profiles are only hypothetical, since real data that relates urease levels with cell concentration is not available yet; however, it is believed that the model reproduces with accuracy the effect cell concentration and urease activity have on the gel system.
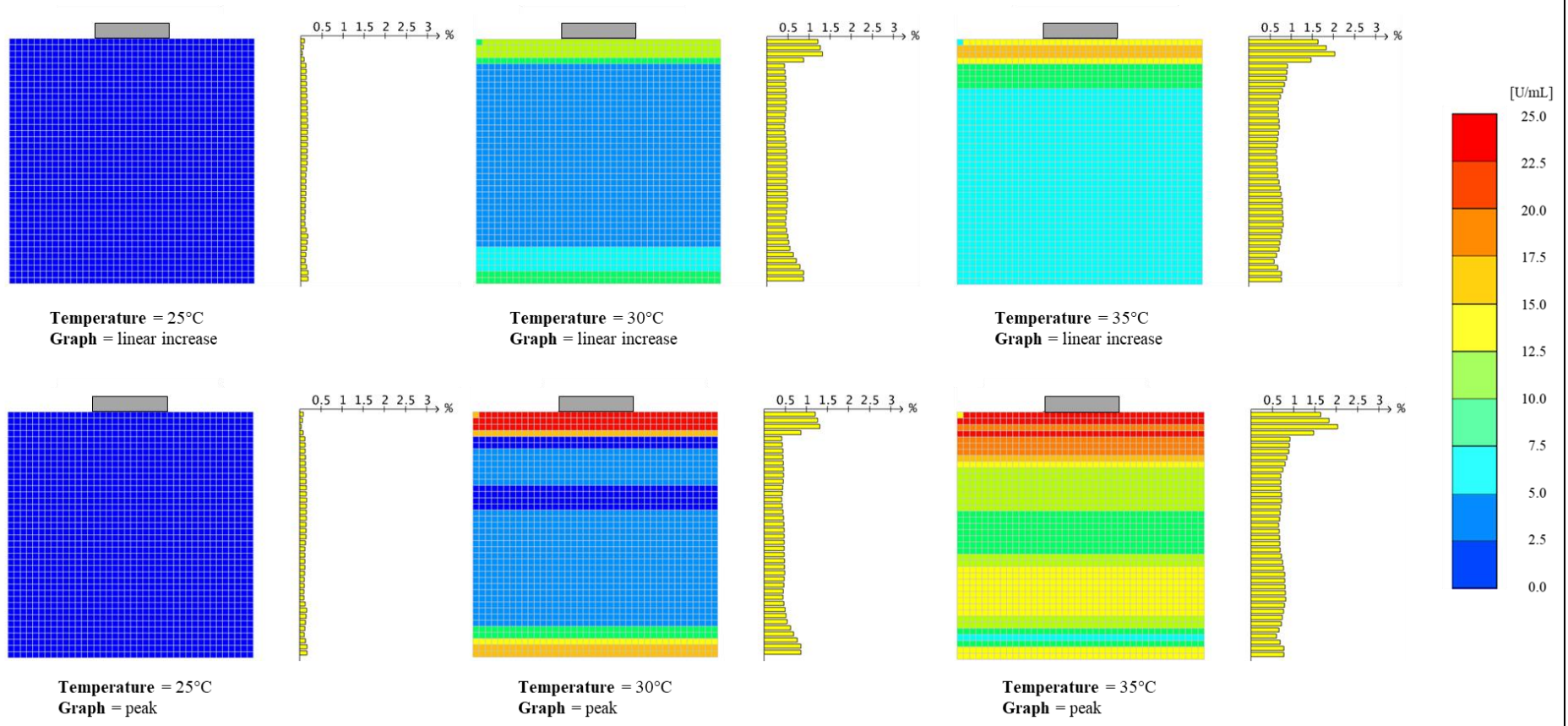
Figure 5-21. Simulations showing urease activity distribution with respect to cell concentration. The top simulations show the effect of a linear increase relationships while the bottom simulations show the effect of a peak relationship

5.4.7. Mode 7 – Urease Activity relative to Pore pressure

As described in section 5.3.6. Integrated system, this mode simulates the behaviour of a pressure-sensitive urease-producing strain of bacteria homogenously distributed within the gel. For this case, the urease activity is not time-dependent and does not depend on cell concentration, i.e. it is assumed that cells do not grow and therefore the system generates the same urease activity over time. Therefore, the only parameter affecting the expression of urease is the level of stress at each location. The model, however, is time-dependent since pore pressures are used for the analysis and, as described in previous section, pore pressure dissipation occurs upon consolidation.

This mode allows the user to explore the *sensitivity* of the system to different urease activity profiles, by selecting the desired *Expression Ratio* relative to the pore pressures generated within the system upon loading. This section therefore shows several simulations generated using different *Expression Ratio* profiles and the results can be seen in Figure 5-22, Figure 5-23 and Figure 5-24.

The simulations from Figure 5-22 show the effect of a <u>linear</u> *Expression Ratio – Stress* relationship, where the urease expression patterns over time are identical to those found in Figure 5-16 (Pore pressure dissipation). The reason for that is that, for a linear relationship, the urease activity is governed proportionally by the level of stress: higher pressures lead to higher urease activity (and under the right conditions, to more crystals precipitated), consequently displaying a simulation with identical colour distribution to the one produced for Mode 2.

Thus, this scenario amplifies the urease activity where higher pore pressures develop, and as pore pressure dissipate and become smaller, the expression ratio relative to the *baseline urease expression* also decreases. In addition, as it can be seen at the top left corner of Figure 5-22, the coefficient of consolidation selected for the simulations was 0.5 m^2/year. If higher c_v values are selected, the pore pressures generated within the system will dissipate at a higher rate, leading to reduced levels of urease expression over time.

Additionally, Figure 5-23 and Figure 5-24 show series of simulations with two different *Expression Ratio – Stress Level* relationships: a peak profile for Figure 5-23, and a less likely three-peak profile for Figure 5-24. Similarly to the previous section, this peak profiles show

amplified levels of urease expression (or increased *expression ratio*) for specific levels of stress.

The three sets of simulations obtained for different profiles show a significantly different behaviour, demonstrating that changes in the *urease activity – stress* profiles can considerably change the macro-scale properties of the hydrogels, and lead to different levels and shapes of crystal precipitation within the gel.

From a practical point of view, however, discussing these results in detail might seem inappropriate since they purely rely on hypothetical data, depend on many limitations and do not contain any real biological information. Therefore, a critical discussion will be provided in the next section (5.4.8. Mode 8 – Bio-mechanical integrated system), which combines the behaviour represented in this mode with the simulations obtained in Mode 6, relative to cell concentration data and likely urease activity profiles.
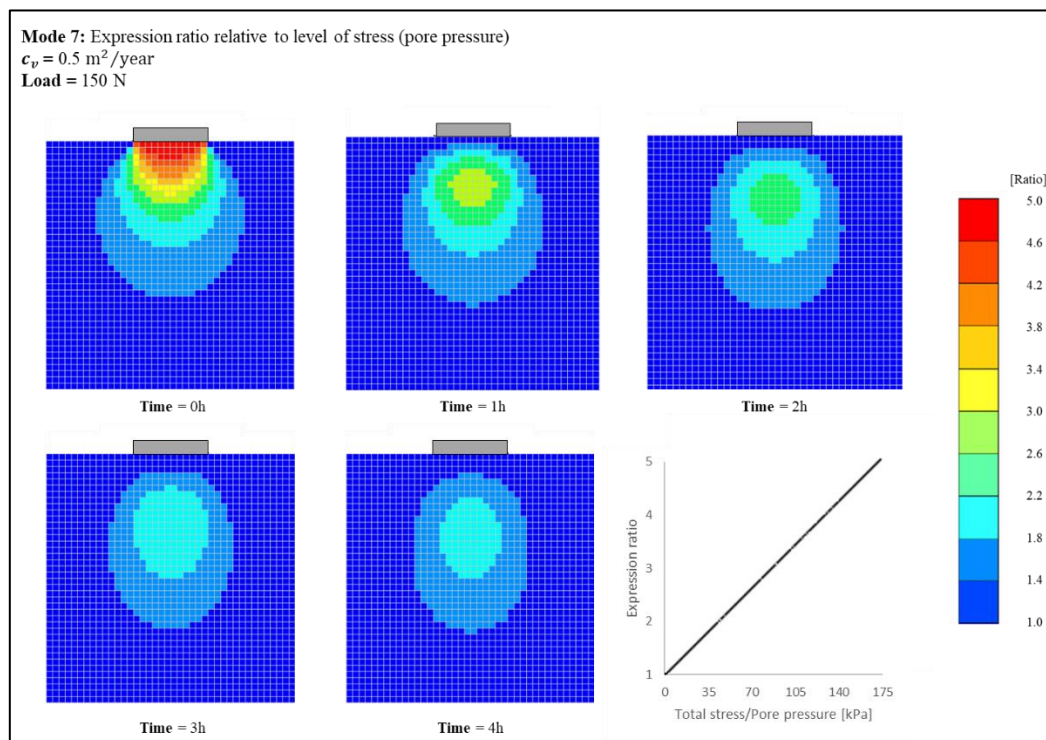
Figure 5-22. Simulations showing Expression Ratio values for a volume of gel loaded with 150N. The relationship between Expression Ratio and level of stress is linear
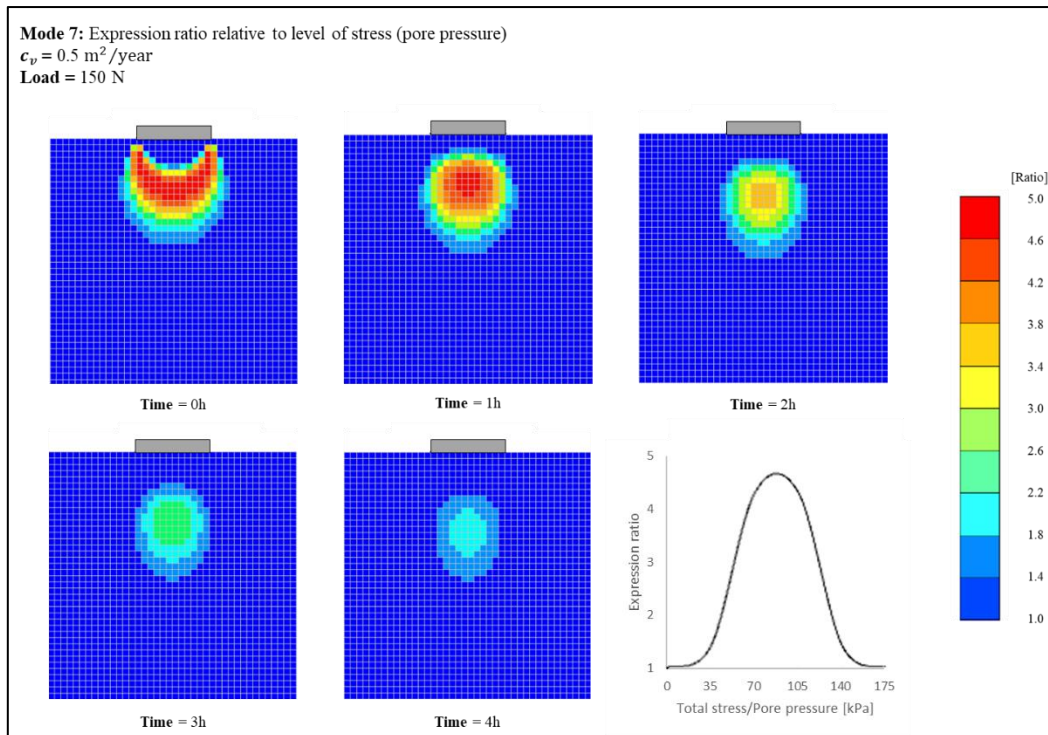
Figure 5-23. Simulations showing Expression Ratio values for a volume of gel loaded with 150N. The relationship between Expression Ratio and level of stress shows sensitivity to a range of pressure around 90kPa
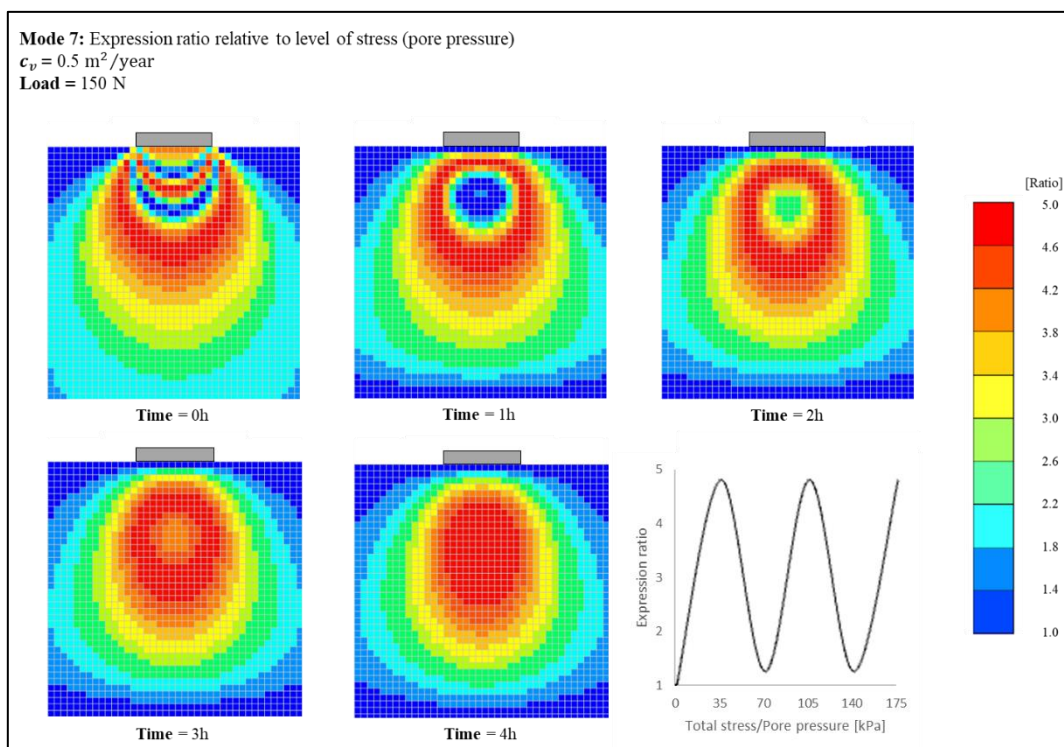
Figure 5-24. Simulations showing Expression Ratio values for a volume of gel loaded with 150N. The relationship between Expression Ratio and level of stress shows sensitivity to a range of pressures around 35kPa, 105 and 175 kPa

5.4.8. Mode 8 – Bio-mechanical integrated system

The simulations displayed in Mode 6 represent a relatively simple case where the urease activity levels across the gel are only dictated by the presence of bacteria cells. For a linear relationship, the amount of urease is proportional to the amount of bacteria cells, which is believed to be the most likely scenario.

On the other hand, mode 7 represents a different scenario where the urease activity levels across the gel are only dictated by the stresses developed under loading, independently of the concentration of cells present in the gel (for more details about the processes and techniques to engineer bacteria cells to sense pressure changes, see section 2.5.3. Computational Colloids and Thinking Soils Projects for an overview, or Guyet et al. (2018) for a more detailed description).

Therefore, as described in section 5.3.6. Integrated system, this mode aimed to combine the outcomes from Mode 6 and Mode 7, by developing a bio-mechanical integrated system that models the levels of urease across a volume of gel in relation to different loading conditions and incorporates real biological data.

In a similar way to mode 7, this Mode assumes that cells are homogeneously seeded within the gel. However, the growth rate and distribution of colonies is now taken into consideration, by implementing the relationship between cell concentration and urease activity described in *Mode 6: Urease Activity relative to Cell Concentration*. Therefore, different concentrations of bacteria colonies are expected to develop within the gel volume, depending on the growth conditions, location and time point.

Figure 5-25 shows three model simulations where three different *Expression Ratio – Pore Pressure* profiles are selected. The relationship between urease activity [U/mL] and cell concentration [%] has been set to linear, as it can be seen on the upper part of Figure 5-25, since it is believed to be the most likely scenario. The model, however, allows for selection of different profiles, such as the peak or the linear decrease relationships presented in Figure 5-11. The model is time-dependent since both of the aspect dictating the behaviour of the system (bacteria growth and pore pressure) depend on the time factor. The simulations presented in Figure 5-25 were captured at t=3h.
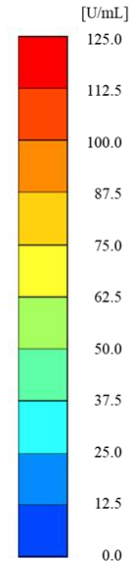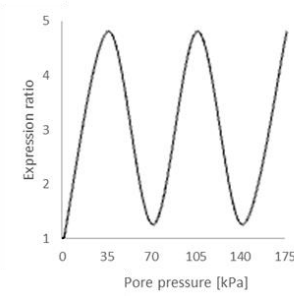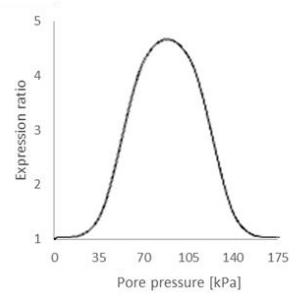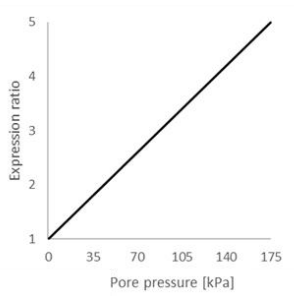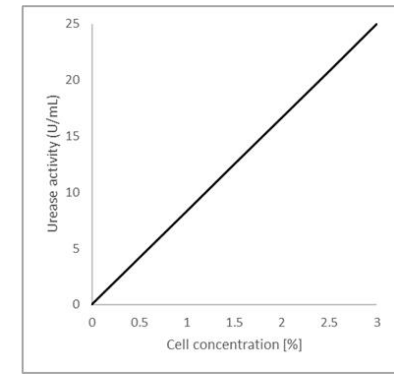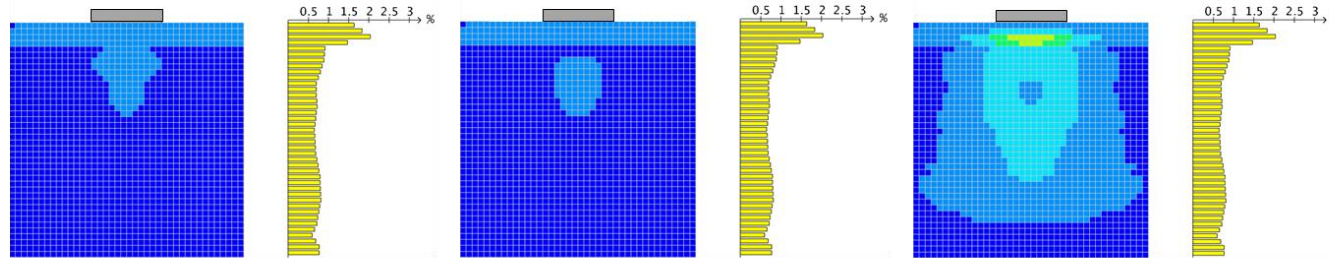
Figure 5-25. Simulations showing the effect of the bio-mechanical coupled model for three different Expression Ratio – Pore Pressure profiles
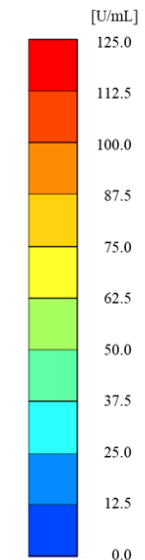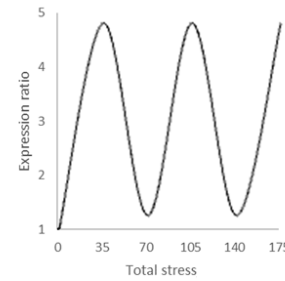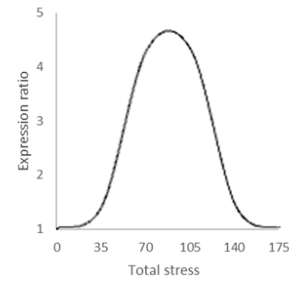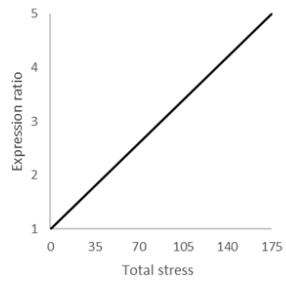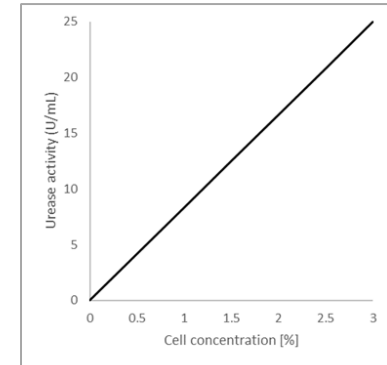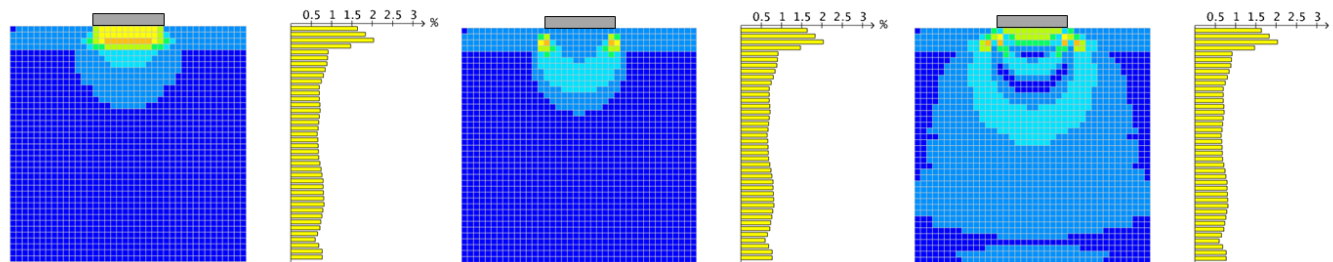
Figure 5-26. Simulations showing the effect of the bio-mechanical coupled model for three different Expression Ratio – Total stress profiles

The simulations displayed in Figure 5-25 demonstrate how the system responds to both concentration of cells and level of stress, by displaying high urease activity levels in areas of the gel containing more bacteria cells and subjected to higher stresses. The model also demonstrates that changing the pressure-sensitivity profiles of bacteria cells leads to significant changes in the amount and distribution of crystals precipitated. This suggests that by altering the behaviour of the genes at the nano-scale it is possible to change the macro-scale properties of the gel. From a practical point of view, developing such a responsive living system that can sense changes in its environment would have implications for many fields (more discussion is provided in Chapter 6).

As mentioned above, these simulations are time-dependent since pore pressure is one of the parameters that govern the outcomes of the system. From consolidation theory, and shown in Mode 2, the pore pressure levels decrease significantly over time, due to the dissipation effect upon drainage. This suggests that the coefficient of consolidation (a value of 0.5 m^2/year was selected for the simulations) plays an important role in determining the levels of urease present in the gel. However, as further discussed in section 5.5. Model limitations, there is the possibility that cells could also detect total stresses or a combination of total stresses and pore pressures. Therefore, a series of simulations are presented in Figure 5-26, with the exact same conditions specified for Figure 5-25, but with the differences that total stresses are now considered, instead of pore pressures. With this scenario proposed, the model is still time-dependent due to the variance in cell concentration over time, but the total stresses do not dissipate over time and the effect on the urease activity levels is not time-dependent.

With this configuration, much higher urease levels are obtained at t=3h, for the three Expression Ratio – Total Stress relationships analysed. By looking at the linear relationship (Figure 5-26, simulation on the left), it can be appreciated how levels of urease approximately 10-fold higher do appear in the areas beneath the loading platform. Furthermore, if urease activity is associated to crystal formation (as described in previous sections), this would lead to a much larger concentration of crystals in the areas of the gel where higher concentration of cells are present as well as higher stresses develop. From a practical point of view, this behaviour is expected to increase the bearing capacity of the gel and reduce the settlement upon loading, amongst other benefits.

Therefore, it can be confirmed by the results obtained in Mode 8 that the computational model has succeeded in combining the pressure-sensitivity ability of engineered bacteria cells (nano-scale behaviour) with their growth rate and distribution of colonies (micro-scale behaviour), and is ultimately able to visually represent the effect produced at the macro-scale.

5.5. Model limitations

This section discusses the limitations of the model that have not been detailed in the main body of the chapter. These limitations are summarised as follows:

- Total stress v pore water pressure

As described in Chapter 4, *B. subtilis* cells are relatively bigger than the micropores present in 6% agarose gels. When the solution containing the cells solidifies into the gel, the cells become embedded to the 3D fibrous microstructure, and it is assumed that their movement is restricted. Thus, when a load is applied and stresses develop within the gel matrix, the cells become pressurised by the forces that the fibres transmit to the cell membrane as well as the uniform pressure generated by the pore water.

The computational model assesses the stresses developed in the gel and their effect on the engineered bacteria cells by applying two different analysis modes: *total stresses* and *pore pressures*. However, if the above-presented scenario is confirmed to be accurate, a new type of analysis should be considered where part of the stresses transmitted to the cells remain constant (i.e. the stress transmitted by the fibres of the gel) and part of these stresses reduce over time (i.e. the pressure applied by the pore water).

Effectively, the stresses transmitted to the cell membrane could be split into two components: a *static* component associated to the stresses generated by the fibres, which does not fluctuate over time, and a *dynamic* component related to the pore pressure values and their dissipation upon consolidation.

- Structural changes upon cell growth

Following on from the above model limitation, the movement of the cells is impeded due to their size being bigger than the pore throats. Hence, the only way the cells can divide upon growth and form colonies of thousands of cells is by cracking the fibres surrounding their membrane to create space for themselves. This phenomena will potentially affect the way stresses distribute and, to a certain extent, reduce the strength of the gel.

The computational model does not consider any changes in the structure produced by the cells upon colony forming, however, the author recommends studying further this behaviour so that it can be determined whether any strength changes occur.

Additionally, as bacteria cells grow and divide by breaking the gel fibres, additional forces act on the cell membrane. These forces might amplify the expression of urease if the engineered strain is very sensitive to pressure changes and may need to be considered in the model.

- Bacteria growth

The bacterial growth analysis performed by the computational model is uni-dimensional – i.e. the model assumes that the growth rate is the same for every depth considered (i.e. alongside a horizontal plane). However, areas near the mould walls are more likely to have a different growth rate due to the availability of space for cell movement. Further research needs to be done in order to characterise the three-dimensional distribution of bacteria and growth rate in a more accurate way.

- Consolidation analysis

The expressions used to analyse the consolidation behaviour of the gel and pore pressure dissipation effect are based on soils saturated with water. Section 5.3.4. Mechanical behaviour describes the assumptions adopted for the analysis in hydrogels. However, one effect not considered in the analysis is the viscosity of the pore water. As cells grow within the micropores, the cells-nutrients-water solution becomes thicker/more viscous, which

ultimately leads to a higher resistance to movement. Therefore, this change in media composition will gradually prolong the time needed for drainage, potentially maintaining higher pressures in the gel micropores for longer periods of time.

- Changes in gel structure

As mentioned in previous sections, one of the objectives of the project is to be able to grow and monitor crystal formation within the hydrogel, potentially demonstrating a higher density of crystals in areas with higher urease expression (see section 6.5. Recommendations for future work for more details about the gel-based physical demonstrator). Hence, this precipitation of crystals within the gel micropores will gradually change its composition, ultimately leading to changes in the gel strength as well as changes in the stress distribution behaviour and pore pressure dissipation rate. The formation of crystals significantly increases the strength of soil samples, as reviewed in Chapter 2, due to the crystals bonding soil particles together and forming a cement-like matrix. However, the extend of this effect in agarose gels is unknown, and therefore, one of the objectives of the physical demonstrator will be to assess the changes in strength in relation to the amount of crystals precipitated.

- Plasticity of the gel

The mathematical expressions used for stress distribution analysis and settlement calculation are based on elasticity laws. However, as it was confirmed in Chapter 3, hydrogels are an elasto-plastic material, and as such, they are composed by both elastic and plastic behaviour. The elastic range is considerably bigger than in soils, however, due to the high coefficient of volume compressibility, hydrogels also experience plastic deformations which, ultimately, lead to changes in the stress-strain behaviour upon loading. Therefore, the repercussion these plastic deformations have on the stress-strain relationship will have to be considered in order to model with accuracy some of the properties of the gel system (e.g. stress distribution or total settlements). However, it is

believed that these plastic strains will have a minimal effect on the behaviour since agarose hydrogels mainly behave elastically, as demonstrated in Chapter 3.

5.6. Concluding remarks

Chapter 5 describes the core methodology development of a computational model designed to assess the response of a pressure-sensitive biomineralization gel-based system that has similar geotechnical properties to soft saturated soils. This responsive system is based on a volume of gel homogenously seeded with pressure-sensitive bacteria cells to which a certain load is applied on the surface, generating a distribution of stresses throughout the gel volume. The engineered bacteria cells present in the gel are modelled in such a way that they detect these pressure changes and respond by releasing a reporter enzyme (urease) associated to the level of stress. This relationship is what we call gene expression profile, and it dictates the amount of urease released in relation to the pressure value.

The model developed in this chapter is based on the model described in Dade-Robertson et al. (2018), however, it has been tailored to the specific needs of this study by:

1) Characterising the behaviour of agarose hydrogels under loading with the experimental data obtained in Chapter 3.
2) Integrating real biological data that describes the growth behaviour and distribution of bacteria colonies in agarose hydrogels.
3) Incorporating hypothetical values of urease activity as the reporting parameter to characterise the behaviour of the system.

The urease activity profiles associated to the stresses in the system are based on hypothetical data, however, the range of values selected for the analysis were obtained from the literature.

The different modelling components and parameters described throughout the chapter were successfully integrated in a user-friendly application that allows exploration of the impact different conditions have on the model, and helps to characterise the response of the pressure-responsive gel-based system to different inputs.

The model is able to predict cell concentration values over time throughout the whole 3D volume of gel for specific conditions, however, it should be noted that the model is not truly predictive, since it cannot simulate scenarios beyond these conditions. The simulations of the computational model showed the response of this pressure-responsive system to different loading scenarios and environmental conditions, and demonstrates how small changes in gene expression profiles (i.e. nano-scale behaviour of engineered bacteria) might alter substantially the behaviour of the system at the macro-scale. This can be appreciated by the different 'cementation' patterns that can be generated depending on the gene profile selected.

The computational model has succeeded in integrating the mechanical and biological components of the system, by simulating the behaviour of small-scale geotechnical scenarios in a gel-based medium, and illustrating the relationships between multiple scales. The results obtained from Mode 8 describe the behaviour of the so-called pressure-responsive bio-cementation system which is based on living bacteria cells and is able to operate across multiples and under different conditions.

The model, however, still relies in hypothetical data relative to the release of urease from the cells. As work in *Thinking Soils* progresses, the relationship between cell concentration and urease activity will be better understood. This will lead to a much better control over the initial conditions of the gel-based system, and will provide with accurate simulations of the urease distribution throughout the gel.

On the other hand, the model also uses gene expression profiles of a hypothetic pressure-sensitive strain of bacteria. This is presented as a bigger challenge since it involves the use of SynBio techniques to modify the nano-scale behaviour of a cell. However, as work progresses and the engineered strain is develop, the associated gene expression profiles will be integrated in the computational model, and simulations will be provided that describe the behaviour of the this pressure-responsive biomineralization system.

All limitations aside, this computational model is presented as a tool for the development, testing and monitoring of engineered responsive systems, and as work progresses within the *Thinking Soils* research group, and some of the model limitations are overcome, it is

believed that the model will be critical in demonstrating the applicability of the system and will provide a key contribution towards the validation of the proof of concept.

As a conclusion, the model describes the behaviour of a responsive living system which is able to combine computation (i.e. design of specific gene expression profiles) and material synthesis (biomineralization) due to the engineered behaviour of bacteria cells, and their ability to be designed to sense changes from the environment and respond in a useful way. A responsive system of this kind has never been developed before and it is expected to provide many benefits across several fields. A discussion about the potential benefits of using engineered responsive living systems for different applications can be found in chapter 6 (Concluding remarks).

Chapter 6

Conclusions

6.1. Introduction

This chapter summarises the main findings and significance of this research. The conclusions from the three experimental chapters of the thesis are described accordingly. Chapter 3 demonstrates the feasibility of using agarose hydrogels as a soil substitute for the development of responsive bio-mediated ground improvement methods by analysing their mechanical and physical properties and comparing them to certain types of soils. Chapter 4 further develops this idea by studying the growth behaviour and distribution of bacterial cells across the 3D matrix of agarose hydrogels. Chapter 5 describes the development of a computational model that integrates the data obtained from Chapter 3 (behaviour of agarose gels under loading) with the outcomes from Chapter 4 (growth behaviour and colonies distribution of bacteria-seeded hydrogels). Additionally, the computational model also incorporates hypothetical values of gene expression (urease activity, in particular) associated to stress levels in order to simulate the behaviour of the so-called responsive bio-cementation system in a gel-based medium. The contribution of this work to the *Thinking Soils* project is also discussed alongside some actions/recommendations to consider for further work. In addition, section 6.8. Concluding remarks reviews the overall findings and implications of this research and discusses its applicability in the field of engineered responsive living systems.

6.2. Agarose Hydrogel as a Soil Analogue

The development of bacteria-based Engineered Responsive Systems requires cultivation, monitoring and testing in a highly controllable material, biologically clean (i.e. absence of other microorganisms) and with well-understood mechanical and physical properties.

Agarose gels possess all these attributes and are, therefore, presented as an attractive option as a soil analogue for researchers working in a laboratory environment on bio-mediated responsive ground improvement systems.

Agarose gels are commonly used for biomedical applications, however, their geotechnical properties and their behaviour under induced loading of this type and magnitude have never been studied. Thus, Chapter 3 of this thesis describes an experimental investigation to assess the suitability of agarose LM (Low Melting Point) gels as a soil analogue by examining some of their relevant mechanical and physical properties. Scanning Electron Microscopy indicated that the pore-fibre structure of the gels is very similar to that found in organic soils such as peats. In addition, the size of the pores (0.3 µm on average) is similar to those found in homogeneous clay soils, although agarose gels have a considerably higher water content (1583%), porosity (0.96) and void ratio (26) than granular materials. The stress-strain relationship was also measured and the elastic modulus (309 kPa) was found to be smaller than the typical values of saturated cohesive soils. In addition, agarose gels present a much more elastic behaviour upon loading in comparison to soils.

On the contrary, the maximum undrained shear strength (27 kPa) and maximum axial strain (18%) are very similar to that found in medium-firm saturated cohesive soils.

The consolidation behaviour was also investigated and the coefficient of consolidation of agarose gel was found to range between 0.10 and 1.36 m^2/year. These values are very similar to those found in organic silts, glacial clays and Chicago silty clays. Additionally, the coefficient of compressibility was obtained (1.82-4.78 m^2/MN), suggesting that the rate of deformability under loading is very similar to that of sensitive clays and highly organic soils. Finally, the hydraulic conductivity of agarose gel was also analysed, and the values obtained (4.1-8.8E-11 m/s) suggest that agarose has a very low permeability, similar to that of homogeneous clay soils.

Although not all of the mechanical and physical properties of saturated cohesive soils are reproduced well by this type of agarose, the outcomes obtained from the experimental programme suggest that the properties required to develop the gel-based computational model/demonstrator are comparable, and in some cases identical. However, if the aim is

to model the behaviour of cohesionless soil types – such as sands – under loading, hydrogels are not fit for the purpose, since they present a different stress-strain, consolidation and pore pressure dissipation behaviour.

Chapter 3 demonstrates that agarose gels are suitable to model the geotechnical behaviour of saturated cohesive soils and it is expected that an agarose-based physical demonstrator will mimic the behaviour of saturated cohesive soils under induced loading, including stress distribution, pore pressure dissipation and rate of deformation. Furthermore, the benefit of using agarose gels in the early-stage development of engineered responsive systems is that they allow complex biological systems – such as Genetically Modified Organisms – to be studied in detail before being tested in a soil environment.

6.3. Growth and Distribution of Bacteria Colonies in Agarose Hydrogel

Agarose gels have been presented as a highly-controllable material in which bacteria colonies can be grown and monitored. The next step to achieve a complete control over the performance of a bacteria-based system was to understand the growth and distribution of the microbes and how they behave under different environmental conditions. The concentration of bacteria cells is one of the main parameters that dictates the rate and magnitude of crystal formation through the process of Microbially-Induced Calcite Precipitation (MICP). Thus, a critical factor to consider when developing responsive ground improvement methods based on MICP is understanding the formation of bacterial colonies in agarose gels and characterising the concentration of cells throughout a volume of gel over time.

Chapter 4, section 4.3.3. Bacteria-seeded agarose gel preparation, introduces a new method to produce homogeneously bacteria-seeded 3D agarose gels. The low gelling temperature of LM agarose is a key factor of the production process since it prevents causing thermal shock to the bacteria cells suspended in the liquid mixture. After gelation, the cells embedded within the matrix of the gel begin to form networks of colonies by breaking the

fibrous web-like structure and growing in number. The methods to visualise and monitor the 3D distribution and growth rate in agarose are also introduced, which rely on the glowing effect of engineered cells when exposed to fluorescence light.

Chapter 4, section 4.4.4. Bacteria growth in agarose hydrogels, evaluates the behaviour of bacterial colonies within the three-dimensional matrix of agarose hydrogels and describes the effect pH, temperature and initial dilution have on the growth rate, cell distribution and colony formation throughout a gel volume. The growth behaviour in hydrogels is demonstrated to differ significantly from the growth in liquid cultures, mainly due to the limitations of space and oxygen availability. The results suggest that an acidic environment (pH6) promotes a higher growth rate of bacteria compared to a more alkali environment (pH8). It was also found that higher temperatures (35°C) result in an increased growth rate in comparison to lower incubation temperatures (25°C), but were followed by an accelerated decay rate (due to cell death), resulting in a similar cell concentration after 24h.

Chapter 4, section 4.4.5. Growth characterisation in cylinders, focuses on characterising the growth rate of colonies throughout the length of a hydrogel cylinder. To do that, 20 slices were taken from each cylindrical sample and the concentration of cells was counted at different time lengths using the same procedure. Furthermore, growth profiles were also obtained for each layer of the gel and each condition analysed. The results obtained showed that a differential (uneven) growth rate appears between the different layers of the gels, with layers closer to the top surface and bottom of the cylinders showing higher concentrations over time.

Finally, a series of growth profiles in the form of numerical expressions were obtained for the different growth conditions. This data represents the macro-distribution of bacteria colonies throughout a volume of hydrogel as well as the growth rate of such colonies and, similarly to the mechanical properties obtained in Chapter 3, it allows modelling and simulation of the cell concentration over time under different environmental conditions.

The work performed in this chapter has characterised the behaviour of bacteria in hydrogels and provides an additional control over the performance of a bacteria-based system. The results obtained in the study have implications on both the *Thinking Soils*

project and the overall development of engineered responsive systems. However, these results also suggest that more work is necessary in order to better understand the growth behaviour of bacteria, especially when they are exposed to less controlled environments, such as soils.

6.4. Modelling of a Gel-based Pressure-responsive System

Chapter 5 describes the modelling of a bacteria-based pressure-responsive system which combines the data obtained in Chapters 3 and 4 with gene expression profiles associated to the behaviour of a pressure-sensitive urease-producing strain of bacteria (Figure 6-1). The model simulates the behaviour of agarose gels under loading and uses the data obtained from the experimental program on hydrogels in conjunction with various governing equations to describe how the stresses and deformations distribute throughout a 3D volume. This is referred as the ***macro-scale*** behaviour of the system. The model also integrates the data relevant to the growth and distribution of bacteria colonies described in Chapter 4. This data describes the ***micro-scale*** behaviour of the system and allows a high degree of control over the concentration of cells present in the 3D gel volume over time by varying temperature and initial inoculum. The computational model is further designed to simulate the behaviour of a pressure-sensitive urease-producing strain of bacteria homogeneously seeded in the matrix of the gel. The pressure-sensitivity is achieved by modifying the ***nano-scale*** behaviour of bacteria cells. The ultimate aim of this computational model is to illustrate how the system interacts across the different scales, and establish the fundaments of a system – based on the use of living organisms – that can change the properties at the macro-scale, by synthesizing biocements in response to pressure changes.
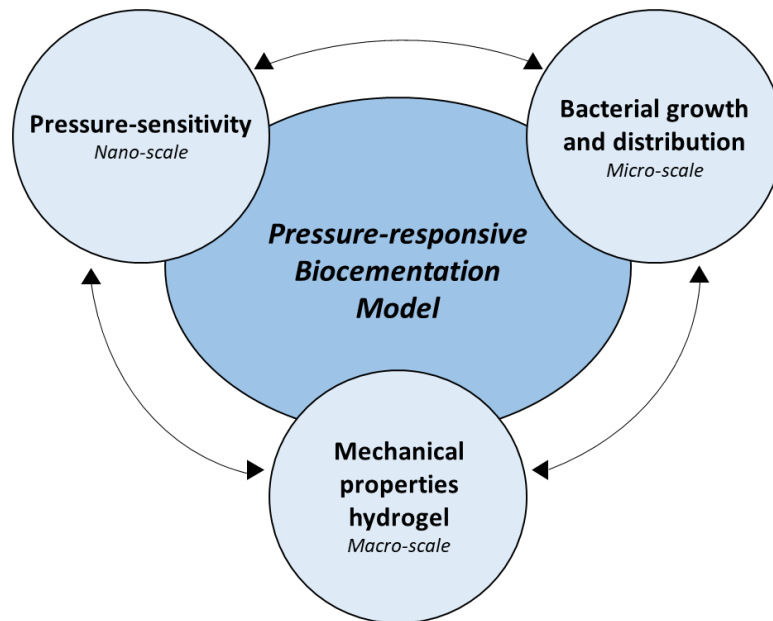
Figure 6-1. Components of the computational model

The chapter is divided into two parts; section 5.3. Model development describes the development of the model and how all the different components were integrated into a user-friendly application. Section 5.4. Model simulations focuses on the performance of the system under different mechanical, physical and biological conditions and provides a series of time-dependent simulations that illustrate how the system behaves. The simulations represent small-scale geotechnical scenarios – based on the behaviour of a shallow foundation under loading – and illustrate how the system is able to reinforce the gel volume by releasing urease and inducing biocementation in response to pressure. This behaviour is achieved due to the pressure-sensitivity of engineered bacteria cells and their associated gene expression profiles.

The simulations generated from the several modes intend to provide an insight into the sensitivity of the model to different parameters. In particular, modes 6, 7 and 8 provide with series of simulations that explore how sensible the model is to variables such as cell concentration, urease activity profile, load applied or coefficient of consolidation.

Referring to the latter, the simulations from mode 8, underpinned by the results from mode 2, clearly show how sensible the model is to the coefficient of consolidation, which

190

reiterates the importance of developing a more robust understanding of the consolidation behaviour of agarose hydrogels.

Moreover, the results also show how the non-uniform distribution of bacteria colonies throughout the gel volume plays an important role in the biocementation performance of the system. Furthermore, the integration of different gene expression profiles allows visualisation of the different biocementation areas that develop depending on the conditions selected.

The simulations obtained from the model have clear implications for the *Thinking Soils* project, and it is intended to use the model as the design framework for the future physical demonstrator that will validate the proof-of-concept of the pressure-responsive system. But more importantly, the model has succeeded in integrating real data related to the mechanical and biological components of the system, and it has been able to create a system that combines computation (i.e. design of specific gene expression profiles) and material synthesis (biomineralization) by using living organisms that have the ability to sense stimuli from the environment and respond in a useful way. Furthermore, the model presented in this study and the soil-based model introduced in Dade-Robertson et al. (2018) are the first ones that combine engineered organisms and material synthesis, and they are expected to underpin the development of more responsive systems with potential applications for the environment.

6.5. Recommendations for future work

While this study has succeeded in achieving the main aim of characterising a gel-based pressure-responsive system from the micro to the macro-scale, there are still numerous limitations and questions associated to the design and implementation of such system that need to be tackled. The author suggests a series of actions and experimental procedures that could be performed to build on the findings from this project and the overall research. These include the following:

- _Gel Mechanics_

- Exploring further the plastic deformations that occur to agarose gels under loading and how it affects the stresses developed. Also, understanding the long-term creep effect of the gels is believed to be important since it might alter the value of the stresses within the gel and the total settlement values. Therefore, an additional triaxial testing programme should be performed to agarose gel samples subjected to long-term induced loading.

- Understand how pore pressures develop upon loading and the rate at which they dissipate upon drainage. This will most likely involve the use of a triaxial apparatus and pressure-volume controllers in order to assess how pore pressures dissipate upon consolidation.

- As bacteria colonies grow within the microstructure of the gels, it is believed that changes occur to the fibre-pore matrix. The pore throats of the gel are considerably smaller than bacteria cells, therefore, the only way colonies can grow and distribute through the gel is by breaking the fibrous structure as they increase in number. Understanding the extent to which the cells change the mechanical properties of the gel is a crucial aspect of the project. The author suggest a series of experiments where the stress-strain relationship of bacteria-saturated gels is analysed. This might involve the use of a triaxial apparatus and similar tests to the ones described in Chapter 3. Furthermore, exploring visually this effect through SEM inspection might also help understand this behaviour.

- _Bacterial Behaviour_

- The model currently contains data on the concentration of cells over time for three specific temperatures (25°C, 30°C and 35°C) and two initial concentration of cells (high = 1/100 dilution; and low = 1/1000 dilution). The author suggest exploring further the growth behaviour in order to incorporate growth profiles for a wider range of conditions. Ultimately, the model should include the governing equations that describe the growth and distribution of bacteria in 3D agarose gels in order to be able to simulate every possible scenario and make it purely predictive.

- The addition of a calcium source is a crucial parameter for calcium carbonate precipitation to occur. However, the model does not take into account the consequences of adding calcium into the gel and how it affects the growth rate of bacteria. Hence, the author suggests an experimental programme where hydrogel samples are prepared with various concentrations of calcium and the growth rate of bacteria is assessed by using the methods described in Chapter 4. Furthermore, the author also recommends exploring the impact of adding inorganic compounds – e.g. calcium chloride – on the mechanical properties of the gel.

- Understanding the relationship between urease activity and cell concentration is another important parameter that needs exploration. The urease enzyme catalyses the hydrolysis of urea and dictates the rate at which calcite crystals precipitate through MICP. Therefore, a deeper understanding is needed on the factors that activate *B. subtilis* urease in vivo and the pathways that regulate its activity.

- One of the key aspects of the overall research project is the development of a *pressure-responsive* strain of bacteria which is capable of sensing pressure-changes and responding in a meaningful way (for example, by releasing specific levels of urease activity at certain stress values). The successful creation of such engineered strain will bring our research to the next level, and will establish the basis of a new type of responsive system based on engineered living organisms. This work will require an in-depth understanding of Synthetic Biology techniques and will involve the collaboration between researchers from several fields and a vast amount of resources.

- Crystal Formation

- Another important aspect to consider in future work is the process of biomineralization through MICP and the different pathways for calcite precipitation in agarose gels. In particular, understanding the relationship between cell concentration and crystal formation as well as the different parameters that dictate the rate at which crystals precipitate is essential for the further development of our responsive biocementation system.

- Following from the previous point, it is also important to understand how crystals attach to the fibres of the gel and how the new composition of the matrix changes the mechanical properties of the gel. Once the pathways for calcite precipitation in agarose are understood and controlled, the author suggests an experimental programme involving triaxial and oedometer tests in order to assess the stress-strain relationship of "biocemented" agarose samples at varying crystal concentrations.

- The author also suggests a series of experiments involving visualisation of crystal-precipitated agarose gels using a technique called *quantitative X-ray Diffraction (XRD).* This will allow monitoring and quantification of the amount and type of biomineralization occurring under different conditions. Additionally, it might also be worth performing a series of *X-ray Computing Tomography (XRT/CT)* tests to biocemented gel samples. This type of analysis allows dynamic exploration of 3D structures, and in our case, it would allow visualisation of the 3D precipitated crystal structure within the gel.

- Computational Modelling

The simulations obtained from the model are subjected to various limitations, which are discussed in section 5.5. Model limitations. Some of these limitations can be overcome by studying further the behaviour of the different components of the system, and some suggested actions are discussed above. Additionally, the author proposes a list of actions to improve the certainty and applicability of the model. These are:

- Understanding the different stresses generated at the bacterial cell membrane. The model currently uses pore pressures as the input value to compute urease activity levels for the *bio-mechanical* integrated simulations. However, as discussed in section 5.5. Model limitations, the engineered cells are also expected to sense a *stationary* or total stress contribution from the fibres enclosing the cell membrane. Therefore, understanding the contribution of the different stresses generated and how they evolve over time is crucial for the future implementation of the system.

- The author also suggests an experimental programme where the settlement values obtained from the model simulations are compared to results obtained experimentally from a similar physical setup. This might involve the use of an oedometer cell to quantify both elastic and consolidation settlements under different stress levels. By doing this, the accuracy and validity of the model can be assessed.

6.6. Parallel studies

Some of the author's recommendations mentioned in the previous section have already become individual work packages in the *Thinking Soils* project and have been running in parallel to this study. One of these work packages, carried out at Newcastle University, aims to understand the relationship between cell concentration and crystal formation as well as the different pathways for calcite precipitation within the matrix of agarose gels and the parameters that dictate the rate of precipitation. Achieving homogeneous crystal precipitation within the gel's structure is a crucial aspect of the *Thinking Soils* project. Most of the procedures used to produce bacteria-seeded gels and some of the techniques employed to monitor the precipitation of minerals within the gels are described in this thesis.

Preliminary results from this work package have demonstrated that it is possible to induce calcite precipitation within agarose gels. Figure 6-2 (left) shows a slice of a bacteria-seeded agarose gel observed with a light microscope, in which crystals of different sizes have precipitated. Qualitative X-Ray Diffraction analysis confirmed that the large-size crystals are indeed calcium carbonate precipitation, induced by the process of MICP. Note that these precipitated crystals can be appreciated with the naked eye. Additionally, Figure 6-2 (right) shows an SEM image of a $CaCl_2$ particle embedded within the fibrous structure of the gel. These samples were prepared by adding calcium chloride to the agarose solution and processing several gel slices in accordance to the ultrafast freezing technique described in section 3.3.3. Scanning Electron Microscope (SEM) imaging. The image shows how particles become embedded within the honeycomb structure of the gel upon gelation, and it is assumed that the same behaviour occurs with inoculated bacteria cells

but at a smaller scale (Note that the concentration of agarose for these samples was 2% m/v, hence the relatively large pore size).
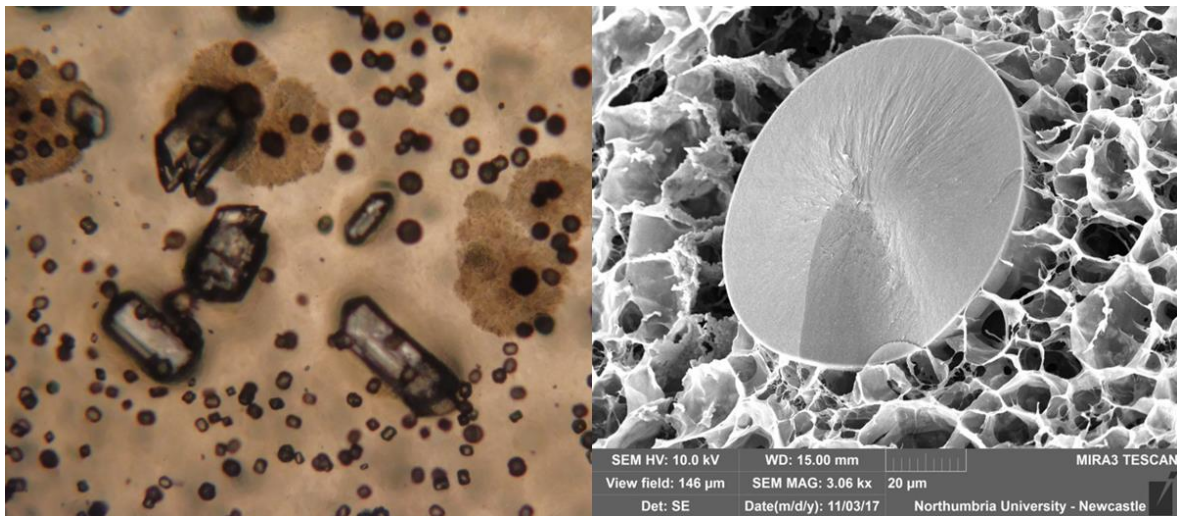
Figure 6-2. CaCO$_3$ induced by MICP (left) and CaCl$_2$ embedded within the structure of the gel (right)

Our project partners (Northumbria University) are also investigating the Microbially-Induced Calcite Precipitation phenomenon. In particular, they are conducting a study on the activation of *B. subtilis* urease in vivo. As described in this thesis, urease is an enzyme produced by some bacteria strains that catalyses the hydrolysis of urea into ammonia and carbon dioxide. This process is responsible for the formation of calcium carbonate (if a calcium source is available), hence, understanding the pathways that regulate urease expression is hugely valuable for the overall research.

The model presented in this thesis incorporates hypothetical profiles of gene expression and, although the simulations clearly demonstrate the potential of the system, it is recognised that the integration of real gene profiles into the model would considerably improve the significance of the model and would assist towards the development of the prototyped responsive system. Therefore, a considerable next step in the development of the gel-based computational model is the incorporation of real urease activity levels associated with the expression of the engineered pressure-sensitive bacteria strain. Preliminary results from a pressure-sensitive *E.coli* strain are reported in Guyet et al.

(2018), however, work continues at the Centre for Bacterial Cell Biology (Newcastle University) in order to find better strain candidates and refine the pressure sensitivity.

6.7. The ethical aspect

An aspect that has not been discussed on this thesis is the ethical conduct of the overall research project. As described throughout the body of the thesis, the *Thinking Soils* project involves the use of GMOs for environmental applications. The release of these engineered organisms into the geo-environment raises concerns of biosafety and sustainability. For instance, a possible impact associated to the use of GMOs for in-situ applications is the effect on indigenous species and the potential alteration of their behaviour due to horizontal gene transfer of recombinant DNA from the engineered organism or the release of GEM-derived metabolites (Urgun-Demirtas et al., 2006).

On the other hand, from a socio-economic point of view, one of the main concerns of governmental bodies in relation to the development of GMOs are the processes involving DNA recombinant techniques and pathogenic organisms, which under uncontrolled conditions, might lead to the generation and use of these engineered pathogens with malevolent purposes.

Although in many cases the use of GMOs to deal with environmental problems is presented as a very attractive option in comparison to traditional processes, the above-mentioned environmental concerns are the main cause of their poor commercialisation for in-situ practices (Megharaj et al., 2011).

In relation to the *Thinking Soils* project, at this stage the work conducted is purely exploratory, very far from field applications; hence, these concerns about biosafety and sustainability are still not considered in the development of the project. Further, for all the experimental packages that require dealing with GMOs, the work is performed in Containment Level 2 laboratories and under the narrow supervision of extremely qualified staff.

For more details about the potential risks associated to Synthetic Biology practices, and the current strategies to deal with these concerns, see König et al. (2013) and Ramos et al. (2011).

6.8. Concluding remarks

The world of Geotechnical Engineering is becoming interested in the use of Genetically Modified Organisms (GMOs) to deal with geo-environmental problems since they provide benefits that conventional microorganisms are not able to offer. Of particular interest to this project is the process of bio-mineralisation through Microbially-Induced Calcite Precipitation (MICP) as an effective and sustainable solution to deal with ground improvement problems. The work described in this thesis interacts with *Thinking Soils*, an EPSRC-funded research project that aims to develop a responsive ground improvement technique, based on an engineered strain of bacteria capable of sensing pressure changes in soils (e.g. due to induced loading) and able to respond by synthesizing bio-cements that increase the strength of the soil where it is needed.

The main aim of the study described in this thesis was to characterise at the micro and macro-scale an agarose-based system capable of testing engineered bacteria in a safe environment, monitoring their response and simulating the effect of a pressure-sensitive bio-cementation system. The implementation of such gel-based system offers many advantages, like enabling cell cultivation in a biologically clean medium where the physical, chemical and mechanical properties are controllable.

The development of this system has clear implications for the *Thinking Soils* project since it will be used for the development of the pressure-responsive bacteria strain as well as for preliminary tests to assess the behaviour of the engineered cells under different conditions. Additionally, the proposed system will ultimately support the validation of the proof-of-concept.

However, we believe a system of this kind can be used for many other applications, even for studies where the effect of mechanical forces are not used as an input. In particular, we believe our gel-based system can be beneficial to researchers working with engineered

living systems for environmental purposes. For example, a current trend of research is focusing on the development of engineered strains for bio-remediation purposes. A benefit of using our gel-based system would be the ability to mimic the biological and chemical properties of the ground and monitoring the remediation performance of the engineered cells. Additionally, another field of research where our gel-based system could be beneficial is in the development of biological sensors for different environmental applications. Therefore, we introduce this gel-based physical and computational model as a tool for the development, testing and monitoring of engineered responsive systems.

As a conclusion, this study has presented the design and modelling of a gel-based physical and computational demonstrator that can be used to study the performance of living engineered bacteria-based systems that can adapt and respond to changes in their environment. Furthermore, the successful implementation of such gel-based demonstrator, accompanied by the corresponding proof-of-concept validation supported by the computational model, would establish the first steps towards the development of a new type of biotechnology in which a material is able to remodel itself in response to physical forces from its environment.

References

Abid, M.M. and Pyrah, I.C., 1988. Guidelines for using the finite element method to predict one-dimensional consolidation behaviour. Comput. Geotech. 5, 213–226.

AC, K., 1999. Bacterial diversity in agroecosystems. Agric Ecosyst Env. 74, 65–76.

Achal, V., Pan, X., 2014. Influence of calcium sources on microbially induced calcium carbonate precipitation by Bacillus sp. CR2. Appl. Biochem. Biotechnol. 173, 307–317.

Anbu, P., Kang, C.-H., Shin, Y.-J., So, J.-S., 2016. Formations of calcium carbonate minerals by bacteria and its multiple applications. Springerplus 5, 250. https://doi.org/10.1186/s40064-016-1869-2

Ann-Muriel, S., Fortin, M., Arguin, C., Hugo, P., 2001. Detection of a Decrease in Green Fluorescent Protein Fluorescence for the Monitoring of Cell Death: An Assay Amenable to High-Throughput Screening Technologies 243, 237–243. https://doi.org/10.1002/cyto.10024

Aymard*, P., Martin, D.R., Plucknett, K., Foster, T.J., Clark, A.H., Norton, I.T., 2001. Influence of Thermal History on the Structural and Mechanical Properties of Agarose Gels. Biopolymers 59, 131–144.

Bachmeier, K.L., Williams, A.E., Warmington, J.R., Bang, S.S., 2002. Urease activity in microbiologically-induced calcite precipitation. J. Biotechnol. 93, 171–181.

Bang, S., Min, S., Bang, S., 2011. Application of Microbially Induced Soil Stabilization Technique for Dust Suppression. Int. J. Geo-Engineering 3, 27–37.

Barkay, T., Schaefer, J., 2001. Metal and radionuclide bioremediation: issues, considerations and potentials. Curr. Opin. Microbiol. 4, 318–323.

Benzerara, K., Miot, J., Morin, G., Ona-Nguema, G., Skouri-Panet, F., Ferard, C., 2011. Significance, mechanisms and environmental implications of microbial biomineralization. Comptes Rendus Geosci. 343, 160–167.

Bhaskar, P. V., Bhosle, N.B., 2005. Microbial extracellular polymeric substances in marine biogeochemical processes. Curr. Sci. 88, 45–53.

Blauw, M., Lambert, J.W.M., Latil, M.N., 2009. BIOSEALING : A METHOD FOR IN SITU SEALING OF LEAKAGES 978–981.

Boquet, E., Boronat, A., Ramos Cormenzana, A., 1973. Production of calcite (calcium carbonate) crystals by soil bacteria is a general phenomenon. Nature 246, 527–529.

Boussinesq, J., 1871. Théorie de l'intumescence liquide, appelée onde solitaire ou de translation, se propageant dans un canal rectangulaire. Comptes Rendus l'Academie Des Sci. 72, 755–759.

Boving, T.B., Blanford, W.J., McCray, J.E., Divine, C.E., Brusseau, M.L., 2008. Comparison of line-drive and push-pull flushing schemes. Gr. Water Monit. Remediat. 28, 75–86. https://doi.org/10.1111/j.1745-6592.2007.00182.x

Bowles, J.E., 1996. Foundation Analysis and Design, 5th editio. ed. McGraw-Hill.

Brandreth, D.A., 1968. Some practical aspects of curve fitting. J. Chem. Educ. 45, 657. https://doi.org/10.1021/ed045p657

British Standard 1377, 1990a. BS-1377: part 7. Methods of test for soils for civil engineering purposes. Shear strength tests (total stress).

British Standard 1377, 1990b. BS-1377: part 6. Methods of test for soils for civil engineering purposes. Consolidation and permeability tests in hydraulic cells and with pore pressure measurement.

British Standard 1377, 1990c. NBS 1377-5:1990. Methods of test for soils for civil engineering purposes. Compressibility, permeability and durability tests.

British Standard 1377, 1990d. BS-1377: part 2. Methods of test for soils for civil engineering purposes. Classification tests.

Burbank, M., Kavazanjian, E., Weaver, T., Montoya, B.M., Hamdan, N., Bang, S.S., Esnault-Filet, A., Tsesarsky, M., Aydilek, A., Ciurli, S., Tanyu, B., Manning, D. a. C., Larrahondo, J., Soga, K., Chu, J., Dejong, J.T., Cheng, X., Kuo, M., Al Qabany, A., Seagren, E. a., Van Paassen, L. a., Renforth, P., Laloui, L., Nelson, D.C., Hata, T., Burns, S., Chen, C.Y., Caslake, L.F., Fauriel, S., Jefferis, S., Santamarina, J.C., Inagaki, Y., Martinez, B., Palomino, A., 2013. Biogeochemical processes and geotechnical applications: progress, opportunities and challenges. Géotechnique 63, 287–301. https://doi.org/10.1680/geot.SIP13.P.017

Burbank, M.B., Weaver, T.J., Green, T.L., Williams, B.C., Crawford, R.L., 2011. Precipitation of Calcite by Indigenous Microorganisms to Strengthen Liquefiable Soils. Geomicrobiol. J. 28, 301–312. https://doi.org/10.1080/01490451.2010.499929

Burns, R.G., 1982. Enzyme activity in soil: location and a possible role in microbial ecology. Soil Biol. Biochem. 14, 423–427.

Carter, M., Bentley, S.P., 1991. Correlations of soil properties. Pentech Press, London.

Castanier, S., Métayer-Levrel, G. Le, Perthuisot, J.-P., 1999. Cacarbonates precipitation and limestone genesis -- the microbiogeologist point of view. Sediment. Geol 126, 9–23.

Chapelle, F.H., 2001. Ground-water microbiology and geochemistry, 2nd ed. Wiley, New York.

Cheng, L., Cord-Ruwisch, R., Shahin, M.A., 2013. Cementation of sand soil by microbially induced calcite precipitation at various degrees of saturation. Can. Geotech. J. 50, 81–90. https://doi.org/10.1139/cgj-2012-0023

Cheng, L., Shahin, M., 2015. Assessment of different treatment methods by microbial-induced calcite precipitation for clayey soil improvement.

Cheng, L., Shahin, M.A., Addis, M., Hartanto, T., Elms, C., 2014. Soil Stabilisation by Microbial-Induced Calcite Precipitation (MICP): Investigation into Some Physical and Environmental Aspects 10–14.

Choi, S.-G., Wu, S., Chu, J., 2016. Biocementation for Sand Using an Eggshell as Calcium Source. J. Geotech. Geoenvironmental Eng. 142, 6016010. https://doi.org/10.1061/(ASCE)GT.1943-5606.0001534

Christensen, H., Hansen, M., Sørensen, J.A.N., Icrobiol, A.P.P.L.E.N.M., 1999. Counting and Size Classification of Active Soil Bacteria by Fluorescence In Situ Hybridization with an rRNA Oligonucleotide Probe 65, 1753–1761.

Chu, J., Ivanov, V., Lee, M.F., Oh, X.M., He, J., 2009. Soil and waste treatment using biocement, in: Proceedings of the International Symposium on Ground Improvement Technologies and Case Histories, ISGI. Vol. 9. pp. 165–170.

Chu, J., Stabnikov, V., Ivanov, V., 2012. Microbially Induced Calcium Carbonate Precipitation on Surface or in the Bulk of Soil. Geomicrobiol. J. 29, 544–549. https://doi.org/10.1080/01490451.2011.592929

Chu, J., Varaksin, S., Klotz, U., Mengé, P., 2009. Construction processes, Proceedings of the 17th International Conference on Soil Mechanics and Geotechnical Engineering: The Academia and Practice of Geotechnical Engineering. https://doi.org/10.3233/978-1-60750-031-5-3006

Dade-Robertson, M., 2015. Computational Colloids: Escherichia coli pressure sensing for material computation.

Dade-Robertson, M., Mitrani, H., Rodriguez Corral, J., Zhang, M., Hernan, L., Guyet, A., Wipat, A., 2018. Design and modelling of an engineered bacteria-based, pressure-sensitive soil. Bioinspir. Biomim. https://doi.org/10.1088/1758-5090/0/0/000000

Dade-Robertson, M., Rodriguez-Corral, J., Guyet, A., Mitrani, H., Wipat, A., Zhang, M., 2017. Synthetic Biological Construction: Beyond "bio-inspired" in the design of new materials and fabrication systems., in: 3rd International Conference Biodigital: Architecture & Genetics. Barcelona: UIC.

Dade-Robertson, M., Rodriguez-Corral, J., Mitrani, H., Zhang, M., Wipat, A., Ramirez-Figueroa, C., Hernan, L., 2016. Thinking Soils: A synthetic biology approach to material based design computation., in: ACADIA 2016 - Posthuman Frontiers: Data, Designers and Cognitive Machines. Ann Arbor, Michigan: Association for Computer Aided Design in Architecture.

De Gennes, P.G., 1979. Scaling Concepts in Polymer Physics. Ithaca, NY.

De Jong, J.T., Martinez, B.C., Mortensen, B.M., Nelson, D.C., Waller, J.T., Weil, M.H., Ginn, T.R., Weathers, T., Barkouki, T., Fujita, Y., Redden, G., Hunt, C., Major, D., Tanyu, B., 2009. Upscaling of bio-mediated soil improvement. Proc. 17th Int. Conf. Soil Mech. Geotech. Eng. Acad. Pract. Geotech. Eng. 3, 2300–2303. https://doi.org/10.3233/978-1-60750-031-5-2300

De Muynck, W., De Belie, N., Verstraete, W., 2010. Microbial carbonate precipitation in construction materials: A review. Ecol. Eng. 36, 118–136. https://doi.org/10.1016/j.ecoleng.2009.02.006

Decho, A.W., 2010. Overview of biopolymer-induced mineralization: What goes on in biofilms? Ecol. Eng. 36, 137–144. https://doi.org/10.1016/j.ecoleng.2009.01.003

DeJong, Jason T., Michael B. Fritzges, and K.N., 2006. Microbially induced cementation to control sand response to undrained shear. J. Geotech. Geoenvironmental Eng. 132, 1381–1392. https://doi.org/10.1061/(ASCE)1090-0241(2006)132:11(1381)

DeJong, J.T., Mortensen, B., Martinez, B., 2007. Bio-soils interdisciplinary science and engineering initiative, Final Report on Workshop, 84 pp." Arlingon, VA, USA: National Science Foundation.

DeJong, J.T., Mortensen, B.M., Martinez, B.C., Nelson, D.C., 2010. Bio-mediated soil improvement. Ecol. Eng. 36, 197–210. https://doi.org/10.1016/j.ecoleng.2008.12.029

DEJONG, J.T., SOGA, K., KAVAZANJIAN, E., BURNS, S., PAASSEN, L.A.V., QABANY, A. AL, AYDILEK, A., S.S.BANG, BURBANK, M., CASLAKE, L.F., C.Y.CHEN, CHENG, X., CHU, J., CIURLI, S., A.ESNAULT-FILET, FAURIEL, S., HAMDAN, N., HATA, T., INAGAKI, Y., S. JEFFERIS19, M. KUO2, L. LALOUI14, J. LARRAHONDO20, D. A. C. MANNING21, B. MARTINEZ22, B. M. MONTOYA23, D. C. NELSON24, A. PALOMINO25, P. RENFORTH26, J.C.SANTAMARINA4, E. A. SEAGREN27, B. TANYU28, M.T. and T.W., Consideration, 2013. Biogeochemical processes and geotechnical applications : progress , opportunities and challenges 287–301.

Dettling, M., Yavitt, J., Cadillo-Quiroz, H., Sun, C., Zinder, S., 2007. Soil-Methanogen interactions in two peatlands (Bog, Fen) in Central New York State. Geomicrobiol. J. 24, 247–259.

Dhami, N.K., Reddy, M.S., Mukherjee, A., 2013. Biomineralization of calcium carbonate polymorphs by the bacterial strains isolated from calcareous sites. J. Microbiol. Biotechnol 23, 707–714.

Doran, P.T., Fritsen, C.H., McKay, C.P., Priscu, J.C., Adams, E.E., 2003. Formation and character of and ancient 19-m ice cover and underlying trapped brine in an "ice-sealed" east Antarctic lake, in: Proc. Natl. Acad. Sci. U.S.A.,. pp. 26–31.

Dupraz, S., Ménez, B., Gouze, P., Leprovost, R., Bénézeth, P., Pokrovsky, O.S., Guyot, F., 2009. Experimental approach of CO 2 biomineralization in deep saline aquifers. Chem. Geol. 265, 54–62.

Edwards, K., Bach, W., McCollom, T., 2005. Geomicrobiology in oceanography: microbe-mineral interactions at and below the seafloor. Trends Microbiol 13, 449–456.

Ehrlich, H., 1996. How microbes influence mineral growth and dissolution. Chem. Geol. 132, 5–9.

Ehrlich, H.L., 1998. Geomicrobiology: its significance for geology. Earth-Science Rev. 45, 45–60.

Elowitz, M., Leibler, S., 2000. A synthetic oscillatory network of transcriptional regulators. Nature 403, 335–8.

Endy, D., 2005. Foundations for engineering biology. Nature 438, 449–53. https://doi.org/10.1038/nature04342

Fadum, R.E., 1948. Influence values for estimating stresses in elastic foundations, in: 2nd Int. Conf. SMFE Rotterdam Vol 3. pp. 77–84.

Ferris, F.G., Phoenix, V., Fujita, Y., Smith, R.W., 2004. Kinetics of calcite precipitation induced by ureolytic bacteria at 10 to 20 C in artificial groundwater. Geochim. Cosmochim. Acta 68,

1701–1710.

Flemming, H.C., Wingender, J., Griegbe, T., Mayer, C., 2000. Physico-chemical properties of biofilms., in: Biofilms: Recent Advances in Their Study and Control. Amsterdam: Harwood Academic Publishers, pp. 19–34.

Fortin, M., Steff, A.M., Hugo, P., 2005. High-throughput technology: green fluorescent protein to monitor cell death. Methods Mol Med. 110, 121–137.

Fragaszy, R.J., Santamarina, J.C., Amekudzi, A., Assimaki, D., Bachus, R., Burns, S.E., Cha, M., Cho, G.C., Cortes, D.D., Dai, S., Espinoza, D.N., Garrow, L., Huang, H., Jang, J., Jung, J.W., Kim, S., Kurtis, K., Lee, C., Pasten, C., Phadnis, H., Rix, G., Shin, H.S., Torres, M.C., Tsouris, C., 2011. Sustainable Development and Energy Geotechnology – Potential Roles for Geotechnical Engineering 15, 611–621. https://doi.org/10.1007/s12205-011-0102-7

Frankel, R.B., Bazylinski, D.A., 2003. Biologically induced mineralization by bacteria. Rev. Mineral. Geochemistry 54, 95–114.

Fujita, Y., Taylor, J.L., Wendt, L.M., Reed, D.W., Smith, R.W., 2010. Evaluating the potential of native ureolytic microbes to remediate a 90Sr contaminated environment. Environ. Sci. Technol. 44, 7652–7658. https://doi.org/10.1021/es101752p

Fukue, M., Ono, S., Sato, Y., 2011. Cementation of Sands Due To Microbiologically-Induced Carbonate Precipitation. Soils Found. 51, 83–93. https://doi.org/10.3208/sandf.51.83

G.A.M. van Meurs, W. van der Zon, J. Lambert, C.C.D.F. van R., 2006. The challenge to adapt soil properties, in: Proc. 5th ICEG: Environ. Geotechnics: Opportunities, Challenges and Responsibilities for Environ. pp. 1192–1199.

Gadd, G.M., 2010. Metals, minerals and microbes: geomicrobiology and bioremediation. Microbiology 156, 609–643.

Gadd, G.M., 2007. Geomycology: biogeochemical transformations of rocks, minerals, metals and radionuclides by fungi, bioweather- ing and bioremediation. Mycol Res 111, 3–49.

Gardner, T., Cantor, C., Collins, J., 2000. Construction of a genetic toggle switch in Escherichia coli. Nature 403, 339–42.

Ginn, T., Wood, B.D., Nelson, K.E., Scheibe, T.D., Murphy, E.M., Clement, T.P., 2002. Processes in microbial transport in the natural subsurface. Adv. Water Resour. 25, 1017–1042.

Goering, R., Dockrell, H., Zuckerman, M., Chiodini, P., Roitt, I., 2013. Mims' medical microbiology

(5th ed.). Philadelphia: Elsevier/Saunders.

Gram, H.C., 1884. Method of distinguishing between two major classes of bacteria. Friedländer's J. Fortschritte der Medizin.

Greenhalgh, R., Greenhalgh, M., Alshareef, F., Robson, G.D., 2017. Application of green fluorescent protein to measure antimicrobial efficacy and the kinetics of cell death against Escherichia coli. J. Microbiol. Methods 141, 67–72. https://doi.org/10.1016/j.mimet.2017.08.005

Gu, W.Y., Yao, H., Huang, C.Y., Cheung, H.S., 2003. New insight into deformation-dependent hydraulic permeability of gels and cartilage, and dynamic behavior of agarose gels in confined compression. J. Biomech. 36, 593–598. https://doi.org/10.1016/S0021-9290(02)00437-2

Guyet, A., Dade-Robertson, M., Wipat, A., Casement, J., Smith, W., Mitrani, H., Zhang, M., 2018. Mild hydrostatic pressure triggers oxidative responses in Escherichia coli. PLoS One 13.

Hamilton, W.A., 2003. Microbially influenced corrosion as a model system for the study of metal microbe interactions: a unifying electron transfer hypothesis. Biofouling 19, 65–76.

Hammes, F., Boon, N., Villiers, J. de, Verstraete, W., Siciliano, S.D., 2003. Strain-specific ureolytic microbial calcium carbonate precipitation. Appl. Environ. Microbiol. 69, 4901–9.

Harkes, M.P., van Paassen, L.A., Booster, J.L., Whiffin, V.S., van Loosdrecht, M.C.M., 2010. Fixation and distribution of bacterial activity in sand to induce carbonate precipitation for ground reinforcement. Ecol. Eng. 36, 112–117. https://doi.org/10.1016/j.ecoleng.2009.01.004

Haro, M.A., De Lorenzo, V., 2001. Metabolic engineering of bacteria for environmental applications: Construction of Pseudomonas strains for biodegradation of 2-chlorotoluene. J. Biotechnol. 85, 103–113. https://doi.org/10.1016/S0168-1656(00)00367-9

Harry, E., Monahan, L., Thompson, L., 2006. Bacterial cell division: the mechanism and its precision. Int. Rev. Cytol 253, 27–94.

Hattori, T., 1973. Microbial life in the soil. Dekker, New York, USA.

Hauser, J.R., 2009. Numerical Methods for Nonlinear Engineering Models. Springer, North Carolina.

Hazen, R., Papineau, D., Bleeker, W., Downs, R., Ferry, J., McCoy, T., Yang, H., 2008. Mineral

evolution. Am Min. 93, 1693–1720.

Horn, J.M., Meike, A., 1995. Microbial Activity at Yucca Mountain. Lawrence Livermore National Laboratory, Chicago.

Inc., R., 2007. Settle3D: Settlement and consolidation analysis.

Ivanov, V., Chu, J., 2008. Applications of microorganisms to geotechnical engineering for bioclogging and biocementation of soil in situ. Rev. Environ. Sci. Biotechnol. 7, 139–153. https://doi.org/10.1007/s11157-007-9126-3

Ivanov, V., Chu, J., Stabnikov, V., 2015. Basics of Construction Microbial Biotechnology, in: Biotechnologies and Biomimetics for Civil Engineering. Springer International Publishing.

Jeppsson, J.O., Laurell, C.B., Franzén, B., 1979. Agarose gel electrophoresis. Clin. Chem. 25, 629–38.

Jiang, G., Noonan, M.J., Ratecliffe, T.J., 2006. Effects of soil matric suction on retention and percolation of Bacillus subtilis in intact soil cores. Water Air Soil Pollut 177, 211–226.

Jiang G, Noonan MJ, R.T., 2006. Effects of soil matric suction on retention and percolation of Bacillus subtilis in intact soil cores. Water Air Soil Pollut 177, 211–226.

Johnson, E.M., Berk, D.A., Jain, R.K., Deen, W.M., 1995. Diffusion and partitioning of proteins in charged agarose gels. Biophys. J. 68, 1561–1568. https://doi.org/10.1016/S0006-3495(95)80328-0

Johnson, E.M., Deen, W.M., 1996. Hydraulic permeability of agarose gels. AIChE J. 42, 1220–1224. https://doi.org/10.1002/aic.690420504

Jonkers, H.M., Thijssen, A., Muyzer, G., Copuroglu, O., Schlangen, E., 2010. Application of bacteria as self-healing agent for the development of sustainable concrete. Ecol. Eng. 36, 230–235. https://doi.org/10.1016/j.ecoleng.2008.12.036

Karol, R.H., 2003. Chemical grouting and soil stabilization, 3rd ed. New York.

Kato, C., Barlet, D.H., 1997. The molecular biology of barophilic bacteria. Extremophiles 1, 111–116.

Khalil, A.S., Collins, J.J., 2010. Synthetic biology: applications come of age. Nat. Rev. Genet. 11, 367–79. https://doi.org/10.1038/nrg2775

Kile, D.E., Eberl, D.D., Hoch, A.R., Reddy, M.M., 2000. An assessmentof calcite crystal growth

mechanisms based on crystal size distributions. Geochim. Cosmochim. Acta 64, 2937–2950.

Kleanthous, C., Armitage, J.P., 2015. The bacterial cell envelope. Philos. Trans. R. Soc. B Biol. Sci. 370, 20150019. https://doi.org/10.1098/rstb.2015.0019

Kohnhauser, K., 2007. Introduction to geomicrobiology. Malden, MA.

Konhauser, K., 2007. Introduction to geomicrobiology, European Journal of Soil Science. https://doi.org/10.1111/j.1365-2389.2007.00943_4.x

König, H., Frank, D., Heil, R., Coenen, C., 2013. Synthetic Genomics and Synthetic Biology Applications Between Hopes and Concerns 11–24.

Kucharski, E.S., Cord-ruwisch, R., Whiffin, V., Al-thawadi, S.M., 2008. Microbial Biocementation (Patent).

Kumar, D., Dhane, G., Priyadarshee, A., 2015. Performance of Different Form of Soil Reinforcement : a Review. Int. J. Sci. Technol. Manag. 4, 667–677.

Laurent, C.T., 1967. Determination of the structure of agarose gels ny gel chromatography. Biochim. Biophys. Acta 136, 199–205.

Lear, G., Lewis, G.D., 2012. Microbial biofilms: current research and applications. Horizon Scientific Press.

Lebron, I., Suarez, D.L., 1996. Calcite nucleation and precipitation kinetics as affected by dissolved organic matter at 25 C and pH> 7.5. Geochim. Cosmochim. Acta 60, 2765–2776.

Li, M., Cheng, X., Guo, H., 2013. Heavy metal removal by biomineralization of urease producing bacteria isolated from soil. Int. Biodeterior. Biodegradation 76, 81–85. https://doi.org/10.1016/j.ibiod.2012.06.016

Lian, B., Hu, Q., Chen, J., Ji, J., Teng, H.H., 2006. Carbonate biomineralization induced by soil bacterium Bacillus megaterium. Geochim. Cosmochim. Acta 70, 5522–5535. https://doi.org/10.1016/j.gca.2006.08.044

Liu, Q., Subhash, G., Moore, D.F., 2011. Loading velocity dependent permeability in agarose gel under compression. J. Mech. Behav. Biomed. Mater. 4, 974–982. https://doi.org/10.1016/j.jmbbm.2011.02.009

LM, P., JP, H., DA, K., 2002. Microbiology, 5th ed. The McGraw-Hill Company.

Lopez-Garcia, P., Kazmierczak, J., Benzerara, K., Kempe, S., Guyot, F., Moreira, D., 2005. Bacterial

diversity and carbonate precipitation in the giant microbialites from the highly alkaline Lake Van, Turkey. Extremophiles 9, 263–274.

Loren L. Looger, Mary A. Dwyer, J.J.S.& H.W.H., Department, 2003. Computational design of receptor andsensorproteinswithnovel functions. Nature 423, 185–190. https://doi.org/10.1038/nature01578.1.

Lowenthal, R.E., Marais, G.V.R., 1976. Carbonate chemistry of aquatic systems.

Madigan, M.T., Martinko, J.M., Dunlap, P.V., Clark, D.P., 2008. Brock biology of microorganisms, 12th ed. Benjamin Cummings.

Madigan, M.T., Martinko, J.M., Parker, J., 2000. Brock—Biology of Microorganisms, 9th ed. Prentice–Hall, Upper Saddle River, N.J.

Maier, R.M., Pepper, I.L., Gerba, C.P., 2009. Environmental microbiology, 2nd editio. ed. Elsevier Science.

Mankins, J.C., 1995. Technology Readiness Levels. White Pap. April 5. https://doi.org/10.1080/08956308.2010.11657640

Manning, D.A.C., 2008. Biological enhancement of soil carbonate precipitation: passive removal of atmospheric CO2. Mineral. Mag. 72, 639–649.

Mapelli, F., Marasco, R., Balloi, A., Rolli, E., Cappitelli, F., Daffonchio, D., Borin, S., 2012. Mineral–microbe interactions: biotechnological potential of bioweathering. J. Biotechnol. 157, 473–481.

Martinez, B.C., Barkouki, T.H., DeJong, J.D., Ginn, T.R., 2011. Upscaling Microbial Induced Calcite Precipitation in 0.5 m Columns: Experimental and Modeling Results. Geo-Frontiers 2011 4049–4059.

Martinez, B.C., DeJong, J.T., Ginn, T.R., Montoya, B.M., Barkouki, T.H., Hunt, C., Tanyu, B., Major, D., 2013. Experimental Optimization of Microbial-Induced Carbonate Precipitation for Soil Improvement. J. Geotech. Geoenvironmental Eng. 139, 587–598. https://doi.org/10.1061/(ASCE)GT.1943-5606.0000787

Megharaj, M., Ramakrishnan, B., Venkateswarlu, K., Sethunathan, N., Naidu, R., 2011. Bioremediation approaches for organic pollutants: A critical perspective. Environ. Int. 37, 1362–1375. https://doi.org/10.1016/j.envint.2011.06.003

Mitchell, A.C.., Ferris, F.G., 2005. The coprecipitation of Sr into calcite precipitates induced by

bacterial ureolysis in artificial groundwater: temperature and kinetic dependence. Geochim. Cosmochim. Acta 69, 4199–4210.

Mitchell, A.C., Dideriksen, K., Spangler, L.H., Cunningham, A.B., Gerlach, R., 2010. Microbially enhanced carbon capture and storage by mineral-trapping and solubility-trapping. Environ. Sci. Technol. 44, 5270–5276.

Mitchell, J.K., 1975. Fundamentals of soil behavior. Wiley, New York, USA.

Mitchell, J.K., Santamarina, J.C., 2005a. Biological Considerations in Geotechnical Engineering. J. Geotech. Geoenvironmental Eng. 131, 1222–1233. https://doi.org/10.1061/(ASCE)1090-0241(2005)131:10(1222)

Mitchell, J.K., Santamarina, J.C., 2005. Biological Considerations in Geotechnical Engineering. J. Geotech. Geoenviron. Eng. 131, 1222–1233.

Mitchell, J.K., Santamarina, J.C., 2005b. Biological Considerations in Geotechnical Engineering. J. Geotech. Geoenvironmental Eng. 131, 1222–1233. https://doi.org/10.1061/(ASCE)1090-0241(2005)131:10(1222)

Mobley, H., Island, M., Hausinger, R., 1995. Molecular biology of microbial ureases. Microbiol Rev 59, 451–580.

Montoya, B.M., 2012. Bio-Mediated Soil Improvement and the Effect of Cementation on the Behavior, Improvement, and Performance of Sand.

Montoya, B.M., DeJong, J.T., Boulanger, R.W., 2013. Dynamic response of liquefiable sand improved by microbial induced calcite precipitation. Géotechnique 63, 302–312.

Morris, V., 1986. Gelation of polysaccharides, in: Mitchell JR, L. DA (Ed.), Functional Properties of Food Macromole- Cules. Elsevier, London, pp. 121–170.

Moseley, M.P., Kirsch, K., 2004. Ground Improvement. New York, USA.

Motulsky, H., Christopoulos, A., 2003. Fitting Models to Biological Data using Linear and Nonlinear Regression. A practical guide to curve fitting. https://doi.org/10.1002/pst.167

Nakano, M.M., Zuber, P., 1998. Anaerobic growth of a "strict aerobe" (Bacillus subtilis). Annu. Rev. Microbiol. 52, 165–190.

Narayanan, J., Xiong, J.-Y., Liu, X.-Y., 2006. Determination of agarose gel pore size: Absorbance measurements vis a vis other techniques. J. Phys. Conf. Ser. 28, 83–86.

https://doi.org/10.1088/1742-6596/28/1/017

Nemati, M., Greene, E.A., Voordouw, G., 2005. Permeability profile modification using bacterially formed calcium carbonate: Comparison with enzymic option. Process Biochem. 40, 925–933. https://doi.org/10.1016/j.procbio.2004.02.019

Ng, W., Lee, M., Hii, S., 2012. An Overview of the Factors Affecting Microbial-Induced Calcite Precipitation and its Potential Application in Soil Improvement 723–729.

Nguyen, P.Q., Courchesne, N.M.D., Duraj-Thatte, A., Praveschotinunt, P., Joshi, N.S., 2018. Engineered Living Materials: Prospects and Challenges for Using Biological Systems to Direct the Assembly of Smart Materials. Adv. Mater. 30, 1–34. https://doi.org/10.1002/adma.201704847

Nordstrom, D.K., Alpers, C.N., 1999. Geochemistry of acid mine waters. Rev. Econ. Geol. 6, 133–160.

Normand, V., Lootens, D.L., Amici, E., Plucknett, K.P., Aymard, P., 2000. New insight into agarose gel mechanical properties. Biomacromolecules 1, 730–738. https://doi.org/10.1021/bm005583j

Oflaz, H., Baran, O., 2014. A new medical device to measure a stiffness of soft materials. Acta Bioeng. Biomech. 16, 125–131. https://doi.org/10.5277/abb140115

Ogston, A.G., 1958. THE SPACES IN A UNIFORM RANDOM SUSPENSION OF FIBRES. Trans. Faraday Soc. 1754–1757.

Ogston, A.G., Preston, B.N., Wells, J.D., 1973. On the Transport of Compact Particles Through Solutions of Chain-Polymers. Proc. R. Soc. A Math. Phys. Eng. Sci. 333, 297–316. https://doi.org/10.1098/rspa.1973.0064

Okwadha, G.D.O., Li, J., 2010. Optimum conditions for microbial carbonate precipitation. Chemosphere 81, 1143–1148. https://doi.org/10.1016/j.chemosphere.2010.09.066

Omoregie, A.I., Khoshdelnezamiha, G., Senian, N., Ong, D.E.L., Nissom, P.M., 2017. Experimental optimisation of various cultural conditions on urease activity for isolated Sporosarcina pasteurii strains and evaluation of their biocement potentials. Ecol. Eng. 109, 65–75. https://doi.org/10.1016/j.ecoleng.2017.09.012

Ouzounov, N., Nguyen, J.P., Bratton, B.P., Jacobowitz, D., Gitai, Z., Shaevitz, J.W., 2016. MreB Orientation Correlates with Cell Diameter in Escherichia coli. Biophys. J. 111, 1035–1043.

https://doi.org/10.1016/j.bpj.2016.07.017

Paul, E.A., Clark, F.E., 1996. Soil microbiology and biochemistry. Academic, New York, USA.

Pernodet, N., Maaloum, M., Tinland, B., 1997. Pore size of agarose gels by atomic force microscopy. Electrophoresis 18, 55–58. https://doi.org/10.1002/elps.1150180111

Phadnis, H.S., Santamarina, J.C., 2011. Bacteria in sediments: pore size effects. Géotechnique Lett. 91–93. https://doi.org/10.1680/geolett.11.00008

Phang, I.R.K., Chan, Y.S., Wong, K.S., Lau, S.Y., 2018. Isolation and characterization of urease-producing bacteria from tropical peat. Biocatal. Agric. Biotechnol. 13, 168–175. https://doi.org/10.1016/j.bcab.2017.12.006

Phillips, A.J., Gerlach, R., Lauchnor, E., Mitchell, A.C., Cunningham, A.B., Spangler, L., 2013. Engineered applications of ureolytic biomineralization: a review. Biofouling 29, 715–733.

Pluen, A., Netti, P.A., Jain, R.K., Berk, D.A., 1999. Diffusion of macromolecules in agarose gels: comparison of linear and globular configurations. Biophys. J. 77, 542–52. https://doi.org/10.1016/S0006-3495(99)76911-0

Poulos, H.G., Davis, E.H., 1974. Elastic solutions for soil and rock mechanics. New York.

Powrie, W., 2014. Soil Mechanics: Comcepts and Applications. CRC Press, London.

Prindle, A., Samayoa, P., Razinkov, I., Danino, T., Tsimring, L.S., Hasty, J., 2012. A sensing array of radically coupled genetic "biopixels." Nature 481, 39–44. https://doi.org/10.1038/nature10722

Purushothama, P.R., 2005. Ground improvement techniques.

Qabany, A.A., Mortensen, B., Martinez, B., Soga, K., DeJong, J., 2011. Microbial carbonate precipitation: correlation of S-wave velocity with calcite precipitation. Geotech. Spec. Publ. 3993–4001.

Ramos, J.L., Marqués, S., van Dillewijn, P., Espinosa-Urgel, M., Segura, A., Duque, E., Krell, T., Ramos-González, M.I., Bursakov, S., Roca, A., Solano, J., Fernádez, M., Niqui, J.L., Pizarro-Tobias, P., Wittich, R.M., 2011. Laboratory research aimed at closing the gaps in microbial bioremediation. Trends Biotechnol. 29, 641–647. https://doi.org/10.1016/j.tibtech.2011.06.007

Rebata-landa, V., Santamarina, J., 2012. Mechanical effects of biogenic nitrogen gas bubbles in

soils. J Geotech Geoenviron Eng 138, 128–137.

Rezanezhad, F., Price, J.S., Quinton, W.L., Lennartz, B., Milojevic, T., Van Cappellen, P., 2016.
Structure of peat soils and implications for water storage, flow and solute transport: A
review update for geochemists. Chem. Geol. 429, 75–84.
https://doi.org/10.1016/j.chemgeo.2016.03.010

Ripp, S., Nivens, D.E., Ahn, Y., Werner, C., Jarrell IV, J., Easter, J.P., Cox, C.D., Burlage, R.S., Sayler,
G.S., 2000. Controlled field release of a bioluminescent genetically engineered
microorganism for bioremediation process monitoring and control. Environ. Sci. Technol.
34, 846–853. https://doi.org/10.1021/es9908319

Rivadeneyra, M.A., Delgado, G., Soriano, M., Ramos-Cormenzana, A., Delgado, R., 2000.
Precipitation of carbonates by Nesterenkonia halobia in liquid media. Chemosphere 41,
617–624.

Rivadeneyra, M.A., Párraga, J., Delgado, R., Ramos-Cormenzana, A., Delgado, G., 2004.
Biomineralization of carbonates by Halobacillus trueperi in solid and liquid media with
different salinities. FEMS Microbiol. Ecol. 48, 39–46.

Robards, A., 1991. Rapid-freezing methods and their applications., in: Electron Microscopy of
Plant Cells. pp. 257–312.

Rodriguez-Corral, J., Mitrani, H., Dade-Robertson, M., Zhang, M., Maiello, P., 2018. Agarose Gel
as a Soil Analogue for the Development of Advanced Bio-mediated Soil Improvement
Methods.

Rogers, J.R., Bennett, P.C., 2004. Mineral stimulation of subsurface microorganisms: release of
limiting nutrients from silicates. Chem. Geol. 203, 91–108.

S, S., DN, S., P, P., 2014. Soil characterization for comprehending stability of geotechnical
structures., in: Methods and Recent Advances in Geomechanics. Taylor & Francis Group,
London, pp. 1661–1665.

Sarikaya, M., 1999. Biomimetics: materials fabrication through biology. Proc. Natl. Acad. Sci. 96,
14183–14185.

Schaeffer, P., Miller, K., Aubert, J., 1965. Catabolic Repression of Bacterial Sporulation Author (s
): Pierre Schaeffer , Jacqueline Millet , Jean-Paul Aubert Source : Proceedings of the
National Academy of Sciences of the United States of America , Published by : National
Academy of Sciences Stab, in: Proceedings of the National Academy of Sciences of the

United States of America. National Academy of Sciences, pp. 704–711.

Shahin, M.A., 2016. Some Innovative Solutions for Dealing with Problematic Soils in Infrastructure Developments 1–22.

Shashank, B.S., Sharma, S., Sowmya, S., Latha, R.A., Meenu, P.S., Singh, D.N., 2016a. State-of-the-art on geotechnical engineering perspective on bio-mediated processes. Environ. Earth Sci. 75, 1–16. https://doi.org/10.1007/s12665-015-5071-6

Shashank, B.S., Sharma, S., Sowmya, S., Latha, R.A., Meenu, P.S., Singh, D.N., 2016b. State-of-the-art on geotechnical engineering perspective on bio-mediated processes. Environ. Earth Sci. 75, 1–16. https://doi.org/10.1007/s12665-015-5071-6

Silver, P.A., Way, J.C., Arnold, F.H., Meyerowitz, J.T., 2014. Engineering explored. Nature 506, 166–167. https://doi.org/10.1073/pnas.1321321111

Singh, A.K., Singh, M., Verma, N., 2017. Extraction, purification, kinetic characterization and immobilization of urease from Bacillus sphaericus MTCC 5100. Biocatal. Agric. Biotechnol. 12, 341–347. https://doi.org/10.1016/j.bcab.2017.10.020

Singh, J.S.., Abhilash, P.C.., Singh, H.B.., Singh, R.P.., Singh, D., P., 2011. Genetically engineered bacteria: an emerging tool for environmental remediation and future research perspectives. Gene 480, 1–9.

Sinha, J., Reyes, S.J., Gallivan, J.P., 2010. Reprogramming bacteria to seek and destroy an herbicide. Nat. Chem. Biol. 6, 464–470. https://doi.org/10.1038/nchembio.369

Skempton, A.W., 1954. "The pore-pressure coefficient A and B." Geo- Tech. 4, 143–147.

Skempton, A.W., 1951. The bearing capacity of clays.

Slonczewski, J.L., Foster, J.W., 2013. Microbiology: an evolving science, 3rd ed.

Smith, C.B., Anderson, J.E., Fischer, R.L., Webb, S.R., 2002. Stability of green fluorescent protein using luminescence spectroscopy: Is GFP applicable to field analysis of contaminants? Environ. Pollut. 120, 517–520. https://doi.org/10.1016/S0269-7491(02)00227-0

Smith, I.K., 2014. Smith's Elements of Soil Mechanics, 9th Edition.

Soon, N.W., Lee, L.M., Khun, T.C., Ling, H.S., 2013. Improvements in engineering properties of soils through microbial-induced calcite precipitation. KSCE J. Civ. Eng. 17, 718–728. https://doi.org/10.1007/s12205-013-0149-8

Spencer, M., 1982. Reverse salt gradient chromatography of tRNA on unsubstituted agarose. III. Physical and chemical properties of different batches of sepharose 4B. J. Chromatogr. A 238, 317–325. https://doi.org/10.1016/S0021-9673(00)81317-5

Stabnikov, V., Ivanov, V., Chu, J., 2015. Construction Biotechnology: a new area of biotechnological research and applications. World J. Microbiol. Biotechnol. 31, 1303–1314. https://doi.org/10.1007/s11274-015-1881-7

Staudt, C., Horn, H., Hempel, D.C., Neu, T.R., 2004. Volumetric measurements of bacterial cells and extracellular polymeric substance glycoconjugates in biofilms. Biotechnol. Bioeng. 88, 585–592.

Stellwagen, J., Stellwagen, N.C., 1995. Internal Structure of the Agarose Gel Matrix. J. Phys. Chem. 99, 4247–4251. https://doi.org/10.1021/j100012a054

Stocks-Fischer, S., Galinat, J.K., Bang, S.S., 1999. Microbiological precipitation of CaCO3. Soil Biol. Biochem. 31, 1563–1571. https://doi.org/10.1016/S0038-0717(99)00082-6

Sutherland, I.W., 2001. Biofilm exopolysaccharides: a strong and sticky framework. Microbiology 147, 3–9.

Tabak, H.H., Lens, P., Van Hullebusch, E.D., Dejonghe, W., 2005. Developments in bioremediation of soils and sediments polluted with metals and radionuclides - 1. Microbial processes and mechanisms affecting bioremediation of metal contamination and influencing metal toxicity and transport. Rev. Environ. Sci. Biotechnol. 4, 115–156. https://doi.org/10.1007/s11157-005-2169-4

Takahashi, I., MacKenzie, L., 1981. Effect of various inhibitors on sporulation of Bacillus subtilis. Cana J Microbiol 30, 80–86.

Takigawa, T., Morino, Y., Urayama, K., Masuda, T., 1996. Poisson's Ratio of Polyacrylamide (PAAm) Gels. Polym. Gels Networks 4, 1–5. https://doi.org/10.1016/0966-7822(95)00013-5

Taylor, D.W., 1948. Fundamentals of soil mechanics. John Wiley, New York.

Terzaghi, K., 1943. Theoretical Soil Mechanics. John Wiley and Sons, New York.

Terzaghi, K., 1925. Principles of soil mechanics. Engineering 93, 874–878.

Trang, P.T.K., Berg, M., Viet, P.H., Van Mui, N., Van Der Meer, J.R., 2005. Bacterial bioassay for rapid and accurate analysis of arsenic in highly variable groundwater samples. Environ. Sci. Technol. 39, 7625–7630. https://doi.org/10.1021/es050992e

Tuson, H.H., Renner, L.D., Weibel, D.B., 2012. Polyacrylamide hydrogels as substrates for studying bacteria. Chem. Commun. 48, 1595–1597. https://doi.org/10.1039/C1CC14705F

Tuvikene, R., Truus, K., Kollist, A., Volobujeva, O., Mellikov, E., Pehk, T., 2008. Gel-forming structures and stages of red algal galactans of different sulfation levels. J. Appl. Phycol. 20, 527–535. https://doi.org/10.1007/s10811-007-9229-9

Umar, M., Kassim, K.A., Ping Chiet, K.T., 2016. Biological process of soil improvement in civil engineering: A review. J. Rock Mech. Geotech. Eng. 8, 767–774. https://doi.org/10.1016/j.jrmge.2016.02.004

Unger, I., Kennedy, A., Muzika, R.-M., 2009. Flooding effects on soil microbial communities. Appl Soil Ecol 42, 1–8.

Urgun-Demirtas, M., Stark, B., Pagilla, K., 2006. Use of Genetically Engineered Microorganisms (GEMs) for the Bioremediation of Contaminants. Crit. Rev. Biotechnol. 26, 145–164.

Urgun-demirtas, M., Stark, B., Pagilla, K., Urgun-demirtas, M., 2017. Use of Genetically Engineered Microorganisms (GEMs) for the Bioremediation of Contaminants Use of Genetically Engineered Microorganisms (GEMs) for the Bioremediation of Contaminants 8551. https://doi.org/10.1080/07388550600842794

van Paassen, L.A., 2011. Bio-mediated ground improvement: from laboratory experiment to pilot applications., in: Proc. GeoFrontiers 2011: Advances in Geotechnical Engineering. pp. 4099–4108.

van Paassen, L.A., Daza, C.M., Staal, M., Sorokin, D.Y., van der Zon, W., van Loosdrecht, M.C., 2010. Potential soil reinforcement by biological denitrification. Ecol. Eng. 36, 168–175.

Vidal, H., 1969. The principle of reinforced earth. Highw. Res. Rec. 282.

Voigt, C., 2012. Synthetic biology. ACS Synth. Biol. 1, 1–2.

Voigt, C.A., 2006. Genetic parts to program bacteria. Curr. Opin. Biotechnol. 17, 548–557. https://doi.org/10.1016/j.copbio.2006.09.001

Whiffin, V.S., van Paassen, L.A., Harkes, M.P., 2007. Microbial Carbonate Precipitation as a Soil Improvement Technique. Geomicrobiol. J. 24, 417–423. https://doi.org/10.1080/01490450701436505

Whitman, W.B., Coleman, D.C., Wiebe, W.J., 1998. Prokaryotes: the unseen majority. Proc. Natl. Acad. Sci. 95, 6578–6583.

Wierzchos, J., Ascaso, C., 1998. Mineralogical transformation of bioweathered granitic biotite, studied by HRTEM: evidence for a new pathway in lichen activity.

Wilson, S.C., Jones, K.C., 1993. Bioremediation of soil contaminated with polynuclear aromatic hydrocarbons (PAHs): a review. Environ. Pollut. 81, 229–249.

Xiao, L.P., Shi, Z.J., Xu, F., Sun, R.C., 2012. Hydrothermal carbonization of lignocellulosic biomass. Bioresour. Technol. 118, 619–623.

Xu, F., Sridharan, B., Durmus, N.G., Wang, S., Yavuz, A.S., Gurkan, U.A., Demirci, U., 2011. Living bacterial sacrificial porogens to engineer decellularized porous scaffolds. PLoS One 6. https://doi.org/10.1371/journal.pone.0019344

Yañez, F., Gomez-Amoza, J.L., Magariños, B., Concheiro, A., Alvarez-Lorenzo, C., 2010. Hydrogels porosity and bacteria penetration: Where is the pore size threshold? J. Memb. Sci. 365, 248–255. https://doi.org/10.1016/j.memsci.2010.09.012

Zwietering, M.H., Jongenburger, I., Rombouts, F.M., Riet, K. V., 1990. Modeling of the Bacterial Growth Curve. Appl Env. Microbiol 56, 1875–1881.

Appendix A. Unconsolidated Undrained Triaxial tests and moisture content calculation

Triaxial data

	SAMPLE 1		SAMPLE 2		SAMPLE 3		SAMPLE 4		SAMPLE 5	
Diameter (mm)	37.36		37.28		37.3		37.03		37.46	
Length (mm)	75.72		73.17		74.8		74.95		74.29	
Cell pressure (kPa)	100 kPa		200 kPa		300 kPa		400 kPa		500 kPa	
	Axial Strain (%)	Deviator Stress (kPa)	Axial Strain (%)	Deviator Stress (kPa)	Axial Strain (%)	Deviator Stress (kPa)	Axial Strain (%)	Deviator Stress (kPa)	Axial Strain (%)	Deviator Stress (kPa)
	0.00	0.09	0.00	-0.08	0.00	1.21	0.00	0.57	0.00	0.85
	0.13	0.55	4.24	14.17	0.13	1.64	0.00	0.78	0.00	0.76
	0.30	1.10	4.41	14.49	0.30	2.24	0.18	0.98	0.18	1.39
	0.46	1.56	4.58	14.89	0.47	2.85	0.27	0.97	0.39	2.23
	0.63	2.02	4.75	15.28	0.63	3.36	0.32	1.56	0.61	3.07
	0.79	2.39	4.92	15.77	0.80	3.86	0.58	2.60	0.81	3.72
	0.96	2.84	5.09	16.16	0.97	4.36	0.84	3.54	1.02	4.48
	1.12	3.38	5.26	16.63	1.14	4.86	1.10	4.48	1.24	5.25
	1.29	3.83	5.43	17.19	1.30	5.44	1.37	5.51	1.47	5.98
	1.45	4.37	5.60	17.66	1.47	5.84	1.63	6.33	1.68	6.77
	1.62	4.81	5.77	18.12	1.64	6.42	1.89	7.24	1.90	7.56
	1.78	5.26	5.94	18.59	1.80	6.90	2.15	8.23	2.11	8.08
	1.95	5.78	6.11	19.14	1.97	7.47	2.42	9.03	2.33	8.85
	2.11	6.22	6.29	19.68	2.14	7.85	2.68	10.01	2.54	9.58
	2.28	6.66	6.46	20.13	2.30	8.42	2.94	10.78	2.76	10.29
	2.44	7.18	6.63	20.58	2.47	8.80	3.20	11.65	2.97	10.91
	2.61	7.62	6.80	21.11	2.64	9.36	3.47	12.61	3.17	11.66
	2.77	8.05	6.97	21.56	2.81	9.91	3.73	13.41	3.39	12.33
	2.94	8.31	7.14	22.08	2.97	10.28	3.99	14.25	3.62	13.09
	3.10	8.90	7.31	22.60	3.13	10.60	4.25	15.07	3.83	13.63
	3.27	9.32	7.48	23.12	3.31	11.28	4.52	15.89	4.05	14.42
	3.43	9.74	7.65	23.63	3.47	11.64	4.78	16.70	4.26	15.12
	3.60	10.25	7.82	24.14	3.64	12.17	5.04	17.59	4.48	15.80
	3.75	10.67	8.00	24.65	3.81	12.61	5.30	18.38	4.69	16.48
	3.93	11.08	8.16	25.16	3.98	13.05	5.56	19.16	4.91	17.15
	4.09	11.58	8.34	25.58	4.14	13.49	5.83	20.12	5.12	17.90
	4.26	12.08	8.51	26.16	4.31	14.01	6.09	20.98	5.33	18.62
	4.42	12.34	8.68	26.65	4.48	14.43	6.35	21.73	5.55	19.28
	4.59	12.98	8.85	27.14	4.65	14.95	6.61	22.57	5.77	20.00
	4.75	13.38	9.02	27.63	4.81	15.37	6.88	23.49	5.98	20.71
	4.92	13.87	9.19	28.20	4.98	15.79	7.14	24.31	6.20	21.49
	5.08	14.36	9.36	28.76	5.15	16.29	7.40	25.12	6.42	22.34
	5.23	14.67	9.53	29.24	5.31	16.71	7.66	26.10	6.63	23.10
	5.41	15.15	9.70	29.71	5.48	17.20	7.93	26.89	6.85	23.70
	5.58	15.63	9.87	30.18	5.65	17.69	8.19	27.76	7.06	24.52
	5.74	16.02	10.04	30.65	5.81	18.09	8.45	28.71	7.26	25.17
	5.91	16.49	10.21	31.11	5.98	18.66	8.71	29.65	7.49	26.00
	6.07	16.96	10.39	31.49	6.15	19.06	8.98	30.59	7.71	26.86
	6.24	17.35	10.56	32.02	6.32	19.53	9.24	31.42	7.92	27.64
	6.41	17.81	10.73	32.48	6.48	19.92	9.50	32.33	8.14	28.42
	6.57	18.36	10.90	33.01	6.65	20.47	9.76	33.23	8.35	29.26
	6.74	18.74	11.07	33.46	6.82	20.94	10.03	34.12	8.57	30.17
	6.90	19.20	11.24	33.90	6.99	21.48	10.26	34.85	8.78	30.93
	7.07	19.58	11.41	34.50	7.15	21.86	10.53	35.98	8.98	31.68
	7.23	19.95	11.58	35.01	7.32	22.40	10.79	36.75	9.20	32.60
	7.40	20.31	11.75	35.61	7.49	22.85	11.05	37.65	9.43	33.49
	7.56	20.85	11.92	36.04	7.65	23.22	11.33	38.52	9.64	34.20
	7.73	21.30	12.10	36.62	7.82	23.74	11.59	39.35	9.86	35.06
	7.89	21.66	12.27	37.12	7.99	24.18	11.84	40.14	10.07	35.72

Cont.	SAMPLE 1		SAMPLE 2		SAMPLE 3		SAMPLE 4		SAMPLE 5	
	8.05	22.10	12.44	37.62	8.15	24.62	12.10	41.02	10.29	36.59
	8.22	22.54	12.61	38.27	8.32	24.97	12.38	41.87	10.50	37.45
	8.39	23.06	12.78	38.76	8.49	25.56	12.64	42.67	10.72	38.26
	8.55	23.50	12.95	39.33	8.66	25.90	12.90	43.60	10.93	38.99
	8.72	23.85	13.12	39.89	8.82	26.41	13.16	44.46	11.14	39.74
	8.88	24.28	13.29	40.44	8.99	27.00	13.43	45.26	11.34	40.47
	9.05	24.63	13.46	41.00	9.16	27.24	13.70	46.16	11.58	41.34
	9.21	25.22	13.63	41.55	9.32	27.57	13.96	46.88	11.79	42.03
	9.38	25.64	13.80	42.01	9.49	28.06	14.21	47.74	12.01	42.85
	9.54	26.06	13.97	42.55	9.66	28.54	14.47	48.49	12.22	43.61
	9.71	26.56	14.14	43.17	9.83	29.02	14.75	49.46	12.44	44.40
	9.87	26.91	14.31	43.70	9.99	29.58	15.00	50.12	12.65	45.20
	10.04	27.47	14.49	44.15	10.16	30.06	15.27	51.00	12.87	45.98
	10.20	27.89	14.66	44.75	10.33	30.61	15.54	51.91	13.07	46.70
	10.37	28.38	14.83	45.35	10.49	31.24	15.80	52.67	13.30	47.46
	10.53	28.86	15.00	45.79	10.66	31.70	16.04	53.38	13.52	48.20
	10.69	29.27	15.17	46.22	10.83	32.24	16.30	54.28	13.73	48.95
	10.86	29.75	15.34	46.73	10.99	32.78	16.57	55.07	13.95	49.82
	11.03	30.15	15.51	47.32	11.16	33.23	16.83	55.77	14.16	50.55
	11.19	30.62	15.68	47.74	11.33	33.83	17.10	56.42	14.38	51.34
	11.36	31.10	15.85	48.23	11.50	34.35	17.35	56.87	14.59	52.10
	11.52	31.49	16.02	48.81	11.66	34.87	17.63	57.49	14.81	52.94
	11.69	31.96	16.20	49.21	11.83	35.46	17.89	57.74	15.01	53.49
	11.85	32.35	16.37	49.54	12.00	35.97	18.14	57.78	15.24	54.15
	12.02	32.73	16.54	49.95	12.16	36.56	18.40	57.61	15.45	55.08
	12.18	33.19	16.71	50.43	12.33	37.05	18.66	56.78	15.67	55.80
	12.35	33.65	16.88	50.82	12.50	37.64	18.92	52.99	15.88	56.58
	12.51	34.18	17.05	51.14	12.67	38.21	19.18	46.16	16.10	57.35
	12.68	34.64	17.22	51.53	12.83	38.81	19.45	38.52	16.31	58.18
	12.84	35.01	17.39	51.76	13.00	39.37	19.52	36.86	16.53	58.93
	13.01	35.53	17.56	52.06	13.17	39.89			16.74	59.78
	13.17	35.90	17.73	52.37	13.33	40.48			16.95	60.36
	13.34	36.34	17.90	52.52	13.50	41.02			17.17	61.10
	13.50	36.78	18.07	52.59	13.67	41.62			17.39	61.88
	13.67	37.29	18.25	52.73	13.84	42.18			17.60	62.18
	13.83	37.73	18.41	52.80	14.00	42.71			17.82	62.78
	14.00	38.24	18.59	52.71	14.17	43.24			18.03	63.24
	14.16	38.66	18.76	52.40	14.34	43.92			18.25	63.75
	14.33	39.09	18.93	52.09	14.51	44.43			18.46	64.20
	14.49	39.51	19.10	50.07	14.67	44.95			18.68	64.56
	14.66	40.01	19.27	45.84	14.84	45.61			18.88	64.71
	14.82	40.35			15.01	46.19			19.11	64.69
	14.99	40.84			15.17	46.69			19.32	64.68
	15.15	41.18			15.34	47.27			19.54	64.11
	15.32	41.58			15.51	47.92			19.75	61.56
	15.48	41.91			15.67	48.56			19.97	50.23
	15.65	42.28			15.84	49.03			20.18	18.69
	15.81	42.72			16.01	49.58			20.22	17.20
	15.98	43.16			16.18	50.13				
	16.15	43.68			16.34	50.76				
	16.31	44.11			16.51	51.29				
	16.48	44.62			16.68	51.83				
	16.64	45.05			16.84	52.43				
	16.81	45.47			17.01	52.87				
	16.97	45.89			17.18	53.47				
	17.14	46.39			17.35	53.90				
	17.30	46.73			17.51	54.41				
	17.46	47.22			17.68	55.00				
	17.63	47.63			17.85	55.50				
	17.80	47.80			18.01	55.99				
	17.96	48.12			18.18	56.48				
	18.12	47.99			18.35	56.89				
	18.29	47.78			18.51	57.37				
	18.45	47.34			18.68	57.77				
	18.62	46.68			18.85	57.86				
	18.78	44.67			19.02	58.03				
	18.95	38.46			19.18	58.19				
	19.11	30.64			19.35	58.21				
					19.52	58.14				
					19.68	58.08				
					19.85	57.50				

Undrained shear strength

	SAMPLE 1	SAMPLE 2	SAMPLE 3	SAMPLE 4	SAMPLE 5
Max. deviator stress (kPa)	48.12	52.80	58.21	57.78	64.71
Max. axial strain (%)	17.95	18.41	19.35	18.14	18.88
Membrane correction (kPa)	1.75	1.80	1.90	1.80	1.85
Corrected deviator stress (kPa)	46.37	51.00	56.31	55.98	62.86
Undrained shear strength, Cu (kPa)	23.19	25.50	28.15	27.99	31.43
Average Cu (kPa)	27.25				

Moisture content

		Before drying (g)	After drying (g)	Water evaporated (g)	Dry sample (g)	Moisture content (%)	Average moisture content (%)
SAMPLE 1	Tin	82.54				1591.41	1583.68
	Tin + sample	116.03	84.52	31.51	1.98		
SAMPLE 2	Tin	81.79				1556.06	
	Tin + sample	103.65	83.11	20.54	1.32		
SAMPLE 3	Tin	82.22				1603.55	
	Tin + sample	115.78	84.19	31.59	1.97		

Appendix B. Oedometer tests

Sample 1	
Diameter =	49.99 mm
Height =	20.45 mm
Loading stage	0 kPa --> 6 kPa
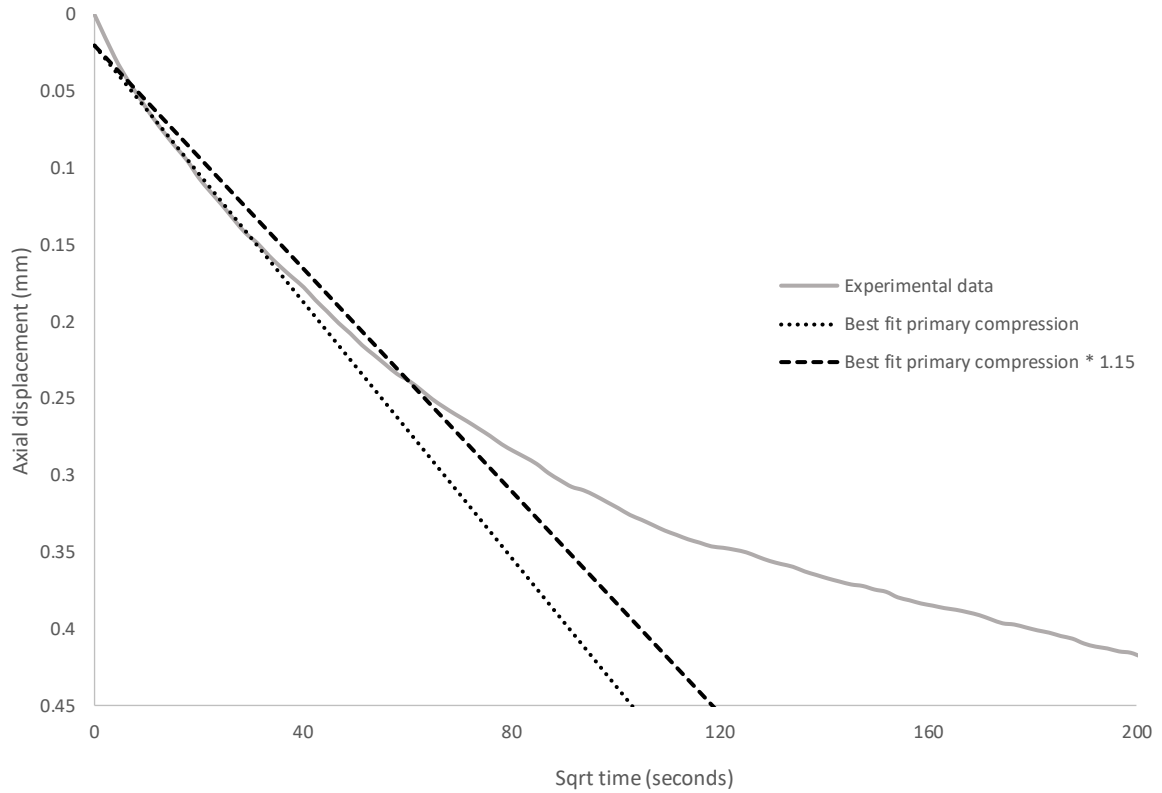
$$C_v = \frac{0.446 * \overline{H}^2}{t_{90}} \qquad m_v = \left(\frac{H_2 - H_1}{H_1}\right)\left(\frac{1000}{P_2 - P_1}\right)$$

√t₉₀ =	65		H₁ =	20.45	mm
t₉₀ =	4225	s	H₂ =	20.03	mm
H =	20.24	mm	P₁ =	0	kPa
Cᵥ =	0.04	mm2/s	P₂ =	6	kPa
Cᵥ =	1.36	m2/yr	mᵥ =	3.45	m2/MN

Sample 2	
Diameter =	49.79 mm
Height =	20.08 mm
Loading stage	12 kPa --> 25 kPa

Axial displacement (mm) vs sqrt time (seconds)

- Experimental data
- Best fit primary compression
- Best fit primary compression * 1.15
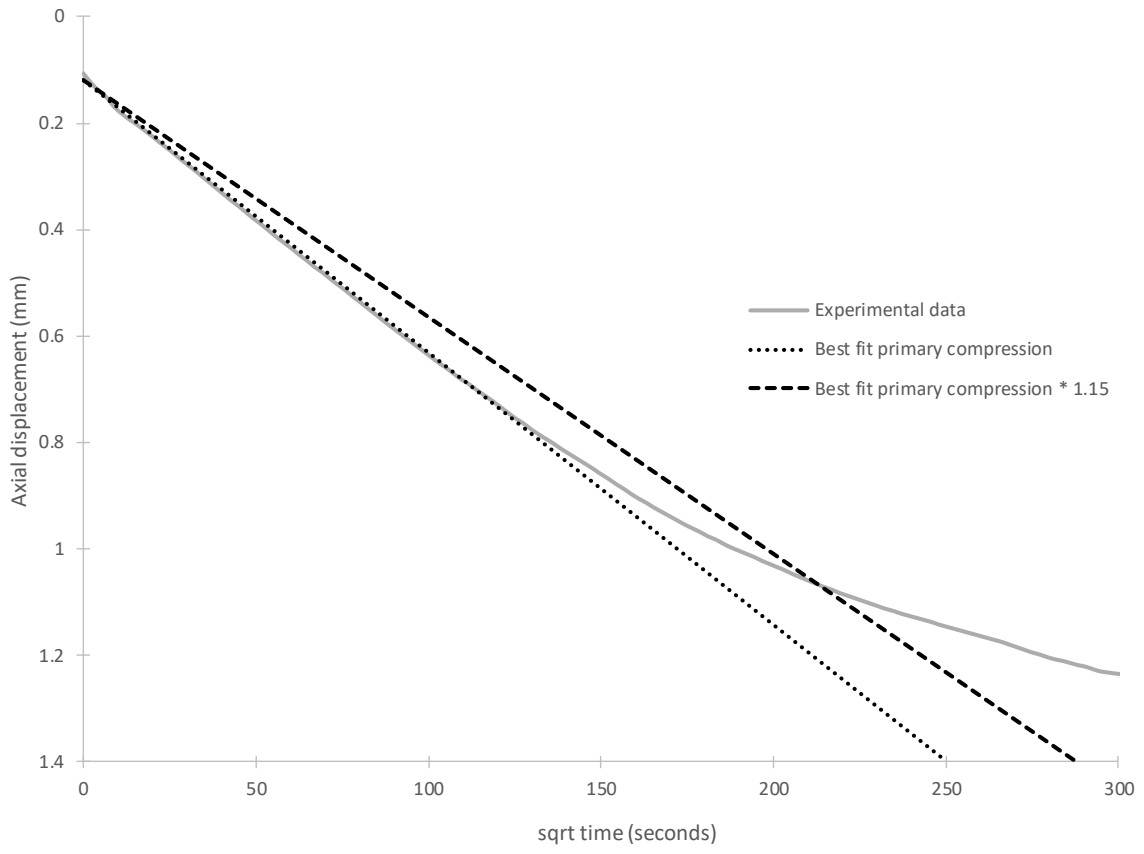
$$C_v = \frac{0.446 * \overline{H}^2}{t_{90}} \qquad m_v = \left(\frac{H_2 - H_1}{H_1}\right)\left(\frac{1000}{P_2 - P_1}\right)$$

√t₉₀ =	210	**H₁ =**	19.97 mm
t₉₀ =	44100 s	**H₂ =**	18.84 mm
H =	19.40 mm	**P₁ =**	12 kPa
C_v =	0.00 mm2/s	**P₂ =**	25 kPa
C_v =	0.12 m2/yr	**m_v =**	4.39 m2/MN

Sample 2

Diameter =	49.79 mm
Height =	20.08 mm
Loading stage	25 kPa --> 50 kPa
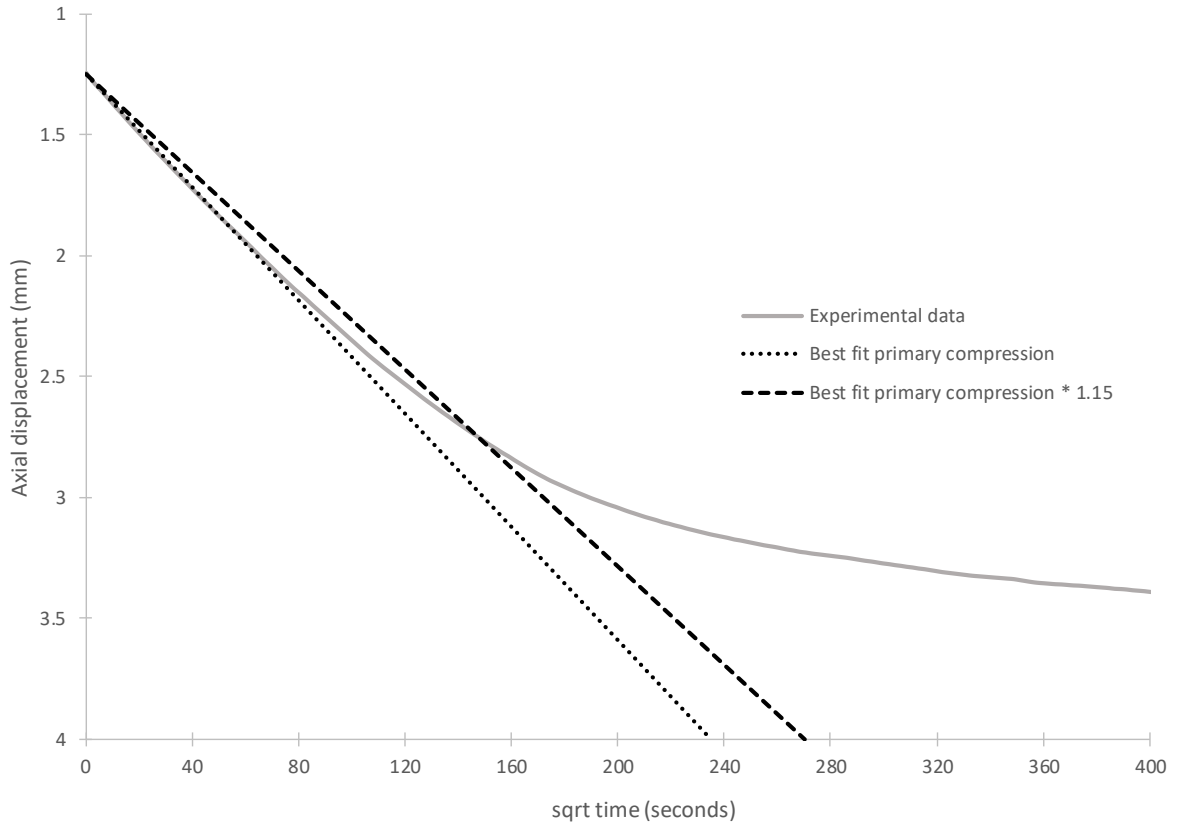
$$C_v = \frac{0.446 * \overline{H}^2}{t_{90}} \qquad\qquad m_v = \left(\frac{H_2 - H_1}{H_1}\right)\left(\frac{1000}{P_2 - P_1}\right)$$

√t₉₀ =	150		**H₁ =**	18.84	mm
t₉₀ =	22500	s	**H₂ =**	16.58	mm
H =	17.71	mm	**P₁ =**	25	kPa
Cᵥ =	0.01	mm2/s	**P₂ =**	50	kPa
Cᵥ =	0.20	m2/yr	**mᵥ =**	4.78	m2/MN

Sample 3

Diameter =	49.36 mm
Height =	20.26 mm
Loading stage	0 kPa --> 6 kPa

Axial displacement (mm) vs sqrt time (seconds)

- Experimental data
- Best fit primary compression
- Best fit primary compression * 1.15
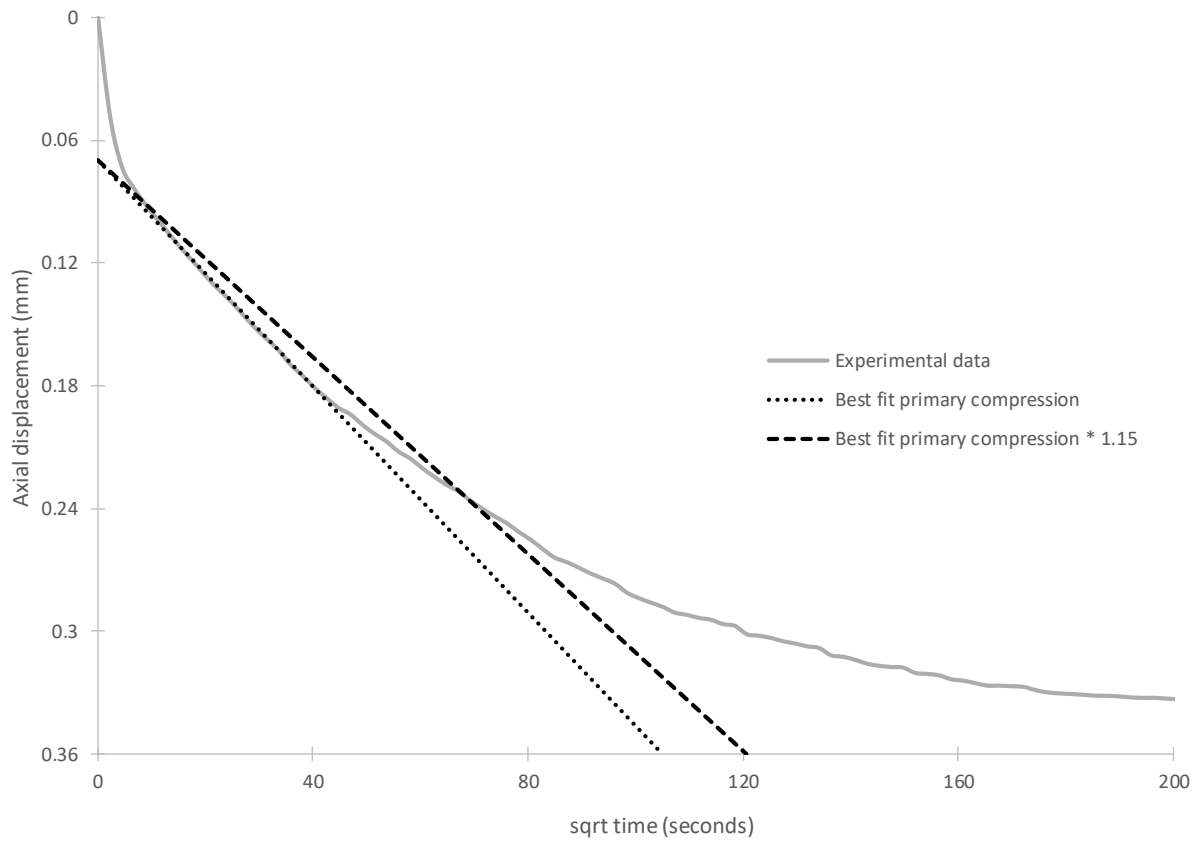
$$C_v = \frac{0.446 * \overline{H}^2}{t_{90}} \qquad\qquad m_v = \left(\frac{H_2 - H_1}{H_1}\right)\left(\frac{1000}{P_2 - P_1}\right)$$

√t₉₀ =	68		**H₁ =**	20.26	mm
t₉₀ =	4624	s	**H₂ =**	19.92	mm
H =	20.09	mm	**P₁ =**	0	kPa
C$_v$ =	0.04	mm2/s	**P₂ =**	6	kPa
C$_v$ =	1.23	m2/yr	**m$_v$ =**	2.80	m2/MN

226

Sample 4	
Diameter =	49.87 mm
Height =	20.86 mm
Loading stage	12 kPa --> 25 kPa
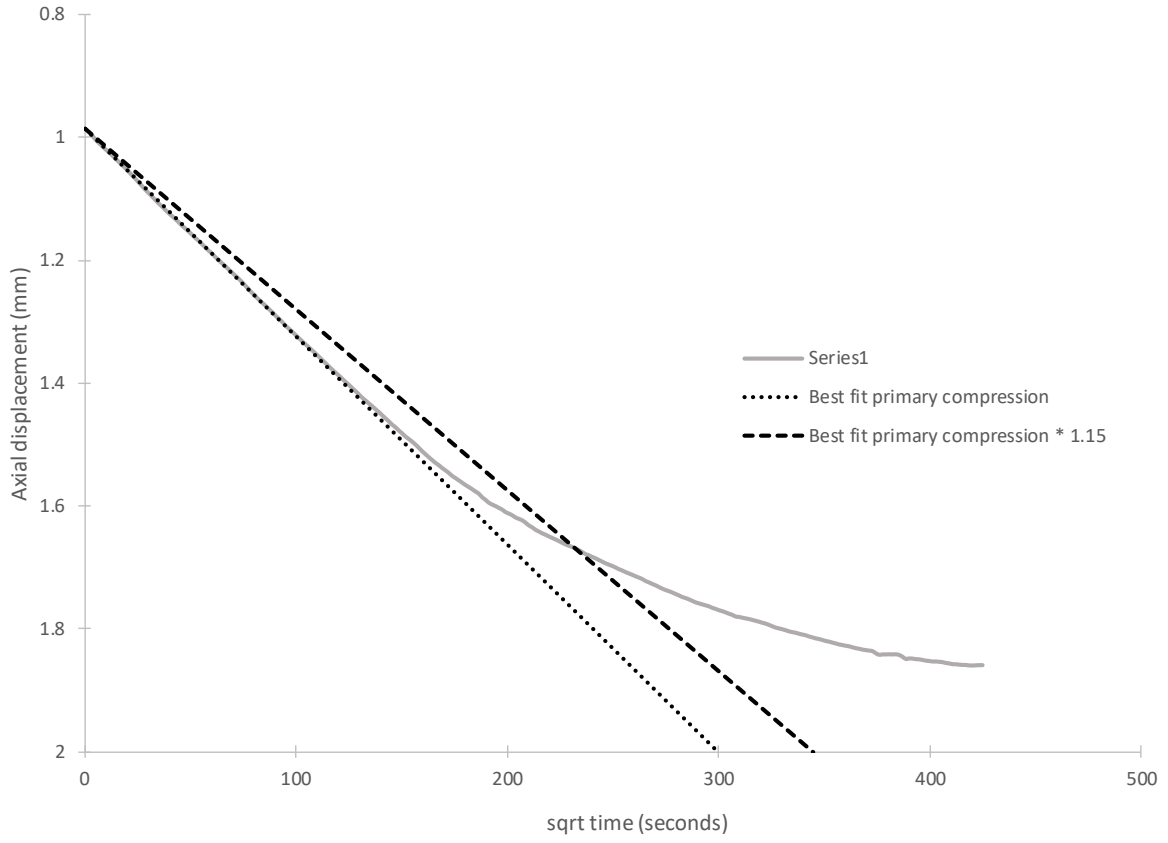
$$C_v = \frac{0.446 * \overline{H}^2}{t_{90}} \qquad\qquad m_v = \left(\frac{H_2 - H_1}{H_1}\right)\left(\frac{1000}{P_2 - P_1}\right)$$

$\sqrt{t_{90}}$ =	225	H_1 =	19.87 mm
t_{90} =	50625 s	H_2 =	18.86 mm
H =	19.37 mm	P_1 =	12 kPa
C_v =	0.00 mm2/s	P_2 =	25 kPa
C_v =	0.10 m2/yr	m_v =	3.93 m2/MN

Sample 5

Diameter =	49.12 mm
Height =	20.54 mm
Loading stage	12 kPa --> 25 kPa
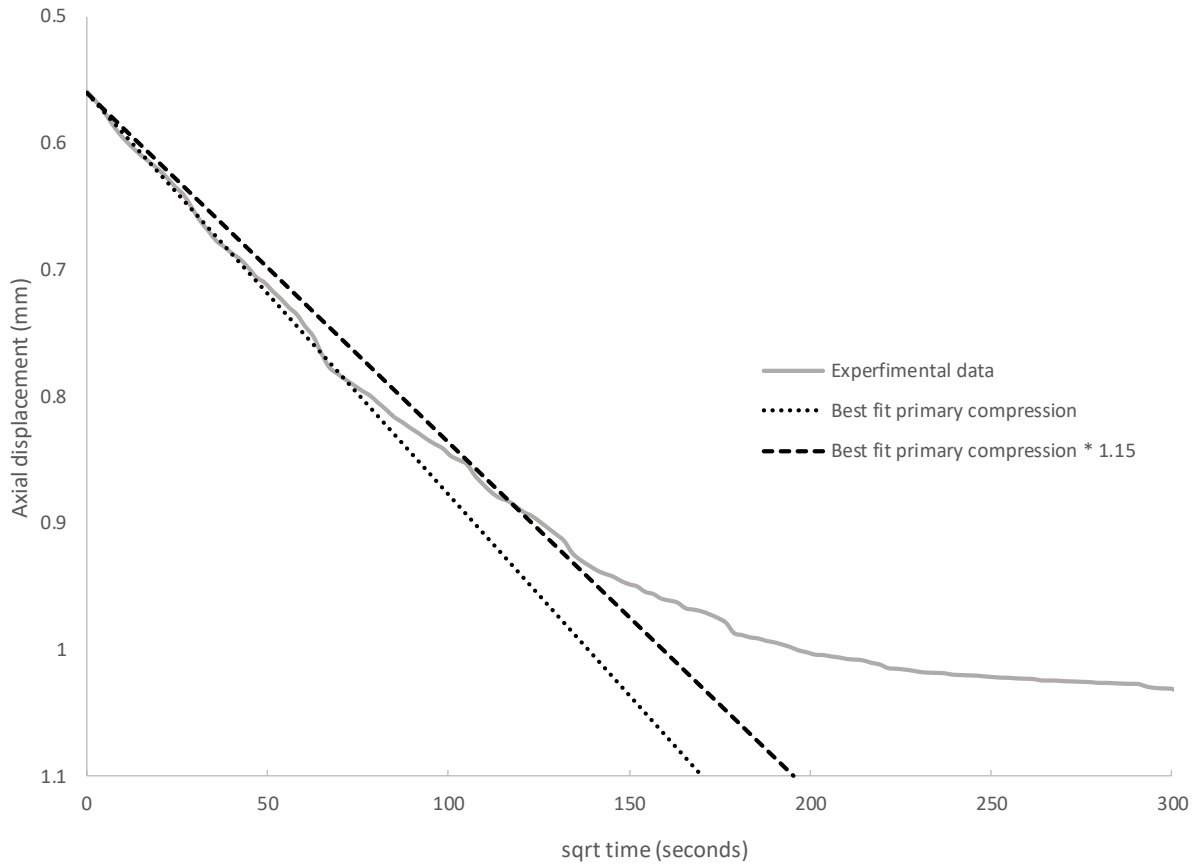
$$C_v = \frac{0.446 * \overline{H}^2}{t_{90}} \qquad\qquad m_v = \left(\frac{H_2 - H_1}{H_1}\right)\left(\frac{1000}{P_2 - P_1}\right)$$

√t₉₀ =	120		**H₁ =**	19.98 mm
t₉₀ =	14400 s		**H₂ =**	19.51 mm
H =	19.74 mm		**P₁ =**	12 kPa
Cᵥ =	0.01 mm2/s		**P₂ =**	25 kPa
Cᵥ =	0.38 m2/yr		**mᵥ =**	1.82 m2/MN

Sample 6

Diameter = 49.63 mm

Height = 20.74 mm

Loading stage 12 kPa --> 25 kPa
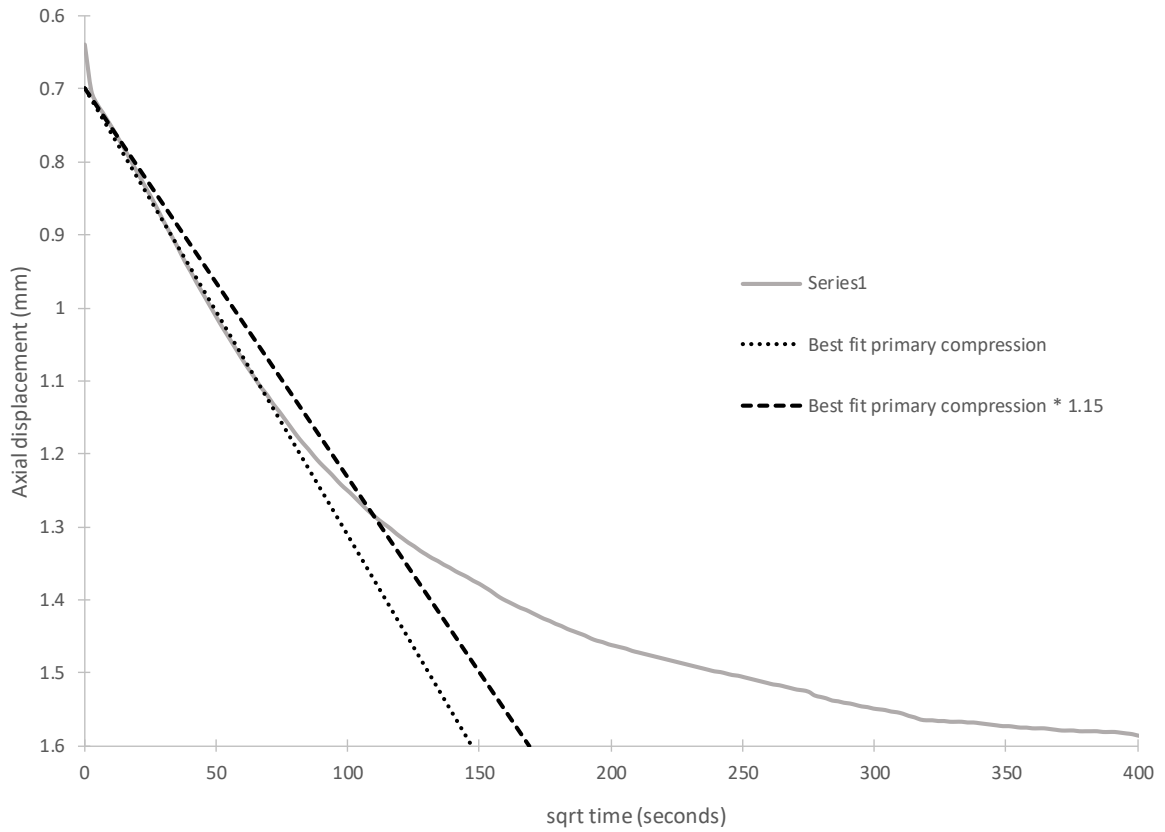
$$C_v = \frac{0.446 * \overline{H}^2}{t_{90}} \qquad m_v = \left(\frac{H_2 - H_1}{H_1}\right)\left(\frac{1000}{P_2 - P_1}\right)$$

$\sqrt{t_{90}}$ =	115		H_1 =	20.74 mm
t_{90} =	13225 s		H_2 =	19.77 mm
H =	20.26 mm		P_1 =	12 kPa
C_v =	0.01 mm2/s		P_2 =	25 kPa
C_v =	0.44 m2/yr		m_v =	3.59 m2/MN

Appendix C. Bacteria growth data

Dilution: 1/1000		Temperature: 25°C																			
		Layer																			
		20	19	18	17	16	15	14	13	12	11	10	9	8	7	6	5	4	3	2	1
Time (h)	0	0.00	0.00	0.00	0.00	0.00	0.00	0.00	0.00	0.00	0.00	0.00	0.00	0.00	0.00	0.00	0.00	0.00	0.00	0.00	0.00
	3	0.26	0.06	0.13	0.12	0.12	0.12	0.10	0.09	0.10	0.11	0.10	0.10	0.10	0.10	0.10	0.11	0.12	0.13	0.12	0.15
	6	0.48	0.12	0.21	0.21	0.21	0.22	0.21	0.20	0.20	0.20	0.18	0.17	0.18	0.20	0.19	0.19	0.21	0.24	0.23	0.25
	9	0.80	0.19	0.36	0.38	0.38	0.39	0.36	0.32	0.33	0.34	0.31	0.28	0.29	0.31	0.30	0.30	0.34	0.38	0.37	0.42
	12	1.46	0.29	0.40	0.44	0.45	0.46	0.44	0.43	0.44	0.45	0.42	0.39	0.40	0.41	0.41	0.41	0.46	0.51	0.48	0.68
	24	5.57	0.90	0.37	0.35	0.30	0.25	0.27	0.29	0.31	0.33	0.32	0.31	0.30	0.28	0.32	0.36	0.36	0.36	0.35	2.21

Dilution: 1/1000		Temperature: 30°C																			
		Layer																			
		20	19	18	17	16	15	14	13	12	11	10	9	8	7	6	5	4	3	2	1
Time (h)	0	0.00	0.00	0.00	0.00	0.00	0.00	0.00	0.00	0.00	0.00	0.00	0.00	0.00	0.00	0.00	0.00	0.00	0.00	0.00	0.00
	3	0.19	0.07	0.14	0.14	0.15	0.16	0.15	0.14	0.14	0.14	0.14	0.15	0.16	0.18	0.18	0.18	0.16	0.14	0.13	0.12
	6	0.91	0.32	0.37	0.35	0.37	0.40	0.37	0.34	0.33	0.33	0.31	0.30	0.31	0.33	0.37	0.41	0.36	0.32	0.29	0.35
	9	4.04	0.53	0.44	0.43	0.45	0.46	0.45	0.43	0.41	0.39	0.43	0.48	0.45	0.43	0.45	0.48	0.44	0.41	0.47	1.94
	12	7.30	0.55	0.50	0.45	0.46	0.46	0.44	0.42	0.39	0.36	0.39	0.41	0.41	0.41	0.45	0.49	0.48	0.48	0.63	2.78
	24	8.89	0.92	0.48	0.30	0.29	0.28	0.28	0.29	0.27	0.26	0.26	0.25	0.26	0.28	0.30	0.32	0.32	0.32	0.51	0.65

Dilution: 1/1000		Temperature: 35°C																			
		Layer																			
		20	19	18	17	16	15	14	13	12	11	10	9	8	7	6	5	4	3	2	1
Time (h)	0	0.00	0.00	0.00	0.00	0.00	0.00	0.00	0.00	0.00	0.00	0.00	0.00	0.00	0.00	0.00	0.00	0.00	0.00	0.00	0.00
	3	0.37	0.45	0.17	0.22	0.23	0.23	0.22	0.20	0.21	0.23	0.20	0.16	0.24	0.31	0.29	0.27	0.24	0.22	0.17	0.38
	6	2.04	1.15	0.41	0.39	0.43	0.46	0.40	0.34	0.39	0.45	0.48	0.51	0.45	0.38	0.45	0.53	0.53	0.54	0.49	2.66
	9	6.38	1.42	0.50	0.30	0.36	0.41	0.36	0.30	0.32	0.35	0.36	0.37	0.32	0.28	0.31	0.34	0.34	0.34	0.27	2.07
	12	6.64	1.07	0.38	0.23	0.26	0.29	0.25	0.21	0.24	0.26	0.27	0.29	0.26	0.23	0.22	0.20	0.22	0.23	0.16	1.67
	24	7.31	0.58	0.29	0.16	0.16	0.15	0.15	0.16	0.18	0.21	0.20	0.19	0.16	0.14	0.15	0.15	0.14	0.13	0.09	1.19

Dilution: 1/100   Temperature: 25°C

Time (h)	Layer																			
	20	19	18	17	16	15	14	13	12	11	10	9	8	7	6	5	4	3	2	1
0	0.00	0.00	0.00	0.00	0.00	0.00	0.00	0.00	0.00	0.00	0.00	0.00	0.00	0.00	0.00	0.00	0.00	0.00	0.00	0.00
3	0.10	0.05	0.09	0.09	0.10	0.11	0.10	0.09	0.10	0.10	0.10	0.10	0.09	0.08	0.09	0.09	0.09	0.08	0.06	0.14
6	0.71	0.34	0.51	0.53	0.53	0.53	0.57	0.61	0.58	0.54	0.53	0.51	0.55	0.59	0.58	0.57	0.52	0.47	0.45	0.63
9	2.69	1.05	1.11	1.09	1.01	0.94	0.91	0.88	0.88	0.88	0.91	0.93	0.89	0.86	0.81	0.77	0.84	0.91	0.96	1.77
12	5.13	1.70	1.23	1.21	1.19	1.17	1.03	0.90	0.96	1.02	1.00	0.98	0.95	0.91	0.87	0.83	0.98	1.14	1.31	2.70
24	15.24	2.21	0.48	0.41	0.43	0.44	0.42	0.39	0.41	0.43	0.49	0.54	0.54	0.54	0.59	0.64	0.62	0.60	0.54	10.52

Dilution: 1/100   Temperature: 30°C

Time (h)	Layer																			
	20	19	18	17	16	15	14	13	12	11	10	9	8	7	6	5	4	3	2	1
0	0.00	0.00	0.00	0.00	0.00	0.00	0.00	0.00	0.00	0.00	0.00	0.00	0.00	0.00	0.00	0.00	0.00	0.00	0.00	0.00
3	1.35	1.32	0.41	0.45	0.46	0.47	0.44	0.42	0.45	0.47	0.48	0.48	0.48	0.49	0.47	0.44	0.50	0.55	0.70	0.86
6	4.62	3.02	0.86	0.90	0.91	0.92	0.94	0.96	0.93	0.91	0.93	0.94	0.99	1.04	1.12	1.19	1.23	1.28	1.59	2.76
9	9.32	2.24	1.03	0.92	0.95	0.97	0.97	0.97	0.93	0.90	0.93	0.96	0.95	0.94	0.92	0.90	0.94	0.98	1.24	6.29
12	11.66	1.81	0.97	0.68	0.71	0.74	0.76	0.78	0.72	0.65	0.69	0.72	0.75	0.77	0.75	0.74	0.72	0.70	0.92	11.07
24	16.33	1.17	0.56	0.57	0.62	0.67	0.64	0.62	0.61	0.61	0.58	0.56	0.55	0.54	0.58	0.61	0.49	0.37	0.46	5.20

Dilution: 1/100   Temperature: 35°C

Time (h)	Layer																			
	20	19	18	17	16	15	14	13	12	11	10	9	8	7	6	5	4	3	2	1
0	0.00	0.00	0.00	0.00	0.00	0.00	0.00	0.00	0.00	0.00	0.00	0.00	0.00	0.00	0.00	0.00	0.00	0.00	0.00	0.00
3	1.22	2.04	0.91	0.88	0.80	0.72	0.72	0.71	0.69	0.66	0.67	0.69	0.74	0.79	0.80	0.81	0.77	0.73	0.60	0.77
6	12.92	5.33	1.21	1.20	1.11	1.01	0.96	0.92	0.98	1.03	1.06	1.08	1.14	1.20	1.20	1.20	1.10	1.00	1.20	9.65
9	19.01	4.04	0.94	0.81	0.90	0.99	0.92	0.86	0.97	1.08	1.00	0.93	0.99	1.05	1.01	0.97	0.97	0.97	0.86	9.36
12	15.24	1.18	0.71	0.60	0.61	0.62	0.68	0.75	0.79	0.83	0.77	0.70	0.78	0.85	0.79	0.73	0.64	0.54	0.59	5.01
24	6.90	0.53	0.30	0.24	0.27	0.30	0.30	0.30	0.29	0.28	0.28	0.28	0.30	0.32	0.28	0.24	0.26	0.27	0.23	1.44

Appendix D. Bacteria growth expressions

| Layer | Temperature: 25°C | |
	Initial dilution: 1/1000	Initial dilution: 1/100
20	y = 54253.7806 + (-54253.69251)/(1+(x/2371.69267)^2.00298)	y = 21.62367 + (-21.660544)/(1+(x/17.79452)^2.91665)
19	y = 13846.8786 + (-13846.86254)/(1+(x/8812.31230)^ 1.63591)	y = 2.25532 + (-2.23795)/(1+(x/9.26264)^4.18813)
18	y = 7.6451915 * (x + 0.16534)/((x^2 - 13.395334*x + 245.27145))	y = 5.1083385 * (x - 1.17732)/((x^2 - 18.563593*x + 122.91609))
17	y = 5.3056227 * (x + 0.23625)/((x^2 - 17.454946*x + 210.96046))	y = 4.3653414 * (x - 0.87994)/((x^2 - 18.508544*x + 118.16362))
16	y = 3.9105753 * (x + 0.47995)/((x^2 - 18.4203*x + 184.91571))	y = 4.5766511 * (x - 0.61966)/((x^2 - 18.838105*x + 125.99945))
15	y = 2.9714405 * (x + 0.72718)/((x^2 - 18.508266*x + 160.4001))	y = 4.7227103 * (x - 0.30965)/((x^2 - 19.303282*x + 135.32045))
14	y = 3.3678768 * (x + 0.35317)/((x^2 - 18.660021*x + 174.66581))	y = 5.113891 * (x - 0.6876)/((x^2 - 17.228378*x + 119.46884))
13	y = 3.5005918 * (x + 0.47344)/((x^2 - 20.124859*x + 200.48739))	y = 5.2319009 * (x - 0.99304)/((x^2 - 15.035661*x + 100.88425))
12	y = 3.7637502 * (x + 0.57873)/((x^2 - 20.337208*x + 208.89915))	y = 5.2913667 * (x - 0.80621)/((x^2 - 16.252215*x + 113.29719))
11	y = 4.0310572 * (x + 0.67998)/((x^2 - 20.54698*x + 217.22483))	y = 5.1796165 * (x - 0.5869)/((x^2 - 17.599531*x + 125.5917))
10	y = 3.7598837 * (x + 0.73654)/((x^2 - 21.462333*x + 228.61361))	y = 5.9851984 * (x - 0.81863)/((x^2 - 17.139284*x + 127.62262))
9	y = 3.6746207 * (x + 0.96289)/((x^2 - 21.814672*x + 241.90862))	y = 0.21989538 * (x + 7.98487) * (x - 0.44822)/((x^2 - 15.013151*x + 88.032033))
8	y = 3.6063968 * (x + 0.87815)/((x^2 - 21.086114*x + 227.20887))	y = 0.2373095 * (x + 8.00328) * (x - 0.77738)/((x^2 - 13.922898*x + 80.442694))
7	y = 3.619267 * (x + 0.60615)/((x^2 - 19.184974*x + 199.66929))	y = 0.28564284 * (x + 4.99855) * (x - 1.08212)/((x^2 - 12.465655*x + 66.468124))
6	y = 4.1305408 * (x + 0.64345)/((x^2 - 20.448117*x + 231.03146))	y = 0.38476607 * (x + 1.47406) * (x - 1.16125)/((x^2 - 10.864125*x + 53.969569))
5	y = 5.1227398 * (x + 0.65093)/((x^2 - 20.333545*x + 261.13605))	y = 0.47989016 * (x + 0.29219) * (x - 1.42938)/((x^2 - 9.0872761*x + 43.106168))
4	y = 4.630249 * (x + 0.76652)/((x^2 - 20.494672*x + 232.58672))	y = 8.4915638 * (x - 0.84968)/((x^2 - 17.082752*x + 155.95229))
3	y = 4.5128826 * (x + 0.78925)/((x^2 - 19.928425*x + 210.47514))	y = 6.7222404 * (x - 0.91146)/((x^2 - 19.500927*x + 155.12537))
2	y = 4.6939082 * (x + 0.5139)/((x^2 - 19.093157*x + 209.09295))	y = 5.2246271 * (x - 1.01742)/((x^2 - 20.872343*x + 150.16363))
1	y = 39848.7658 + (-39848.72277)/(1+(x/ 6689.31671)^1.74429)	y = 51757.7937 + (-51757.82528)/(1+(x/2068.63365)^1.90685)

Layer	Temperature: 30°C	
	Initial dilution: 1/1000	Initial dilution: 1/100
20	y = 8.96553 + (-8.84562)/(1+(x/9.32440)^5.58214)	y = 17.80218 + (-17.754875)/(1+(x/8.99344)^2.42137)
19	y = 1.18174 + (-1.19642)/(1+(x/11.32573)^1.62120)	y = 0.78717698 * (x + 1.85022) * (x - 0.02461)/((x^2 - 7.7898198*x + 22.968998))
18	y = 0.43767731 * (x + 0.10533) * (x - 0.21042)/((x^2 - 3.6281843*x + 28.446359))	y = 10.221162 * (x - 0.05676)/((x^2 - 9.2308904*x + 90.892631))
17	y = 5.737994 * (x - 0.14571)/((x^2 - 10.063578*x + 125.91537))	y = 0.36245445 * (x + 3.46178) * (x + 0.06758)/((x^2 - 6.7856899*x + 27.496979))
16	y = 5.5404972 * (x - 0.15589)/((x^2 - 9.4727742*x + 112.49402))	y = 0.42053787 * (x + 2.23518) * (x + 0.07001)/((x^2 - 6.3881033*x + 25.076142))
15	y = 5.2859621 * (x - 0.165)/((x^2 - 9.1381264*x + 100.84517))	y = 0.48026895 * (x + 1.27028) * (x + 0.08121)/((x^2 - 5.9943584*x + 22.680058))
14	y = 0.12023635 * (x + 16.98812) * (x - 0.03692)/((x^2 - 9.5172945*x + 66.474695))	y = 0.44582922 * (x + 1.73145) * (x + 0.07444)/((x^2 - 6.5743421*x + 25.49448))
13	y = 0.13599315 * (x + 11.95428) * (x - 0.00628)/((x^2 - 9.5969344*x + 64.69567))	y = 0.41480046 * (x + 2.13676) * (x + 0.06211)/((x^2 - 7.13787*x + 28.051996))
12	y = 0.14042091 * (x + 9.93742) * (x - 0.0007)/((x^2 - 8.9501672*x + 58.088215))	y = 0.42796317 * (x + 1.29763) * (x + 0.08988)/((x^2 - 6.5764174*x + 23.546709))
11	y = 0.14488697 * (x + 7.91384) * (x + 0.00492)/((x^2 - 8.3098929*x + 51.053436))	y = 0.44109961 * (x^2 + 0.44990129*x + 0.082776693)/((x^2 - 6.1178589*x + 19.139987))
10	y = 0.099970009 * (x + 17.66236) * (x + 0.16207)/((x^2 - 10.454526*x + 71.569875))	y = 0.38621885 * (x + 2.60492) * (x + 0.06495)/((x^2 - 6.5689121*x + 24.752613))
9	y = 3.9170916 * (x - 0.06848)/((x^2 - 12.377804*x + 109.65975))	y = 0.33002157 * (x + 5.64073) * (x + 0.05345)/((x^2 - 7.043495*x + 30.477425))
8	y = 4.7184789 * (x + 0.01209)/((x^2 - 10.470842*x + 112.71369))	y = 0.33837345 * (x + 4.50578) * (x + 0.0369)/((x^2 - 7.2135947*x + 28.677945))
7	y = 5.7541462 * (x + 0.03243)/((x^2 - 7.7732748*x + 114.20107))	y = 0.34748314 * (x + 3.49631) * (x + 0.01577)/((x^2 - 7.346072*x + 27.027606))
6	y = 0.059083984 * (x + 73.86094) * (x + 0.00098)/((x^2 - 8.4737931*x + 92.364379))	y = 0.42349055 * (x^2 - 0.19539413*x + 0.02302418)/((x^2 - 7.1620068*x + 20.175032))
5	y = 0.10825806 * (x + 31.10619) * (x - 0.03698)/((x^2 - 8.7779117*x + 76.995684))	y = 0.48627387 * (x - 0.00569) * (x - 2.01446)/((x^2 - 6.8243735*x + 14.716684))
4	y = 0.026385956 * (x + 211.01765) * (x - 0.04933)/((x^2 - 9.6210881*x + 119.03792))	y = 0.32118968 * (x + 1.53677) * (x + 0.03533)/((x^2 - 8.0372577*x + 24.055345))
3	y = -0.23174324 * (x - 0.05508) * (x - 53.47035)/((x^2 - 13.207026*x + 257.444))	y = 0.16671602 * (x + 12.20408) * (x + 0.00891)/((x^2 - 8.8987902*x + 31.639668))
2	y = 6.7063468 * (x + 0.20551)/((x^2 - 20.450977*x + 233.06281))	y = 0.19393527 * (x + 15.446) * (x - 0.01278)/((x^2 - 8.8763006*x + 32.924581))
1	y = 0.24008209 * (x^2 - 2.130873*x + 15.359838)/((x^2 - 20.325968*x + 111.48009))	y = 36.466208 * (x + 0.16336)/((x^2 - 25.231834*x + 198.90429))

Layer	Temperature: 35℃	
	Initial dilution: 1/1000	Initial dilution: 1/100
20	y = 7.06215 + (-6.88847)/(1+(x/6.82920)^7.52943)	y = 3.5514848 * (x + 4.72767) * (x - 1.43801)/((x^2 - 13.193476*x + 56.82352))
19	y = 0.19423508 * (x + 18.45054) * (x + 0.32584)/((x^2 - 11.416085*x + 57.970653))	y = 0.10547681 * x * (x^2 - 33.667588*x + 294.32248)/((x^2 - 14.408748*x + 65.674894))
18	y = 0.16081868 * (x + 4.80274) * (x + 0.27538)/((x^2 - 8.9337465*x + 43.186248))	y = 6.0371622 * (x + 0.00353)/((x^2 - 5.6649801*x + 27.870644))
17	y = 0.10749663 * (x + 2.5385) * (x + 0.01677)/((x^2 - 7.0040372*x + 20.079209))	y = 4.3397634 * (x - 0.01367)/((x^2 - 6.6476497*x + 25.610083))
16	y = 0.07037939 * (x + 13.78097) * (x + 0.01956)/((x^2 - 7.6954498*x + 29.780034))	y = 5.1677497 * (x + 0.01603)/((x^2 - 6.2863491*x + 29.422096))
15	y = 0.035935134 * (x + 43.6375) * (x + 0.03635)/((x^2 - 8.5809715*x + 38.761199))	y = 6.7236463 * (x + 0.03947)/((x^2 - 5.2287143*x + 35.813396))
14	y = 0.061515363 * (x + 18.15312) * (x + 0.03183)/((x^2 - 7.7311943*x + 32.610629))	y = 6.7236463 * (x + 0.03947)/((x^2 - 5.2287143*x + 35.813396))
13	y = 0.09106702 * (x + 6.3459) * (x + 0.02673)/((x^2 - 6.770933*x + 24.356891))	y = -0.63868656*(x - 0.00059)*(x - 38.92415)/((x^2 + 5.1143522*x + 71.690473))
12	y = 0.11844005 * (x + 2.54503) * (x + 0.03605)/((x^2 - 6.9474792*x + 21.160841))	y = -0.43292464 * (x + 0.00277) * (x - 40.11181)/((x^2 - 2.5018902*x + 68.988684))
11	y = 0.14429253 * (x + 0.48026) * (x + 0.11448)/((x^2 - 6.9961873*x + 18.779935))	y = -0.32848764 * (x + 0.01606) * (x - 41.002)/((x^2 - 6.4837141*x + 68.348274))
10	y = 0.13591688 * (x + 0.31345) * (x + 0.14368)/((x^2 - 7.7328609*x + 21.367416))	y = -0.18699047 * (x + 0.00606) * (x - 53.11654)/((x^2 - 6.4716775*x + 52.428987))
9	y = 0.12962818 * (x + 0.27727) * (x - 0.08808)/((x^2 - 8.3871923*x + 23.668561))	y = -0.06335273 * (x - 0.00043) * (x - 107.28892)/((x^2 - 6.7643554*x + 40.129818))
8	y = 0.10678813 * (x + 3.15356) * (x - 0.01276)/((x^2 - 7.3747326*x + 21.310044))	y = -0.10375101 * (x - 0.00321) * (x - 81.15097)/((x^2 - 6.2491495*x + 42.659617))
7	y = 0.079072098 * (x + 10.22963) * (x - 0.003)/((x^2 - 5.5864257*x + 17.718212))	y = -0.15809908 * (x - 0.00468) * (x - 65.96907)/((x^2 - 5.645834*x + 45.713659))
6	y = 0.086825881 * (x + 4.81339) * (x + 0.01592)/((x^2 - 7.2009843*x + 19.625153))	y = -0.14356379 * (x - 0.00411) * (x - 63.5638)/((x^2 - 5.9790705*x + 41.448524))
5	y = 0.084159665 * (x + 3.91697) * (x + 0.09933)/((x^2 - 8.0275096*x + 21.818148))	y = -0.13888566 * (x - 0.00334) * (x - 58.38914)/((x^2 - 6.2855487*x + 38.20864))
4	y = 0.074493038 * (x + 5.60308) * (x + 0.06145)/((x^2 - 8.4120102*x + 24.300229))	y = -0.11295342 * (x + 0.01426) * (x - 65.54696)/((x^2 - 6.286213*x + 37.830835))
3	y = 0.066215988 * (x + 7.22353) * (x + 0.00891)/((x^2 - 8.843119*x + 26.828079))	y = -0.088408493 * (x + 0.03448) * (x - 76.13849)/((x^2 - 6.2696577*x + 37.451246))
2	y = 0.043318064 * (x + 7.13871) * (x + 0.07439)/((x^2 - 9.3378501*x + 27.1485))	y = 0.037175311 * (x + 81.23337) * (x - 0.01257)/((x^2 - 8.8282006*x + 33.162469))
1	y = 0.88154094 * (x + 0.00217) * (x - 1.96438)/((x^2 - 8.6998536*x + 24.221705))	y = -0.042434928 * x * (x - 0.421) * (x - 42.77729)/((x^2 - 12.863437*x + 46.594581))

Appendix E. Processing code

```
// Computational model to represent and predict the behaviour of agarose gels, bacteria growth and effect
stress-sensitive urease-producing engineered bacteria on the matrix of the gel

import controlP5.*; //Graphic user interface

import peasy.*; //3D cam

import nervoussystem.obj.*;

PeasyCam cam; //Initialise the cam

ControlP5 cp5; //Initialise the GUI

Slider2D lp1;

// Variables for initiation and reset of the interface.

boolean set = false; //Turns to true after the initial stress simulation and prevends the stress values resetting.

boolean run = false; //Runs the simulation

boolean reset = false; // Resets all values and sets run to false

boolean drainage = false; //Allows/restricts vertical drainage of water out of the sample

boolean one_way = false; //Changes the drainage from 2 way to 1 way

boolean local_stress = false; //Allows/restricts the generation of local stresses due to a reduced foundation

boolean lock = false; //Locks the movement of the hydrogel sample

boolean low = false; //Initial concentration of bacteria cells

boolean high = true; //Initial concentration of bacteria cells

boolean linear_increase_1 = false; //Graph gene expression

boolean linear_decrease_1 = false; //Graph gene expression

boolean linear_increase_2 = false; //Graph gene expression

boolean linear_decrease_2 = false; //Graph gene expression

boolean peak_1 = false; //Graph gene expression

boolean peak_2 = false; //Graph gene expression

boolean isobars = false; //Allows the representation of the stresses in terms of isobars

boolean record = false;

float amount = 0; //Initialises the variable amount

float load = 1000; //Initialises the variable load (in N)

float cv = 1; //Initialises the coefficient of Consolidation (square METER/YEAR)

float skempton_factor = 6.2;

float cu = 27;

float ultimate_bearing_capacity = skempton_factor*cu; //Calculates the ultimate bearing capacity of the gel
(considering a semi-infinite space)
```

```
int temperature = 30; //Initialises the variable temperature
// Initialise the  arrays
float[][][]recording_pressure; //updates to track changes in pore pressure over time
float[][][]static_stress; //records total stress due to loading
float[][][]immediate_settlement;
float[][][]total_immediate_settlement;
float[][][]consolidation_settlement;
float[][][]total_consolidation_settlement;
float[][][]bacteria_growth;
float[][][]amount_urease;
float counter = 0; //counter used to display timer (MINUTES)
float time_threshold =4; //variable to stop the simulation at a certain time (in HOURS)
//Dimnesions of the analysis area and the foundation
float ratio = 4;
float number_boxes_length = 40; //number of total boxes
float number_boxes_breadth = 40; //number of total boxes
float number_boxes_depth = 40; //number of total boxes
float gel_length_real = 100; //real dimensions of the volume of hydogel (mm)
float gel_length_virtual = gel_length_real*ratio;   //virtual dimensions of the volume of hydrogel (pixels)
float gel_breadth_real = 100;    //(mm)
float gel_breadth_virtual = gel_breadth_real*ratio;  //(pixels)
float gel_depth_real = 100;     //(mm)
float gel_depth_virtual = gel_depth_real*ratio;    //(pixels)
float foundation_length;    //real dimensions of the foundation(mm)
float foundation_depth = 20;    //virtual dimensions of the foundation (pixels)
float box_size_virtual = gel_length_virtual/number_boxes_length;  //virtual dimensions of the boxes (pixels)
float box_size_real = gel_length_real/number_boxes_length; //real dimensions of the boxes (mm)
int slice = 1;


int Simulation_Mode = 1; //Initialises the variable silation_mode
//Properties of the hydrogel
float mu=0.45;
float young=300;
float Cc=0.41;
```

```
float e0=27;

float Ip=0.9; ////for rigid foundations and L/B=1

float mv=0.5;

float Val2_0 = 0; //Initialises the values for graph 2

float Val2_35 = 0.8;

float Val2_70 = 1.6;

float Val2_105 = 2.4;

float Val2_140 = 3.2;

float Val2_175 = 4;

float Val1_0 = 0; //Initialises the values for graph 1

float Val1_0_5 = 4.16;

float Val1_1 = 8.32;

float Val1_1_5 = 12.5;

float Val1_2 = 16.65;

float Val1_2_5 = 20.8;

float Val1_3 = 25;

int box_height = 150; //size of the graphs

int box_width = 150; //size of the graphs

int box_x = 1400; //x location of the graphs

int box_y_1 = 70; //y location of graph 1

int box_y_2 = 450; //y location of graph 2

float max_expression_1 = 25; //max expression of graph 1 (y axis)

float max_expression_2 = 4; //max expression of graph 2 (y axis)

boolean hit_line = false; //variable that identifies the x coordinate of the graphs

int[][]graph_matrix_1 = new int[box_width][box_height]; //Initialise the 2D array for graph 1

int[][]graph_matrix_2 = new int[box_width][box_height]; //Initialise the 2D array for graph 2


float y_value_1; //Initialises the variable y_value_1

float y_value_2; //Initialises the variable y_value_2

boolean export_2d = true;


/////////////////////////////////////////////SETUP/////////////////////////////////////////////

void setup(){

  frameRate(60); //SLOWS DOWN THE COUNTER
```

```
reset = false;

size(1600, 800, OPENGL); //size of the GUI

cam = new PeasyCam(this, 700);  //Initialize the  cam

cam.setMinimumDistance(700);

cam.setMaximumDistance(1000);

cam.lookAt(200, 200,200);

//cam.rotateX(0.0);

cam.setYawRotationMode(); //Allows only rotation on the y direction

cam.setResetOnDoubleClick(false);  //Avoid the camera resetting when double-clickling


//setup sliders of the GUI                              cp5.addSlider("cv")

cp5 = new ControlP5(this);                               .setPosition(30, 480)

 cp5.addToggle("run")                                    .setSize(150, 20)

 .setPosition(30, 60)                                    .setRange(0, 3)

  .setSize(50, 50)                                       .setValue(0)

   .setValue(false)                                      .setColorCaptionLabel(1)

    .setColorCaptionLabel(1)                              .setNumberOfTickMarks(31)

     ;                                                   ;

cp5.addSlider("load")                            cp5.addSlider("Simulation_Mode")

 .setPosition(30, 130)                                  .setPosition(30, 230)

  .setSize(150, 20)                                     .setSize(150, 20)

   .setRange(0, 1000)                                   .setRange(1, 8)

    .setValue(150)                                      .setValue(5)

     .setColorCaptionLabel(1)                            .setColorCaptionLabel(1)

                                                          .setNumberOfTickMarks(8)

 ;                                                       ;

 cp5.addSlider("foundation_length")             cp5.addToggle("one_way")

 .setPosition(30, 180)                                  .setPosition(80, 330)

  .setSize(150, 20)                                     .setSize(10, 10)

   .setRange(10, 100)                                   .setValue(false)

    .setValue(30)                                       .setColorCaptionLabel(1)

     .setColorCaptionLabel(1)                            ;

      .setNumberOfTickMarks(10)               cp5.addToggle("drainage")

       ;                                               .setPosition(30, 330)
```

240

```
    .setSize(10, 10)                                    .setSize(10, 10)

      .setValue(true)                                     .setValue(false)

        .setColorCaptionLabel(1)                            .setColorCaptionLabel(1)

          ;                                                   ;

  cp5.addToggle("local_stress")                     cp5.addToggle("high")

   .setPosition(130, 330)                            .setPosition(130, 430)

    .setSize(10, 10)                                  .setSize(10, 10)

      .setValue(true)                                  .setValue(true)

        .setColorCaptionLabel(1)                         .setColorCaptionLabel(1)

          ;                                               ;

  cp5.addSlider("time_threshold")                  cp5.addSlider("Val2_0")

   .setPosition(30, 280)                            .setPosition(1350, 630)

    .setSize(150, 20)                                .setSize(10, 100)

      .setRange(0, 10)                                .setRange(0, 4)

        .setValue(4)                                   .setValue(0)

          .setColorCaptionLabel(1)                       .setColorCaptionLabel(1)

            .setNumberOfTickMarks(11)                     .setColorValue(color(0, 0, 0))

              ;                                             //.setColorBackground(color(0, 0, 0))

  cp5.addSlider("temperature")             //.setColorForeground(color(255,0,0))

   .setPosition(30, 380)                               ;

    .setSize(150, 20)                            cp5.addSlider("Val2_35")

      .setRange(25, 35)                           .setPosition(1390, 630)

        .setValue(30)                              .setSize(10, 100)

          .setColorCaptionLabel(1)                  .setRange(0, 4)

            .setNumberOfTickMarks(3)                  .setValue(0.8)

              ;                                         .setColorCaptionLabel(1)

  cp5.addToggle("lock")                                 .setColorValue(color(0, 0, 0))

   .setPosition(460, 650)                                ;

    .setSize(10, 10)                            cp5.addSlider("Val2_70")

      .setValue(false)                           .setPosition(1430, 630)

        .setColorCaptionLabel(1)                  .setSize(10, 100)

          ;                                         .setRange(0, 4)

  cp5.addToggle("low")                               .setValue(1.6)

   .setPosition(60, 430)                               .setColorCaptionLabel(1)
```

```
          .setColorValue(color(0, 0, 0))                    .setSize(10, 10)

       ;                                                    .setValue(false)

cp5.addSlider("Val2_105")                                   .setColorCaptionLabel(1)

  .setPosition(1470, 630)                                  ;

    .setSize(10, 100)                           cp5.addToggle("peak_1")

      .setRange(0, 4)                             .setPosition(1550, 750)

        .setValue(2.4)                              .setSize(10, 10)

          .setColorCaptionLabel(1)                  .setValue(false)

            .setColorValue(color(0, 0, 0))           .setColorCaptionLabel(1)

       ;                                               ;

cp5.addSlider("Val2_140")                    cp5.addToggle("linear_increase_2")

  .setPosition(1510, 630)                      .setPosition(1350, 380)

    .setSize(10, 100)                            .setSize(10, 10)

      .setRange(0, 4)                              .setValue(false)

        .setValue(3.2)                               .setColorCaptionLabel(1)

          .setColorCaptionLabel(1)                    ;

            .setColorValue(color(0, 0, 0))   cp5.addToggle("linear_decrease_2")

       ;                                       .setPosition(1440, 380)

cp5.addSlider("Val2_175")                      .setSize(10, 10)

  .setPosition(1550, 630)                        .setValue(false)

    .setSize(10, 100)                              .setColorCaptionLabel(1)

      .setRange(0, 4)                                ;

        .setValue(4)                       cp5.addToggle("peak_2")

          .setColorCaptionLabel(1)           .setPosition(1550, 380)

            .setColorValue(color(0, 0, 0))    .setSize(10, 10)

       ;                                        .setValue(false)

cp5.addToggle("linear_increase_1")              .setColorCaptionLabel(1)

  .setPosition(1350, 750)                         ;

    .setSize(10, 10)                    cp5.addSlider("Val1_0")

      .setValue(false)                    .setPosition(1350, 250)

        .setColorCaptionLabel(1)            .setSize(10, 100)

       ;                                      .setRange(0, 25)

cp5.addToggle("linear_decrease_1")             .setValue(5)

  .setPosition(1440, 750)                        .setColorCaptionLabel(1)
```

242

```
                .setColorValue(color(0, 0, 0))
                  //.setColorBackground(color(0, 0, 0))
//.setColorForeground(color(255,0,0))
                    ;
    cp5.addSlider("Val1_0_5")
      .setPosition(1390, 250)
        .setSize(10, 100)
          .setRange(0, 25)
            .setValue(5)
              .setColorCaptionLabel(1)
                .setColorValue(color(0, 0, 0))

                  ;
    cp5.addSlider("Val1_1")
      .setPosition(1430, 250)
        .setSize(10, 100)
          .setRange(0, 25)
            .setValue(5)
              .setColorCaptionLabel(1)
                .setColorValue(color(0, 0, 0))
                  ;
    cp5.addSlider("Val1_1_5")
      .setPosition(1470, 250)
        .setSize(10, 100)
          .setRange(0, 25)
            .setValue(5)
              .setColorCaptionLabel(1)
                .setColorValue(color(0, 0, 0))
                  ;
    cp5.addSlider("Val1_2")
      .setPosition(1510, 250)
        .setSize(10, 100)
          .setRange(0, 25)
            .setValue(5)
```

```
                .setColorCaptionLabel(1)
                  .setColorValue(color(0, 0, 0))
                    ;
    cp5.addSlider("Val1_2_5")
      .setPosition(1550, 250)
        .setSize(10, 100)
          .setRange(0, 25)
            .setValue(5)
              .setColorCaptionLabel(1)
                .setColorValue(color(0, 0, 0))
                  ;
    cp5.addSlider("Val1_3")
      .setPosition(1590, 250)
        .setSize(10, 100)
          .setRange(0, 25)
            .setValue(5)
              .setColorCaptionLabel(1)
                .setColorValue(color(0, 0, 0))
                  ;
    cp5.addToggle("isobars")
      .setPosition(460, 130)
        .setSize(10, 10)
          .setValue(true)
            .setColorCaptionLabel(1)
              ;
    cp5.addSlider("slice")
      .setPosition(30, 630)
        .setSize(150, 20)
          .setRange(1, 40)
            .setValue(20)
              .setColorCaptionLabel(1)
                //.setColorValue(color(0, 0, 0))
                  ;
    cp5.addSlider("mu")
```

```
    .setPosition(30, 580)

     .setSize(150, 20)

      .setRange(0.4, 0.49)

       .setValue(0.45)

        .setColorCaptionLabel(1)

         .setNumberOfTickMarks(10)

          //.setColorValue(color(0, 0, 0))

           ;
  cp5.addSlider("mv")

    .setPosition(30, 530)

     .setSize(150, 20)

      .setRange(0,1)

       .setValue(0.5)

        .setColorCaptionLabel(1)

         .setNumberOfTickMarks(11)

          //.setColorValue(color(0, 0, 0))

           ;
  cp5.addToggle("export_2d")

    .setPosition(1200, 30)

     .setSize(50, 50)

      .setValue(false)

      .setColorCaptionLabel(1)

        ;
  cp5.setAutoDraw(false);

}
```

```
////////////////////////////////////////////DRAW////////////////////////////////////////////
void draw(){
background(255);
  //Draws the arrow
 //pushMatrix();
 //translate(190,-200,200);
 //stroke(1);
 //fill(100);
 //rect(0,0,20,100);
 //triangle(-10,100,30,100,10,120);
 //popMatrix();
  //Set the dimensions of the volume of gel
pushMatrix();
translate(200,202.5,200);
noFill();
stroke(1);
box(gel_length_virtual, gel_depth_virtual, gel_breadth_virtual); //Dimensions of the bix box
popMatrix();
 //Draws the foundation
if (drainage == false || local_stress == false){
pushMatrix();
translate(200,-7.5,200);
stroke(1);
fill(150);
box(100*ratio,foundation_depth,100*ratio);
popMatrix();
} else {
pushMatrix();
translate(200,-7.5,200);
stroke(1);
fill(150);
box(foundation_length*ratio,foundation_depth,foundation_length*ratio);
 popMatrix();
```

```
}

//Draws the confinement
if (run == false){
pushMatrix();
translate(-5,202.5,100);
fill(100);
stroke(1);
//box(10, gel_depth_virtual, gel_breadth_virtual/2);
popMatrix();
pushMatrix();
translate(405,202.5,100);
fill(100);
stroke(1);
//box(10, gel_depth_virtual, gel_breadth_virtual/2);
popMatrix();
pushMatrix();
translate(200,407.5,100);
fill(100);
stroke(1);
//box(gel_length_virtual+20, 10, gel_breadth_virtual/2);
popMatrix();
pushMatrix();
translate(200,207.5,-5);
fill(100);
stroke(1);
//box(gel_length_virtual+20, gel_depth_virtual+10, 10);
popMatrix();
}
if (lock == true){
cam.setActive(false); //Restricts rotation
}else{
cam.setActive(true); //Allows rotation
}
```

```
if (linear_increase_1 == true && linear_decrease_1 == false && peak_1 == false){ //linear increase graph

  Val2_0 = 0;

  Val2_35 = 0.8;

  Val2_70 = 1.6;

  Val2_105 = 2.4;

  Val2_140 = 3.2;

  Val2_175 = 4;

}

  if (linear_decrease_1 == true && peak_1 == false){ //linear decrease graph

  Val2_0 = 4;

  Val2_35 = 3.2;

  Val2_70 = 2.4;

  Val2_105 = 1.6;

  Val2_140 = 0.8;

  Val2_175 = 0;

}

  if (linear_increase_1 == false && linear_decrease_1 == false && peak_1 == true){ //peak graph

  Val2_0 = 0;

  Val2_35 = 0.5;

  Val2_70 = 3.5;

  Val2_105 = 3.5;

  Val2_140 = 0.5;

  Val2_175 = 0;

}

   if (linear_increase_2 == true && linear_decrease_2 == false && peak_2 == false){ //linear increase graph

  Val1_0 = 0;

  Val1_0_5 = 4.16;

  Val1_1 = 8.32;

  Val1_1_5 = 12.5;

  Val1_2 = 16.65;

  Val1_2_5 = 20.8;

  Val1_3 = 25;

  }
```

```
if (linear_decrease_2 == true && peak_2 == false){ //linear decrease graph

Val1_0 = 25;

Val1_0_5 = 20.8;

Val1_1 = 16.65;

Val1_1_5 = 12.5;

Val1_2 = 8.32;

Val1_2_5 = 4.16;

Val1_3 = 0;

}

if (linear_increase_2 == false && linear_decrease_2 == false && peak_2 == true){ //peak graph

Val1_0 = 0;

Val1_0_5 = 3;

Val1_1 = 19;

Val1_1_5 = 23;

Val1_2 = 19;

Val1_2_5 = 3;

Val1_3 = 0;

}

float Es = young*(1-mu)/((1+mu)*(1-2*mu));

if (run==true) {

counter = counter + 1;

if (((load*1000)/(foundation_length*foundation_length)) > ultimate_bearing_capacity){    //if the stress
generated exceeds the ultimate bearing capacity of the gel...

        println("Bearing capacity exceeded");

} else {

        if (set == false) { //Turns to true after the initial stress simulation and prevents the stress values
resetting.

    //Initialises the  arrays of 40x40x40 boxes

    static_stress = new
float[int(number_boxes_length+1)][int(number_boxes_breadth+1)][int(number_boxes_depth+1)];

    recording_pressure = new
float[int(number_boxes_length+1)][int(number_boxes_breadth+1)][int(number_boxes_depth+1)];

    immediate_settlement = new
float[int(number_boxes_length+1)][int(number_boxes_breadth+1)][int(number_boxes_depth+1)];

    total_immediate_settlement = new
float[int(number_boxes_length+1)][int(number_boxes_breadth+1)][int(number_boxes_depth+1)];
```

```
    consolidation_settlement = new
float[int(number_boxes_length+1)][int(number_boxes_breadth+1)][int(number_boxes_depth+1)];

    total_consolidation_settlement = new
float[int(number_boxes_length+1)][int(number_boxes_breadth+1)][int(number_boxes_depth+1)];

    bacteria_growth = new
float[int(number_boxes_length+1)][int(number_boxes_breadth+1)][int(number_boxes_depth+1)];

    amount_urease = new
float[int(number_boxes_length+1)][int(number_boxes_breadth+1)][int(number_boxes_depth+1)];

    for (int i = 1; i < (number_boxes_length+1); i++) {

      for (int j = 1; j < (number_boxes_breadth+1); j++) {

        for (int k = 1; k < (number_boxes_depth+1); k++) {

          if (local_stress == false){

          static_stress[i][j][k] = StressDistribution((i-(gel_length_real-foundation_length)/5)*2.5-1.25, (j-
(gel_breadth_real-foundation_length)/5)*2.5-1.25, k*2.5-1.25, load, foundation_length,
foundation_length);

          recording_pressure[i][j][k] = (load*1000)/(100*100);

          }

          if (local_stress == true){

          static_stress[i][j][k] = StressDistribution((i-(gel_length_real-foundation_length)/5)*2.5-1.25, (j-
(gel_breadth_real-foundation_length)/5)*2.5-1.25, k*2.5-1.25, load, foundation_length,
foundation_length);

          recording_pressure[i][j][k] = StressDistribution((i-(gel_length_real-foundation_length)/5)*2.5-
1.25, (j-(gel_breadth_real-foundation_length)/5)*2.5-1.25, k*2.5-1.25, load, foundation_length,
foundation_length);

          total_immediate_settlement[i][j][k] = (static_stress[i][j][k]/Es)*box_size_real;

          total_consolidation_settlement[i][j][k] = static_stress[i][j][k]*box_size_real*mv/1000;

        }

        }

      }

    }

      set = true;

    }

  for (int i = 1; i < number_boxes_length+1; i++) {

   for (int j = slice; j < slice+1; j++) {

    for (int k = 1; k < number_boxes_depth+1; k++) {

     pushMatrix();

     translate(i*box_size_virtual-5, k*box_size_virtual-2.5, j*box_size_virtual+5);

     bacteria_growth[i][j][k] = bacteria_amount(k,counter/60); //The values for the 3D array
bacteria_growth depend on the function bacteria_amount and the vertical layer (k)
```

```
    if (drainage == false){

        static_stress[i][j][k] = (load*1000)/(100*100); //Static stress equals load/dimensions across the gel
if foundation dimensions equals confinement dimensions

        float pore_pressure = static_stress[i][j][k]; //PWP equals static stress if drainage is not allowed

        if (Simulation_Mode == 1) {

        println(static_stress[20][20][1]);

        noStroke();

        fill(255,255-static_stress[i][j][k]*2.5,255-static_stress[i][j][k]*2.5);

        box(box_size_virtual);

        }

        if (Simulation_Mode == 2) {

        noStroke();

        println(pore_pressure);

        //if ((static_stress[i][j][k]-recording_pressure[i][j][k]) > 10){

        //fill(pore_pressure/1, 0, 255-(pore_pressure/1));

        fill(255-pore_pressure*2.5,255-pore_pressure*2.5,255);

        //fill(0);

        box(box_size_virtual);

        //}

        }

    }

    if (drainage == true){

      if (foundation_length == 100){


        static_stress[i][j][k] = (load*1000)/(100*100); //Static stress equals load/dimensions across the gel
if foundation dimensions equals confinement dimensions

        float pore_pressure = recording_pressure[i][j][k]; //PWP dissipation in the vertical direction

        if (Simulation_Mode == 1) {

        println(static_stress[20][20][1]);

        noStroke();

        fill(255,255-static_stress[i][j][k]*2.5,255-static_stress[i][j][k]*2.5);

        box(box_size_virtual);

        }

        if (Simulation_Mode == 2) {

        noStroke();
```

```
    fill(255-pore_pressure*2.5,255-pore_pressure*2.5,255);

    box(box_size_virtual);

    println(pore_pressure);

      if (isobars == true){ //Represents the pwp in the form of isobars

    if(recording_pressure[i][j][k] > 157.7){

      fill(245,13,5);

    } else if (recording_pressure[i][j][k] > 140 && recording_pressure[i][j][k] < 157.7){

      fill(247,81,15);

    } else if (recording_pressure[i][j][k] > 122.5 && recording_pressure[i][j][k] < 140){

      fill(255,126,5);

    } else if (recording_pressure[i][j][k] > 105 && recording_pressure[i][j][k] < 122.5){

      fill(255,191,13);

    } else if (recording_pressure[i][j][k] > 87.5 && recording_pressure[i][j][k] < 105){

      fill(255,255,0);

    } else if (recording_pressure[i][j][k] > 70 && recording_pressure[i][j][k] < 87.5){

      fill(182,255,0);

    } else if (recording_pressure[i][j][k] > 52.5 && recording_pressure[i][j][k] < 70){

      fill(0,255,99);

    } else if (recording_pressure[i][j][k] > 35 && recording_pressure[i][j][k] < 52.5){

      fill(0,255,249);

    } else if (recording_pressure[i][j][k] > 17.5 && recording_pressure[i][j][k] < 35){

      fill(0,146,255);

    } else {

      fill(0,0,255);

    }

    stroke(200);

    box(box_size_virtual);

    }

    }

    }

    if (foundation_length < 100){ //local stresses develop if the dimensions of the foundation are smaller
than the confinement

    static_stress[i][j][k] = StressDistribution((i-(gel_length_real-foundation_length)/5)*2.5-1.25, (j-
(gel_breadth_real-foundation_length)/5)*2.5-1.25, k*2.5-1.25, load, foundation_length,
foundation_length);;

    float pore_pressure = recording_pressure[i][j][k]; //PWP dissipation in the vertical direction
```

```processing
immediate_settlement[i][j][k] = (static_stress[i][j][k]/Es)*box_size_real;

consolidation_settlement[i][j][k] = (static_stress[i][j][k]-pore_pressure)*box_size_real*mv/1000;

if (Simulation_Mode == 1) {

println(static_stress[20][20][k]);

stroke(200);

fill(255,255-static_stress[i][j][k]*2,255-static_stress[i][j][k]*2);

box(box_size_virtual);

if (isobars == true){ //Represents the stress in the form of isobars

  if(static_stress[i][j][k] >= 157.7){

    fill(245,13,5);

  } else if (static_stress[i][j][k] > 140 && static_stress[i][j][k] < 157.7){

    fill(247,81,15);

  } else if (static_stress[i][j][k] > 122.5 && static_stress[i][j][k] < 140){

    fill(255,126,5);

  } else if (static_stress[i][j][k] > 105 && static_stress[i][j][k] < 122.5){

    fill(255,191,13);

  } else if (static_stress[i][j][k] > 87.5 && static_stress[i][j][k] < 105){

    fill(255,255,0);

  } else if (static_stress[i][j][k] > 70 && static_stress[i][j][k] < 87.5){

    fill(182,255,0);

  } else if (static_stress[i][j][k] > 52.5 && static_stress[i][j][k] < 70){

    fill(0,255,99);

  } else if (static_stress[i][j][k] > 35 && static_stress[i][j][k] < 52.5){

    fill(0,255,249);

  } else if (static_stress[i][j][k] > 17.5 && static_stress[i][j][k] < 35){

    fill(0,146,255);

  } else {

    fill(0,0,255);

  }

  stroke(200);

  box(box_size_virtual);

}

}

if (Simulation_Mode == 2) {
```

```
if (counter/60 <= time_threshold){

stroke(200);

fill(255-recording_pressure[i][j][k]*2,255-recording_pressure[i][j][k]*2,255);

box(box_size_virtual);

println(recording_pressure[20][20][k]);

 if (isobars == true){ //Represents the pwp in the form of isobars

 if(recording_pressure[i][j][k] > 157.7){

   fill(245,13,5);

 } else if (recording_pressure[i][j][k] > 140 && recording_pressure[i][j][k] < 157.7){

   fill(247,81,15);

 } else if (recording_pressure[i][j][k] > 122.5 && recording_pressure[i][j][k] < 140){

   fill(255,126,5);

 } else if (recording_pressure[i][j][k] > 105 && recording_pressure[i][j][k] < 122.5){

   fill(255,191,13);

 } else if (recording_pressure[i][j][k] > 87.5 && recording_pressure[i][j][k] < 105){

   fill(255,255,0);

 } else if (recording_pressure[i][j][k] > 70 && recording_pressure[i][j][k] < 87.5){

   fill(182,255,0);

 } else if (recording_pressure[i][j][k] > 52.5 && recording_pressure[i][j][k] < 70){

   fill(0,255,99);

 } else if (recording_pressure[i][j][k] > 35 && recording_pressure[i][j][k] < 52.5){

   fill(0,255,249);

 } else if (recording_pressure[i][j][k] > 17.5 && recording_pressure[i][j][k] < 35){

   fill(0,146,255);

 } else {

   fill(0,0,255);

 }

 stroke(200);

 box(box_size_virtual);

}

}

if(counter/60 >= time_threshold){

   cv = 0;

stroke(200);
```

```
fill(255-recording_pressure[i][j][k]*2,255-recording_pressure[i][j][k]*2,255);

box(box_size_virtual);

println(recording_pressure[20][20][2]);

  if (isobars == true){ //Represents the pwp in the form of isobars

  if(recording_pressure[i][j][k] > 157.7){

    fill(245,13,5);

  } else if (recording_pressure[i][j][k] > 140 && recording_pressure[i][j][k] < 157.7){

    fill(247,81,15);

  } else if (recording_pressure[i][j][k] > 122.5 && recording_pressure[i][j][k] < 140){

    fill(255,126,5);

  } else if (recording_pressure[i][j][k] > 105 && recording_pressure[i][j][k] < 122.5){

    fill(255,191,13);

  } else if (recording_pressure[i][j][k] > 87.5 && recording_pressure[i][j][k] < 105){

    fill(255,255,0);

  } else if (recording_pressure[i][j][k] > 70 && recording_pressure[i][j][k] < 87.5){

    fill(182,255,0);

  } else if (recording_pressure[i][j][k] > 52.5 && recording_pressure[i][j][k] < 70){

    fill(0,255,99);

  } else if (recording_pressure[i][j][k] > 35 && recording_pressure[i][j][k] < 52.5){

    fill(0,255,249);

  } else if (recording_pressure[i][j][k] > 17.5 && recording_pressure[i][j][k] < 35){

    fill(0,146,255);

  } else {

    fill(0,0,255);

  }

  stroke(200);

  box(box_size_virtual);

}

}

}

 if (Simulation_Mode ==3){ // IMMEDIATE SETTLEMENT

  stroke(200);

  fill(255-total_immediate_settlement[i][j][k]*10,255,255-total_immediate_settlement[i][j][k]*10);

   box(box_size_virtual);
```

```
        if (isobars == true){

        if (total_immediate_settlement[i][j][k] >= 4.5){

          fill(245,13,5);

    }else if (total_immediate_settlement[i][j][k] >= 4 && total_immediate_settlement[i][j][k] < 4.5){

          fill(247,81,15);

    }else if (total_immediate_settlement[i][j][k] >= 3.5 && total_immediate_settlement[i][j][k] < 4){

          fill(255,126,5);

    }else if (total_immediate_settlement[i][j][k] >= 3 && total_immediate_settlement[i][j][k] < 3.5){

          fill(255,191,13);

    }else if (total_immediate_settlement[i][j][k] >= 2.5 && total_immediate_settlement[i][j][k] < 3){

          fill(255,255,0);

    }else if (total_immediate_settlement[i][j][k] >= 2 && total_immediate_settlement[i][j][k] < 2.5){

          fill(182,255,0);

}else if (total_immediate_settlement[i][j][k] >= 1.5 && total_immediate_settlement[i][j][k] < 2){

          fill(0,255,99);

}else if (total_immediate_settlement[i][j][k] >= 1 && total_immediate_settlement[i][j][k] < 1.5){

          fill(0,255,249);

}else if (total_immediate_settlement[i][j][k] >= 0.5 && total_immediate_settlement[i][j][k] < 1){

          fill(0,146,255);

      }else{

        fill(0,0,255);

      }

      stroke(200);

      box(box_size_virtual);

      }
println(static_stress[20][20][1],immediate_settlement[20][20][1],total_immediate_settlement[20][20][1]);

      }

      if (Simulation_Mode ==4){ // CONSOLIDATION SETTLEMENT

      if (counter/60 <= time_threshold){

      stroke(200);

fill(255-total_consolidation_settlement[i][j][k]*100,255,255-total_consolidation_settlement[i][j][k]*100);

      box(box_size_virtual);

      if (isobars == true){

      if (total_consolidation_settlement[i][j][k] >= 4.5){
```

```
                fill(245,13,5);
        }else if (total_consolidation_settlement[i][j][k] >= 4 && total_consolidation_settlement[i][j][k] < 4.5){
                fill(247,81,15);
        }else if (total_consolidation_settlement[i][j][k] >= 3.5 && total_consolidation_settlement[i][j][k] < 4){
                fill(255,126,5);
        }else if (total_consolidation_settlement[i][j][k] >= 3 && total_consolidation_settlement[i][j][k] < 3.5){
                fill(255,191,13);
        }else if (total_consolidation_settlement[i][j][k] >= 2.5 && total_consolidation_settlement[i][j][k] < 3){
                fill(255,255,0);
        }else if (total_consolidation_settlement[i][j][k] >= 2 && total_consolidation_settlement[i][j][k] < 2.5){
                fill(182,255,0);
        }else if (total_consolidation_settlement[i][j][k] >= 1.5 && total_consolidation_settlement[i][j][k] < 2){
                fill(0,255,99);
        }else if (total_consolidation_settlement[i][j][k] >= 1 && total_consolidation_settlement[i][j][k] < 1.5){
                fill(0,255,249);
        }else if (total_consolidation_settlement[i][j][k] >= 0.5 && total_consolidation_settlement[i][j][k] < 1){
                fill(0,146,255);
                }else{
                 fill(0,0,255);
                }
                stroke(200);
                box(box_size_virtual);
                }
                println(consolidation_settlement[20][20][1],total_consolidation_settlement[20][20][1]);
                }
                if (counter/60 >= time_threshold){
                cv = 0;
                stroke(200);
fill(255-total_consolidation_settlement[i][j][k]*100,255,255-total_consolidation_settlement[i][j][k]*100);
                box(box_size_virtual);
                if (isobars == true){
                 if (total_consolidation_settlement[i][j][k] >= 4.5){
                 fill(245,13,5);
                }else if (total_consolidation_settlement[i][j][k] >= 4 && total_consolidation_settlement[i][j][k] <
4.5){
```

256

```processing
      fill(247,81,15);

      }else if (total_consolidation_settlement[i][j][k] >= 3.5 && total_consolidation_settlement[i][j][k] <
4){

      fill(255,126,5);

      }else if (total_consolidation_settlement[i][j][k] >= 3 && total_consolidation_settlement[i][j][k] <
3.5){

      fill(255,191,13);

      }else if (total_consolidation_settlement[i][j][k] >= 2.5 && total_consolidation_settlement[i][j][k] <
3){

      fill(255,255,0);

      }else if (total_consolidation_settlement[i][j][k] >= 2 && total_consolidation_settlement[i][j][k] <
2.5){

      fill(182,255,0);

      }else if (total_consolidation_settlement[i][j][k] >= 1.5 && total_consolidation_settlement[i][j][k] <
2){

      fill(0,255,99);

      }else if (total_consolidation_settlement[i][j][k] >= 1 && total_consolidation_settlement[i][j][k] <
1.5){

      fill(0,255,249);

      }else if (total_consolidation_settlement[i][j][k] >= 0.5 && total_consolidation_settlement[i][j][k] <
1){

      fill(0,146,255);

      }else{

      fill(0,0,255);

      }

      stroke(200);

      box(box_size_virtual);

      }

      println(consolidation_settlement[20][20][1],total_consolidation_settlement[20][20][1]);

      }

    }

    if (Simulation_Mode ==5){ // CONSOLIDATION SETTLEMENT

  float total_settlement = total_immediate_settlement[i][j][k]+total_consolidation_settlement[i][j][k];

      if (counter/60 <= time_threshold){

      stroke(200);

      fill(255-total_settlement*100,255,255-total_settlement*100);

      box(box_size_virtual);
```

```
if (isobars == true){
 if (total_settlement >= 9){
  fill(245,13,5);
 }else if (total_settlement >= 8 && total_settlement < 9){
  fill(247,81,15);
 }else if (total_settlement >= 7 && total_settlement < 8){
  fill(255,126,5);
 }else if (total_settlement >= 6 && total_settlement < 7){
  fill(255,191,13);
 }else if (total_settlement >= 5 && total_settlement < 6){
  fill(255,255,0);
 }else if (total_settlement >= 4 && total_settlement < 5){
  fill(182,255,0);
 }else if (total_settlement >= 3 && total_settlement < 4){
  fill(0,255,99);
 }else if (total_settlement >= 2 && total_settlement < 3){
  fill(0,255,249);
 }else if (total_settlement >= 1 && total_settlement < 2){
  fill(0,146,255);
 }else{
  fill(0,0,255);
 }
 stroke(200);
 box(box_size_virtual);
 }
println(total_immediate_settlement[20][20][1]+total_consolidation_settlement[20][20][1]);
 }
 if (counter/60 >= time_threshold){
 cv = 0;
 stroke(200);
 fill(255-total_settlement*100,255,255-total_settlement*100);
 box(box_size_virtual);
 if (isobars == true){
  if (total_settlement >= 9){
```

```
      fill(245,13,5);
    }else if (total_settlement >= 8 && total_settlement < 9){
      fill(247,81,15);
    }else if (total_settlement >= 7 && total_settlement < 8){
      fill(255,126,5);
    }else if (total_settlement >= 6 && total_settlement < 7){
      fill(255,191,13);
    }else if (total_settlement >= 5 && total_settlement < 6){
      fill(255,255,0);
    }else if (total_settlement >= 4 && total_settlement < 5){
      fill(182,255,0);
    }else if (total_settlement >= 3 && total_settlement < 4){
      fill(0,255,99);
    }else if (total_settlement >= 2 && total_settlement < 3){
      fill(0,255,249);
    }else if (total_settlement >= 1 && total_settlement < 2){
      fill(0,146,255);
    }else{
      fill(0,0,255);
    }
    stroke(200);
    box(box_size_virtual);
    }
    println(total_immediate_settlement[20][20][1]+total_consolidation_settlement[20][20][1]);
    }
   }
  }
 }
hit_line = false;
if (Simulation_Mode == 6){ //Represents enzyme activity w.r.t. amount of bacteria (Graph 1)
   amount = bacteria_growth[i][j][k];
   //println(bacteria_growth[i][j][1],y_value_1);
   float value_of_x_1 = (float(box_width)/3)*amount;
    for (int l = 0; hit_line == false; l++) {
```

```
if (graph_matrix_1[int(value_of_x_1)][l] < -2) {

    float y_value_1 = max_expression_1-(l*(max_expression_1/box_height));

    println(y_value_1);

    float voxel_size = y_value_1/450;

    //noStroke();

    //fill(0,255,0);

    //fill(0);

    //box(voxel_size);

    if (isobars == true){

      if (y_value_1 >= 22.5){

fill(245,13,5);

      }else if (y_value_1 >= 20 && y_value_1 < 22.5){

fill(247,81,15);

      }else if (y_value_1 >= 17.5 && y_value_1 < 20){

fill(255,126,5);

      }else if(y_value_1 >= 15 && y_value_1 < 17.5){

fill(255,191,13);

      }else if(y_value_1 >= 12.5 && y_value_1 < 15){

fill(255,255,0);

      }else if(y_value_1 >= 10 && y_value_1 < 12.5){

fill(182,255,0);

      }else if(y_value_1 >= 7.5 && y_value_1 < 10){

fill(0,255,99);

      }else if(y_value_1 >= 5 && y_value_1 < 7.5){

fill(0,255,249);

      }else if(y_value_1 >= 2.5 && y_value_1 < 5){

fill(0,146,255);

      }else{

fill(0,0,255);

      }

      //noStroke();

      stroke(200);

      box(box_size_virtual);

    }
```

```
        hit_line = true;

      }

    }

}

    if (Simulation_Mode == 7) { //Represents enzyme activity w.r.t. level of stress (Graph 2)

     float example_pressure = recording_pressure[i][j][k];

     float value_of_x_2 = (float(box_width)/175)*example_pressure;

     for (int l = 0; hit_line == false; l++) {

      //println(graph_matrix[int(0)][0]);

      if (graph_matrix_2[int(value_of_x_2)][l] < -2) {

        float y_value_2 = max_expression_2-(l*(max_expression_2/box_height))+1;

        println(y_value_2);

        float voxel_size = y_value_2/450;

        stroke(0);

        fill(0,255,0);

        //box(voxel_size);

        if (isobars == true){

          if (y_value_2 >= 4.6){

       fill(245,13,5);

          }else if (y_value_2 >= 4.2 && y_value_2 < 4.6){

       fill(247,81,15);

          }else if (y_value_2 >= 3.8 && y_value_2 < 4.2){

       fill(255,126,5);

          }else if(y_value_2 >= 3.4 && y_value_2 < 3.8){

       fill(255,191,13);

          }else if(y_value_2 >= 3 && y_value_2 < 3.4){

       fill(255,255,0);

          }else if(y_value_2 >= 2.6 && y_value_2 < 3){

       fill(182,255,0);

          }else if(y_value_2 >= 2.2 && y_value_2 < 2.6){

       fill(0,255,99);

          }else if(y_value_2 >= 1.8 && y_value_2 < 2.2){

       fill(0,255,249);

          }else if(y_value_2 >= 1.4 && y_value_2 < 1.8){
```

```
          fill(0,146,255);

            }else{

        fill(0,0,255);

            }

            //noStroke();

            stroke(200);

            box(box_size_virtual);

          }

          hit_line = true;

        }

      }

    }

    if (Simulation_Mode == 8){ //Couples simulation 6 and 7

      float amount = bacteria_growth[i][j][k];

      float example_pressure = recording_pressure[i][j][k];

      float value_of_x_1 = (float(box_width)/3)*amount;

      float value_of_x_2 = (float(box_width)/175)*example_pressure;

        for (int l = 0; hit_line == false; l++) {

          if (graph_matrix_1[int(value_of_x_1)][l] < -2){

            float y_value_1 = max_expression_1-(l*(max_expression_1/box_height));

          for (int l2 = 0; hit_line == false; l2++) {

            if (graph_matrix_2[int(value_of_x_2)][l2] < -2){

              float y_value_2 = max_expression_2-(l2*(max_expression_2/box_height))+1;

              float integrated_response = y_value_1*(y_value_2);

              noStroke();

              fill(255-integrated_response/4);

              println(y_value_1, y_value_2, integrated_response);

              //box(box_size_virtual);


              if (isobars == true){

            if (integrated_response >= 112.5){

        fill(245,13,5);

              }else if (integrated_response >= 100 && integrated_response < 112.5){

        fill(247,81,15);
```

```
        }else if (integrated_response >= 87.5 && integrated_response < 100){
    fill(255,126,5);
        }else if(integrated_response >= 75 && integrated_response < 87.5){
    fill(255,191,13);
        }else if(integrated_response >= 62.5 && integrated_response < 75){
    fill(255,255,0);
        }else if(integrated_response >= 50 && integrated_response < 62.5){
    fill(182,255,0);
        }else if(integrated_response >= 37.5 && integrated_response < 50){
    fill(0,255,99);
        }else if(integrated_response >= 25 && integrated_response < 37.5){
    fill(0,227,255);
        }else if(integrated_response >= 12.5 && integrated_response < 25){
    fill(0,146,255);
        }else{
    fill(0,0,255);
        }
        //noStroke();
        stroke(200);
        box(box_size_virtual);
      }
            hit_line = true;
        }
        }
        }
        }
        }
    popMatrix();
    }
    }
    }
    if (Simulation_Mode == 6 || Simulation_Mode == 8){ //Represents bacteria growth by drawing lines next
to each layer
    for (int i=1; i<41; i++){
      amount = bacteria_amount(i,counter/60);
```

263

```
    pushMatrix();

    translate(-20,0,200);

    stroke(0);

    fill(0);

    line(500,-5,730,-5);

    line(730,-5,725,-10);

    line(730,-5,725,0);

    line(535,-10,535,0);

    line(570,-10,570,0);

    line(605,-10,605,0);

    line(640,-10,640,0);

    line(675,-10,675,0);

    line(710,-10,710,0);

    line(500,-5,500,420);

    line(500,420,495,415);

    line(500,420,505,415);

    textMode(SHAPE);

    textSize(20);

    text("0.5",520,-13);

    text("1",565,-13);

    text("1.5",590,-13);

    text("2",635,-13);

    text("2.5",660,-13);

    text("3",705,-13);

    text("%",740,0);

    stroke(0);

    fill(255,255,0);

    rect(500,(i*10.1-10),amount*70,7);

    popMatrix();

    //println(bacteria_amount(1,counter/60),counter/60);

  }

}

///////////CALCULATION SETTLEMENT////////////////////////

cam.beginHUD();
```

```
    //float immediate_ement = ((1-
mu*mu)*load*foundation_length*Ip)/(young*foundation_length*foundation_length); //It occurs in all
types of soil due to elastic compression.It is determined from elastic theory.

    //float first_parameter = Cc/(1+e0);

    //float consolidation_settlement = first_parameter*gel_depth_real*0.5*log((load*1000)/(100*100));

    if (drainage == true && local_stress == false){

      textSize(15);

      stroke(1);

      fill(0);

      //text("Total settlement (mm) =",500,700);

      //text(consolidation_settlement,700,700);

    }

    if (drainage == true && local_stress == true && foundation_length<100){

      textSize(15);

      stroke(1);

      fill(0);

      //text("Total settlement (mm) =",500,700);

      //text(immediate_settlement+consolidation_settlement,700,700);

    }

    cam.endHUD();

    float time_inc = 1;   //MINUTES!//

    float beta = (cv*1000000*time_inc)/(525600*box_size_real*box_size_real); //Variable used to control
the pwp dissipation

    if (one_way == false){ //Drainage through top and bottom

      for (int i = 1; i < number_boxes_length+1; i++) {

        for (int j = 1; j < number_boxes_breadth+1; j++) {

          for (int k = 1; k < number_boxes_depth+1; k++) {

            if (k==1){

              recording_pressure[i][j][k] = 0; //pwp at the top layer becomes 0

            }

            if (k>1 && k<number_boxes_depth){

recording_pressure[i][j][k] = recording_pressure[i][j][k] + beta*(recording_pressure[i][j][k-1] +
recording_pressure[i][j][k+1] - 2*recording_pressure[i][j][k]); //Expression that updates pwp with time

            }

            if (k==number_boxes_depth){

              recording_pressure[i][j][k] = 0; //pwp at the bottom layer becomes 0
```

```
            }

          }

        }

      }

    }

    if (one_way == true){ //Only drainage through the top

      for (int i = 1; i < number_boxes_length+1; i++) {

        for (int j = 1; j < number_boxes_breadth+1; j++) {

          for (int k = 1; k < number_boxes_depth+1; k++) {

            if (k==1){

              recording_pressure[i][j][k] = 0; //pwp at the top layer becomes 0

            }

            if (k>1 && k<number_boxes_depth){

recording_pressure[i][j][k] = recording_pressure[i][j][k] + beta*(recording_pressure[i][j][k-1] +
recording_pressure[i][j][k+1] - 2*recording_pressure[i][j][k]); //Expression that updates pwp with time

            }

            if (k==number_boxes_depth){

              //recording_pressure[i][j][k] = 0;

            }

          }

        }

      }

    }

    for (int i = 1; i < number_boxes_length+1; i++) {

      for (int j = 1; j < number_boxes_breadth+1; j++) {

        for (int k = 1; k < number_boxes_depth+1; k++) {

          if (k+1<41){

            total_immediate_settlement[i][j][k] = total_immediate_settlement[i][j][k+1] +
immediate_settlement[i][j][k];

            total_consolidation_settlement[i][j][k] = total_consolidation_settlement[i][j][k+1] +
consolidation_settlement[i][j][k];

          }

        }

      }

    }

  }
```

266

```
  } ///////////////////////////////// END RUN ////////////////////////////////////////
if (export_2d == true) {
  saveFrame("Screen_Shot-####.png");
  export_2d = false;
}
// Draw in the 2D window overlaying 3D
cam.beginHUD();
//////////////////////// DRAW THE LEGENDS AND TEXT ON THE GUI //////////////////////////
if (run == true){
  if (drainage == false){
   if (Simulation_Mode ==1){
    for (int i=1; i<11; i++){
    stroke(0);
    fill(255,0 +30*i,0+30*i);
    rect(1050,250+20*i,20,20);
    textSize(12);
    fill(0);
    text("100kPa",1073,275);
    text("50kPa",1073,374);
    text("0kPa",1073,473);
    }
   }
   if (Simulation_Mode ==2){
    for (int i=1; i<11; i++){
    stroke(0);
    fill(0 +30*i,0+30*i,255);
    rect(1050,250+20*i,20,20);
    textSize(15);
    fill(0);
    text("100kPa",1073,275);
    text("50kPa",1073,374);
    text("0kPa",1073,473);
    }
   }
```

```
    }
  if (drainage == true && local_stress == false){
  if (Simulation_Mode ==1){
    for (int i=1; i<11; i++){
    stroke(0);
    fill(255,0 +30*i,0+30*i);
    rect(1050,250+20*i,20,20);
    textSize(12);
    fill(0);
    text("100kPa",1073,275);
    text("50kPa",1073,374);
    text("0kPa",1073,473);
    }
  }
  if (Simulation_Mode ==2){
  for (int i=1; i<11; i++){
  stroke(0);
  fill(0 +30*i,0+30*i,255);
  rect(1050,250+20*i,20,20);
  textSize(15);
  fill(0);
  text("100kPa",1073,275);
  text("50kPa",1073,374);
  text("0kPa",1073,473);
  }
  }
  }
  if (drainage == true && local_stress == true){
  if (Simulation_Mode ==1){
    for (int i=1; i<11; i++){
    stroke(0);
    fill(255,0 +30*i,0+30*i);
    rect(1050,250+20*i,20,20);
    textSize(12);
```

```
        fill(0);

        text("160kPa",1073,275);

        text("800kPa",1073,374);

        text("0kPa",1073,473);

        }

      }

      if (Simulation_Mode ==2){

      for (int i=1; i<11; i++){

      stroke(0);

      fill(0 +30*i,0+30*i,255);

      rect(1050,250+20*i,20,20);

      textSize(15);

      fill(0);

      text("160kPa",1073,275);

      text("80kPa",1073,374);

      text("0kPa",1073,473);

        }

      }

    }

  }

  textSize(12);

  fill(20);

  int upper_margin = 30;

  int margin = 250;

  int spacer = 220;

  textSize(18);

  //text("Computational model to represent and predict the behaviour of agarose gels, bacteria growth",
  180,40);

  //text("and effect stress-sensitive urease-producing engineered bacteria on the matrix of the gel", 200,65);

  textSize(15);

  fill(255, 0, 0);

  if (run == true) {

    text("Stop and reset", 85, 110);

  } else {

    text("Run", 85, 110);
```

```
}

fill(0);

textSize(10);

text("Load (N)", margin - spacer, 160);

text("Coefficient of consolidation (square meter/year)", margin - spacer, 510);

text("Coefficient of compressibility (square meter/megaNewton)", margin - spacer, 560);

text("Poisson's ratio", margin - spacer, 610);

text("Time threshold (HOURS)", margin - spacer, 310);

text("Length (mm)", margin - spacer, 210);

text("Temperature (C)", margin - spacer, 410);

textSize(12);

text("Initial Concentration Cells", margin - spacer, 190);

textSize(10);

if (Simulation_Mode == 1) {

  text("Stress Static", margin - spacer, 260);

}

if (Simulation_Mode == 2) {

  text("Dissipation Excess PWP", margin - spacer, 260);

}

if (Simulation_Mode == 3) {

  text("Immediate settlement", margin - spacer, 260);

}

if (Simulation_Mode == 4) {

  text("Consolidation settlement", margin - spacer, 260);

}

if (Simulation_Mode == 5) {

  text("Total settlement", margin - spacer, 260);

}

 if (Simulation_Mode == 6) {

  text("Enzyme activity w.r.t. cell concentration (Graph 1)", margin - spacer, 260);

}

if (Simulation_Mode == 7) {

  text("Enzyme activity w.r.t. stress (Graph 2)", margin - spacer, 260);

}
```

```
if (Simulation_Mode == 8) {

  text("Enzyme activity w.r.t. cell concentration and stress", margin - spacer, 260);

}

textSize(12);

text("Counter (time in MINUTES):", margin-spacer, upper_margin + 680);

text(counter, margin, upper_margin + 680);

text("Counter (time in HOURS):", margin-spacer, upper_margin + 730);

text(counter/60, margin, upper_margin + 730);

cp5.draw();

///////////////////////////////////////////GRAPH 1///////////////////////////////////////

//draw the gene expression graph to the screen

noStroke();

fill(255);

rect(box_x, box_y_2, box_width, box_height);

fill(0);

float tick_marks_x_1 = 6;

float tick_marks_x_2 = 5;

float tick_marks_y_1 = 5;

float tick_marks_y_2 = 4;

stroke(1);

for (int i = 0; i< (tick_marks_y_1+1); i++) { //Y AXIS

  float tick_distance = box_height/(tick_marks_y_1);

  stroke(1);

  line(box_x-5, (box_y_1+box_height)-(i*tick_distance), box_x-1, (box_y_1+box_height)-(i*tick_distance));

  float axis_y_value = (max_expression_1/tick_marks_y_1)*i;

  textSize(10);

  text(nf(axis_y_value, 1, 0), box_x-25, (box_y_1+box_width)-(i*tick_distance));

}

for (int i = 0; i< (tick_marks_x_1+1); i++) { // X AXIS

  float x_tick_distance = box_width/(tick_marks_x_1);

  stroke(1);

  line(box_x+(i*x_tick_distance), box_y_1+box_height, box_x+(i*x_tick_distance),
(box_y_1+box_height+5));

  float axis_x_value = (3/(tick_marks_x_1))*i; //changes the spacing of the x values of the graph

  textSize(10);
```

```
    text(nf(axis_x_value, 1, 0), box_x+(i* x_tick_distance)-5, box_y_1+box_height+20); //moved 10 pixels to
the left

  }

//////////////////////////////////// CURVE OF THE GRAPH //////////////////////////////////////

  noFill();

  stroke(1);

  beginShape();

  curveVertex(translated_point_x(box_x, 0, box_width,3), translated_point_y_1(box_y_1, Val1_0,
box_height,25));

  curveVertex(translated_point_x(box_x, 0, box_width,3), translated_point_y_1(box_y_1, Val1_0,
box_height,25));

  curveVertex(translated_point_x(box_x, 0.5, box_width,3), translated_point_y_1(box_y_1, Val1_0_5,
box_height,25));

  curveVertex(translated_point_x(box_x, 1, box_width,3), translated_point_y_1(box_y_1, Val1_1,
box_height,25));

  curveVertex(translated_point_x(box_x, 1.5, box_width,3), translated_point_y_1(box_y_1, Val1_1_5,
box_height,25));

  curveVertex(translated_point_x(box_x, 2, box_width,3), translated_point_y_1(box_y_1, Val1_2,
box_height,25));

  curveVertex(translated_point_x(box_x, 2.5, box_width,3), translated_point_y_1(box_y_1, Val1_2_5,
box_height,25));

  curveVertex(translated_point_x(box_x, 3, box_width,3), translated_point_y_1(box_y_1, Val1_3,
box_height,25));

  curveVertex(translated_point_x(box_x, 3, box_width,3), translated_point_y_1(box_y_1, Val1_3,
box_height,25));

  endShape();

///////////////////////////////////////////GRAPH 2///////////////////////////////////////////////

  //draw the gene expression graph to the screen

  noStroke();

  fill(255);

  rect(box_x, box_y_2, box_width, box_height);

  fill(0);

  stroke(1);

/////////////////// Y AXIS GRAPH ///////////////////

for (int i = 0; i< (tick_marks_y_2+1); i++) {

  float tick_distance = box_height/(tick_marks_y_2);

  stroke(1);

  line(box_x-5, (box_y_2+box_height)-(i*tick_distance), box_x-1, (box_y_2+box_height)-(i*tick_distance));
```

```
    float axis_y_value = ((max_expression_2)/tick_marks_y_2)*i;

    textSize(10);

    text(nf(axis_y_value+1, 1, 0), box_x-25, (box_y_2+box_width)-(i*tick_distance));

  }
```

/////////////////////////////////// X AXIS GRAPH ///

```
  for (int i = 0; i< (tick_marks_x_2+1); i++) {

    float x_tick_distance = box_width/(tick_marks_x_2);

    stroke(1);

    line(box_x+(i*x_tick_distance), box_y_2+box_height, box_x+(i*x_tick_distance),
(box_y_2+box_height+5));

    float axis_x_value = (175/(tick_marks_x_2))*i; //changes the spacing of the x values of the graph

    textSize(10);

    text(nf(axis_x_value, 1, 0), box_x+(i* x_tick_distance)-10, box_y_2+box_height+20); //moved 10 pixels to
the left

  }
```

 /////////////////////////////////// CURVE OF THE GRAPH ///////////////////////////////////////

```
  noFill();

  stroke(1);

  beginShape();

  curveVertex(translated_point_x(box_x, 0, box_width,175), translated_point_y_2(box_y_2, Val2_0,
box_height,4));

  curveVertex(translated_point_x(box_x, 0, box_width,175), translated_point_y_2(box_y_2, Val2_0,
box_height,4));

  curveVertex(translated_point_x(box_x, 35, box_width,175), translated_point_y_2(box_y_2, Val2_35,
box_height,4));

  curveVertex(translated_point_x(box_x, 70, box_width,175), translated_point_y_2(box_y_2, Val2_70,
box_height,4));

  curveVertex(translated_point_x(box_x, 105, box_width,175), translated_point_y_2(box_y_2, Val2_105,
box_height,4));

  curveVertex(translated_point_x(box_x, 140, box_width,175), translated_point_y_2(box_y_2, Val2_140,
box_height,4));

  curveVertex(translated_point_x(box_x, 175, box_width,175), translated_point_y_2(box_y_2, Val2_175,
box_height,4));

  curveVertex(translated_point_x(box_x, 175, box_width,175), translated_point_y_2(box_y_2, Val2_175,
box_height,4));

  endShape();

  cam.endHUD();
```

```
////////////////////////// PICKS THE VALUES OFF GRAPH 1 //////////////////////////
for (int l = 0; l< box_width; l++) {
  for (int m = 0; m< box_height; m++) {
    graph_matrix_1[l][m] = get(l+box_x, m+box_y_1);
  }
}
////////////////////////// PICKS THE VALUES OFF GRAPH 2 //////////////////////////
for (int l = 0; l< box_width; l++) {
  for (int m = 0; m< box_height; m++) {
    graph_matrix_2[l][m] = get(l+box_x, m+box_y_2);
  }
}
if (run==false) {
  set = false;
  counter = 0;
 }
}
///////////////////////////////////////END DRAW///////////////////////////////////////

///////////////////////////////////////// FUNCTIONS /////////////////////////////////////////
float StressDistribution(float l, float b, float z, float load, float pad_length, float pad_breadth) {
  float m1 = b/z;
  float n1 = l/z;
  float I1 = Influence(m1, n1);
  float m2 = (pad_length - b)/z;
  float n2 = l/z;
  float I2 = Influence(m2, n2);
  float m3 = (pad_length - b)/z;
  float n3 = (pad_breadth - l)/z;
  float I3 = Influence(m3, n3);
  float m4 = b/z;
  float n4 = (pad_breadth - l)/z;
  float I4 = Influence(m4, n4);
  float stress = (load/(pad_length*pad_breadth))*(I1+I2+I3+I4)*1000; // in kPa
```

274

```
  return stress;

}

float Influence(float m, float n) {

 float I =
(1/(2*PI))*(atan((m*n)/sqrt(m*m+n*n+1))+((m*n)/sqrt(m*m+n*n+1))*((1/(1+m*m))+(1/(1+n*n))));

  return I;

}
```

////////////////////////////////EQUATIONS BACTERIA GROWTH/////////////////////////////////

```
float bacteria_amount(int layer, float time){

  if (counter/60 > time_threshold){

    counter = counter-1; //to counteract the counter value

  } else {

  if (low == true && high == false){

   if (temperature == 25){

            if(layer == 1){

            amount=54253.7806 + ((-54253.69251)/(1+pow((time/2371.69267),2.00298)));

            }

  }
```

/////////////////ADD HERE THE REST OF CONDITIONS AND GROWTH EXPRESSIONS/////////////////

```
  if (amount < 0){

    amount = 0;

    return amount;

  } else {

  return amount;

  }

}
```

/////////////////////////////////////GENE LEVEL GRAPH///

```
float translated_point_x(int margin_x, float pressure_val, float box_w, float max_value_x) {

  float point_location =  ((box_w /max_value_x)*pressure_val) + margin_x;

  return point_location;

}

float translated_point_y_2(int margin_y, float expression_value, float box_l, float max_expression) {

  float point_location =  (-((box_l/max_expression)*expression_value) + margin_y)+box_l;
```

```
    return point_location;
}
float translated_point_y_1(int margin_y, float expression_value, float box_l, float max_expression) {
   float point_location =  (-((box_l/max_expression)*expression_value) + margin_y)+box_l;
   return point_location;
}
```